Inaugural dissertation

for

obtaining the doctoral degree

of the

Combined Faculty of Mathematics, Engineering and Natural Sciences

of the

Ruprecht - Karls - University

Heidelberg

presented by

Anna Hartley, M.Sc.

born in Troisdorf, Germany

Oral examination: 29th April 2024

Reprogramming human cells using SMAR vectors and Potentiation of H-1PV oncolysis by Ledipasvir

Referees: Prof. Dr. Ralf Bartenschlager

Dr. Richard P Harbottle

Preamble

This thesis represents a culmination of work undertaken across two distinct phases. I joined the LOVIT laboratory under the supervision of Dr Antonio Marchini in November 2019, and began working on the oncolytic virus H-1PV. Due to the closure of the LOVIT laboratory at the end of 2021, I moved to the DNA Vector Group under Dr Richard Harbottle to continue my work on H-1PV. As part of this move, I also initiated a project aiming to reprogram human cells using DNA vectors. Accordingly, this thesis is split into two distinct chapters: Chapter 1 explores reprogramming of human cells using episomal SMAR vectors, and Chapter 2 delves into the mechanism of action of a novel drug combination with the oncolytic virus H-1PV.

Summary

This two-part thesis explores the utility of non-viral DNA vectors for reprogramming human cells, as well as the potentiation of the oncolytic virus H-1 parvovirus (H-1PV) by a novel combination with the antiviral drug Ledipasvir.

Pluripotent stem cells are an attractive tool for regenerative medicine due to their capacity for unlimited self-renewal and their ability to differentiate into any somatic cell type. However, the generation of pluripotent stem cells from human embryos raises ethical challenges and is strictly regulated as a result. The advent of cellular reprogramming has now made it possible to generate induced pluripotent stem cells (iPSCs) from a patient's own cells, or for derivation of off-the-shelf cell therapies without the ethical concerns of embryonic stem cells. Nevertheless, current methods for the generation of iPSCs for clinical application cause concerns due to the use of viruses and viral components. Lentiviral transduction is a popular method to introduce reprogramming factors into cells, however they carry with them a high risk of insertional mutagenesis. iPSCs which are currently employed in a therapeutic manner in clinical trials are exclusively derived using the oriP/EBNA-1 vector system, which makes use of the Epstein Barr Virus Nuclear Antigen 1, a protein which has been implicated in oncogenesis, and is known to induce immune activation in iPSCs. Thus, there is a clear need to improve the safety of the reprogramming process to generate iPSCs with the least possible damage and immune activation.
In this thesis, I show for the first time that DNA vectors which comprise Scaffold/Matrix Attachment Regions (S/MARs) can be used to reprogram healthy neonatal human dermal fibroblasts, eliminating the need for viral components. SMAR vectors are retained episomally in cells without integration, but require only a single transfection for successful reprogramming, a feature which is highly attractive for current good manufacturing practice (cGMP). SMAR iPSCs can be generated at practical efficiencies and are phenotypically indistinguishable from traditional EBNA iPSCs. They also show strong similarity to human embryonic stem cell lines in their gene expression. Importantly, SMAR iPSCs show differentiation capacity into cell of all three embryonic lineages, confirming their pluripotency. Surprisingly, modifications to the vectors to reduce their immunogenicity and improve their retention in cells proved counterproductive, as these optimised nanoSMAR vectors were unable to fully reprogram cells. The genetic stability of SMAR iPSCs is comparable to that of EBNA iPSCs, and they show the potential for loss of the vector after reprogramming to generate vector free iPSCs. Further fine-tuning of the SMAR vector system to ensure passive vector loss after reprogramming is discussed. This work thus represents a step towards virus free, vector free and factor free reprogramming for clinical applications.

Summary

The field of oncolytic virotherapy has enjoyed increasing clinical success in the past decade, with the worldwide approval of four oncolytic viruses to date. One of the oncolytic viruses under clinical evaluation is H-1PV, a rodent protoparvovirus which is non-pathogenic to humans and possesses natural oncolytic activity. Its replication is strictly dependent on a transformed phenotype in human cells, giving it a good safety profile for clinical use. This virus has shown considerable promise in early-stage clinical trials for the treatment of both high-grade glioma and pancreatic ductal adenocarcinoma (PDAC), two cancer modalities for which treatment options remain limited and prognosis is dismal. H-1PV treatment in these settings was safe and well tolerated, with some early signs of efficacy including evidence of viral replication in the tumour bed and immune conversion of the tumour microenvironment, as well as an improvement in patient survival in comparison to historical controls. Nonetheless, H-1PV monotherapy was not curative under the regimes used, highlighting a need for the improvement of oncolytic H-1PV therapy.

One approach for this with rapid translational potential is the combination therapy of H-1PV with other drugs to improve its oncolytic activity. This approach has already shown promise in the successful potentiation of H-1PV in combination with the histone deacetylase inhibitor valproic acid and pro-apoptotic BH3 mimetics, such as ABT-737. Here I present a high-throughput screening approach which identified the FDA-approved antiviral drug Ledipasvir as a potentiator of H-1PV oncolysis in human cells. Importantly, Ledipasvir co-treatment improves the oncolytic capabilities of H-1PV in a wide range of cancer cell lines spanning diverse tumour types, including primary patient-derived PDAC cultures. I determined that the cell death induced by the Ledipasvir-H-1PV combination is at least in part apoptotic, but the drug is unable to improve viral replication. Instead, Ledipasvir improves the oncotoxic properties of the major effector protein NS1, albeit without directly binding to NS1. A series of unbiased screening approaches revealed a complex interplay between Ledipasvir, H-1PV, and the pro-survival PI3K/Akt/mTOR signalling pathway. While H-1PV alone activates Akt signalling, this becomes hyperactivated upon the addition of Ledipasvir, and may serve to improve the functionality of NS1. Further downstream, inhibition of mTOR by the small molecule Torin was able to abrogate the combinatorial effects of H-1PV and Ledipasvir, without affecting oncolysis by H-1PV alone. I propose a tentative model in which the combination of Ledipasvir and H-1PV modulate components of the PI3K/Akt/mTOR pathway to improve the functionality and oncotoxic capabilities of the H-1PV NS1 protein, ultimately improving viral oncolysis.

Zusammenfassung

Diese zweiteilige Arbeit untersucht die Verwendung nichtviraler DNA-Vektoren für die Reprogrammierung menschlicher Zellen sowie die Potenzierung der onkolytischen Eigenschaften des H-1 Parvovirus (H-1PV) durch eine neuartige Kombination mit dem antiviralen Wirkstoff Ledipasvir.

Pluripotente Stammzellen sind aufgrund ihrer Fähigkeit zur unbegrenzten Selbsterneuerung und ihrer Fähigkeit, sich in jeden somatischen Zelltyp zu differenzieren, ein attraktives Werkzeug für die regenerative Medizin. Die Gewinnung pluripotenter Stammzellen aus menschlichen Embryonen wirft jedoch ethische Probleme auf und ist daher streng geregelt. Seit dem Aufkommen der zellulären Reprogrammierung ist es nun möglich, induzierte pluripotente Stammzellen (iPSCs) aus adulten patienteneigenen Zellen oder aus patientenfremden Zellen zu erzeugen und erlauben damit gebrauchsfertige und standardisierte Zelltherapien ohne die ethischen Bedenken die mit der Nutzung embryonaler Stammzellen verbunden sind. Die derzeitigen Methoden zur Gewinnung von iPSCs für die klinische Anwendung sind jedoch aufgrund der Verwendung von Viren und viralen Komponenten risikobehaftet. Die lentivirale Transduktion ist eine beliebte Methode, um Reprogrammierungsfaktoren in die Zellen einzubringen, birgt jedoch die Gefahr der Insertionsmutagenese. iPSCs, die derzeit in klinischen Versuchen therapeutisch eingesetzt werden, werden ausschließlich mit dem oriP/EBNA-1-Vektorsystem erzeugt, das das Epstein-Barr-Virus-Nuklearantigen 1 verwendet, ein Protein, das mit Onkogenese in Verbindung gebracht wird und dafür bekannt ist, dass es in iPSCs eine Immunaktivierung auslöst. Diese Ausgangssituation verlangt nach einer sichereren Reprogrammierungsmethode, um iPSCs mit möglichst geringer Schädigung und Immunaktivierung zu generieren.
In dieser Arbeit zeige ich zum ersten Mal, dass DNA-Vektoren, die Scaffold/Matrix Attachment Regions (S/MARs) enthalten, zur Reprogrammierung gesunder, neonataler, menschlicher Hautfibroblasten verwendet werden können, ohne dass virale Komponenten erforderlich sind. SMAR-Vektoren integrieren nicht ins Genom sondern verbleiben episomal in den Zellen, erfordern aber nur eine einzige Transfektion für eine erfolgreiche Reprogrammierung und sind daher ideal für die hohen Anforderungen der Arzneimittelherstellung (Good Manufacturing Practice, GMP), geeignet. SMAR iPSCs können mit praktikabler Effizienz erzeugt werden und sind phänotypisch nicht von herkömmlichen EBNA iPSCs zu unterscheiden. Auch in ihrer Genexpression weisen sie große Ähnlichkeit mit humanen embryonalen Stammzelllinien auf. Besonders hervorzuheben ist, dass SMAR-iPSCs die Fähigkeit zur Differenzierung in Zellen aller drei embryonalen Abstammungslinien aufweisen, was ihre Pluripotenz bestätigt. Überraschenderweise erwiesen sich Modifikationen an den Vektoren zur Verringerung ihrer Immunogenität und zur Verbesserung ihrer anhaltenden

Präsenz in den Zellen als kontraproduktiv, da diese optimierten nanoSMAR-Vektoren nicht in der Lage waren, Zellen vollständig zu reprogrammieren. Die genetische Stabilität von SMAR iPSCs ist mit der von EBNA iPSCs vergleichbar, und sie zeigen das Potenzial, den Vektor nach der Reprogrammierung zu verlieren, was die Erzeugung vektorfreier iPSCs ermöglichen würde. Eine weitere Optimierung des SMAR-Vektorsystems, um den passiven Vektorverlust nach der Reprogrammierung sicherzustellen, ist geplant. Diese Arbeit stellt somit einen Schritt in Richtung virenfreier, vektorfreier und faktorfreier Reprogrammierung für klinische Anwendungen dar.

Der Bereich der onkolytischen Virotherapie ist in den letzten zehn Jahren zunehmend klinisch erfolgreich geworden, wobei bisher vier onkolytische Viren weltweit als Arzneimittel zugelassen wurden. Eines der in der klinischen Prüfung befindlichen onkolytischen Viren ist H-1PV, ein Nagetier-Protoparvovirus, das für den Menschen nicht pathogen ist und eine natürliche onkolytische Aktivität besitzt. Seine Replikation ist in menschlichen Zellen streng auf einen tumorartig transformierten Phänotyp begrenzt, was ihm ein gutes Sicherheitsprofil für den klinischen Einsatz verleiht. Dieses Virus hat sich in frühen klinischen Versuchen als vielversprechend für die Behandlung von hochgradigen Gliomen und duktalen Adenokarzinomen der Bauchspeicheldrüse (engl.: PDAC) erwiesen, zwei Krebsarten, für die es nach wie vor nur begrenzte Behandlungsmöglichkeiten gibt und deren Prognose sehr schlecht ist. Die H-1PV-Behandlung in diesen Fällen war sicher und gut verträglich, und zeigte erste Anzeichen für eine Wirksamkeit, darunter Hinweise auf virale Replikation im Tumorbett und Immunumwandlung der Tumormikroumgebung sowie eine Verbesserung der Überlebensrate der Patienten im Vergleich zu historischen Kontrollen. Dennoch war die H-1PV-Monotherapie mit den verwendeten Therapieschemata nicht kurativ, was die Notwendigkeit einer Verbesserung der onkolytischen H-1PV-Therapie unterstreicht.
Ein Ansatz mit schnellem Umsetzungspotenzial ist die Kombinationstherapie von H-1PV mit anderen bereits zugelassenen Medikamenten zur Verbesserung seiner onkolytischen Aktivität. Dieser Ansatz hat sich bereits in der erfolgreichen Potenzierung der onkolytischen Eigenschaften von H-1PV in Kombination mit dem Histon-Deacetylase-Inhibitor Valproinsäure und pro-apoptotischen BH3-Mimetika wie ABT-737 als vielversprechend erwiesen. Hier stelle ich einen Hochdurchsatz-Screening-Ansatz vor, mit dem das von der FDA zugelassene antivirale Medikament Ledipasvir als Verstärker der H-1PV-Onkolyse in menschlichen Zellen identifiziert wurde. Die gleichzeitige Behandlung mit Ledipasvir verbessert die onkolytischen Fähigkeiten von H-1PV in einem breiten Spektrum von Krebszelllinien verschiedener Tumorarten, einschließlich primärer PDAC-Kulturen, die von Patienten stammen. Ich habe herausgefunden, dass der durch die Ledipasvir-H-1PV-Kombination ausgelöste Zelltod zumindest teilweise apoptotisch ist, das Medikament aber nicht in der Lage ist, die virale Replikation

zu verbessern. Stattdessen fördert Ledipasvir die onkotoxischen Eigenschaften des Haupteffektorproteins NS1, ohne jedoch direkt an NS1 zu binden. Eine Reihe von Screening-Ansätzen ergab ein komplexes Zusammenspiel zwischen Ledipasvir, H-1PV und dem überlebensfördernden PI3K/Akt/mTOR-Signalweg. Während H-1PV allein den Akt-Signalweg aktiviert, wird dieser bei Zugabe von Ledipasvir hyperaktiviert und kann dazu dienen, die Funktionalität von NS1 zu verbessern. Die Hemmung von mTOR durch den small-molecule Inhibitor Torin konnte die kombinatorischen Effekte von H-1PV und Ledipasvir aufheben, ohne die Onkolyse durch H-1PV allein zu beeinflussen. Ich schlage ein vorläufiges Modell vor, bei dem die Kombination von Ledipasvir und H-1PV Komponenten des PI3K/Akt/mTOR-Stoffwechsels moduliert, um die Funktionalität und die onkotoxischen Fähigkeiten des NS1-Proteins von H-1PV zu verbessern, was letztendlich die virale Onkolyse steigert.

Acknowledgements

There are many people I want to thank for their support, help, and guidance over the past four years.

Firstly, to my supervisors, Antonio, and Richard. Antonio, thank you for taking me on as a PhD student and giving me the opportunity to do this work. Thank you for continuing to care about the project and helping me from afar, even while you embarked on a whole new life. Richard, thank you for supporting me right from the start and adopting me into your group. Thank you for helping me to not take everything in life quite so seriously and reminding me to consider what I have achieved, instead of always focussing on what's missing. Joining your lab is one of the best decisions I could have made; thank you for making it possible.

Thank you to my thesis advisers and committee – Ralf Bartenschlager, Dirk Grimm, Moritz Mall, Hrvoje Miletic, Martin Hoogduijn, and Dirk Nettelbeck. Your help and input shaped both of these projects greatly. In particular, thank you to Dirk Grimm for introducing me to the worlds of virology, gene therapy and reprogramming in the first place! To Dirk Nettelbeck – thank you for always including me in everything oncolytic viruses and making me feel welcome, even though I was not in your group. To Martin – thank you for introducing me to Mehrnaz and fostering our collaboration, as well as welcoming me in Rotterdam and inviting me to join your group.

To everyone in both of my labs, past and present – Tiago, Clemens, Annabel, Gayatri, Tiina, Valérie, Toros, Ali, Manu, Julia, Alice, Luisa, Francisca, João, Conny, Patrick, Silvia, and Malte. Thank you for the lunches, coffee chats, Christmas market and summer festival visits and support both inside and out of the lab. A good lab environment makes such a difference to a PhD experience, and I feel very lucky to have had just that. Special thanks to Annabel, for your cell culture help and lab management, guiding us through the pandemic with nary a tip box lacking. To Luisa, thank you for all the conversations, crazy theories, and surprising results you've talked through with me. Thank you for your patience when I needed to vent and for reading most of my thesis so carefully when you yourself are so busy! Thank you to Valérie and Tiina for your generosity with your time and data to allow me to continue this project. To my two Masters intern students, Toros and Conny – thank you for trusting me to guide you, and your patience with me when I had no more of a clue than you! You two have taught me at least as much as I taught you.

On to the science: Yunhee, thank you for your bioinformatics wizardry and patience when I came to you *yet again* with another request! Catarina, thank you for your advice on autophagy and generosity with reagents when I came to you for help. Jonny, thanks for all of the conversations inside and outside the ATV when we were really both there to work, ranging from qPCRs to figure design. Theresa and Christine, thank you for the discussions and your generosity with data from your studies. Claudia, thank you for your willingness to share your cells with me to make my experiments possible. Assia, Alex and Milena – thank you for all of your help with the PDAC spheroid experiments, and your willingness to try again and again, even at the cost of your own experiments. Jürg – thank you for cheering me on from the sidelines, supporting me and helping me with ideas, and for always having an open door when I had questions. Thanks also to Aubry Miller for your advice on the CETSA assay, and to Oli Heil for your help with Chipster. Thank you as well to all the people working behind-the-scenes to even make this possible – particularly the kitchen staff of ATV 2nd floor east. Without your hard work, ours would ground to a halt! Cheers to Kai, who was always a friendly face when coming in to work or leaving late. And finally, to Mehrnaz, Lieke and Tracy – thank you for welcoming me with open arms in Rotterdam, dealing with my incessant questions and sharing protocols, space, and reagents with me. You really made me feel at home!

Of course, I have to thank my friends for keeping me sane and cheering me on in the last four years. To my best friend, Sammy – these few years have been tumultuous to say the least, but I'm so grateful to know that I always have you in my corner and I'm sure we have both come out the other side stronger. To my friends from Adelaide – Isaac, Vanessa, and Lauren – thank you for always picking up where we left off even though I am home so seldomly. I am lucky to still be in touch with many people from my Masters studies: Anne, Pavle, Marghi, Jonas (Koeppel and Becker!), Dani, and Cindy. I always enjoy catching up with each of you; thank you for your support and ideas whenever we do. To my wonderful PhD friends: Yunhee, Simay, Cansu, Paul, Flávio, and Aga. It has been a privilege to go on this journey with you; thank you for the commiserations, the celebrations, the pandemic-era all day bike rides and Zoom calls, and later the dinners running late into the night. To Mo – thank you for all your encouragement, and the many late-night Chinese dinners in the lab! And of course, thank you to my wonderful new friends from Rotterdam: Steven, Camilla, and Amanda. You made me feel so welcome and I am very grateful to have met you!

To my friends at the Musikfreunde Heidelberg, especially Selma, Stephanie, Sebastian, Heidrun, Annika, Stefan(s), Margaret, Matthias, Colin, Bastian, Ralf, Uta, and Rebecca. Tuesday evenings were my escape from the ups and downs of the lab, and I couldn't think of anything better. Thank you for welcoming me with open arms and making me feel like I belong, even though I still can't remember which note is H and which note is B! Thank you also to Renè for pouring your heart and soul into the orchestra to make it possible.

Suchira – I have no words to express how grateful I am to you. Thank you for pouring hours and hours into my projects, the marathon data discussions, sometimes into the small hours of the morning. Thank you for looking after me when I couldn't do it myself, for coaching me through the failures and celebrating the wins with me. This thesis would not be what it is without your guidance and support, both scientifically and personally. Thank you.

And finally, to my family – Daniel, Esther, and David. You raised me to be curious, to be confident in my abilities, and to persevere. Without this I would never have managed this work. Thank you for coming to look after me in particularly stressful periods of the PhD and talking me through every trial and tribulation. Your support and love have helped me immensely to reach this point, and I am truly grateful.

Declaration of Contributions

Reprogramming work

Experiments	Contributors
Cloning and validating vectors	Alicia Roig-Merino, Anna Hartley, Cornelia Wincek
Reprogramming cells (transfection, maintenance, picking)	Anna Hartley, Cornelia Wincek, Annabel Grewenig
Characterisation of iPSC clones (immunofluorescence, qRT-PCR, trilineage differentiation, CNV analysis)	Mehrnaz Ghazvini, Lieke Dons, Tracy Li, Anna Hartley
PCR for vector retention	Anna Hartley

H-1PV work

Experiments	Contributors
Screening to identify Ledipasvir	Valérie Palissot, Tiina Marttila, Gian Mario Dore, Laurent Brino, Anne Maglott-Roth
Validation screening for Ledipasvir	Valérie Palissot, Tiina Marttila, Gian Mario Dore
Characterisation of Ledipasvir in cell line panel	Valérie Palissot, Tiina Marttila
U373-MG and AsPC-1 cell lines	Valérie Palissot, Tiina Marttila, Anna Hartley
Primary PDAC 2D cell cultures	Anna Hartley
Viral qPCR	Gian Mario Dore, Anna Hartley
Western blots for viral proteins	Anna Hartley, Toros Taşgın
HeLa/HEK-NS1 experiments, including CETSA	Anna Hartley, Toros Taşgın
Cell Painting	Laurent Brino, Zahra Hanifehlou
PamGene kinase profiling	Valérie Palissot, Tiina Marttila, Anna Hartley, PamGene
RNA sequencing	Valérie Palissot, Tiina Marttila, Gian Mario Dore, Anna Hartley, Yunhee Jeong
Inhibitor treatments	Anna Hartley

Publications and Awards

Publications arising from this work

Hartley, A.*, Kavishwar, G.*, Salvato, I., and Marchini, A., 2020. **A Roadmap for the Success of Oncolytic Parvovirus-Based Anticancer Therapies**, Annu Rev Virol, 7: 537-57. https://doi.org/10.1146/annurev-virology-012220-023606

Hartley, A., Wincek, C., Urban, M., Roig-Merino, A., Burger, L., Taşgın, T., Grewenig, A., Ghazvini, M., Dons, L., Li, T., Hoogduijn, M., Harbottle, R., 2024. **Safe and simple generation of human iPSCs using S/MAR DNA Vectors**, Genes, manuscript submitted.

Hartley, A., Wincek, C., Urban, M., Roig-Merino, A., Burger, L., Taşgın, T., Grewenig, A., Ghazvini, M., Dons, L., Li, T., Hoogduijn, M., Harbottle, R., 2024. **Safe and simple generation of human iPSCs using S/MAR DNA Vectors**, Genes, manuscript in preparation.

Schäfer, T., Knol, L., Haas, F., **Hartley, A.**, Pernickel, S., Jády, A., Finkbeiner, M., Achberger, J., Arelaki, S., Modic, Ž., Schröer, K., Zhang, W., Schmidt, B., Schuster, P., Haferkamp, S., Doerner, J., Gebauer, F., Ackermann, M., Kvasnicka, HM., Kulkarni, A., Bots, S., Kemp, V., Poetsch, A., Hoeben, R., Erhardt, A., Marchini, A., Ungerechts, G., Ball, C., Engeland, C., 2024. **Biomarker Screen for Efficacy of Oncolytic Virotherapy in Patient-derived Pancreatic Cancer Cultures**, EBioMedicine, manuscript in revision.

Presentations associated with the work in this thesis

Hartley, A., Palissot, V., Marttila, T., Taşgın, T., Jeanty, C., Dore, GM., Brino, L., Maglott-Roth, A., Harbottle, R., Marchini, A., 2022. **Identification of an Antiviral Drug as a Novel Potentiator of H-1PV-Mediated Oncolysis**. 25th Annual meeting American Society of Gene and Cell Therapy, poster presentation.

Hartley, A., Palissot, V., Marttila, T., Taşgın, T., Jeanty, C., Dore, GM., Brino, L., Maglott-Roth, A., Harbottle, R., Marchini, A., 2022. **Identification of an Antiviral Drug as a Novel Potentiator of H-1PV-Mediated Oncolysis**. 15th International PhD Student Cancer Conference, poster presentation.

Hartley, A., Palissot, V., Marttila, T., Taşgın, T., Jeanty, C., Dore, GM., Brino, L., Maglott-Roth, A., Harbottle, R., Marchini, A., 2022. **Identification of an Antiviral Drug as a Novel Potentiator of H-1PV-Mediated Oncolysis**. XVIII International Parvovirus Workshop, short talk.

Hartley, A., Du, Z., Urban, M., Roig-Merino, A., Peterson, J., Ghazvini, M., Hoogduijn, M., Harbottle, R., 2023. **Generation And Persistent Genetic Modification Of Virus- And Factor-Free Human iPSCs Into Kidney Organoids Using S/MAR DNA Vectors**. 26th Annual meeting American Society of Gene and Cell Therapy, poster presentation.

Hartley, A., Burger, L., Taşgın, T., Urban, M., Roig-Merino, A., Peterson, J., Ghazvini, M., Harbottle, R., 2023. **Generation And Persistent Genetic Modification Of Virus- And Factor-Free Human iPSCs For Cell-Based Cancer Therapies**. 16th International PhD Student Cancer Conference, short talk.

Awards

DKFZ International PhD Program PhD position, November 2019 – November 2022.

Outstanding Poster Award, 25th Annual meeting American Society of Gene and Cell Therapy, 2022.

Outstanding Poster Award, 26th Annual meeting American Society of Gene and Cell Therapy, 2023.

Runner-up Short Talk Prize, 16th International PhD Student Cancer Conference, 2023.

Short term research fellowship award, DKFZ, August 2023.

Table of Contents

List of Abbreviations

2A	Self-cleaving peptide
4E-BP1	eIF4E-Binding Protein 1
A549	Lung adenocarcinoma cell line
AAV	Adeno-Associated Virus
AdV	Adenovirus
AI	Artificial Intelligence
AKT	Ak Strain Transforming
ANOVA	Analysis of Variance
AP	Alkaline Phosphatase
APAR	Autonomous Parvovirus-Associated Replication
AsPC-1	PDAC cell line
ATF	Activating Transcription Factor
ATM	Ataxia Telangiectasia Mutated kinase
ATP	Adenosine Triphosphate
BBB	Blood-Brain-Barrier
BCA	Bicinchoninic acid
Bcl2	B-cell lymphoma 2
BH3	Bcl2 Homology Domain 3
bp	Base pairs
BSA	Bovine Serum Albumin
BxPC-3	PDAC cell line
CAG	Cytomegalovirus-Actin-Globin Promoter (Synthetic Promoter)
Caki-1	Renal clear cell adenocarcinoma cell line
CAR	Chimeric Antigen Receptor
CD	Cluster of Differentiation
CDK9	Cyclin-Dependent Kinase 9
cDNA	complementary DNA
CEA	Carcinoembryonic Antigen
CETSA	Cellular Thermal Shift Assay
cGAS-STING	cyclic GMP–AMP Synthase - Stimulator of Interferon Genes
cGMP	current Good Manufacturing Practice
CKIIα	Casein Kinase II alpha
CMV	Cytomegalovirus
CNV	Copy Number Variant
COPII	Coat Protein Complex II
CPE	Cytopathic Effect
CpG	Cytosine-Guanine dinucleotide
CREB	cAMP Response Element-Binding Protein
CRM1	Chromosomal Region Maintenance 1

CSCN	Cancer Stem Cell medium
CTLA-4	Cytotoxic T Lymphocyte Associated Protein-4
DAMPs	Damage-Associated Molecular Patterns
DAPI	4′,6-diamidino-2-phenylindole
DC	Dendritic Cell
DMEM	Dulbecco's Modified Eagle's Medium
DMSO	Dimethyl Sulfoxide
DMVs	Double Membrane Vesicles
DNA	Deoxyribonucleic Acid
dNTP	Deoxynucleotide Triphosphate
DU145	Prostate cancer cell line
EBNA-1	Epstein Barr Nuclear Antigen 1
EBV	Epstein Barr Virus
ECL	Enhanced Chemiluminescence
ECM	Extracellular Matrix
EDTA	Ethylenediaminetetraacetic Acid
EGFR	Epidermal Growth Factor Receptor
eIF-4E	eukaryotic Initiation Factor 4E
EMA	European Medicines Agency
ER	Endoplasmic Reticulum
ES cell	Embryonic Stem cell
FACS	Fluorescence Activated Cell Sorting
FBS	Foetal Bovine Serum
FDA	Food and Drug Administration
FDR	False Discovery Rate
(b)FGF	(basic) Fibroblast Growth Factor
FKBP12	FK506-Binding Protein 12
GAP	GTPase Activating Protein
GFP	Green Fluorescent Protein
GM-CSF	Granulocyte Macrophage Colony Stimulating Factor
GMEB	Glucocorticoid Modulatory Element Binding Protein
GSEA	Gene Set Enrichment Analysis
GSK3	Glycogen Synthase Kinase-3
GTPase	Guanosine Triphosphate hydrolysing enzyme
H-1PV	H-1 Parvovirus
HCV	Hepatitis C Virus
HDAC	Histone Deacetylase
HEK-293T	Human Embryonic Kidney 293 cells expressing SV40 virus large T antigen
HEK-NS1	HEK-293T cells with doxycycline-inducible expression of H-1PV NS1 protein
HeLa	Cervical cancer cell line (Henrietta Lacks)

HeLa-NS1	HeLa cells with doxycycline-inducible expression of H-1PV NS1 protein
HEPES	4-(2-hydroxyethyl)-1-piperazineethanesulfonic acid
HLA	Human Leukocyte Antigen
HMGB1	High Mobility Group Box 1
HRP	Horseradish Peroxidase
HSV	Herpes Simplex Virus
HuES	Human Embryonic Stem Cell
ICD	Immunogenic Cell Death
ICP6	Infected Cell Protein 6
IDH1	Isocitrate Dehydrogenase 1
IF	Immunofluorescence
IFN(α2b/β/γ)	Interferon (alpha2b/beta/gamma)
IgG	Immunoglobulin G
IL	Interleukin
IL2RG	Interleukin-2 Receptor Subunit Gamma
iPSC	induced Pluripotent Stem Cell
IRS	Insulin Receptor Substrate
JNK	Jun N-terminal Kinase
kb	Kilobase pairs
kDa	Kilodaltons
KEGG	Kyoto Encyclopedia of Genes and Genomes
LB	Luria Broth
LDH	Lactate Dehydrogenase
LDV	Ledipasvir
LIF	Leukaemia Inhibitory Factor
LOH	Loss Of Heterozygosity
MAPK	Mitogen-Activated Protein Kinase
MEK	MAPK Kinase
MEM	Minimal Essential Medium
mESC	mouse Embryonic Stem Cells
MMP	Matrix Metalloproteinase
MOI	Multiplicity Of Infection
mRNA	messenger RNA
mTOR	mammalian Target Of Rapamycin
mTORC1/2	mTOR Complex 1/2
MV	Measles Virus
MVM	Minute Virus of Mice
NAD	Nicotinamide Adenine Dinucleotide
NCAM	Neural Cell Adhesion Molecule
NDV	Newcastle Disease Virus
NEAA	Non-essential Amino Acids
NHDF	Neonatal Human Dermal Fibroblasts

NK cells	Natural Killer cells
NS 1/2/3/5A/5B	Non-Structural genes/proteins 1/2/3/5A/5B
NSC	Neural Stem Cell
OKSM(L)	Oct3/4, Klf4, Sox2, c/L-Myc, (Lin28), or Yamanaka factors
ORC	Origin Replication Complex
OV	Oncolytic Virus
p70S6K	ribosomal protein S6 Kinase beta-1
Panc-1	PDAC cell line
PAMPs	Pathogen-Associated Molecular Patterns
(D)PBS	(Dulbecco's) Phosphate-Buffered Saline
PC3	Prostate cancer cell line
PC03	PDAC PDX culture, also called HD2205
PC06	PDAC PDX culture, also called HD4435
PC09	PDAC PDX culture, also called HIPO48
PC20	PDAC PDX culture, also called HD5015
PC31	PDAC PDX culture, also called FC14238656
PCA	Principle Component Analysis
PCNA	Proliferating Cell Nuclear Antigen
PCR	Polymerase Chain Reaction
PD-1	Programmed Cell Death Protein-1
PD-L1	Programmed Death-Ligand 1
PDAC	Pancreatic Ductal Adenocarcinoma
PDK1	Phosphoinositide-Dependent Kinase 1
PDX	Patient-Derived Xenograft
PFU	Plaque Forming Units
PI3K	Phosphoinositide 3 Kinase
PIP_2	Phosphatidylinositol (3,4)-Bisphosphate
PIP_3	Phosphatidylinositol (3,4,5)-Trisphosphate
PKC	Protein Kinase C
PKR	Protein Kinase R
PLA2	Phospholipase 2
polyI:C	Polyinosinic:polycytidylic acid
PTEN	phosphatase and tensin homolog
PTK	Phosphotyrosine Kinase
PVDF	Polyvinylidene Difluoride
q(RT)-PCR	quantitative (Reverse-Transcription) Polymerase Chain Reaction
Rheb	Ras Homolog Enriched in Brain
RIG-I	Retinoic acid-Inducible Gene I
RISC	RNA-Induced Silencing Complex
RMA	Robust Multichip Average
RNA	Ribonucleic Acid
ROCK	Rho-Associated Protein Kinase

ROCKi	Rho-Associated Protein Kinase inhibitor
ROS	Reactive Oxygen Species
RPA	Replication Protein A
RPMI (1640)	Roswell Park Memorial Institute medium
RPS6	Ribosomal Protein S6
S6K	Rps6 Kinase
SAF-A	Scaffold Attachment Factor A
SAT protein	Short Alternatively Translated Protein
SATB1	Special AT-Rich Sequence Binding Protein 1
SDS-PAGE	Sodium Dodecyl Sulphate - Polyacrylamide Gel Electrophoresis
SeV	Sendai Virus
SFFV	Spleen Focus-Forming Virus
SGK	Serum- and Glucocorticoid-induced protein Kinase
SMAD4	Mothers Against Decapentaplegic Homolog 4
S/MAR	Scaffold/Matrix Attachment Region
SMAR	Vector containing an S/MAR
SNB-19	Glioma cell line
SOC	Super Optimal broth with Catabolite repression
SSEA-1/4	Stage Specific Embryonic Antigen 1/4
STK	Serine/Threonine Kinase
SV40	Simian Virus 40
T-Vec	Talimogene laherparepvec
TBS	Tris-Buffered Saline
TGFβ	Transforming Growth Factor beta
TLR	Toll-Like Receptor
TME	Tumour Microenvironment
TNF	Tumour Necrosis Factor
TRAIL	TNF-Related Apoptosis-Inducing Ligand
TSC 1/2	Tuberous Sclerosis Complex 1/ 2
TUDCA	Tauroursodeoxycholic Acid
U251	Glioma cell line
U373-MG	Glioma cell line
UKA	Upstream Kinase Analysis
ULK1	Unc 51-Like autophagy activating Kinase 1
UMAP	Uniform Manifold Approximation and Projection
VEGF	Vascular Endothelial Growth Factor
VEGFR	VEGF Receptor
VP 1/2/3	Viral Particle genes/proteins 1/2/3
VPA	Valproic Acid
VSV	Vesicular Stomatitis Virus
VV	Vaccinia Virus
WB	Western Blot

List of Figures

Figures

List of Tables

Chapter 1: Reprogramming human cells using SMAR vectors

1 Introduction

1.1 Overview

In this work, I aimed to establish the reprogramming of human somatic cells using episomal DNA vectors without the aid of viral components. Reprogramming is a hugely useful tool in clinical testing and potentially also patient treatment; however many concerns remain about the safety of induced pluripotent stem cells (iPSCs) for clinical application. The removal of viral components from the reprogramming process should improve the quality of iPSCs generated, improving their safety and applicability in the clinic.

1.2 Reprogramming

1.2.1 Stem cells

Stem cells are undifferentiated cells capable of producing somatic cells in the body. Stemness is defined by an unlimited capacity for self-renewal, as well as the potential to differentiate into more specialised somatic cell types. There is a distinction between stem cells of different potency: totipotent stem cells are those capable of generating all cell types in the body. These are the first few cells of an embryo, also known as 2C cells. They are capable of generating cells of both embryonic and extraembryonic lineages and occur only very early in embryonic development [1]. Pluripotent stem cells are only able to differentiate into cells of embryonic lineages – endoderm, mesoderm, and ectoderm – and if derived from the inner cell mass of the blastocyst, are termed embryonic stem (ES) cells. Later in development, multipotent and even unipotent stem cells also occur, capable of generating only a few or one cell type, respectively. Such stem cells can occur within adult tissues, to replenish the cells of that tissue type, such as in the haematopoietic system. These tissue-specific stem cells can produce progenitor cells, which are no longer considered stem cells as they have lost their unlimited self-renewal capacity. In general, stem cells undergo asymmetric division, producing one copy of the original stem cell, and one daughter cell with reduced potency, which continues to produce progenitor cells until the lineage ends in fully differentiated somatic cells.

1.2.2 Cellular reprogramming

Early in stem cell research, it was accepted that the asymmetric division of stem cells to produce more differentiated daughter cells was a one-way process. This is exemplified by the epigenetic landscape proposed by Conrad Waddington in 1957 [2], in which a cell is depicted as a marble rolling down a landscape with several local minima, or differentiation possibilities (Figure 1). However, studies by John Gurdon showed that direct injection of nuclei from fully differentiated adult cells into enucleated oocytes can produce phenotypically normal frogs [3]. Thus, the

genetic information present in each nucleated somatic cell is sufficient for pluripotency. This paved the way for landmark studies by Takahashi and Yamanaka, showing that the differentiation of murine and human somatic cells can be reversed, and that these cells can return to an embryonic-like state by retroviral-mediated gene transfer, a process they named "reprogramming" [4; 5]. Astonishingly, this was achieved with the expression of only four defined transcription factors: Oct3/4, also known as POU5F1, Klf4, Sox2, and c-Myc, known today as OKSM or Yamanaka factors. Due to the immense clinical and research potential of these cells, termed induced pluripotent stem cells (iPSCs), Gurdon and Yamanaka shared the 2012 Nobel Prize in Medicine. In the years since their discoveries, the method of reprogramming has been greatly expanded upon.

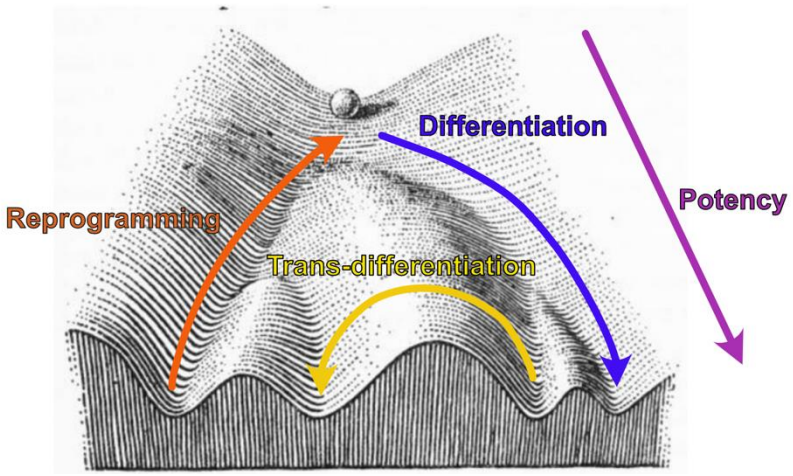

Figure 1. Waddington's epigenetic landscape. Diagram depicts a marble rolling down a landscape, with several local minima emerging as it rolls. The marble represents a pluripotent stem cell, and the landscape its potency (magenta arrow). The downward path (blue arrow) represents differentiation - the stem cell loses potency as it differentiates into committed daughter cells. Reprogramming (orange arrow) involves restoring potency to a differentiated cell allowing it to move back up the landscape and become pluripotent once more. Trans-differentiation, or direct reprogramming (yellow arrow), involves the direct conversion of one cell type to another without an intermediary pluripotent state. Figure modified from Waddington [2].

1.2.3 Methods for reprogramming

Takahashi and Yamanaka initially delivered the reprogramming factors to cells by retroviral-mediated gene transfer [4]. However, even at this earliest of stages, it was clear that retroviral gene transfer carries a large oncogenic risk due to insertional mutagenesis. Thus, this method has since undergone substantial development, to reduce this tumourigenic risk and advance iPSCs closer to clinical applications (Figure 2A). Retroviral vectors were quickly succeeded by lentiviral vectors due to their favourable safety profile and improved efficiency [6; 7]. Lentiviral vectors remain a popular means of Yamanaka factor expression today. Other viral vectors such as adeno-associated viruses (AAVs) have also been applied in reprogramming [8], however these also still carry the potential for

integration [9], particularly when genome editing is applied simultaneously [10]. The RNA Sendai virus (SeV) is a popular vector for reprogramming, used as a non-transmissible form of SeV for delivery of reprogramming factors without integration and available as a ready-to-use kit [11].

Viral vectors are to date the most common reprogramming methods, as they offer easy of delivery of the reprogramming factors to cells. Nonetheless, nonviral delivery of reprogramming factors has also been explored to address safety concerns. Direct delivery of messenger RNA (mRNA) proved effective in reprogramming human fibroblasts after daily transfection (minimum five transfections) [12; 13], as well as delivery of proteins extracted from ES cells in murine cardiac and skin fibroblasts [14]. Delivery of proteins to the cytoplasm of cells is technically challenging and stressful to cells, so the Yamanaka factors have also been fused with cell-penetrating peptides for cellular delivery. This led to successful synthetic protein-based reprogramming of both human and mouse cells in 2009 [15]. Small molecules have even been used successfully to reprogram human cells *in vitro* [16].

Finally, cellular reprogramming has also been achieved using non-viral DNA-mediated delivery of reprogramming factors. Transposons, which are mobile genetic elements, have been used to generate iPSCs of various species. They can be integrated into host genomes by a transposase enzyme, and an advantage over retroviral transfer is that integration-deficient transposases can also be used to re-excise the transposon out of the genome after completion of reprogramming [17]. However, as with retroviruses, this requirement for integration into the genome for functional gene expression causes concern over genomic integrity. The Yamanaka group has worked extensively with plasmid-based reprogramming, firstly establishing multi-transfection protocols with traditional plasmids [18; 19]. These protocols were however laborious, as the expression of the reprogramming factors does not persist for long enough to establish fully reprogrammed cells without repeated transfection. A refinement of this strategy came from the Thomson group in the form of so-called episomal vectors, incorporating the oriP/*EBNA-1* (Epstein Barr Nuclear Antigen 1) genes from Epstein Barr Virus (EBV) [20]. Episomal vectors are non-viral circular DNA vectors, which are capable of self-replication using host cell machinery without integration into the genome. Once again, the Yamanaka group further developed this strategy by incorporating knockdown of p53 and exchanging c-Myc for L-Myc to improve reprogramming efficiency while reducing the oncogenic potential of Myc overexpression [21; 22]. These vectors are commonly known as EBNA vectors and have become one of the most widely used methods for reprogramming. Indeed, there are to date two registered clinical trials in phase III using iPSC-derived cellular therapies, both of which use allogeneic iPSCs reprogrammed using the EBNA vector system [23-25]. There are also advances in reprogramming using synthetic DNA, such as

doggybone DNA (dbDNA), to generate iPSCs [26]. Doggybone vectors are linear, double-stranded DNA with closed ends which were used to generate iPSCs at a similar efficiency to EBNA vectors, which showed improved pluripotency and genomic stability compared with EBNA iPSCs.

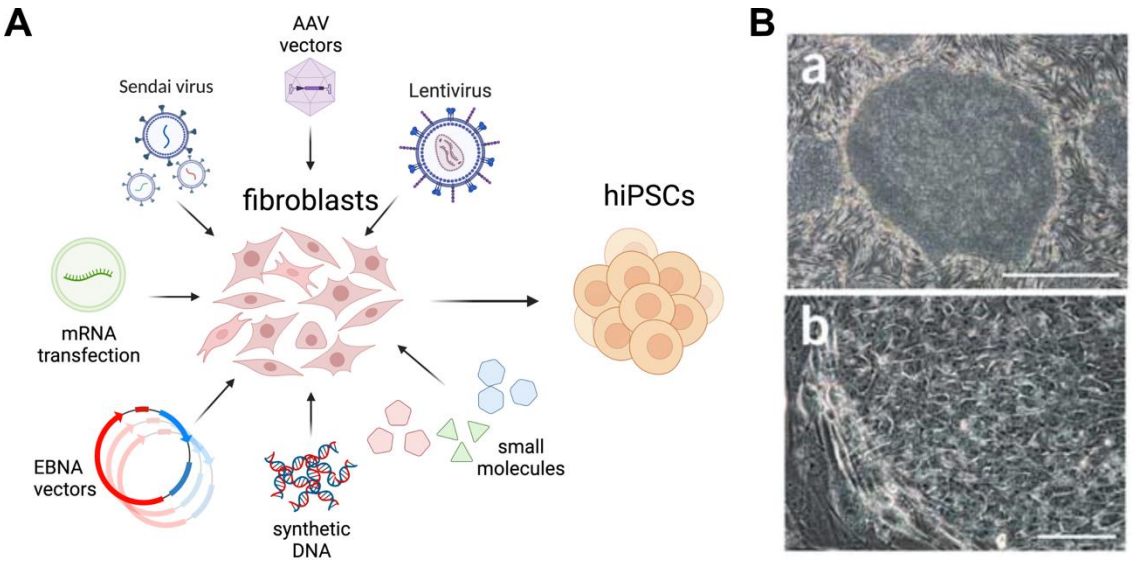

Figure 2. Generation of iPSCs and their characteristics. A Schematic showing different (non-exhaustive) possibilities for generating iPSCs from fibroblast cells. **B** Phenotypic characteristics of iPSCs in brightfield microscopy, exemplifying the round, shiny-bordered colony morphology and no clear borders between cells as compared to bordering fibroblasts (a), and large nuclei with little cytoplasm (b). Scale = 1mm (a), 100µm (b). Figure A generated using BioRender, figures in B reproduced from Okita, Matsumura et al. [21].

1.2.4 Transdifferentiation

Another major advance in cellular reprogramming came with the advent of trans-differentiation, or direct reprogramming. Here, differentiated cells are directly converted into different lineages without an intermediate pluripotent state (Figure 1). In this case, the factors required for transdifferentiation depend on the desired cell type. Typically, these factors are transcription factors or non-coding RNAs which are involved in defining the cell type of interest. The first example of this was found in mouse embryonic fibroblasts, which could be converted directly into myoblasts by overexpression of the transcription factor MyoD *in vitro* [27]. Although these two cell types originate from the same embryonic lineage, later studies expanded this principle to transdifferentiate cells between lineages as well [28; 29]. Transdifferentiation is particularly interesting, as it offers the possibility of *in situ* reprogramming for regenerative therapies without some of the drawbacks of pluripotency, discussed below. However, safe *in vivo* delivery of factors and robust efficiencies of transdifferentiation remain major clinical barriers for this field [28]. Importantly, a vector system capable of reprogramming cells into iPSCs should also be capable of transdifferentiation, simply by altering the factors expressed.

1.2.5 Applications for iPSCs

iPSCs can in principle be utilised in any situation where ES cells would be beneficial while bypassing the ethical concerns surrounding the use of ES cells, particularly in humans. Given their unlimited growth capacity, iPSCs are an ideal basis cell type for off-the-shelf cell therapies. Moreover, reprogramming also offers new possibilities that even ES cells do not; namely, a patient's own cells can now be reprogrammed and used for patient-specific disease models or drug testing. In addition, autologous therapies are now feasible, if not yet clinically applied. Lost or damaged tissue can in theory be replaced by autologous cells through reprogramming and directed differentiation. As well as direct replacement of tissue, genetic defects can be corrected in iPSCs *in vitro*, and the patient's own corrected cells can be reintroduced to minimise immune response. In fact, the first person ever treated with iPSC-derived cell therapy in 2014 was a Japanese woman with age-related macular degeneration. A skin biopsy was taken from the patient, from which fibroblasts were reprogrammed into iPSCs and differentiated into retinal pigment epithelium cells. A sheet of these retinal pigment epithelium cells was transplanted back into the patient's eye, and her vision stabilised and remained stable up to four years later [30; 31]

As of early 2021, there are approximately 81 ongoing clinical trials involving iPSCs [32]. Of these, most nontherapeutic trials are based in the United States, such as disease modelling, drug screening, and creating cell banks. Roughly one quarter of these trials are therapeutic, mostly based in Japan, and mostly using allogeneic iPSCs. This is likely for ease of regulatory approval, as each iPSC line created must be rigorously screened for quality. However, four of these 81 trials are already generating and using autologous iPSCs for cell-based therapies. The most commonly targeted organ for iPSC-based clinical trials is unsurprisingly the circulatory system, given the ease of administration. However, there is much interest in iPSC-based therapies of the nervous and visual systems as well. To date, there are two registered phase III clinical trials testing iPSC-derived cell therapies, both using allogeneic cell products. The first, based in Kyoto, aims to treat Parkinson's disease by the transplantation of iPSC-derived dopaminergic neurons, and has also gained approval to begin trials in the United States [23; 24]. Secondly, an Australian trial targeting osteoarthritis involves the injection of iPSC-derived mesenchymal stem cells, with participant enrolment recently completed [25; 33].

1.2.6 Limitations of current iPSCs

Despite the many advantages of reprogramming, there are some limitations to current iPSC-based therapies. As noted above, the majority of current iPSC-based clinical trials use allogeneic iPSCs [32]. This is because autologous iPSCs for treatment are costly and difficult to generate; not only does this approach take a long time from patient sample to finished product, but the quality of the cell

product must be stringently assayed for every patient. Therefore, there has been a shift in approach to "cloak" allogeneic iPSCs from immune recognition by editing the human leukocyte antigen (HLA) loci [34; 35]. Mismatching of HLA types between donor (iPSC-derived cells) and recipient (patient) can cause rejection of the iPSC-based cell product [36; 37]. While allogeneic iPSC products do need to be closely matched in HLA type to their recipient, editing iPSCs to generate homozygous HLA types is fraught, as this can cause unintended hemizygosity [38]. Other approaches involve building cell banks of naturally homozygous HLA-typed iPSCs to match a majority of the population [21; 39].

In addition to immune compatibility, the tumourigenic potential of iPSC-based therapies is a concern. Indeed, one of the original proofs of pluripotency of iPSCs was their ability to form teratomas *in vivo* [4; 5]. Therefore, any incompletely differentiated cell products derived from iPSCs could pose significant danger to patients. Simultaneously, iPSC-derived cell products must be homogenous with respect to their differentiation and expression patterns to avoid variability in the end product and its effectiveness or safety [40]. The long-term effects of iPSC-based therapies are unknown, as reprogramming is a relatively new technology – as the first patient was treated in 2014, a maximum of 10 years' of follow up data are available to date [30]. Since reprogramming is a stressful process, cells are prone to enter senescence, or if this is blocked by p53 suppression, to genetic aberration [41-43]. This means that it is crucial to ensure the genetic stability of each iPSC line created, adding to the burden of generating autologous treatments by reprogramming. It is therefore of interest to explore reprogramming methods that are scarless, cause the least possible damage.

Many currently established reprogramming methods are either virus-based or retain viral components; lentiviruses, SeV, AAVs, and episomal EBNA vectors being common examples [8; 44]. Lentiviral transduction, although safer than retroviral, still carries the risk of insertional mutagenesis [45]. SeV, as an RNA virus, presents no risk of genomic insertion of its transgenes, however the virus often persists in reprogrammed cells and must be actively removed, causing concerns that iPSCs still harbouring the SeV vectors may not be capable of full differentiation into target cell types [46; 47]. The episomal EBNA vector system employs the *EBNA-1* gene from EBV, which has been implicated in oncogenesis [21; 48; 49]. In addition, infection of cells with viruses or the presence of viral components during the reprogramming process can trigger a low-level immune activation, which persists even in fully reprogrammed cells [26].

1.3 SMAR vectors

1.3.1 Potential of S/MARs for reprogramming

Due to the established risks and drawbacks of viral-based reprogramming, I aimed in this study to improve upon the current reprogramming protocols by removing viral components. It is well established that plasmid-based expression of reprogramming factors does not persist for long enough to establish fully reprogrammed cells without repeated transfection [18]. Indeed, the purpose of the *EBNA-1* gene and oriP region in the EBNA reprogramming vectors is to extend the kinetics of reprogramming factor expression beyond that of a normal plasmid [20]. The EBNA-1 protein binds to the oriP region on each episomal vector, tethering it to the nuclear matrix and facilitating replication of the vector synchronously with the cell cycle [50]. This is highly reminiscent of human Scaffold/Matrix Attachment Regions (S/MARs). S/MARs are human AT-rich DNA sequences involved in chromosomal organisation in the nucleus. They anchor the chromatin to the nuclear matrix, interacting with and defining transcription factories by interactions with transcription factors and structural proteins [51; 52]. In this way, S/MARs are involved in the orchestration of both transcription and genome replication [53]. The inclusion of an S/MAR sequence on a plasmid vector can facilitate episomal retention of the vector, resulting in stable, heritable transgene expression without insertion into the genome (reviewed recently by Kreppel and Hagedorn [50]). Thus, the safety profile of iPSCs for clinical application may be improved by replacing the oriP/*EBNA-1* region in the EBNA reprogramming system, currently the most clinically advanced reprogramming method, with a human S/MAR sequence (Figure 3). These vectors which include genomic S/MAR sequences will henceforth be referred to as SMAR vectors.

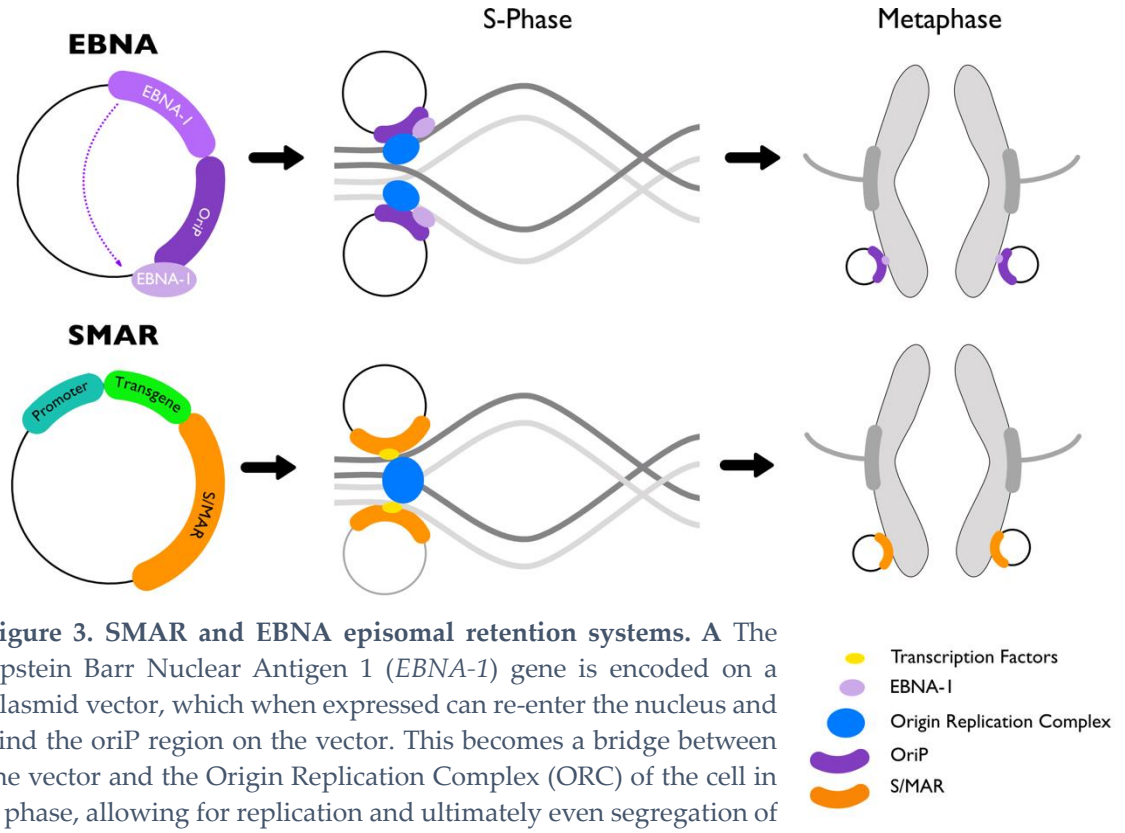

Figure 3. SMAR and EBNA episomal retention systems. A The Epstein Barr Nuclear Antigen 1 (*EBNA-1*) gene is encoded on a plasmid vector, which when expressed can re-enter the nucleus and bind the oriP region on the vector. This becomes a bridge between the vector and the Origin Replication Complex (ORC) of the cell in S phase, allowing for replication and ultimately even segregation of vectors in mitosis. **B** Human Scaffold/Matrix Attachment Region sequences are binding sites for human structural and transcription factors, allowing a vector encoding an S/MAR sequence to tether to the cellular ORC. S/MAR sequences encourage the replication of the vector and ensure even segregation of vector progeny into daughter cells during mitosis. Figure designed by Alicia Roig-Merino [54].

1.3.2 S/MARs: structure and function

S/MAR sequences are present across the human genome, as evolutionary conserved sequences which contribute to the structure and organisation of the genome in 3D space. S/MARs orchestrate both gene transcription and DNA replication through their structure and interaction with proteins in the nucleus. S/MARs are bound by structural proteins such as scaffold attachment factor A (SAF-A) and special AT-rich sequence binding protein 1 (SATB1) [51; 52]. Through these interactions, the genome becomes tethered to the nuclear lamina or matrix within the nuclear membrane, forming chromatin loops in between each S/MAR sequence [55] (Figure 4A).

The partitioning of the genome during interphase by S/MAR sequences defines transcription factories [56]. Importantly, although S/MARs are often found near enhancer elements [57], this chromatin loop structure is cell type specific, defined by protein expression. Differential expression of S/MAR-binding proteins alters the architecture of the chromatin, with alternate tethering of S/MARs to the nuclear matrix allowing for cell type specific transcription programs [51]. S/MAR

sequences can also act as insulators, preventing the spread of epigenetic silencing by DNA methylation [58-60].

In addition to the regulation of gene transcription, S/MAR sequences also facilitate the replication of DNA, and these two functions are heavily interconnected [61]. They are composed of approximately 70% A-T content, so are readily able to unwind, and are capable of doing so stably to reduce torsional strain in the genomic structure [57]. This can then form an easily accessible region for the start of DNA synthesis. An association between S/MAR sequences and topoisomerase II has been reported *in vitro*, also supporting the hypothesis that S/MARs can function as an origin of replication in the human genome. After DNA replication, the interactions of S/MAR sequences with the SAF-A protein aid the even segregation of chromosomes in mitosis [52].

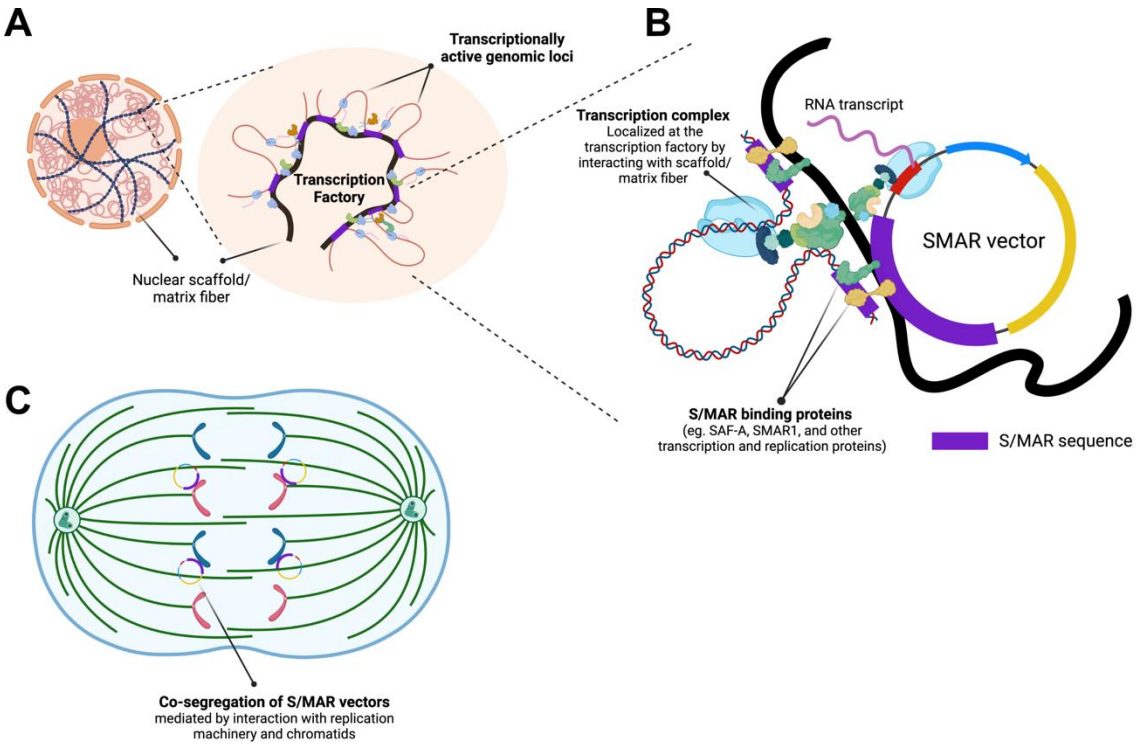

Figure 4. Scaffold Matrix Attachment (S/MAR) regions in their native context and in episomal vectors. A Protein fibers form the nuclear scaffold or matrix structure within the nuclear envelope, providing an anchor point for chromatin, which forms clusters of chromatin loops actively transcribed in foci known as transcription factories. These anchors consist of S/MAR sequences bound to nuclear matrix proteins. **B** The incorporation of an S/MAR sequence on a plasmid vector allows the vector to anchor to the nuclear matrix in the same way as the genome, binding nuclear proteins such as SAF-A. This structure also recruits both transcription and replication machinery to drive expression and replication of the episomal vector. **C** In mitosis, S/MAR sequences allow the replicated episomal vector to co-segregate with chromatids. Figure designed by Toros Taşgın using BioRender.

1.4 Current uses of S/MARs

1.4.1 Generation of SMAR vectors

Due to S/MARs association with chromosomal replication, and partly to study their function, an S/MAR element was first incorporated into a plasmid vector, known as pEPI, in 1999 by Hans Lipps' group [62]. This was the first non-viral plasmid vector to rely solely on human components for its episomal retention and transgene expression. The S/MAR element chosen is found upstream of the human interferon-β gene. In the context of plasmid vectors, S/MAR sequences assist in transcriptional activation, prevention of transgene silencing, and provide mitotic stability to the vector in host cells. pEPI was retained in Chinese hamster ovary cells without genomic integration and could be isolated and re-transformed into bacteria, strongly suggesting episomal maintenance, at low copy number. pEPI associates with the nuclear matrix in the same way as genomic S/MAR sequences (Figure 4B) [52; 63]. The original pEPI was designed with an origin of replication derived from the simian virus 40 (SV40), but it was later found that this was dispensable, as the S/MAR itself is capable of recruiting replication machinery. However, it is crucial that active transcription runs into the S/MAR sequence, as removal or inversion of the promoter leads to genomic integration in the presence of selection [61]. The presence of an S/MAR on a plasmid encourages the formation of replication complexes, although these do not exclusively form on the S/MAR itself [64]. The vector establishes in low copy numbers of about five to ten vector copies per cell [63], and its replication coincides with that of the chromosome – once and only once per cell cycle – together with regions that are replicated early in S phase, which suggests an open chromatin structure as found in or around actively transcribed genes (Figure 4C) [64; 65]. This was confirmed by circular chromosome conformation capture, showing that established pEPI-based replicons localise to actively transcribed regions, and that chromosomal localisation of each vector molecule may be heritable depending on the vector construction [66].

1.4.2 Improving SMAR vectors

In the years since its inception, our group has worked on the development of improved SMAR vectors (Figure 5). Careful selection of tissue-specific promoters allowed for extended persistence of the vector, even allowing gene expression for up to six months after *in vivo* delivery to liver cells [60]. Similarly, a reduction of the immunogenicity of the original plasmid by removal of CpG islands resulted in both higher and more persistent gene expression [67]. This was further reduced by the use of a nanobackbone (Aldevron) in place of a plasmid backbone, reducing the bacterial sequences present in the vector to the minimum, approximately 250 base pairs (bp) [68]. This nanobackbone system also incorporates non-antibiotic vector selection, which is highly advantageous for clinical use [69]. Next, reshuffling of the vector structure by moving the selection marker from the

bacterial backbone into the mammalian expression cassette, next to the transgene, improved the retention of the episome as intended without vector breakage [70]. Bacterial DNA contains unmethylated CpG dinucleotides, which become targets for *de novo* methylation in eukaryotic cells. This methylation is able to spread along the vector, eventually silencing the promoter and transgene [71; 72]. Thus, the addition of insulator sequences between the bacterial backbone and mammalian promoter also improved transgene expression by inhibiting this methylation spread [70]. Splice sites were also added around the S/MAR sequence, as this mimics the maturation of endogenous mRNA, stabilising the mRNA transcript without affecting the episomal maintenance function of the S/MAR [70]. Finally, the use of different S/MAR sequences depending on the target cell type allows for fine-tuning of transgene expression and retention. While the original interferon-beta (IFNβ) S/MAR is approximately 2 kilobase pairs (kb) in size, smaller sequences derived from an S/MAR adjacent to the *APOB* gene can help to reduce the size of the vector while retaining their episomal capacity [68; 70].

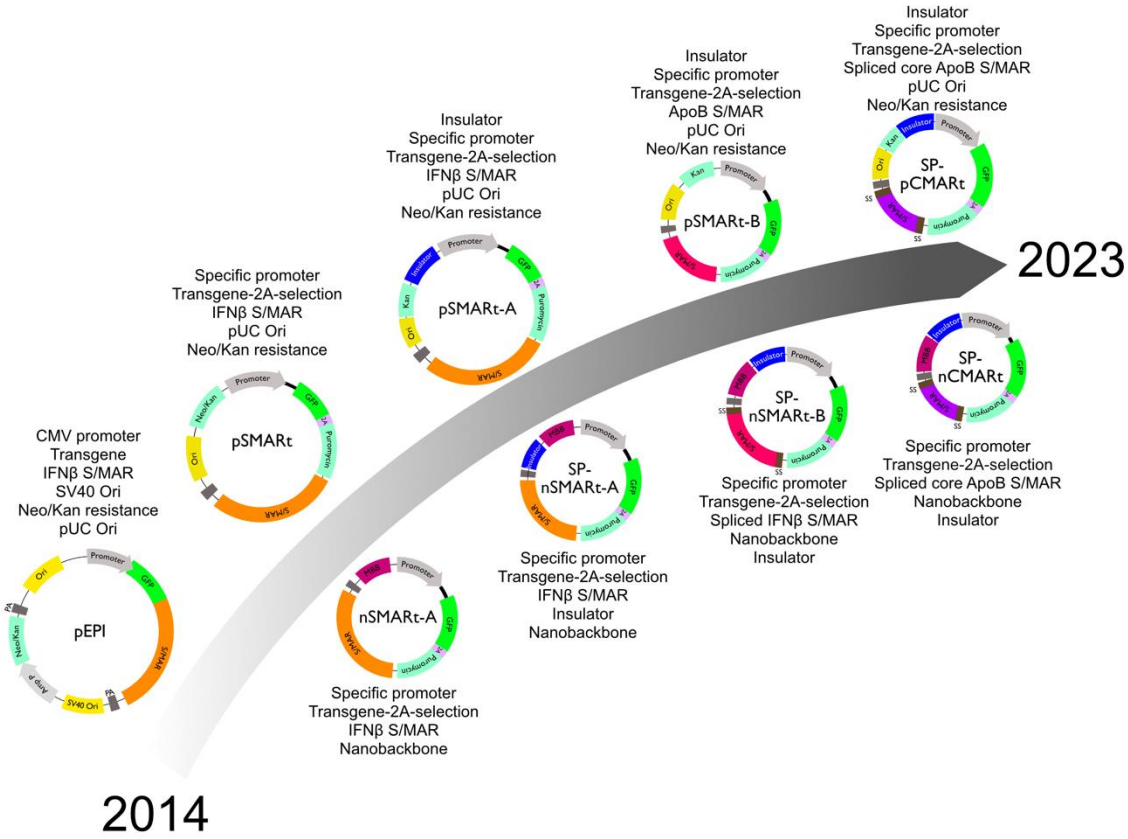

Figure 5. Evolution of SMAR vectors. Schematic overview of the original SMAR vector pEPI (left) and its development over the past nine years. Figure adapted from Alicia Roig-Merino [54].

The modifications and improvements described above have developed SMAR vectors into an exemplary platform for genetic modification. SMAR vectors are efficient and cost-effective to produce, and can be efficiently delivered to cells when optimised [68; 73]. They deliver stable and sustainable transgene expression over long time periods, while not posing any risk of genotoxicity due to their non-

integrative nature. Additionally, they possess no viral elements and only minimal non-human elements, minimising the cellular immune response to the vector. Finally, SMAR vectors have a theoretically unlimited capacity – the largest transgene delivered in an SMAR vector thus far was 135kb [74]. Our group has previously used SMAR vectors to generate chimeric antigen receptor (CAR) – T cells [68]. Vector improvements allowed the efficient transfection of primary T cells, a highly sensitive cell type, with minimal impact on the cell phenotype, and minimal immune response compared with lentiviral transduction. T cells modified with SMAR vectors were at least as efficacious as those transduced with lentiviral constructs expressing the same CAR construct both *in vitro* and *in vivo*. Crucially, due to the ease of manufacturing these vectors, it has now become possible to produce clinical grade CAR T cells at clinically relevant scales in five days.

1.4.3 Using SMAR vectors in human iPSCs

Our group has also previously used optimised SMAR vectors to modify iPSCs (Figure 6). SMARs allow stable transgene expression in human iPSCs over at least 170 days without selection, and with minimal impact on stem cell identity [73; 75]. Importantly for cell banking, this expression is also stable throughout cryopreservation of modified cells. Co-transfection of SMAR vectors carrying green fluorescent protein (GFP) during reprogramming of human fibroblasts using the EBNA vector system resulted in stable GFP-expressing iPSCs, with no effect on pluripotency *in vitro* or *in vivo* in chimera studies. Additionally, stable SMAR-GFP iPSCs could be differentiated into cells corresponding to each germ layer, with minimal loss of transgene expression. These results thus suggest that SMAR vectors can survive the epigenomic reorganisation associated with both reprogramming and differentiation, so these vectors are uniquely resistant to epigenetic silencing. This effect is particularly striking for vectors with the nanobackbone [54].

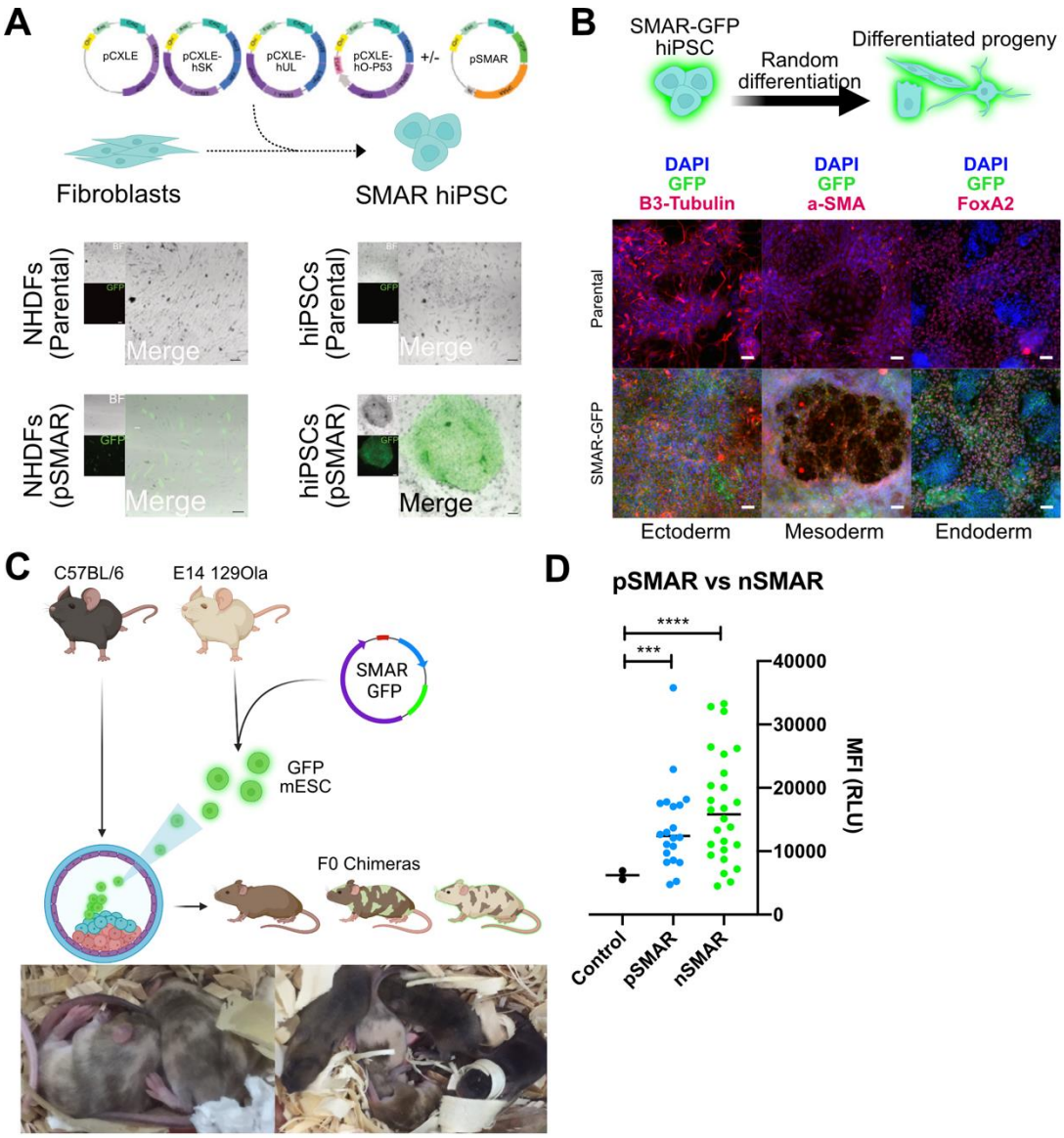

Figure 6. iPSCs can be stably modified using SMAR vectors. A An SMAR vector encoding GFP was co-transfected into neonatal human dermal fibroblasts (NHDFs) together with the EBNA reprogramming system. Fluorescence microscopy shows the retention of GFP signal in pSMAR-modified cells before and after reprogramming. **B** SMAR-GFP modified human iPSCs (hiPSC) were subjected to random differentiation into the three embryonic lineages. Fluorescence microscopy shows the retention of GFP signal (green) together with markers of successful differentiation (red). **C** Mouse embryonic stem cells (mESC) from the129Ola strain (light coat) were modified with an SMAR-GFP vector and microinjected into C57BL/6 embryos (dark coat) to generate chimeric pups. **D** Chimeric pups retained transgenic GFP expression as assessed by ear biopsies (n=49), and GFP expression in nSMAR-modified chimeras was silenced less than pSMAR-modified chimeras. Data published in Roig-Merino, Urban et al. [73]

Given the features of SMAR vectors outlined above, they present a promising alternative to the virus-based EBNA vector system for episomal reprogramming. The optimised SMAR vectors do not contain any viral elements, reducing both the oncogenic risk and the potential for immune activation in the resulting iPSCs. They can sustain transgene expression beyond that of a normal plasmid, which is necessary for reprogramming, without integrating into the genome. Additionally, modification of the resultant iPSCs is possible again using the SMAR vectors, which can survive the differentiation process. Indeed, the most recent work in our group focusses on cellular immunotherapy approaches, generating CAR T and natural killer (NK) cells using SMAR vectors [68]. Therefore, the ultimate goal of this work is to develop an all-in-one vector platform, capable of safely generating and modifying iPSCs for clinical application (Figure 7).

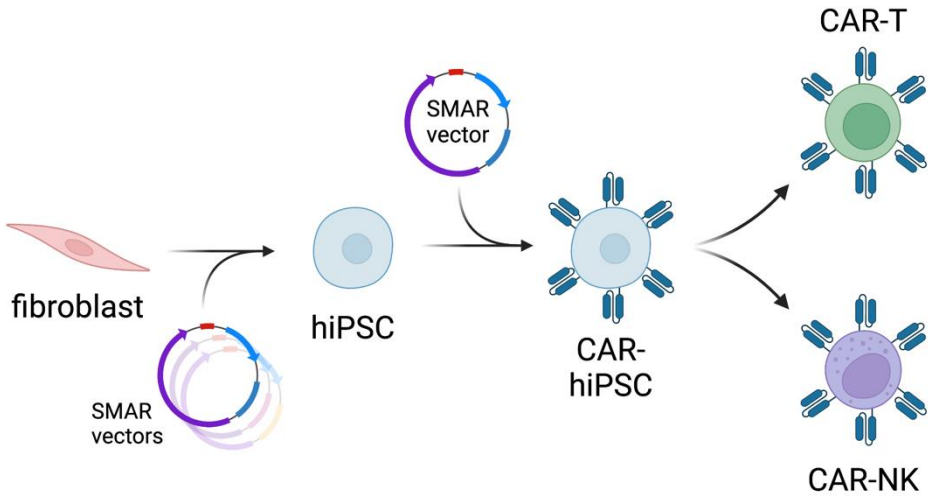

Figure 7. An all-in-one vector platform for the generation and modification of human iPSCs (hiPSCs). Figure generated using BioRender.

2 Results

2.1 Generation of a novel reprogramming platform

To evaluate the potential for SMAR vectors to be used for cellular reprogramming, I used the established four-vector EBNA plasmid series developed by the Yamanaka lab [21] as the current gold standard for episomal reprogramming (Figure 8A). The use of these vectors for feeder-free reprogramming of human somatic cells had already been established in our group by Manuela Urban [75]. Based on these vectors, my colleague Alicia Roig-Merino cloned the SMAR vector series by direct substitution of the oriP/*EBNA-1* region for the IFNβ SMAR on a traditional plasmid background. As SMARs do not rely on protein expression for episomal vector retention, this renders the fourth "EBNA-boost" plasmid (pCXWB-EBNA1) superfluous [76] (Table 1). Therefore, a fourth SMAR vector encoding only GFP and puromycin resistance was generated to allow for monitoring and selection of cells (Figure 8B). Subsequent to the construction of these vectors, our group has implemented the nanovector system (see Section 1.4.2 above) [69] for improved vector performance in mammalian cells. Therefore, I constructed a series of SMAR reprogramming vectors on a nanovector background – the nanoSMAR series (Figure 8C). These also carry the refinement of splice sites flanking the IFNβ SMAR, to stabilise mRNA generated from the vectors [68]. Another vector series made by Alicia, the nano series, comprises each of the reprogramming vectors on a nanovector background without any sequence for episomal retention (Figure 8D). Previous experience in our group suggests that nanovectors express their transgenes at higher levels than plasmid vectors, and it is known that the reprogramming process requires strong, but temporary, expression of ectopic reprogramming factors [77-79]. Therefore, transient expression from nanovectors may be sufficient to reprogram cells while improving the safety profile of the vectors as there is very little chance of vector retention. The potential risks and benefits of reprogramming somatic cells using each vector series are summarised in Table 1.

Figure 8. Vectors used in this study. Schematics of each vector used in this study with representative sizes. **A** EBNA series, designed and generated by the Yamanaka group [21]. EBNA-GFP-p2A-puro is a vector for selection not used in reprogramming and was cloned by Alicia Roig-Merino **B** SMAR series, cloned by Alicia Roig-Merino. SMAR_GFP shP53 is a selection vector not used in reprogramming. **C** nanoSMAR series, cloned in this study. **D** nano series, designed by Alicia Roig-Merino and produced by Nature Technologies.

Table 1. List of reprogramming vector series used in this study and their properties.

	EBNA series	SMAR series	nanoSMAR series	nano series
Bacterial sequences and antibiotic selection	Yes	Yes	No	no
Viral components	Yes	No	No	No
Oncogenic	Potentially	No	No	No
Episomal maintenance	Yes	Yes	Yes	No
Vector size	Large	Medium	Small	Small
Number of vectors needed for reprogramming	Four	Three	Three	Three
Safety profile	Low	Medium	High	Very high
Reprogramming capacity	Yes	Untested	Untested	Untested

2.2 Testing novel reprogramming vectors

I first tested the functionality of the vectors in this study by transfection into HEK-293T cells to assess the expression of each transgene. Each vector was transfected individually, and untransfected cells were used as a negative control. As transfection with the positive control vector pmaxGFP showed expression of the fluorescent reporter gene GFP (Figure 9A), the expression of the reprogramming factors' expression was evaluated by Western blotting. Figure 9B shows that each vector is functional and expresses the expected reprogramming factors. Due to a lack of L-Myc antibody, the expression of this factor could not be assessed. However, expression of Lin28 can be used as an indicator that L-Myc is expressed, as it is transcribed and translated downstream of L-Myc in these vectors.

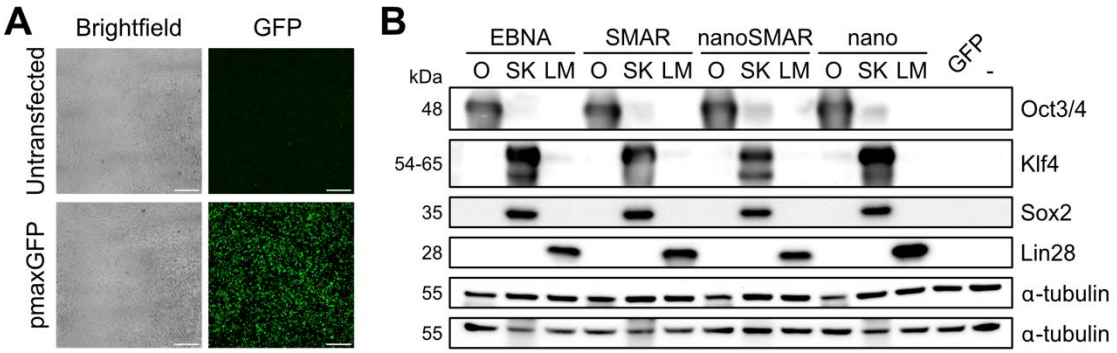

Figure 9. All reprogramming vectors used in this study are functional. A HEK-293T cells were transfected with vectors from the four different reprogramming series and pmaxGFP as a positive control using jetPEI. Cells were imaged 24hpt using a Nikon fluorescence microscope. Cells showed expression of GFP as a proxy of successful transfection. Scale = 500µm. **B** Protein lysates from transfected HEK-293T cells 24hpt were assessed for expression of reprogramming factors Oct3/4, Klf4, Sox2 and Lin28, showing that all reprogramming factors are expressed by each vector series. Experiments were conducted in collaboration with Cornelia Wincek.

Secondly, it was important to establish an accurate method of assessing transfection efficiency in neonatal human dermal fibroblasts (NHDFs), the target cell type for reprogramming in this study. Flow cytometry analysis is considered as the gold standard, as it has the highest sensitivity of those available. However, flow cytometry of NHDFs requires the passaging of cells due to their adherent growth, so this approach precludes the possibility to follow transgene expression over time. To evaluate other methods, NHDFs were transfected with SMAR-GFP resulting in 27% GFP-positive cells after 24 hours, as measured by flow cytometry (Supplementary Figure 1A), which dropped to 3.6% GFP positivity after eight days (Supplementary Figure 1B). In contrast, fluorescent microscopy imaging and automated analysis using an Incucyte instrument (Supplementary Figure 1C) does not require passaging cells and can be done at regular intervals while not disturbing the experiment. A comparison of these two methods, as well as a fluorescent-capable cell counter LUNA, shows that while the Incucyte is not quite as sensitive as flow cytometry, it is able to detect a similar level of GFP expression

(24% vs 27%, Supplementary Figure 1D). In contrast, the LUNA cell counter could only detect the brightest GFP expression, leading to a measurement of 10.4% GFP-positive cells. Therefore, I concluded that Incucyte imaging and analysis of GFP positivity provides an acceptable balance between sensitivity of detection and reduced manipulation of the cells to measure transfection efficiency in future experiments.

2.3 Reprogramming human cells using novel SMAR reprogramming vectors

2.3.1 SMAR vectors can reprogram somatic human cells

After generating and validating the SMAR reprogramming vectors and establishing a method for measuring their transfection efficiency, I moved on to reprogramming somatic NHDFs into iPSCs using these novel vectors. I performed a head-to-head comparison of each vector series (Figure 8), matching the respective conditions as closely as possible to the EBNA-based reprogramming protocol established by Manuela Urban [73; 75]. In this protocol, NHDFs are transfected with 2µg of each vector in the series (either three or four vectors), then expanded and cultured under fibroblast conditions for eight days, after which they are re-plated and cultured under stem cell conditions for another 20-30 days until iPSC colonies form (Figure 10A). A separate transfection of cells with SMAR-GFP allowed quantification of transfection efficiency at 14.4% (Figure 10B), and cells were monitored by microscopy for up to 40 days following transfection. The formation of small colonies was visible by 21 days post transfection in EBNA series transfected cells (Figure 10C), whereas none of the other conditions generated clear colony-like structures with defined borders similar to the colonies shown in Figure 2. However, transfection of NHDFs with SMAR, nanoSMAR, and nano series all caused dramatic changes in cellular morphology and led to the formation of so-called pre-iPSCs by day 40 post transfection, similar to those documented in literature as incompletely reprogrammed cells [80]. While SMAR and nanoSMAR series both produced many such pre-iPSC colonies, the nano series of reprogramming vectors only produced two giant colonies from 90,000 total cells seeded.

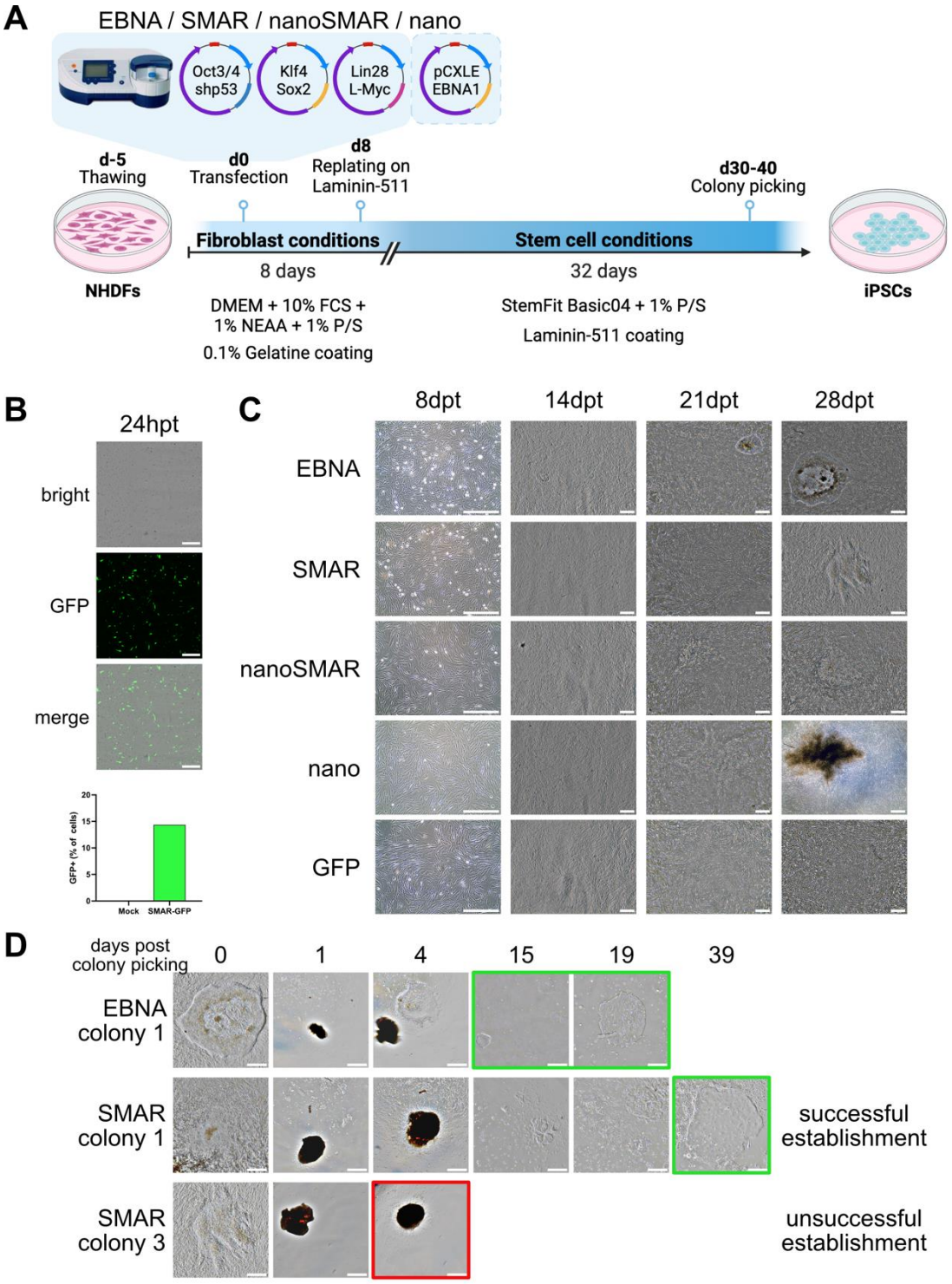

Figure 10. NHDFs can be reprogrammed using SMAR vectors. A Scheme depicting episomal reprogramming by EBNA or (nano)SMAR vectors in neonatal human dermal fibroblasts (NHDFs) as established by Manuela Urban. **B** NHDFs transfected with SMAR-GFP vector were imaged 24 hours post transfection using a Nikon fluorescence microscope and GFP positivity was quantified. Scale = 500µm. **C** Brightfield images taken with an EVOS microscope of iPSC colony formation from the different reprogramming vector series over time. Scale = 500µm. **D** Brightfield images taken with an EVOS microscope following the establishment of iPSC colonies after picking over time. Scale = 500µm. This experiment was done in collaboration with Cornelia Wincek.

As none of the novel vector series produced unequivocal iPSC colonies, the most promising pre-iPSC colonies were picked into fresh plates to evaluate their potential to mature into iPSCs. As shown in Figure 10D, colonies picked from EBNA-transfected cells displayed iPSC morphology within 2 weeks of picking, with colonies of tightly packed cells with shiny, defined edges. The majority of pre-iPSCs rapidly reverted to a fibroblast-like morphology after picking; however, one pre-iPSC colony eventually developed iPSC-like morphology, 40 days after picking, and could be successfully established (Figure 10D, SMAR colony 1). This cell line will henceforth be referred to as SMAR1 iPSCs.

2.3.2 SMAR iPSCs express stemness markers

One of the fundamental processes during reprogramming is a complete restructuring of the epigenome, leading to the expression of marker genes characteristic for stem cells. One such marker traditionally used is alkaline phosphatase (AP), a membrane-bound hydrolase whose expression tends to be much higher in pluripotent stem cells than somatic cells [81]. I stained NHDFs 28 days post transfection with each reprogramming vector series and found only significant AP expression in EBNA series transfected cells (Figure 11A). However, SMAR1 iPSCs also stained positive for AP 60 days post transfection, indicating that these cells continued to mature after picking, and may have developed into *bona fide* iPSCs. Additionally, I examined the expression of the stemness markers Oct3/4, Lin28, Nanog and Tra-160 by immunofluorescence (Figure 11B), only two of which are expressed by the reprogramming vectors themselves. The expression of all four stemness markers was comparable between SMAR1 iPSCs and EBNA iPSCs. Finally, quantitative reverse-transcription polymerase chain reaction (qRT-PCR) on a wider range of marker genes indicated a transcriptional profile very similar to three independent human embryonic stem cell (HuES) lines, and in strong opposition to negative control fibroblast cells (Figure 11C). These results together are a strong indication that SMAR1 iPSCs are indeed stem cells.

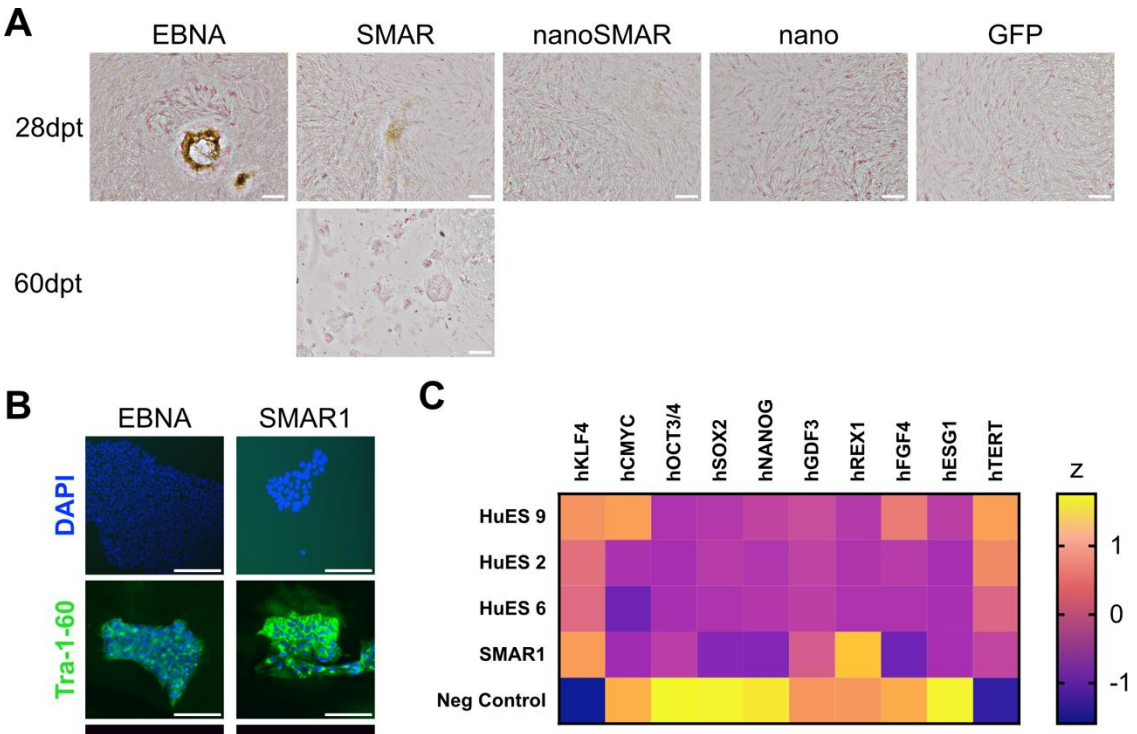

Figure 11. SMAR iPSCs express markers of pluripotency. One colony of SMAR-derived iPSCs (SMAR1) could be established in the first round of reprogramming. **A** SMAR1 iPSCs stained positive for AP, although only 60 days post transfection. Scale = 500µm. **B** SMAR1 iPSCs express pluripotency markers Tra-1-60 (green), Oct3/4 (magenta), Nanog (orange), and Lin28 (yellow) as measured by immunofluorescence. Scale = 200µm, experiments done in collaboration with Toros Taşgın. **C** SMAR1 iPSCs express pluripotency genes as measured by qRT-PCR in a similar pattern to HuES cell lines, and distinctly to fibroblasts (neg control). Data shown is a z-transformation of the fold change of gene expression to the negative control fibroblast line, and was obtained in collaboration with Mehrnaz Ghazvini, Erasmus MC.

2.3.3 SMAR iPSCs are pluripotent

While marker expression and morphology of cell colonies are good indicators of successful reprogramming, the fundamental property of iPSCs is that they are pluripotent; that is, they are capable of differentiation into cells of the three germ layers. Therefore, my collaborators Mehrnaz Ghazvini, Lieke Dons and Tracy Li (Erasmus MC, Rotterdam) subjected SMAR1 iPSCs to trilineage differentiation, together with EBNA iPSCs as a positive control, and stained these cultures for lineage-specific markers Sox17 (endoderm), NCAM (mesoderm), and β-tubulin (ectoderm) (Figure 12A). While SMAR1 iPSCs were not as efficient at differentiation as EBNA iPSCs, a small proportion of cells were positive for each germ layer marker, indicating that there is a sub-population of SMAR1 iPSCs which are truly pluripotent. Additionally, qRT-PCR analysis of differentiated SMAR1 iPSCs indicated similar expression profiles to those of differentiated HuES cell lines (Figure 12B). Thus, these experiments show for the first time that human somatic cells can be reprogrammed into iPSCs using the SMAR vector system.

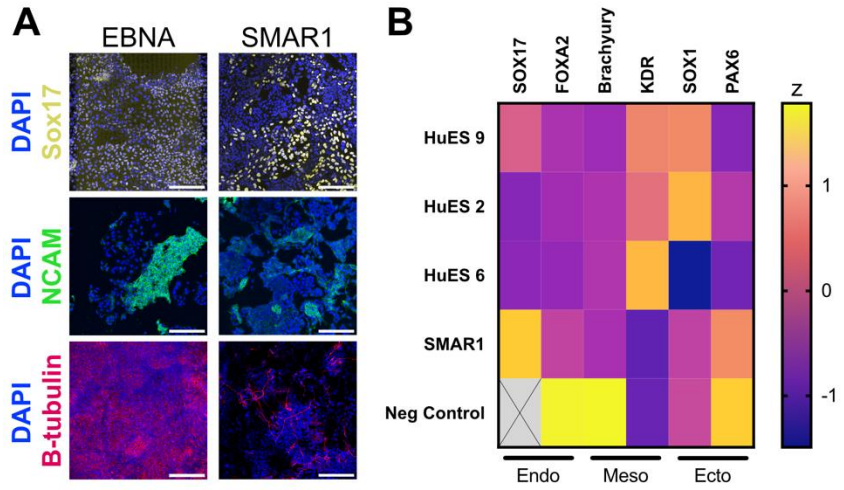

Figure 12. SMAR iPSCs can differentiate into cells of three lineages. SMAR1 iPSCs were subjected to directed trilineage differentiation and then assessed for their capacity to differentiate. **A** Cells derived from SMAR1 iPSCs stain positive for Sox17 (yellow, endoderm), NCAM (green, mesoderm), and B-tubulin (magenta, ectoderm) after directed differentiation into the appropriate lineage as measured by immunofluorescence. Scale = 200μm, EBNA-derived iPSCs are shown for comparison. **B** Cells derived from SMAR1 iPSCs express the appropriate lineage markers as measured by qRT-PCR. Data shown is a z-transformation of the fold change of gene expression to the negative control fibroblast line. All data in this figure was obtained in collaboration with Mehrnaz Ghazvini, Erasmus MC.

2.4 Improving the reprogramming process using novel SMAR reprogramming vectors

2.4.1 Optimisation of transfection in NHDFs

Having proved that SMAR vectors can in principle be used to reprogram human somatic cells, I next optimised the reprogramming protocol to improve the yield of iPSCs generated using SMAR vectors. I decided not to pursue reprogramming using the nano vector series, as this was the condition that showed the least promise in the previous experiments. The transfection efficiency of with a single SMAR-GFP vector could vary from approximately 15-30% (Figure 10B and Supplementary Figure 1D), so I initially focussed on improving this transfection rate. I therefore tested the effect of increased vector mass in the initial transfection, by transfecting NHDFs as previously described, with 2µg (1x), 4µg (2x), or 10µg (5x) of each reprogramming vector (Figure 13A). Separate transfections with both EBNA-GFP and SMAR-GFP vectors controlled for any potential differences in transfection efficiencies between the vector backbones. I quantified GFP expression in these cells both 24 and 48 hours post transfection by Incucyte microscopy (Figure 13B) and saw indeed a slightly higher initial transfection efficiency using the SMAR backbone than the EBNA one. Gratifyingly, a five-fold increase in initial vector mass also resulted in an approximately five-fold increase in transfection efficiency, bringing the transfection rate to almost 50%. However, this boost in transfection also resulted in an initial loss of viability of the cells transfected with the SMAR 5x vector condition (Figure 13C, SMAR5x 7dpt). Cells transfected with the nanoSMAR5x condition did not suffer noticeable toxicity, consistent with observations that the minimal bacterial backbone in nanovectors is less toxic to mammalian cells than traditional plasmids [70; 82]. Cells were monitored during reprogramming, and again the positive control EBNA vector series produced morphological iPSC colonies by day 27 post transfection. In all other conditions, as previously, many clusters of morphological changes and pre-iPSC colonies appeared by this time, most notably in both the SMAR5x and the nanoSMAR5x conditions (Figure 13C).

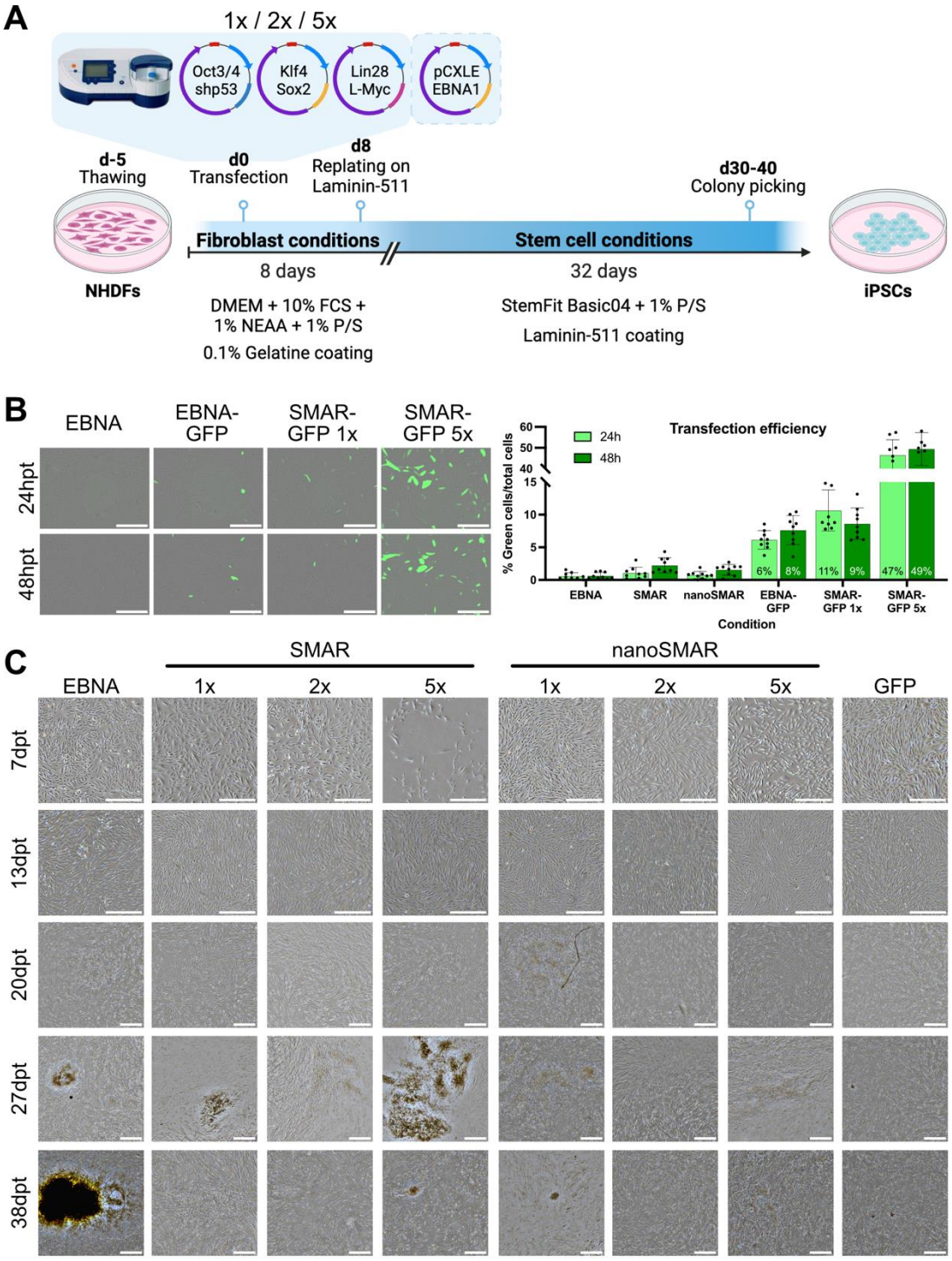

Figure 13. Improving the efficiency of SMAR reprogramming. A Scheme depicting episomal reprogramming by EBNA or (nano)SMAR vectors in neonatal human dermal fibroblasts (NHDFs) as established by Manuela Urban - either 1x, 2x, or 5x the established vector mass was used for transfection. **B** GFP positivity of transfected NHDFs was quantified 24h and 48h post transfection using Incucyte microscopy and software. Scale = 500µm. **C** Brightfield images taken with an EVOS microscope of NHDFs after transfection following the formation of colonies. Scale = 500µm.

To estimate the efficiency of reprogramming with the different vector systems, I fixed and stained cells for AP expression. It is assumed that each iPSC colony derives from a single reprogrammed cell, such that the number of AP-positive colonies can be used to calculate the percentage of successfully reprogrammed cells. AP staining at 31 days post transfection showed a reprogramming efficiency of 0.073% using the EBNA vector series (Figure 14A, right). Conversely, neither SMAR nor nanoSMAR vectors were able to produce AP-positive colonies with the same efficiency in that timeframe. There was a positive correlation between the amount of plasmid transfected (and therefore transfection efficiency) and the reprogramming efficiency, such that SMAR5x gave the highest efficiency at 0.0243%. However, despite an approximately seven-fold higher transfection efficiency in the SMAR5x condition over EBNA (Figure 13B), this is an approximately three-fold lower reprogramming efficiency. This suggests that there are factors other than initial transfection efficiency at play determining the reprogramming efficiency.

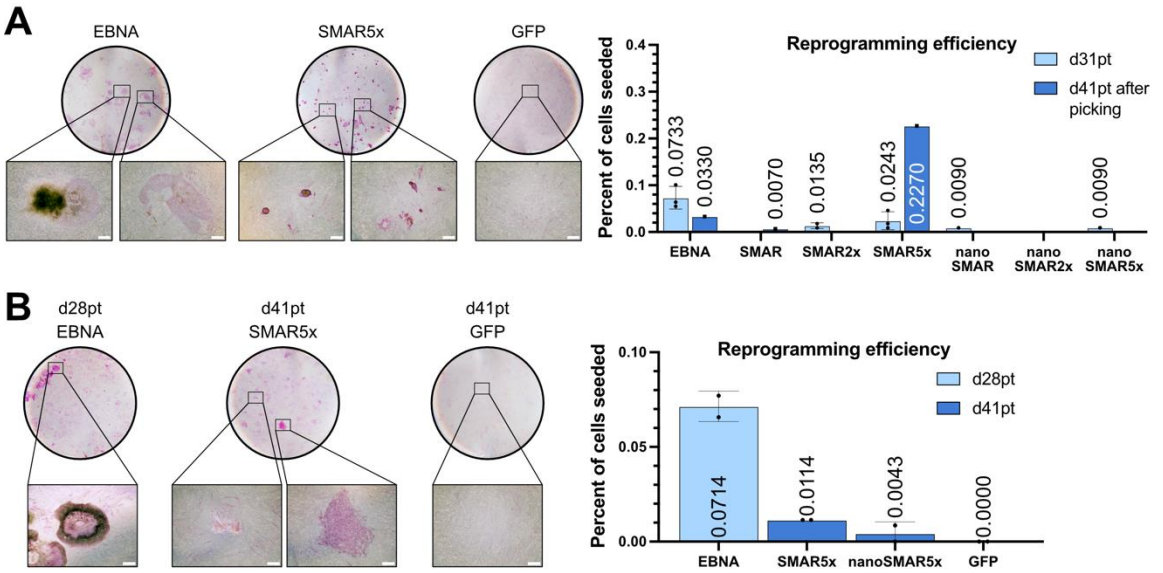

Figure 14. Efficiency of SMAR reprogramming can be improved by increasing transfection efficiency and culture time. NHDFs were transfected with EBNA, SMAR, or nanoSMAR vectors in different amounts and cultured for up to 41 days. Cells were then fixed and stained for alkaline phosphatase (AP). **A** Representative images of AP-stained wells 41 days post transfection, after picking, for EBNA, SMAR5x, and GFP conditions. Reprogramming efficiency of all conditions was calculated by dividing the number of AP-positive colonies by the total cells plated at days 31 or 41 post transfection (right). **B** Cells were reprogrammed as above, and AP staining of EBNA-transfected cells at day 28 post transfection was compared with (nano)SMAR5x transfection at day 41 post transfection. Reprogramming efficiency was quantified as above (right). Scale = 500µm.

NHDFs were also reprogrammed with the optimised protocol for the purpose of establishing iPSC colonies. I therefore cultured these cells for the extended time of up to 41 days, at which time a plethora of small but fully developed iPSC colonies emerged in the SMAR5x condition. To estimate the reprogramming efficiency, I

performed another AP staining at this time. In just 10 days, the efficiency of reprogramming in the SMAR5x condition had increased by nine-fold (Figure 14A, Supplementary Figure 2), and showed a three-fold improvement over EBNA-based reprogramming. It is important to note that the reprogramming efficiency calculated at day 41 post transfection in this experiment is an underestimate, as iPSC clones had already been picked from these plates. However, this experiment suggests that SMAR-based reprogramming of fibroblasts requires a longer timeline than EBNA-based reprogramming. Due to these results, I repeated reprogramming under these conditions, comparing AP staining at day 28 post transfection for EBNA with staining at day 41 post transfection for SMAR5x and nanoSMAR5x conditions. Again, 28 days was sufficient for the formation of mature AP-positive iPSC colonies in the EBNA condition, but cells transfected with SMAR vectors required at least 40 days to show proper colony morphology, with many pre-iPSC colonies also forming (Figure 14B). In this replicate however, the reprogramming efficiency of EBNA outstripped that of SMAR5x by approximately six-fold.

2.4.2 Improved SMAR iPSCs express stemness markers

iPSC colonies generated using the optimised protocol above were picked for further culture. Four EBNA clones were picked, all of which survived, and 10 SMAR5x clones were picked, eight of which survived, and only one of which reverted to a fibroblast-like morphology. I characterised four of the remaining SMAR5x iPSC clones, compared with three EBNA clones. All clones tested showed expression of stemness markers SSEA-1, Nanog, Tra-1-81, and Oct3/4, and all successfully completed directed differentiation into the three germ layers (Figure 15). In fact, some of the SMAR5x iPSC clones showed improved differentiation capacity, particularly into the mesoderm lineage, compared to the EBNA clones tested (Figure 15B, SMAR5x.2, SMAR5x.7). Transcriptional analysis of these cells by qRT-PCR, both before and after directed differentiation, also showed a higher similarity between EBNA- and SMAR5x-derived iPSCs with HuES cells than control fibroblasts, although some variations were present (Figure 16A, C). Principle component analysis of this data showed a tight clustering of the majority of EBNA and SMAR5x iPSC cell lines with HuES cells, with a clear separation of control fibroblasts (Figure 16B, D). Thus, the optimised SMAR reprogramming protocol developed in this study can generate high-quality functional SMAR iPSCs at practical efficiencies.

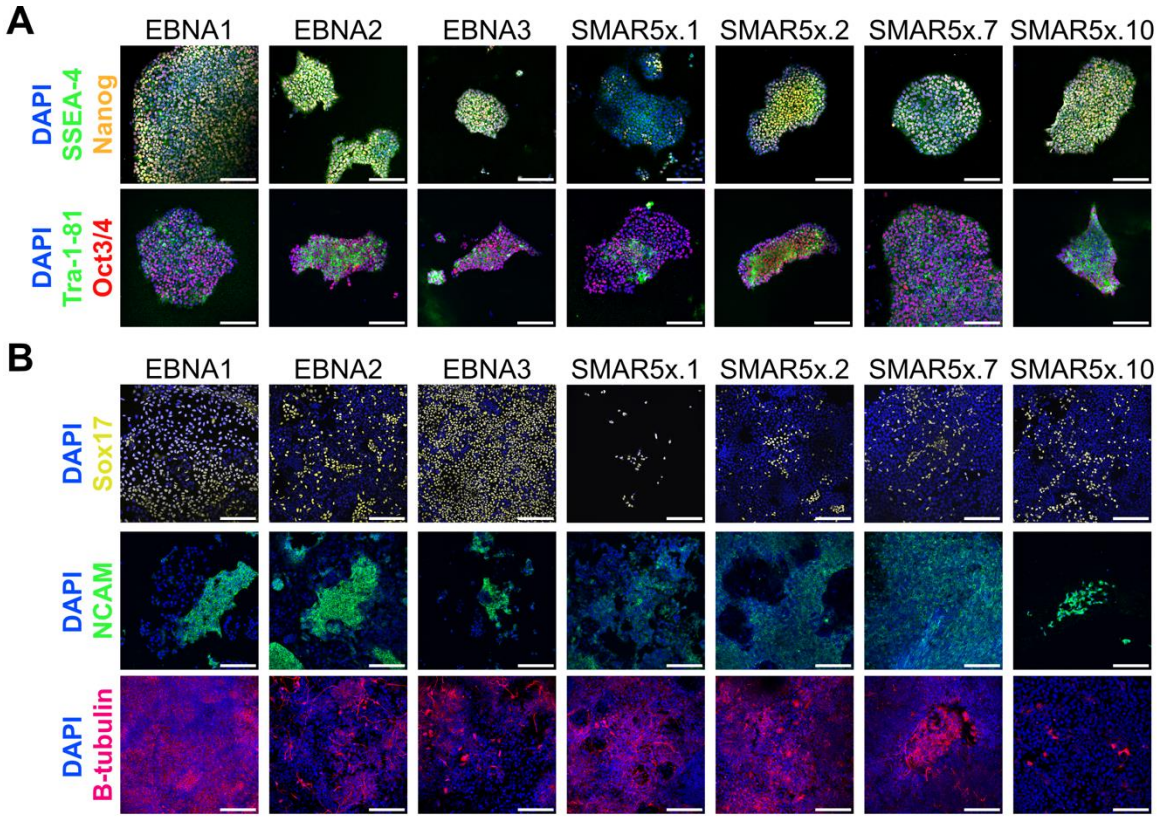

Figure 15. Optimisation of SMAR reprogramming yields high-quality SMAR iPSCs. NHDFs were reprogrammed using the optimised protocol and compared with EBNA-reprogrammed NHDFs. Three EBNA clones and four SMAR5x clones were analysed by immunofluorescence for **A** the expression of stem cell markers SSEA-4 (green), Nanog (orange), Tra-1-81 (green), and Oct3/4 (red), and **B** their ability to differentiate into cells of three distinct lineages. Sox17 (yellow) was used as an endoderm marker, NCAM (green) as a mesoderm marker, and B-tubulin (magenta) as an ectoderm marker. Scale = 200μm.

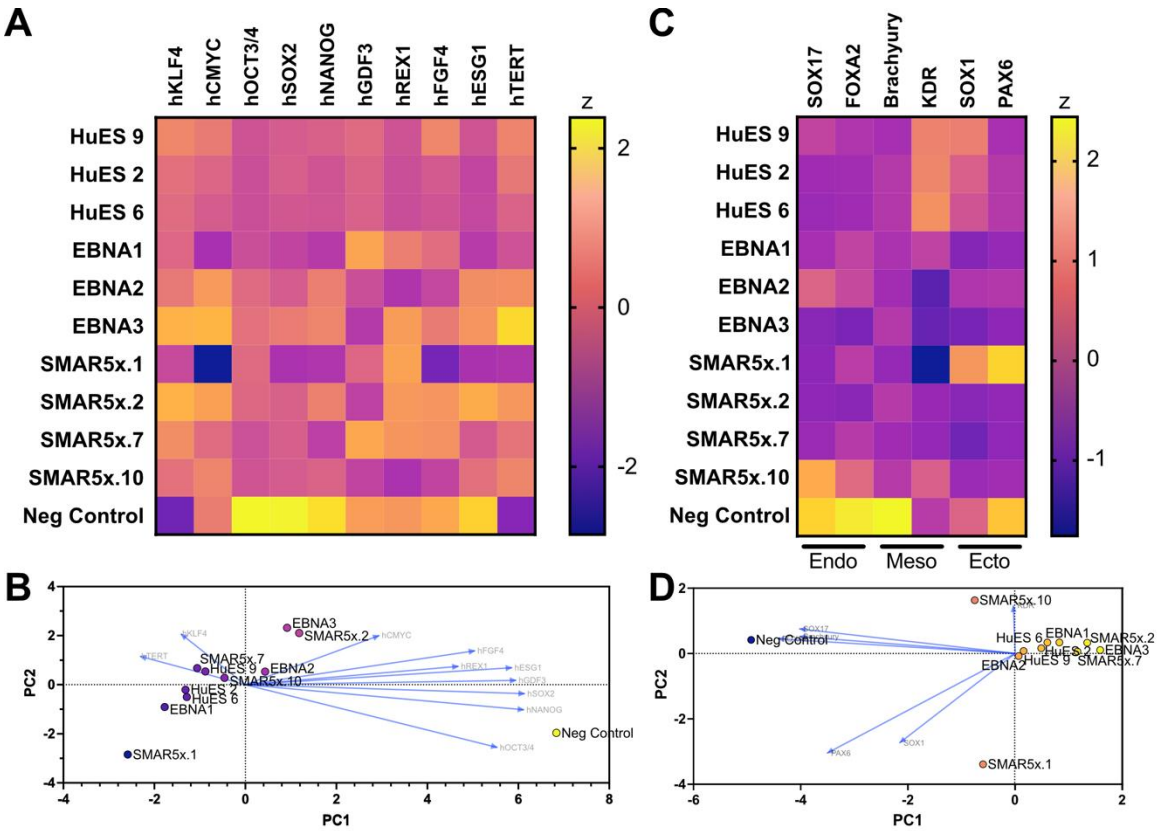

Figure 16. SMAR iPSCs display similar gene expression to human embryonic stem cells. The gene expression of four SMAR-iPSC lines were compared with three EBNA-iPSC lines, as well as three human embryonic stem cell (HuES) lines and one fibroblast cell line (Neg control) by qRT-PCR. In **A** their expression of stemness genes was assessed. Data shown is a z-transformation of the fold change of gene expression to the negative control fibroblast line. **B** Principal component analysis (PCA) of delta Ct expression of stemness genes shows a large separation between fully differentiated negative control fibroblasts and iPSCs or HuES cells analysed, with a smaller spread among iPSC lines. Arrows represent the contribution of each gene to the principal component. In **C** each cell line was subject to directed differentiation into endoderm, mesoderm, or ectodermal lineages, and their expression of lineage-specific markers was assessed. Data shown is a z-transformation of the fold change of gene expression to the negative control fibroblast line. **D** PCA of delta Ct expression of lineage-specific genes again shows a large separation between negative control fibroblasts and iPSCs or HuES cells analysed, with a smaller spread among iPSC lines. Arrows represent the contribution of each gene to the principal component.

2.4.3 Impact of SMAR reprogramming on genomic integrity

Cellular reprogramming is a highly genetically stressful process, involving the reorganisation of the entire genome in a cell [83]. Therefore, it is crucial to monitor the genome of reprogrammed cells for any aberrations that may have occurred during the process. Together with my collaborators in Rotterdam, I performed microarray analysis on the iPSC clones produced in this study, including three EBNA clones, the SMAR1 clone, and four SMAR5x clones. By comparison to the somatic NHDFs used as input cells for all the above iPSC lines, EBNA1 iPSCs show no genetic rearrangements or aberrations (Figure 17). However, SMAR1 iPSCs show several chromosomal duplications in chromosomes 7 and 16, as well as a

partial loss of one copy of chromosome 16. In contrast, SMAR5x clones 1, 2 and 7 show much more minimal genomic damage, limited to no more than two small losses and duplications spread across chromosomes per clone. Therefore, the optimised reprogramming method not only yields a higher reprogramming efficiency and more stable iPSC clones than the original method but improves the genetic stability of SMAR iPSCs as well.

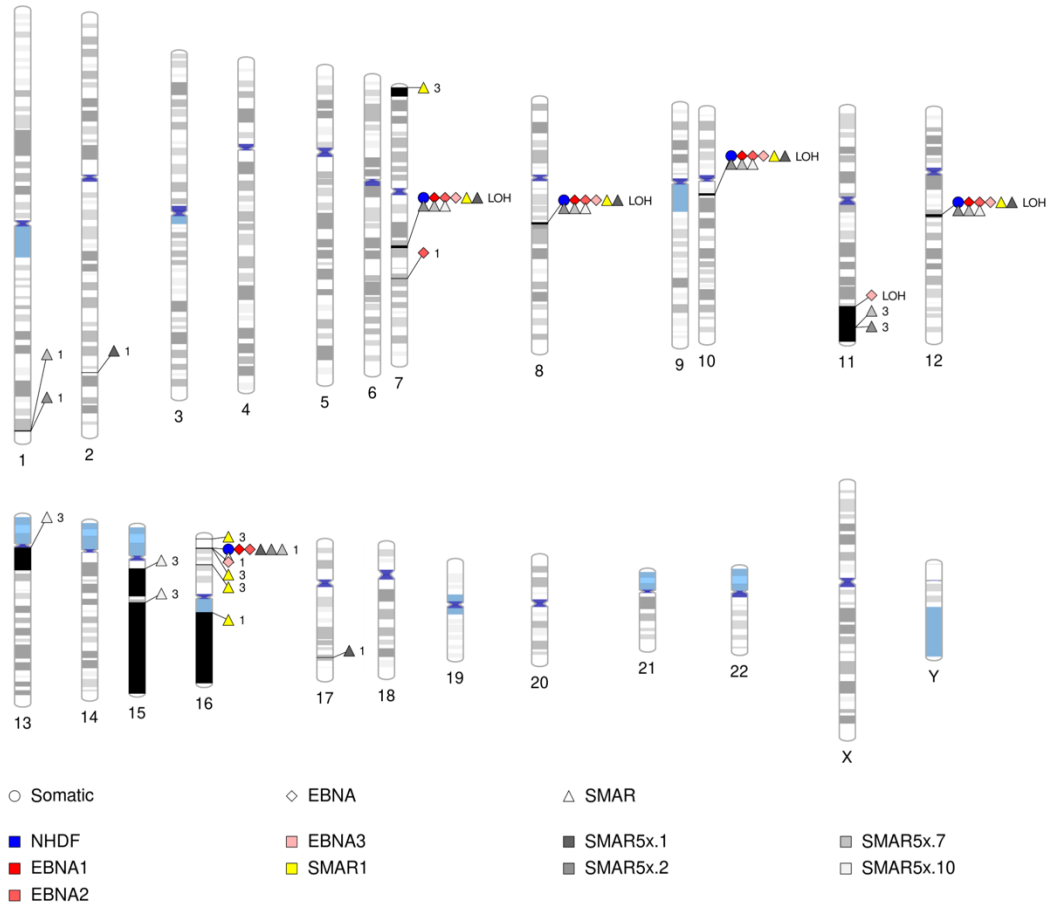

Figure 17. The optimised SMAR reprogramming protocol improves genomic stability of iPSCs generated from fibroblasts (NHDF). Phenogram plot showing all copy number variations (CNVs) detected in somatic NHDFs used as reprogramming inputs (blue circles), EBNA-reprogrammed iPSCs (red diamonds), SMAR-reprogrammed iPSCs from the first reprogramming trial (SMAR1, yellow triangles), and SMAR-reprogrammed iPSCs using the optimised protocol (greyscale diamonds). Annotations denote the copy number call (1 or 3 copies), or loss of heterozygosity (LOH). CNV data was obtained by microarray analysis of genomic DNA from iPSCs on the Illumina Infinium Global Screening Array chip. Data analysis was performed by Lieke Dons, Erasmus MC.

2.4.4 Assessment of vector retention in episomal reprogramming

One major aim of SMAR-based reprogramming was to improve the safety of the reprogramming process with respect to genomic integrity. Ideal iPSCs should be vector free and factor free, so the spontaneous loss of the reprogramming vectors after the reprogramming process is highly desirable. Therefore, I assessed the iPSC clones produced in this study for the presence of the reprogramming vectors.

Presence of at least one reprogramming vector was detected by polymerase chain reaction (PCR) for the bacterial origin of replication present on both EBNA and SMAR vectors (Figure 8A and B, yellow "Ori" segments). As it has previously been reported that approximately 70% of EBNA-reprogrammed cells lose the episomal vectors by passage 20 [21], I tested my iPSC clones at passages 6 and 10 (Figure 18). The presence of the episomal vectors was already undetectable at passage 6 in EBNA clone 1 and SMAR5x clones 5 and 8 and became undetectable in EBNA clone 2 by passage 10. The loss of detectable bacterial backbone in two out of five SMAR5x iPSC clones tested indicates that passive loss of SMAR vectors is possible after reprogramming, although possibly less efficient than loss of EBNA vectors.

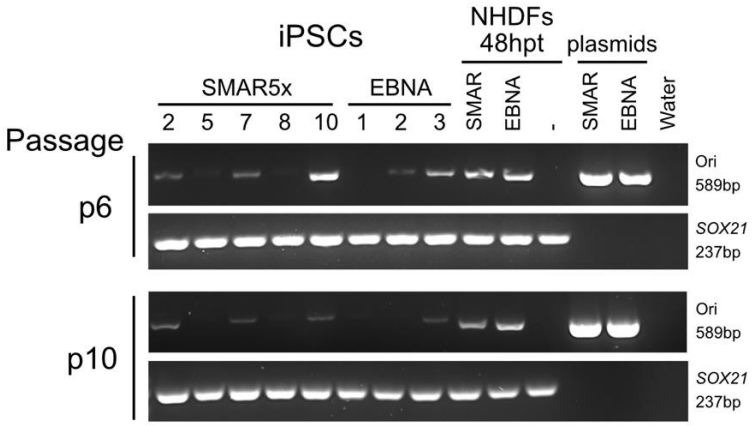

Figure 18. SMAR iPSCs can lose SMAR vectors after successful reprogramming. Presence of the reprogramming vectors was assessed by PCR on genomic DNA for the plasmid origin of replication (Ori, 589bp) at **A** passage 6 and **B** passage 10 after iPSC colony establishment. A 237bp fragment corresponding to the *SOX21* gene was used as an internal control to confirm the presence of genomic DNA template. Five SMAR and three EBNA clones were assessed for presence of the vectors. Two out of three EBNA clones and two out of five SMAR clones had undetectable vector levels at passage 10.

2.5 Summary

In this study, I demonstrated that episomal SMAR vectors can be used to reprogram somatic human fibroblasts. SMAR vectors resulted in a lower efficiency of reprogramming than the well-established EBNA vectors, but optimisation of the protocol improved the yield of iPSC colonies, albeit over a longer timeframe. SMAR iPSCs showed AP activity and were positive for stemness markers such as Nanog, SSEA-1, and Tra-1-81. Crucially, they were as capable of differentiation into cells of all three lineages as EBNA iPSCs, if not more, and gene expression analysis showed a tight clustering of SMAR iPSCs with HuES cells. However, the genetic stability of SMAR iPSCs could be improved in comparison to EBNA reprogramming, and it is not yet certain that SMAR iPSCs lose the episomal reprogramming vectors over time. These are two aspects of SMAR reprogramming that would be crucial to address in the future, to allow for the efficient generation of vector free, factor free, virus free human iPSCs.

3 Discussion

3.1 Current state of the art in reprogramming

Human iPSCs are an exciting technology, as tools for studying development and disease progression, drug modelling, as well as a basis for regenerative medicine. However, their safe and efficient generation is still technically challenging, and currently limits the clinical application of these cells [32].

There have been many protocols developed to reprogram cells into iPSCs (Figure 2), however each requires a compromise on safety, efficiency, or practicality. While lentiviruses are a popular and efficient means of reprogramming, they can cause insertional mutagenesis by integration into the genome, either disrupting tumour suppressor genes or activating oncogenes [84]. Indeed, the United States Food and Drug Administration (FDA) very recently required manufacturers of currently approved CAR T cell products to update safety labelling associated with their products, due to serious risk of T cell malignancies arising from the use of retroviral and lentiviral vectors [85; 86]. Sendai virus-based vectors are also a high-efficiency means of expressing reprogramming factors [11], however the virus can persist in reprogrammed cells for many passages, and may require active removal and screening, hindering its practicality [44; 87]. In addition, there are currently no clinical grade SeV vectors for reprogramming available [87]. Reprogramming by co-transduction of AAV vectors has also been explored by the Grimm group, and shows promise in its capacity for the delivery of Yamanaka factors both *in vitro* and *in vivo* [8]. However, even in this study the authors noted considerable stable integration of AAV vector genomes, of up to three quarters of *in vitro* generated iPSCs, and all *in vivo* generated iPSCs, with obvious implications for the clinical safety of this approach. Finally, the episomal EBNA vector system is widely used due to its safety and practicality, including in clinical settings. However, the use of the *EBNA-1* gene in this system still carries oncogenic potential, and cells reprogrammed with this vector system show immune activation, which may be undesirable for downstream application [26; 48; 49].

Non-viral reprogramming methods offer significant benefit in terms of safety; however, this often comes at the cost of practicality. mRNA transfection can be used to reprogram cells, however this requires at least four daily transfections which is not suitable for clinical grade manufacturing [12; 13]. A survey of 55 laboratories around the world found that 41% were unable to establish RNA-based reprogramming, suggesting that this is a challenging method. Additionally, only fibroblasts could be reprogrammed using RNA transfection [87]. Protein-based reprogramming, while a promising approach, seems mainly hampered by the difficulty in delivering proteins to cells, hindering the efficiency of reprogramming further than other methods [15]. Similarly, small molecule-based reprogramming

currently takes significantly longer than more established methods and involves many hands-on steps and potentially expensive compounds [16]. Another recent idea from the McKay group is to use synthetically modified linear DNA to reprogram cells [26]. The iPSCs generated by this method show favourable stability in their pluripotency and immune profiles, however recent evidence suggests that the dbDNA used in this study might spontaneously integrate into the genome at even a higher rate than traditional plasmids [88].

3.2 Summary of results

Until the present work, complete reprogramming of human cells using SMAR vectors has only been achieved using fibroblasts from patients with Batten disease, which present a lower barrier to reprogramming than cells from healthy donors [54]. Here, I present a protocol for the complete reprogramming of healthy human fibroblasts with SMAR vectors.

SMAR vectors were generated by the replacement of the oriP/*EBNA-1* region on the EBNA reprogramming vectors developed by the Yamanaka group [21] by human S/MAR regions. Surprisingly, additional modifications to the vectors to reduce immunogenicity and stabilise transgene mRNA resulted in only incomplete reprogramming (Figure 10). iPSC generation with SMAR vectors does take slightly longer than with the EBNA vector system (Figure 13), however the efficiency of reprogramming is still within acceptable limits for practicality (Figure 14). I show that SMAR iPSCs are phenotypically indistinguishable from EBNA iPSCs and similar to HuES cells in their protein and gene expression (Figure 15 and Figure 16). However, with the current system, there is still some retention of the SMAR vectors in iPSC cultures (Figure 18). This retention is similar between EBNA and SMAR iPSCs, indicating that there is potential for the spontaneous loss of the vector as reported for the EBNA system [21; 87]. The protocol developed here uses the Amaxa II electroporator, a well-established and common device, making it an easily accessible protocol for any laboratory. Additionally, it requires no weekend hands-on time, as medium changes are only on Mondays, Wednesdays, and Fridays.

3.3 Observations on SMAR reprogramming

3.3.1 Interplay between transfection and reprogramming efficiency

The four different vector series tested for reprogramming in this study differ slightly in their properties and usage (Table 1). The only vector series expressing viral factors is the EBNA series, which uses expression of the EBNA-1 antigen from EBV for episomal maintenance. This is replaced in the SMAR series by a human S/MAR sequence derived from the *IFNB1* gene. The EBNA series includes one

"EBNA-boost" plasmid, to ensure sufficient expression of EBNA-1 for prolonged expression of the Yamanaka factors [21]. However, as the SMAR series does not require protein expression for episomal maintenance, this boost plasmid becomes redundant. Thus, while successful reprogramming can only occur in a cell which is transfected by four EBNA plasmids, only three SMAR plasmids per cell are required. It may therefore be speculated that, given the same initial transfection efficiency, the SMAR series may be more efficient at reprogramming than the EBNA series. Additionally, as the SMAR series are much smaller than the EBNA series of vectors, it can be expected that they would be more easily transfectable into cells. This is indeed consistently the case, as can be seen in Figure 13B; measurement of fluorescence 24 hours post transfection shows only 6% GFP+ cells after EBNA-GFP transfection, as opposed to 11% after SMAR-GFP transfection under equivalent conditions. Interestingly though, the short-term retention rates of EBNA and SMAR vector systems appear to differ; while the measured GFP positivity increased to 8% for EBNA-transfected cells, SMAR-transfected cells reduced to 9%. Therefore, the original transfection efficiency is not the only factor determining reprogramming efficiency. It is possible that the EBNA and SMAR vector systems display different expression dynamics over time, which may explain the differences in both the timing and efficiency of reprogramming between the two systems (Figure 14). A time-course study of vector dynamics comparing EBNA and SMAR vector systems would be prudent for the further development of this system; it was not conducted in this study due to time constraints. Consistent with previous reports, the nano series of vectors with no episomal retention components performed the worst in reprogramming fibroblasts, once again indicating that prolonged expression of Yamanaka factors is crucial in the success of the process [18]. It is likely that the improved vector expression and retention provided by the nanovector backbone still cannot compensate for the lack of an episomal component in this context.

Despite an initially poor transfection efficiency, the EBNA vector series proved more efficient than the SMAR series at reprogramming fibroblasts in all but one experiment (Figure 14A). In addition, the EBNA reprogramming efficiency was also more consistent between experiments than that of the SMAR system. Thus, there are clearly uninvestigated aspects of the SMAR system that influence its ability to reprogram cells. Firstly, the functionality of the shp53 construct present in both vector systems has not been tested in the context of the SMAR vectors. An shp53 was incorporated into the EBNA vector system as this was found to improve the reprogramming efficiency [43]. This was simultaneously linked with the induction of senescence by overexpression of the Yamanaka factors, which the shp53 is then able to bypass [42]. As the IFNβ S/MAR used in this system is known to preferentially associate with RNA polymerase II [66], the efficacy of a shRNA construct driven by an RNA polymerase III promoter on the same vector is unknown. If the efficacy of this shp53 is lower on SMAR vectors than EBNA

vectors, or indeed varying stochastically, this may explain a lower or fluctuating reprogramming efficiency. Secondly, EBNA-1 does not just interact with the episomal vectors in transfected cells; it interacts with other cellular promoters, potentially creating a favourable environment for reprogramming [89]. In particular, EBNA-1 can deregulate c-Myc in multiple cell types by direct binding of the c-Myc promoter [89; 90]. As Myc expression is so central to reprogramming, this is very likely to affect the efficiency of reprogramming with EBNA vectors [91]. Nevertheless, the efficiency of SMAR-based reprogramming is still high enough for practicability, as each experiment resulted in multiple clones that could be picked from a single 6-well of seeded cells.

3.3.2 Influence of the nanobackbone on reprogramming

A surprising finding from this study was that the SMAR vector series was consistently capable of reprogramming human fibroblasts, while the nanoSMAR series was not, despite the two vector systems containing the same basic components. Indeed, the most significant discrepancy between the two vector systems is the bacterial plasmid backbone (Table 1). It is possible that the bacterial components present in the SMAR system cause more stress to transfected cells than the minimal nanobackbone, and in doing so aid the epigenetic remodelling needed for reprogramming. This could be tested by combining the nanoSMAR vectors with low-level agonism of the cyclic GMP–AMP synthase (cGAS)–stimulator of interferon genes (STING) pathway to mimic an inflammatory response. In fact, there is some precedence for cGAS-STING signalling contributing to stemness, for example in T cells [92]. However, not all inflammatory signalling might be beneficial to reprogramming, as other evidence suggests that pro-inflammatory c-Jun N-terminal Kinase (JNK) pathway signalling hinders cellular plasticity in the context of reprogramming [16]. The induction of an innate immune response hampers reprogramming in some contexts, such as daily mRNA transfection. There are however also suggestions that early and low-level immune activation could be beneficial to reprogramming [93; 94]. Indeed, a follow up study by the same authors showed that Toll-Like Receptor 3 (TLR3) stimulation by polyinosinic:polycytidylic acid (polyI:C) treatment is the key to efficient protein-based reprogramming [95]. It is therefore plausible that the use of a nanobackbone in episomal reprogramming vectors, designed to reduce the cell's innate immune response to the vector, inadvertently also renders the vector less capable of reprogramming.

3.3.3 Reprogramming kinetics

Although SMAR vectors can generate *bona fide* iPSCs, these were almost all picked as pre-iPSC colonies and cultured further to mature into iPSCs (Figure 10D; Figure 11A). Indeed, the kinetics of reprogramming studied by Yamanaka and Takahashi indicate that many fibroblasts begin the reprogramming process but never mature

into iPSCs, instead reverting into a fibroblast-like state [96]. This then explains the low reprogramming efficiency seen in all methods. Given an efficient delivery of OKSM factors, approximately 20% of fibroblasts (donor-dependent) express the stemness marker Tra-1-60 within seven days. However, most of these cells will invariably revert to a fibroblast-like state. A crucial phase is around days 11-15, in which the factor Lin28 is particularly effective in encouraging proliferation of Tra-1-60+ cells, improving the percentage of cells maturing into full iPSCs. Other work has used gene expression profiling to divide the reprogramming process into distinct initiation, maturation, and stabilisation phases [97]. This maturation phase of reprogramming is in fact being exploited in aging work as well, where Gill, Parry et al. [98] expressed OKSM factors in fibroblasts until exactly this stage – 10 to 17 days – before withdrawing reprogramming factor expression and observing the reversion of cell fate. The key idea of this study was to rejuvenate older fibroblasts and "reset" both the transcriptome and the epigenome by partial reprogramming, without losing cellular identity and generating stem cells. This work indicates that there is a temporal barrier of approximately 15-17 days in reprogramming, up until which removal of OKSM expression will result in cell fate reversion. The behaviour of SMAR-reprogrammed cells in this study would suggest that the expression of SMAR-delivered OKSML may decline around this time, as a proportion of picked pre-iPSC colonies did in fact revert to a fibroblast-like phenotype. A better knowledge of expression dynamics from SMAR vectors may aid to fine-tune the OKSML dosage and improve reprogramming timing and efficiency.

Importantly, my observation that pre-iPSC colonies can develop into full iPSCs after picking is not a new phenomenon. Gonzalez, Barragan Monasterio et al. [99] also report post-picking maturation of iPSC colonies after one or two transfections with a transient CAG-driven plasmid. In this case, there was no mechanism for the maintenance of the transfected plasmid, and a large majority of iPSC lines were found to have integrated the OKSM cassette. While integration was not specifically assessed in this study, previous evidence shows that SMAR vectors do not integrate into genomic sites, regardless of cell type [68; 73].

3.3.4 Genomic stability of iPSCs

Episomal vectors seem to be able to reprogram cells with lower risk of genomic aberrations than other methods [100; 101]. However, EBNA-1 expression has previously been linked to DNA damage by the induction of reactive oxygen species (ROS) [26; 102]. Thus, it could be expected that removing EBNA-1 expression from the reprogramming process would improve genomic stability of iPSCs. Surprisingly, this was not the case; the genomic stability of SMAR-derived iPSCs was not superior to EBNA-derived iPSCs (Figure 17). Only a single iPSC clone derived in this study, EBNA3, showed CNVs exactly matching the input

NHDFs. This may again be due to differential reprogramming factor expression over time. While EBNA iPSCs could be picked as mature colonies, SMAR iPSCs were matured post-picking, and this extended culturing timeline may increase genomic stresses [103]. Two of the clones tested, SMAR1 and SMAR5x.10 showed significant aberrations in several chromosomes and would clearly not be suitable for further application. These results highlight the importance of screening iPSCs for genomic stability before further use. It is known that the shp53 cassette, present on both EBNA and SMAR vector series, improves the efficiency of reprogramming at the cost of genomic stability [104]. Therefore, removal of this cassette might be the first step towards improving the genomic stability of SMAR iPSCs.

3.4 Future directions

The present work established for the first time SMAR plasmid-based episomal reprogramming in wild-type human cells, establishing a new avenue for non-viral reprogramming strategies. Several aspects of this protocol are however open to refinement, to improve the reprogramming efficiency of SMAR reprogramming and increase its practicality for future use.

Firstly, it is known that only a small proportion of SMAR plasmids transfected into cells move to a favourable nuclear location for episomal establishment, evidenced by a low retention rate of the vector without selection [66; 75]. As vectors that do not establish become diluted in cell proliferation in the same way that non-episomal plasmids do, one strategy to retain longer vector expression would be to limit mitotic divisions in transfected cells. Primary NHDFs in culture exhibit contact inhibition, and can be kept in a confluent state for several weeks without loss of viability [105; unpublished observations]. The protocol established here involves expanding NHDFs two days after transfection, and only taking a small proportion of the resulting cells for reprogramming (see Section 2.3.1 above). It may be beneficial to the reprogramming efficiency to skip this expansion step, and instead directly take all transfected cells for reprogramming, as this would limit mitotic divisions of the cells and potentially increase the transgene OKSML expression in the early stages of reprogramming.

Secondly, the strategy presented here requires successful triple transfection in a single cell for reprogramming to occur, as the OKSML genes are divided into three vectors. It may therefore be beneficial to combine all transgenes on a single cassette, as is the strategy commonly employed in lentiviral reprogramming [6]. In this way, each successfully transfected cell should receive all factors necessary for reprogramming. However, the drawback to this approach is that it would require a large vector (approximately 10kb). This may then be challenging to efficiently transfect into cells.

Another factor in the reprogramming efficiency that was not examined in this study is the initial transfection protocol in NHDFs. The protocol used here with the Amaxa II Nucleofector resulted in on average 10-15% transfection efficiency, which was always sufficiently good for EBNA vector-based reprogramming, so has not been optimised. However, if SMAR vectors are not as efficient in the reprogramming process, optimising their transfection into cells may also boost the efficiency of reprogramming. This was achieved by simply increasing the vector mass by five-fold (Figure 13B), however this amount of SMAR plasmid DNA also caused toxicity to the cells (Figure 13C, SMAR5x 7dpt). Other, more modern nucleofection devices such as the Lonza 4D electroporator or the MaxCyte ExPERT GTx electroporator could be considered instead and may allow for higher transfection efficiencies in these cells without toxic effects.

Finally, several small molecules have been found to be capable of improving reprogramming efficiencies by interactions with key signalling pathways. Inhibitors of histone deacetylates or DNA methyltransferases such as 5-aza-cytidine or valproic acid have been reported to improve reprogramming efficiencies, presumably by encouraging epigenetic remodelling in the cells [106]. A combination of inhibiting mitogen-activated protein kinase (MAPK) and glycogen synthase kinase-3 (GSK3), together with addition of leukaemia inhibitory factor (LIF), is also able to mature mouse neural stem cell (NSC)-derived pre-iPSCs, as well as removing the need for Sox2 and Myc expression [107]. Reprogramming NSCs with fewer factors is however still possible without the aid of small molecules, as Sox2 is endogenously expressed in NSCs and thus dispensable for the reprogramming process [108]. In both mouse and human cells, vitamin C has also been shown to improve reprogramming efficiencies by alleviating senescence [80]. Importantly, vitamin C was found to encourage the maturation phase of reprogramming in this study, helping pre-iPSCs to mature into iPSCs. A combination of the above inhibitors together with transforming growth factor β (TGFβ) inhibition has already been successfully applied to improve the reprogramming efficiency of EBNA-based episomal reprogramming vectors [109]. Thus, the co-treatment of cells with one or more of these small molecules may also boost the reprogramming efficiency of the SMAR vector system.

An overarching goal of the reprogramming field is to produce nonviral vector free, factor free iPSCs, that is, iPSCs that no longer retain the exogenous reprogramming factors or delivery vectors without scars in the genome from vector excision. In this work however, while the SMAR vectors were lost in iPSC lines SMAR5x.5 and SMAR5x.8, they were retained in three other SMAR5x lines tested at passage 10 (Figure 18). This is indeed in line with previous observations that, once established, SMAR vectors can persist for many months in the absence of selection [73; 75]. It is plausible that the reprogramming process itself acts as a selection of sorts, and iPSC colonies which can establish have a higher likelihood of vector retention than

incompletely or unsuccessfully reprogrammed fibroblasts. Two of three EBNA colonies tested lost their plasmid levels to below detectable levels by the same number of passages (Figure 18). It is therefore likely that SMAR vectors are better able to maintain episomal status than EBNA vectors, which are known to be lost, albeit slowly, by mitotic dilution (2-8% per cell division) [110]. However, clever use of promoters may be able to allow for the maintenance of SMAR vectors during the reprogramming process, and their passive removal after stable iPSCs are established. In this work, OKSML expression was driven by the CAG promoter on both EBNA and SMAR vectors, which is particularly resistant to epigenetic silencing during the reprogramming and differentiation processes [54]. It is known that SMAR vectors are lost from cells if silenced [111]. Therefore, future work could focus on the use of cell state-dependent promoters in which expression of reprogramming factors is high in early reprogramming, but silenced later in the process when endogenous expression of OKSM is induced. One such promoter is the spleen focus-forming virus (SFFV) promoter. This promoter is known to be sensitive to epigenetic silencing during cell differentiation [79]. It has been used in lentiviral reprogramming, where it becomes silenced as endogenous Oct4 expression arises [6]. Thus, the use of a cell state-specific promoter such as SFFV on SMAR reprogramming vectors may facilitate silencing of the vectors as iPSCs mature, causing their loss, generating vector free iPSCs.

Importantly, other groups are also continually developing the reprogramming process to improve its safety. This also applies to Shin Yamanaka himself, whose group has recently modified the SeV reprogramming system to aid in more complete and efficient removal of viruses after reprogramming [47]. The dbDNA reprogramming approach employed by the McKay group led to the understanding that ectopic expression of EBNA-1 causes ROS-mediated DNA damage to cells, and that cells reprogrammed using the EBNA vector system displayed increased immune reactivity than dbDNA-reprogrammed cells [26]. This work highlights the necessity of virus free approaches to cellular reprogramming. The SMAR system however has the practical advantage of scalability, as it is relatively cheap and straight-forward to produce even grams of SMAR vectors, and they require no post-processing after bacterial purification [68]. In fact, the SMAR vector system presents a very close alternative to work by Okita and colleagues [19], who showed that four sequential transfections of traditional plasmids can reprogram cells. Again, the SMAR system improves the practicality of this approach, as the capacity of these vectors to be retained episomally allows for a single transfection to perform the same function, which is attractive for current good manufacturing practice (cGMP) application.

4 Supplementary figures

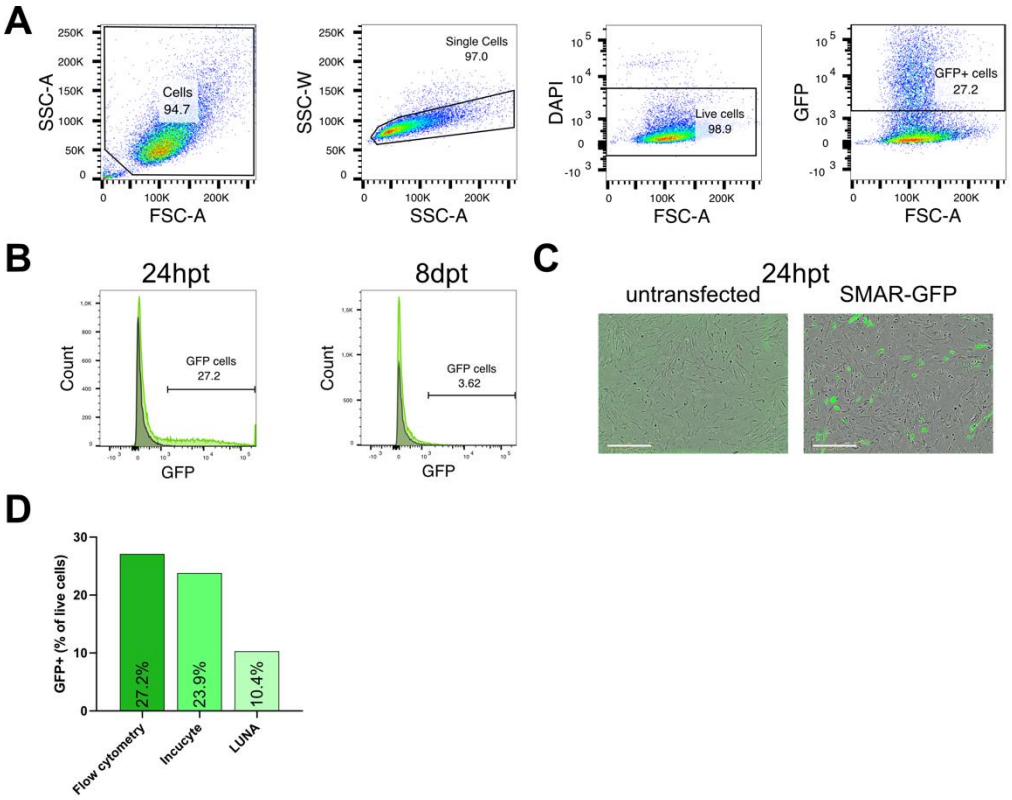

Supplementary Figure 1. Determination of transfection efficiency in NHDFs. NHDFs were transfected with SMAR-GFP vector and analysed by flow cytometry, Incucyte imaging or LUNA cell counting 24 hours post transfection. **A** Example gating strategy to determine GFP positivity in flow cytometry. **B** Comparison histograms of GFP positivity 24 hours and 8 days post transfection showing a decrease of GFP expression over time. **C** Example images from the Incucyte showing GFP expression 24 hours post transfection from NHDFs transfected with SMAR-GFP. Scale = 400µm. **D** Comparison of GFP expression as a percentage of live cells as measured by flow cytometry (taken as a gold standard), Incucyte imaging, and LUNA cell counting. This experiment was conducted in collaboration with Cornelia Wincek.

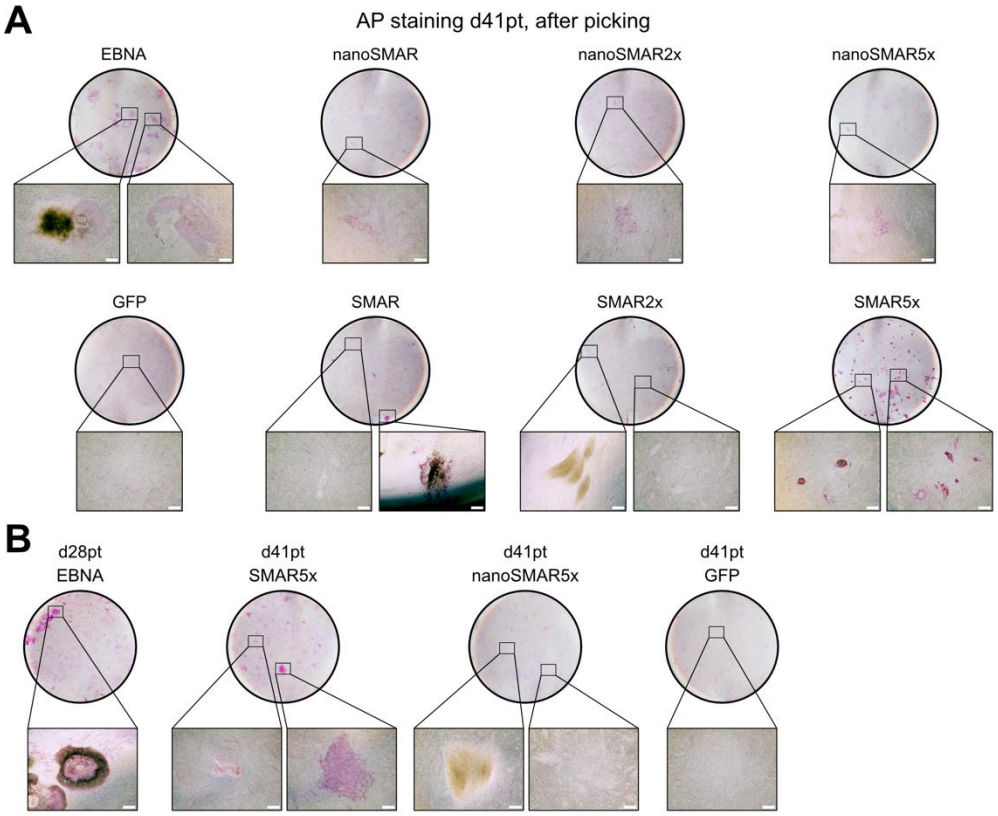

Supplementary Figure 2. Effect of timepoint on alkaline phosphatase staining of reprogrammed NHDFs. NHDFs were transfected with EBNA, SMAR, or nanoSMAR vectors in different amounts and cultured for up to 41 days. Cells were then fixed and stained for alkaline phosphatase (AP). **A** Representative images of AP-stained wells 41 days post transfection, after picking, for all transfection conditions. **B** Cells were reprogrammed as above, and AP staining of EBNA-transfected cells at day 28 post transfection was compared with (nano)SMAR5x transfection at day 41 post transfection. Scale = 500μm.

Chapter 2: Potentiation of H-1PV oncolysis by Ledipasvir

5 Introduction

5.1 Oncolytic viruses – a brief history

The association of viral infection with cancer dates back over a century. The earliest evidence for the interaction of viruses with tumours emerged in the mid-1800s, when some physicians reported evidence of spontaneous tumour regression after a viral infection, such as influenza infection. These limited case studies described infections ranging from influenza to chicken pox or measles, causing unexplained and spontaneous reduction in tumour burden [112]. This phenomenon was particularly well-recognised in leukaemias [113]. Typically, the patients who benefited from this infection tended to be young and often immunocompromised, and remissions were generally short-lived, with very sparse reports of curative infections [112; 114]. These case reports however sparked curiosity, and so in 1949, the observation of an apparent improvement in two patients with Hodgkin's lymphoma after contracting viral hepatitis led to a clinical trial. 21 patients with Hodgkin's lymphoma were infected with serum or tissue from hepatitis patients, of which 13 developed viral hepatitis. Remarkably, seven of these 13 showed some level of remission, although again short-lived and incomplete [115]. This garnered some interest and more trials were conducted, with flaviviruses such as Dengue virus, yellow fever, and particularly West Nile Virus isolate 101 being tested in many clinical trials in the mid-1900s [112; 116]. However, these clinical trials were invariably hampered by either low infection rates of patients or high pathogenicity of the virus, often leading to the death of patients due to the viral infection which would supposedly improve their condition. Interestingly, it was recognised as early as the 1920s that some viruses may possess "oncotropism"; that is, the ability to infect and replicate preferentially in cancer cells instead of healthy cells [116; 117]. This was the birth of the oncolytic virus (OV) as a cancer therapeutic.

Towards the late 1950s, other viruses began to emerge as the front-runners in oncolytic therapies, and remain in use as OV therapies today, such as adenoviruses (AdV), herpes simplex viruses (HSV), paramyxoviruses, picornaviruses, and pox viruses [112]. After a brief lull, renewed interest in OVs began in the 1990s, when genetic engineering of viruses to improve their oncotropism or oncolytic capacity began. The first instance of this was a HSV-1 virus with a mutation in its viral thymidine kinase gene, improving its safety, as well as its oncotropism and oncolytic capabilities in glioblastoma [118]. This work became a catalyst for an explosion of research and development into OVs, culminating in the clinical approval of four OVs globally to date: Rigvir, a picornavirus adapted to treat melanoma, was approved for clinical use in Latvia in 2004 [119]. Oncorine (H101) is an engineered AdV for the treatment of nasopharyngeal carcinoma together with chemotherapies, which was approved in China in 2005 [120]. Talimogene-Laherparepvec, or T-Vec, is an engineered attenuated HSV-1 virus encoding two

copies of the granulocyte macrophage colony stimulating factor (GM-CSF) to improve its immunostimulatory properties. T-Vec was approved for clinical use against recurrent melanoma in the United States and Europe in 2015 [121; 122], with approvals following in Israel and Australia in the years since [123]. Finally, Delytact, or Teserpaturev, is a second engineered HSV-1 strain recently conditionally approved in 2021 for clinical use against malignant glioma in Japan [124]. Delytact has the same attenuating mutations as T-Vec, namely deletion of the *γ34.5* and *α47* genes, as well as an additional inactivation of the infected cell protein 6 (*ICP6)* gene. *γ34.5* deletion improves the oncoselectivity of the virus, as this gene normally inhibits the host cell antiviral response to shut off protein expression. *α47* deletion allows sustained expression of class I major histocompatibility complex on infected cells to enhance the anti-tumour immune response. *ICP6* is normally required for HSV-1 genome replication, so its inactivation further limits replication of Delytact to dividing cells expressing sufficient levels of ribonucleotide reductase to compensate for this loss [124]. A phase II trial of Delytact was in fact terminated early as the primary endpoint of the study was met ahead of time, with the one-year survival rate at 84.2% in 19 patients treated, compared with 15% in historical controls receiving chemo- and radiotherapy [125]. Rigvir was pulled from the Latvian market in 2019, when it emerged that viral doses were substantially lower than advertised, and controversy remains about its effectiveness [126]. Nevertheless, the field of OVs has continued to expand, and in the ten years spanning 2012 to 2022, there were a total of 127 clinical trials for OV therapies [127], with over 408 trials in total conducted, spanning at least 31 distinct viruses (Table 2)[128; 129]. Interestingly, one non-oncolytic AdV vector has also been recently approved by the FDA in December of 2022 for the treatment of invasive bladder cancer unresponsive to immunotherapy [130]. This is a replication-incompetent AdV, named Adstiladrin, which is being used as a gene therapy vector to deliver the cytokine IFNα2b. IFNα2b has both direct antiproliferative effects as well as indirect immune-stimulatory properties, giving this gene therapy vector similar properties to other OVs.

Table 2. Overview of phase III clinical trials involving oncolytic viruses. Data retrieved from ClinicalTrials.gov.

Virus family	Virus name	Cancer	ClinicalTrials.gov identifier
Herpesviridae	Talimogene laherparepvec (T-Vec)	Melanoma, head and neck cancer	NCT01161498 (complete)
			NCT02263508 (complete)
			NCT00769704 (complete)
			NCT01368276 (complete)
	OH2	Melanoma	NCT05868707
Adenoviridae	H101	Hepatocellular carcinoma, non-muscle invasive bladder cancer	NCT03780049
			NCT01438112
			NCT04452591
Poxviridae (Vaccinia Virus)	X-594 (Pexa-Vec)	Hepatocellular carcinoma	NCT02562755 (terminated early)
	Olvimulogene nanivacirepvec (Olvi-Vec)	Ovarian cancer	NCT05281471

5.2 Oncotropism

The oncotropism of OVs, defined as their ability to preferentially infect and replicate in rapidly dividing or transformed cells over healthy cells, can either be naturally occurring or engineered. Naturally oncotropic viruses include HSV, Measles virus (MV), or H-1 protoparvovirus (H-1PV), whereas the oncotropism of AdV-based OVs must be engineered [131]. There are three major determinants of oncotropism, either natural or engineered; (i) interactions with the tumour microenvironment, (ii) cell surface receptors, and (iii) aberrant signalling in cancer cells [131].

i. Interactions with the tumour microenvironment (TME)
   There are many physical barriers for OV therapies, especially in solid tumours, as these are passive particles without autonomous motility. Solid tumours consist of cells within a dense extracellular matrix (ECM), which can physically block viral entry to the tumour site, such as the cases of Semliki Forest Virus or AdV [132]. Numerous strategies have been devised to overcome this physical TME barrier and facilitate OV spread. It has been found that pre-treatment or co-injection of matrix metalloproteinases

(MMPs) allows for the breakdown of some constituents of this ECM, improving viral spread in solid tumours of HSV in melanoma and soft tissue sarcoma models [133; 134]. Extending this idea, when allowed by the packaging capacity of the virus, MMP genes have been inserted as transgenes into OV genomes. For example, MMP-9 inserted into a vaccinia virus (VV) augmented viral oncolysis in a xenograft model of prostate cancer [135]. In addition to ECM, tumours are often poorly vascularised, as tumour cells grow and overwhelm the vascular supply, leading to areas of hypoxia and necrosis within the tumour bed. This poses a barrier to traditional cancer therapies such as chemo- and radiotherapy as well [136]. Poor vascular structure both increases the difficulty for OVs to localise to the tumour cells and means that OVs must be able to replicate under hypoxic conditions within cells. Under hypoxia, cells often shut down protein synthesis, adversely affecting viral replication. Nevertheless, some OVs have a natural capacity to replicate under hypoxic conditions, such as NDV and Reovirus, and are thus suitable for treatment of hypoxic tumours [137]. Another strategy is to increase the hypoxic stress even further in the tumour bed, starving tumour cells of oxygen by targeting endothelial cells. Vesicular stomatitis virus (VSV) preferentially infects tumour vasculature, causing thrombosis and ultimately tumour shrinkage [138]. Other OVs such as AdV have been engineered to produce anti-angiogenic factors, also inhibiting the growth of tumour vasculature and suppressing tumour growth [139; 140]. Interestingly, the latter study employed a pH-sensitive polymer coating to facilitate cellular uptake of the virus in a hypoxic environment [140].

ii. Cell surface receptors

Viruses can be oncotropic simply due to the cell surface receptors that they require as mediators for cell binding and entry. If these receptors happen to be upregulated in transformed cells, the virus will naturally have a better ability to infect cancer cells. This is the case for example in HSV-1, which binds the herpesvirus entry mediator protein and some cell surface nectins, which are often upregulated in some cancers, including melanoma [141]. HSV-1, as a naturally oncolytic virus, is the basis for two of the four currently clinically approved OVs. Similarly, MV binds to CD46 to mediate cell attachment, which is very often upregulated in cancer cells [142]. AdVs, on the other hand, have been engineered to create oncotropism: their natural cell surface receptor is the coxsackie and adenovirus receptor, which is often not expressed by cancer cells. However, modifications to the AdV capsid allows binding to CD46, CD80, CD86, or the carcinoembryonic antigen (CEA) to re-target their binding to cancer cell surfaces (reviewed by [143]).

iii. Aberrant signalling in cancer cells

Finally, once inside the cell, viruses must usurp natural cellular processes to traffic to replication sites, replicate their genomes, produce viral proteins, and assemble progeny virions. Simultaneously, they must avoid cellular anti-viral defences. Each of these processes may be altered in cancer cells, allowing viruses to replicate preferentially in transformed cell types. Normally, viral components such as nucleic acids are detected via pattern recognition receptors such as retinoic acid-inducible gene I (RIG-I), and lead to type I interferon (IFN) production, triggering a plethora of antiviral activity [144]. However, in transformed cells, growth and proliferation pathways are prioritised, often with the side effect of lowering antiviral immunity due to difficulty in producing or responding to type I IFN [144]. Ras overexpression, a common driver of transformation, can cause inactivation of protein kinase R (PKR), one of the downstream targets of RIG-I antiviral signalling [145]. PKR is activated by binding double-stranded RNA, and signals to block protein synthesis, halting viral replication. Many wild-type viruses have developed mechanisms to combat PKR signalling [146], and indeed deletion of the *γ34.5* genes in HSV-1 leads to replication only in PKR-defective cancer cells, a strategy devised to enhance its oncotropism [147]. NDV is another naturally oncotropic virus which is restricted by functional PKR signalling, thus limiting its replication to transformed cells [148]. In addition, NDV shows significantly enhanced oncolytic capability in cells with resistance to apoptosis through overexpression of B-cell lymphoma 2 (Bcl2) family proteins [149]. Alterations in expression of Bcl2 family proteins leading to a resistance to apoptosis is a hallmark of B cell lymphomas [150]. Indeed, many cancers can become "addicted" to overexpression of anti-apoptotic Bcl2 family members [151]. Finally, parvoviruses such as H-1PV require active proliferative signalling for their replication to occur, and are dependent on the expression of cellular S phase factors such as cyclin A as well as expression of factors associated with transformation like Phosphoinositide-dependent kinase 1 (PDK1) and activating transcription factor (ATF) for successful replication (described in detail in Section 5.5.3 below) [152].

5.3 Interactions with the immune system

There has been a growing body of evidence in the OV field that OVs are capable of more than just lysing cancer cells. In addition to this, OVs generate a secondary effect of immune activation as a result of their replication and cell lysis [153]. Lysis of tumour cells can release both cellular material and viral material, defined as damage-associated molecular patterns (DAMPs) and pathogen-associated molecular patterns (PAMPs), respectively. These DAMPs and PAMPs can attract

immune cells to the tumour site and trigger an immune activation towards tumour and virus alike. Death of cells able to cause such an immune response is termed immunogenic cell death (ICD). There are a few well-characterised hallmarks of ICD, such as extracellular ATP, which can act as a "find-me" signal to encourage immune cell homing to the tumour site [154]. The chaperone protein calreticulin, normally localised to the endoplasmic reticulum (ER), can also function as an "eat-me" signal when externalised to the cell surface, encouraging dendritic cell (DC)-mediated phagocytosis [155]. The nuclear protein high mobility group box 1 (HMGB1) can be actively secreted or passively released in necrosis and late apoptosis, and binds to antigen presenting cells, stimulating a pro-inflammatory response [155]. Many OVs are able to trigger this ICD by multi-modal cell death, such as NDV, which induces ICD characterised by ecto-calreticulin and HMGB1 release in a mouse model of glioblastoma [156]. H-1PV activates an antiviral immunity through recognition by toll-like receptors (TLRs), similarly stimulating DC phagocytosis and presentation to cytotoxic T lymphocytes [157-159]. A common strategy is to "arm" OVs with immune stimulatory molecules, such as GM-CSF, to increase the stimulation of antitumour immunity, as has been employed in T-Vec [121]. GM-CSF is a secreted glycoprotein which stimulates the production of granulocytes and monocytes. Importantly, the anti-viral immunity provoked by OV treatment is not necessarily a barrier to OV therapies; this immune activation can convert a "cold" tumour microenvironment to a "hot" one with immune cell infiltration and an inflammatory milieu. In this way, OV therapies can also function as an adjuvant to other immunotherapies, such as checkpoint blockade or cell-based immunotherapies [153; 160].

5.4 Oncolytic viruses as combinatorial therapies

Currently, clinical trials for OV therapies are dominated by oncolytic AdV, followed by HSV and VV (Table 2) [127]. Since its clinical approval by the FDA in 2015, the oncolytic HSV T-Vec has also been tested in contexts outside of its original indication as a melanoma monotherapy [161]. The phase III OPTiM trial which led to the approval of T-Vec showed a complete response in cutaneous melanoma of the head and neck of almost 30%, compared with 0% in controls treated with recombinant GM-CSF [162]. From here, clinical trials have branched out to test T-Vec in other cancer types, such as squamous cell carcinoma, breast cancer, pancreatic cancers, and even paediatric advanced solid tumours [163-166]. In addition, there is a recognition that OVs such as T-Vec may have utility as a neoadjuvant therapy. A trial using T-Vec as a neoadjuvant treatment before surgical resection of melanoma lowered the risk of reoccurrence by an estimated 25% [167].

As well as neoadjuvant therapy, there is a growing understanding that OV-based therapies can synergise well with other modalities of cancer treatments, partly due to their mild side effects compared with other options. These side effects, which are most commonly flu-like symptoms of fever, chills, nausea, and fatigue, do not tend to overlap heavily with the side effects of other therapies such as chemotherapy or radiotherapy, and as such OVs present an attractive option for combination with these treatments.

The combination of OVs with radiotherapy may be able to improve viral replication, thus improving the oncolytic effects of the virus. For example, the replication of an oncolytic AdV expressing the tumour necrosis factor (TNF)-related apoptosis-inducing ligand (TRAIL) is enhanced by radiotherapy of colorectal cancer cells *in vitro* [168]. Here, the combination therapy achieved a cell cycle arrest at G1 phase, followed by a significant increase in caspase-mediated apoptosis compared to either monotherapy, which was also protective in a xenograft mouse model. Alternatively, OV infection of cancer cells can impair the ability of these cells to counteract or tolerate DNA damage, leaving the tumour more vulnerable to radiotherapy-induced damage. Radiotherapy combined with an oncolytic VV strain increased the apoptosis of BRAF-mutant melanoma cells both *in vitro* and *in vivo* in mice, which was independent of viral replication [169]. This increased cytotoxicity led to increased DNA damage and was mediated through inhibition of pro-survival TNFα in tumour cells.

Chemotherapy is another treatment modality with which OVs have been combined. These two treatment regimens both target fast-growing cells, so a combination should lead to higher treatment efficacy, potentially allowing lower doses and thus side effects. Indeed, the oncolytic Reovirus Reolysin has been combined with paclitaxel and carboplatin chemotherapies in a mouse melanoma model, showing synergistic tumour killing *in vitro* and *in vivo* [170]. This work has been extended to the clinic, with a phase II trial in advanced malignant melanoma meeting primary efficacy endpoints with three out of 14 partial responses, although this trial was discontinued in favour of emerging immunotherapeutic treatments for melanoma [171]. A phase III trial with the same combination in squamous cell carcinoma is currently awaiting results (Clinicaltrials.gov: NCT01166542). However, the efficacy of such combination therapies may be cancer specific, as the same combination of paclitaxel and Reolysin in ovarian, tubal, or peritoneal cancer did not improve patient outcomes compared with paclitaxel alone [172].

The capacity of OVs to activate the immune system against both virus and tumour pairs particularly well with immunotherapies [123]. In one study, the combination of the FDA-approved oncolytic HSV T-Vec with mitogen-activated protein kinase (MAPK) Kinase (MEK) inhibition improved the oncolysis of melanoma cells by

improving viral replication, promoting tumour apoptosis as well as anti-viral and anti-tumour CD8 T cell responses in a mouse model of colon cancer [173]. Due to this inflammatory phenotype, in which the immune checkpoint molecules programmed cell death protein-1 (PD-1) and its cognate ligand PD-L1 were upregulated on tumour cells, this combination treatment was rationally combined with anti-PD-1 immunotherapy. This even further improved the survival of mouse models of melanoma and colon cancer to almost curative levels [173]. This observation that OV therapy can induce PD-1 and PD-L1 expression and "heat up" a solid tumour bed has led to several clinical trials combining checkpoint inhibition with OV therapies. Combination of T-Vec with the anti-PD-1 antibody pembrolizumab in melanoma showed very promising results in a phase Ib trial, with an objective response rate of 62% and a complete response rate of 33% [174], however a later phase III trial failed to meet its primary endpoints of efficacy [175]. This has led to speculation that the discrepancy between the two trial outcomes may lie in the timing of treatment; while T-Vec was administered six weeks before pembrolizumab in the phase Ib trial, they were given simultaneously in the phase III trial. The earlier administration of checkpoint inhibition might favour anti-viral immunity and viral clearance, before the OV has a chance to induce immune responses in the tumour [123]. This would align well with the positive results of another phase II trial combining T-Vec with another checkpoint inhibitor, the anti-cytotoxic T lymphocyte associated protein-4 (CTLA-4) antibody ipilimumab, where patients were "primed" twice with T-Vec injection before administration of immunotherapy [176]. These studies highlight the importance of understanding the mechanistic basis underpinning synergistic combination treatments once these combinations have been discovered.

5.5 H-1 Parvovirus

In 1960, Helene Toolan, Alice Moore and colleagues first reported an "unidentified, filtrable agent" isolated from human tumours. This agent was able to cause disease in hamsters including stillbirth and deformities, and it could be passaged in human cancer cell lines [177]. This agent was later recognised as a virus and named H-1 [178], and found to belong to the family *Parvoviridae*, genus *Protoparvovirus*, giving the virus the name H-1PV. Initially, it was unclear whether this virus was actually the cause of the initial tumours in humans, or if it was an opportunistic infection due to a natural oncotropism. However, H-1PV was then found to have antineoplastic effects on AdV-induced tumours in hamsters [179], confirming that it is indeed an oncotropic virus. This work has since extended to recognise the oncolytic effects of H-1PV against human tumours [180; 181], while simultaneously being innocuous for normal tissue [182].

5.5.1 Structure of H-1PV

H-1PV is a small, non-enveloped single-stranded DNA virus with a natural tropism for rodents. The identity of its natural host is somewhat controversial; some argue that it is a rat virus, as it was first isolated from human tumours passaged in rats. In these animals, it causes respiratory disease via the oronasal route [177; 183]. H-1PV can however also infect and propagate in hamsters, causing death or deformities in young animals [184; 185]. Nevertheless, the virus is unable to replicate in mice, even when cells are transformed [183]. The genome of H-1PV is small, around 5.1kb, with two main transcriptional cassettes: the early non-structural (*NS*) genes, and the late viral particle (*VP*) genes. Early gene expression of the non-structural proteins NS1 and NS2 is driven by the p4 promoter, whereas the p38 promoter controls the expression of the late VP1/2 capsid proteins, and the short alternatively translated (SAT) protein. This simple genome is flanked by two palindromic hairpins at either end of the single-stranded DNA, protecting the linear ends and providing a structure for genome replication and encapsidation. Genome replication follows a complex rolling hairpin mechanism, and as such the hairpin ends are not equivalent; the left-hand hairpin forms a Y-shape and drives asymmetric genome replication, whereas the right-hand hairpin has a simpler structure and allows terminal resolution [186].

The capsid of H-1PV is very small, at 25nm, which is approximately the size of a ribosome. This gives the virus an unusual stability in the environment, allowing it to survive for several months [183]. The capsid is icosahedral in shape, with three main structural components: a pore at the five-fold axes, a spike at the three-fold axes, and a dimple at the two-fold axes (Figure 19) [187; 188]. The VP proteins making up this structure are produced by alternative splicing of the same transcript to form either VP1 or VP2. VP2 is then cleaved at its N-terminus to form VP3 during capsid maturation, which then becomes the major constituent of the capsid in mature virions.

Many determinants of the parvovirus structure, life cycle, and oncotoxicity have been studied in other protoparvoviruses, particularly in minute virus of mice (MVM), so these studies have been taken together here to build a complete picture of the protoparvoviral life cycle.

5.5.2 Parvoviral proteins

NS1 is the major effector protein of protoparvoviruses, with an apparent molecular weight of 83 kilodaltons (kDa). It has a characteristic accumulation the nucleus of infected cells, due to its nuclear localisation signal [189]. This multifunctional protein regulates many viral processes, including driving viral gene expression, genome replication, and cytotoxic effects of protoparvovirus infection. It contains an ATP-dependent oligomerisation domain and a DNA binding domain, which

allows it to bind the p38 viral promoter, transactivating the expression of the capsid genes [189-191]. This DNA binding activity is also dependent on the acetylation of NS1 [192]. In addition, NS1 possesses a helicase domain, used to drive viral genome replication and possibly packaging, by analogy to the helicase-containing small Rep proteins of the genus *Dependoparvoviridae* [193; 194]. NS1 is also differentially phosphorylated throughout infection by cellular kinases, which is likely one of the regulatory mechanisms for its many functions [195-197]. Accordingly, NS1 interacts with cellular kinases, including the protein kinase C (PKC) family [198; 199], and casein kinase IIα (CKIIα) [200; 201]. Phosphorylated and acetylated NS1 is then capable of triggering multimodal cell death in infected cells. It induces the accumulation of reactive oxygen species (ROS), leading to a DNA damage response and caspase-dependent apoptosis, [202], cytoskeleton rearrangement and breakdown through its interaction with CKIIα [201], as well as lysosomal cell death by shifting the balance between lysosomal cathepsins and cystatins [203]. In addition, direct interaction of NS1 with factors involved in cell cycle progression such as replication protein A (RPA) causes cell cycle arrest at the G2/M transition, favouring viral replication [193; 202; 204].

NS2 is the second protein produced by the early p4 promoter, although it is less well studied than NS1. NS2 is 25kDa and shares an N-terminus with NS1, with putative roles in genome replication, translation, capsid assembly, and virus cytotoxicity in MVM. Mutations in NS2 can improve viral fitness, possibly due to improvements in viral capsid maturation [205]. In addition, interaction of NS2 with the nuclear export factor Crm1 is vital for the export of progeny virions from the nucleus [206].

The protoparvoviral capsid proteins VP1 and VP2 are both expressed from the late p38 promoter, driven by NS1. VP1 is an 81kDa protein with phospholipase 2 (PLA2) activity in its N-terminus to facilitate endosomal escape and a nuclear localisation signal to target the capsid to the nucleus [207; 208]. The 65kDa VP2 is an alternatively spliced form of VP1, sharing a C-terminus with the former. To form viral capsids, VP1 and VP2 assemble into trimers in the cytoplasm, which translocate to the nucleus and assemble into empty virions with ten copies of VP1 and 50 copies of VP2 [209]. As part of capsid maturation, 18-21 amino acids are cleaved off the N-terminus of VP2 to form VP3 only in intact virions and not empty capsids. Thus, VP3 becomes the major capsid component of protoparvoviruses [188]. Additionally, there is a small alternate reading frame of VP2 consisting of 58 amino acids known as the SAT protein. Porcine parvovirus SAT is found in the ER and is able to induce ER stress [210]. Exogenous expression of MVM SAT is in fact more toxic to cells than exogenous NS1, and mutations to knock out SAT strongly inhibit infectivity [211]. SAT may function as a virus-encoded pore in the plasma membrane as part of the lytic capability of the virus [211].

5.5.3 Parvoviral life cycle

H-1PV is a rodent virus, thus viral replication in human cells is absolutely reliant on host S phase and transforming factors. This reliance also defines H-1PV's oncotropism; while the virus can enter normal and transformed cells with similar efficiency, it is only able to replicate in transformed cells [212].

H-1PV initially binds to sialic acid motifs on laminins, particularly laminin γ1, at the cell surface [187; 213], and gains entry to cells via clathrin-mediated endocytosis which is dependent on galectin-1 (Figure 19) [214; 215]. After cell entry, the capsid requires endosomal acidification to expose the PLA2 domain of VP1, digesting the endosomal membrane and allowing trafficking to the nucleus [207; 215; 216]. While it is clear that the virus needs to enter the nucleus for genome replication, the mechanism by which it does so is more opaque. It is possible that there are several entry pathways, depending on the virus and cellular system examined. Canine parvovirus makes use of cellular dynein to traffic to the nucleus [217]. Interactions of the H-1PV capsid with the nuclear pore complex can cause active nuclear membrane permeabilisation, again dependent on PLA2 activity of VP1 [218]. Interestingly, the activity of caspase 3 plays a role in the nuclear permeabilisation by MVM, through cleavage of lamin B2 [219]. The timing of H-1PV and MVM viral uncoating is still subject to debate; some evidence suggests that capsids enter the nucleus intact through the nuclear pore complex, as in the case of AAVs [220; 221]. However, the viral genome can also be "ejected" from the capsid without disassembly, so partial uncoating and release of the genome into the nucleus is also possible [222; 223].

Parvoviral replication takes place in autonomous parvovirus-associated replication (APAR) bodies within the nucleus [224]. Genome replication takes place by an asymmetric rolling hairpin mechanism, in which the cyclin A/Cdk2 complex defining the initiation of cellular S phase is required to generate the double-stranded replicative form of the genome [225; 226]. This double-stranded replicative intermediate is then the transcription template for viral gene expression [186; 190]. The early p4 promoter is then driven by E2F, Ets, ATF/CREB and SMAD4 transcription factors in transformed cells, producing NS1 and NS2 (Figure 19) [227-230]. Viral DNA is synthesised by a complex of DNA polymerase δ, proliferating cell nuclear antigen (PCNA), replication protein A, and replication factor C [193; 226; 231]. Concatemeric forms of the viral genome are produced, which are resolved by NS1-mediated nicking of the parvoviral genome together with glucocorticoid modulatory element binding protein (GMEB) and HMGB1 and 2 [232; 233]. In this way, single-stranded genomes accumulate and are packaged into capsids over the course of hours following parvoviral infection [186]. Importantly, this replication triggers a cellular DNA damage response, with accumulation of γ-H2AX histone marks, as well as p53 and ataxia telangiectasia mutated (ATM) kinase in APAR bodies. ATM in fact aids MVM replication by

arresting the cell cycle at G2/M phase [234]. This cell cycle arrest is thought to be beneficial to viral replication, as the virus needs time to efficiently transcribe and replicate its genome before cell death. The activation of the pro-survival PDK1/Akt signalling axis by MVM NS1 may also delay host cell death until convenient for the virus [235].

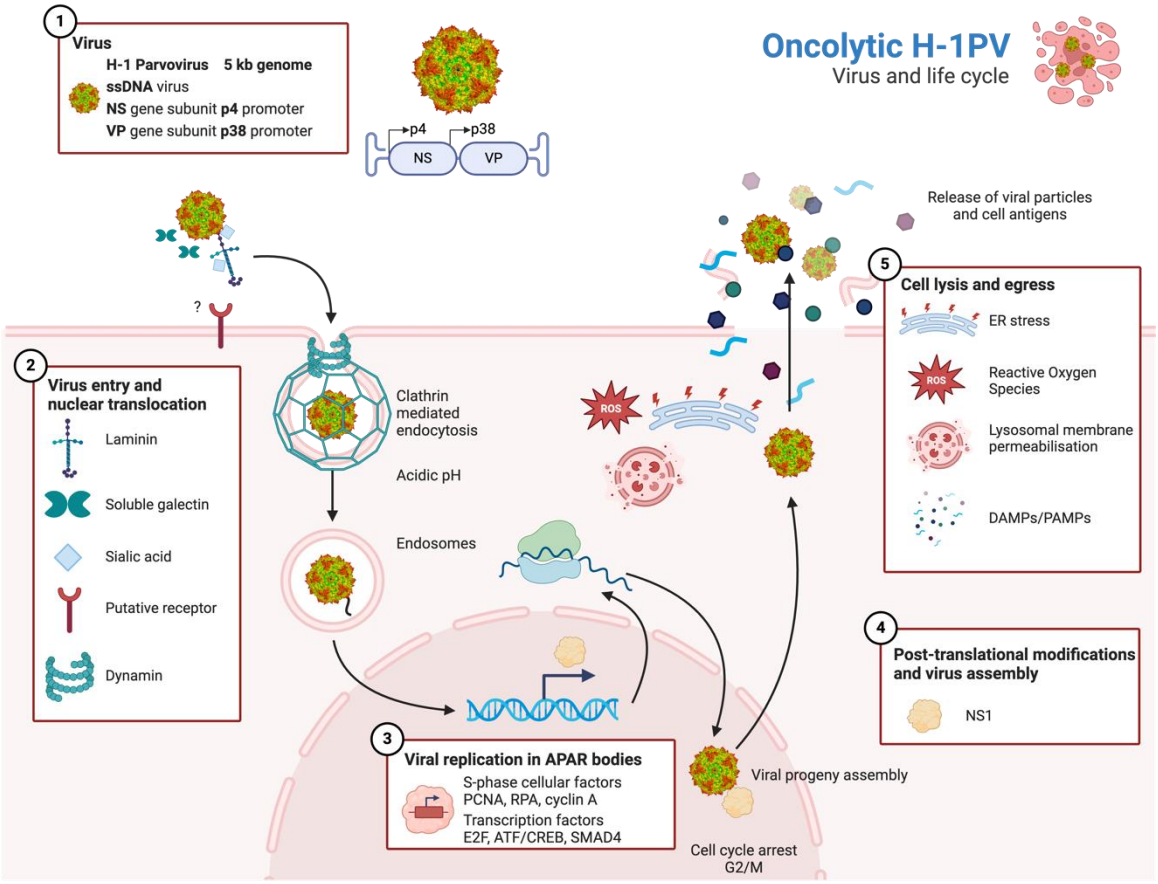

Figure 19. H-1PV structure and life cycle. H-1PV is a single-stranded (ss) DNA virus with a genome of 5kb encoding two transcription cassettes, *NS* and *VP*. The virus binds to sialic acid residues on laminin as well as soluble galectin to mediate cell entry via clathrin-mediated endocytosis. Acidification of endosomes leads to the exposure of the PLA2 domain on VP1 to allow endosomal escape and trafficking to the nucleus. Viral replication takes place in Autonomous Parvovirus-Associated (APAR) bodies and is reliant on S phase cellular factors as well as cellular transcription factors. Expression of the *NS* genes leads to the production of the viral NS1 protein, which drives the *VP* genes as well as causing cell cycle arrest. Viral replication also causes accumulation of reactive oxygen species (ROS) and ER stress. Parvoviral capsids are assembled in the nucleus and virion egress is aided by vesicular transport, before release into the extracellular space by multimodal lytic cell death, including apoptosis, necrosis, and lysosomal membrane permeabilisation. Cellular lysis leads to the release of virions as well as damage- and pathogen-associated molecular patterns (DAMPs/PAMPs). Figure adapted from Kavishwar [236] using BioRender. H-1PV capsid structure retrieved from Allaume, El-Andaloussi et al. [187].

NS1 transactivates the viral p38 promoter, driving the expression of the *VP1* and *VP2* capsid genes. This leads to pre-assembly of VP1/2 trimers in the cytoplasm, which must be phosphorylated by Raf-1 kinase before entry into the nucleus [237]. Here, trimers assemble into empty capsids before packaging of the genome, presumably through the five-fold pore of the assembled capsid [186; 223]. This packaging is assumed to rely on the helicase activity of NS1 to pump the genome into the pre-assembled capsids, analogous to AAV small Rep proteins (Figure 19) [194]. There is much evidence for parvoviral egress following an endosomal trafficking route. In MVM, the exposure and phosphorylation of VP2 in full capsids, as well as an interaction of NS2 with chromosomal region maintenance 1 (CRM1), facilitates rapid nuclear export of progeny virions into coat protein complex II (COPII) vesicles through the ER and Golgi apparatus [238; 239]. The actin-modifying proteins Radixin and gelsolin are also both requires for MVM egress from the nucleus to the cell periphery by reorganisation of the cytoskeleton, driven in part by NS1/CKIIα activity [200; 201; 240; 241]. In addition, newly synthesised MVM capsids colocalise with the endosomal markers Lamp2, cathepsin B and Rab6, indicating an endosomal egress route [240]. Finally, while cell lysis is clearly a major contributor to viral release, there is also some evidence of an active export of virions to the cell surface before final lysis [240].

Ultimately, parvoviral replication follows a lytic infection cycle, resulting in lysis of the host cell to release most progeny virions. H-1PV in particular can cause multimodal cell death, with several pathways including apoptosis, necrosis, and lysosomal cell death implicated (Figure 19). Several studies quickly noted that H-1PV causes caspase 3-dependent apoptotic cell death in rat and human glioma cells [242; 243], and apoptotic hallmarks were also found in H-1PV infected human hepatoma cells [244]. The mechanism for this was later characterised in more detail, with expression of NS1 alone causing cell cycle arrest at G2/M phase, ROS accumulation, DNA damage markers and cleavage of caspase 3 [192; 202]. However, in some systems H-1PV causes features of necrotic cell death in transformed cells together with apoptotic hallmarks. Here it was found that enzymes consuming nicotinamide adenine dinucleotide (NAD) became hyperactivated, driving the cells into necrosis before apoptotic processes could complete [245]. Additionally, glioma cells resistant to apoptotic treatments undergo a lysosomal mode of cell death, driven by accumulation of cathepsins B and L and reductions in cystatin B and C in the cytoplasm [203]. Cytosolic cathepsin activity also rises in pancreatic ductal adenocarcinoma (PDAC) cells infected with H-1PV *in vitro*, although blockage of this pathway does not save cells viral oncolysis [246]. These results together suggest that H-1PV can simultaneously drive multiple cell death pathways, overcoming host resistance to any one cell death pathway.

5.5.4 Clinical studies: successes and shortcomings of H-1PV

H-1PV has been studied extensively in pre-clinical models, including but not limited to melanoma [158; 247], breast and cervical carcinomas [181; 192; 248], neuroblastoma and medulloblastoma [249; 250], glioma [251-255], and pancreatic ductal adenocarcinoma (PDAC) [192; 246]. These studies have culminated in two clinical trials to date (Figure 20).

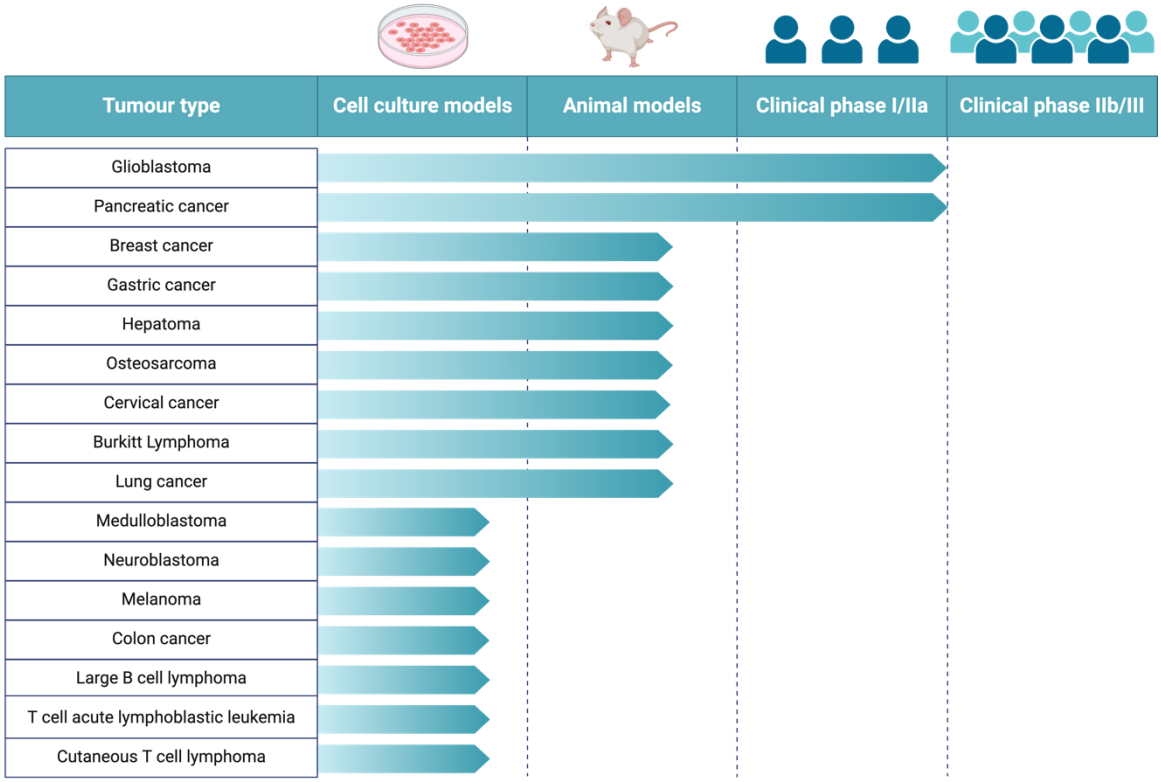

Figure 20. Current progress of H-1PV research: progression towards the clinics. Figure adapted from Hartley, Kavishwar et al. [256] using BioRender.

The first clinical trial, ParvOryx01, was a phase I/IIa clinical trial involving 18 patients with progressive primary or recurrent glioblastoma [257; 258]. This was a dose-escalation trial with two groups of intratumoral or intravenous administration of H-1PV, before tumour resection and a second injection of the virus into the tumour cavity in both groups. All patients were negative for mutations in the isocitrate dehydrogenase 1 (IDH1) gene, a common driver mutation in glioma, and one feature which may actually improve the outcomes OV therapies [259; 260]. Dose-limiting toxicity was not reached in either treatment group, indicating that H-1PV is safe and well tolerated in humans. Pre-clinical studies in rat glioma models indicated that H-1PV is able to cross the blood-brain-barrier (BBB) in rats, presumably due to its small size [254; 255]. This clinical trial then corroborated those findings in humans, showing that H-1PV is also able to cross the BBB and home to the tumour, as viral nucleic acids were measured in tumours from patients who had only received intravenous H-1PV before resection.

While this trial was designed as a small dose-escalation study with heterogenous patients, some evidence of H-1PV efficacy was seen. Viral replication and gene expression, including NS1, were detected in tumours. Cathepsin B expression was induced, particularly in areas with high NS1 expression, matching prior reports of lysosomal-mediated cell death in glioma cells [203]. There was also some evidence of immunogenicity, as immune cells including CD4 and CD8 effector T cells infiltrated into tumours after H-1PV treatment. Similarly, most patients' peripheral T cells were reactive against viral epitopes, and half of the patients tested showed a glioma-specific T cell response [258].

After the success of this trial, H-1PV has also been employed under compassionate use grounds in glioblastoma in combination with immune modulating treatment, specifically bevacizumab, an anti-vascular endothelial growth factor (VEGF) antibody to inhibit formation of blood vessels, and PD-1 inhibitors to block inhibitory signalling from the tumour [261]. Of the nine patients treated under this program, seven displayed an objective response, with two complete responses, highlighting the potential for H-1PV particularly in combination with other therapies.

The second, phase II clinical trial employing H-1PV focussed on metastatic PDAC which was refractory to first-line therapy [262; 263]. Again, dose-limiting toxicity was not reached, and two of seven patients displayed a partial response. All patients showed antiviral T cell responses, and there was some evidence of viral replication in tumours. In agreement with the previous trial, the two responders had T cell infiltration into the tumour, together with an increase of pro-inflammatory markers such as IFNγ, IL-8, IL-9, and IL-12 [263]. This ability of H-1PV to "heat up" a tumour microenvironment is particularly promising in the context of PDAC, where responses to immune checkpoint inhibitors are virtually non-existent [263]. Thus, the use of the virus may encourage better conditions for checkpoint inhibitors to exert their immunostimulatory functions.

The successful outcomes of both clinical trials using H-1PV demonstrate that it is safe to use in humans, with some evidence of efficacy. Nonetheless, H-1PV monotherapy is still not curative, and many open questions remain as to the treatment targets and regimens which would maximise its potential in the clinics.

5.6 Improving H-1PV oncolytic therapies

To improve the oncolytic potential of H-1PV, several strategies can be employed (Figure 21). Firstly, viral engineering can boost the anticancer or immunostimulatory properties of the virus or target it to novel cell types. Secondly, clinical use of the virus can be informed by an understanding of its life cycle and critical factors, producing biomarkers and guiding therapeutic protocols. Finally, novel combinations of H-1PV with other drugs can provide synergistic anticancer effects, with potential for rapid translation to the clinics (Figure 21).

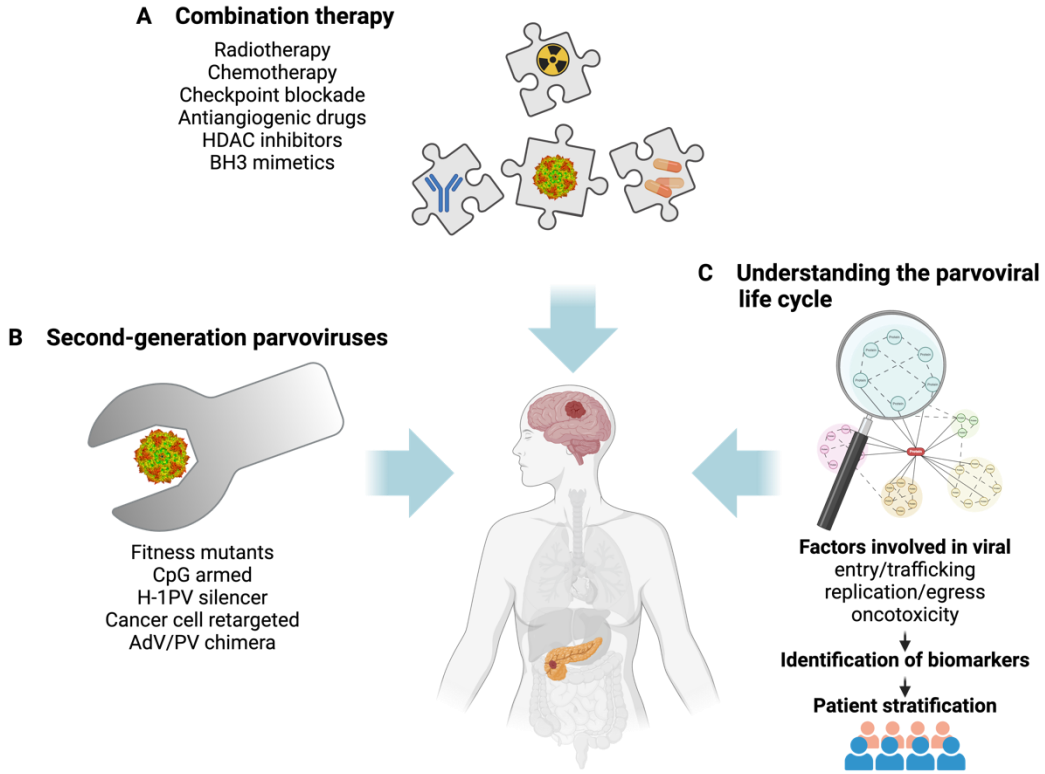

Figure 21. Improving H-1PV oncotherapies. Three main strategies exist to improve H-1PV therapy in a clinical setting. **A** Firstly, combination treatment with other anticancer treatments such as chemotherapy, immunotherapy, radiotherapy, or small molecule inhibitors can improve the outcomes of H-1PV therapy. **B** Secondly, the development of second-generation oncolytic parvoviruses can expand the repertoire of available oncolytic viruses with improved oncolytic and immunostimulatory properties. **C** Finally, a closer understanding of the mechanisms underlying the parvoviral life cycle can lead to identification of biomarkers which can be used to stratify patient groups most likely to respond to H-1PV therapy. Figure adapted from Hartley, Kavishwar et al. [256] using BioRender. H-1PV capsid structure retrieved from Allaume, El-Andaloussi et al. [187].

5.6.1 Viral engineering

H-1PV, as one of the smallest OVs under development, has very limited capacity for genome modification – only additions of less than 200bp can still result in infectious virus production [264]. Nevertheless, Raykov, Grekova and colleagues capitalised on the immunostimulatory properties of H-1PV and added CpG motifs to the viral genome to boost antiviral and antitumour immunity as much as possible. They showed that CpG-H1 viruses can act as an adjuvant from within

tumour cells and increase pro-inflammatory IFNγ, CD80, and CD86 expression in metastatic lymph nodes through TLR9 signalling, even without viral replication [265; 266]. Another strategy for arming H-1PV involves the addition of a short hairpin RNA (shRNA) cassette downstream of the *VP* gene unit, allowing silencing of target genes in the host cell to benefit H-1PV infection [267]. A proof-of-concept study using a shRNA targeting cyclin-dependent kinase 9 (CDK9) was effective at improving the oncolytic capacity of the virus in prostate and PDAC cancer cell lines *in vitro*, as well as a rat xenograft model of PDAC [268].

An alternative strategy for engineering of H-1PV to improve its oncolytic capabilities is capsid modification. Insertion of an RGD-4C peptide into the three-fold axis spike in the H-1PV capsid while ablating its capacity to bind sialic acid successfully retargeted H-1PV to specific integrins, allowing the virus to target melanoma cells *in vitro* [187]. Similarly, addition of VEGF-binding peptides to the MVM capsid simultaneously shields the virus from neutralising antibody responses while stimulating production of anti-VEGF antibodies, allowing it to double as an antiangiogenic treatment [269]. Capsid shuffling between rodent parvoviruses has also shown potential for retargeting them to different tumour types [270]. A final capsid engineering strategy for H-1PV can be found in the generation of chimeric viruses: here, the diminutive nature of the H-1PV genome can become an advantage. The entire H-1PV genome can be inserted into an AdV 5 vector, generating AdV-PV chimeras which can target novel cell types with high-efficiency. Productive infection generates secondary rounds of wild-type H-1PV progeny, so here the AdV 5 vector acts as a kind of Trojan horse [271]. Another advantage of this strategy is that the AdV-PV chimera can be further armed with therapeutic transgenes that would not be possible to insert into the H-1PV genome due to its limited packaging capacity.

5.6.2 Understanding viral mechanisms

Much of the H-1PV life cycle is still unknown and has only been characterised in related viruses such as MVM (see Section 5.5.3 above). A deeper understanding of the critical factors and interactions in H-1PV oncoselectivity and replication could thus aid the discovery of biomarkers to predict good patient responses to H-1PV therapy. Additionally, if critical points of the H-1PV life cycle can be identified, they can be used to inform rational combination of the virus with potential drug candidates to provide synergistic anticancer effects [256].

5.6.3 Novel combination therapies

One such rational combination has already been employed due to the knowledge that H-1PV has an immunogenic effect on DC and T cells in melanoma [158]. Here, Goepfert and colleagues combined H-1PV with ipilimumab, which blocks CTLA-4 and nivolumab, which blocks PD-1 in an *ex vivo* model of human melanoma.

These immune checkpoint inhibitors block inhibitory signals on immune cells and tumour cells, respectively. While H-1PV infection caused an upregulation of checkpoint molecules on melanoma cells, it also improved the cells' ability to mature DCs. Combination with checkpoint inhibition then provided an even stronger immune response, with enhanced cytotoxic T cell activation than the virus alone [272].

H-1PV has also previously been combined with various chemotherapies. In melanoma cells, H-1PV-mediated lysis improved after combination with cisplatin and vincristine, and the immunogenicity of this cell death also increased, as measured by DC maturation and subsequent cytotoxic T cell activation in an *ex vivo* model [247]. Meanwhile, combination of H-1PV with the standard-of-care chemotherapy gemcitabine in PDAC cells *in vitro* showed that those cell lines refractory to gemcitabine could still be effectively killed by the virus. This led to the suggestion that the two agents do not necessarily work together actively, but together can cover a wider range of cancer phenotypes than either treatment alone [273].

Similarly, the combination of H-1PV with ionizing radiation has been tested in high-grade glioma cells *in vitro* [274]. Here, it was discovered that the order of treatments is critical; radiation treatment before H-1PV infection has a much greater combinatorial effect than after infection. Synergistic oncolysis did not always correlate with an increase in NS1 levels, as a proxy for viral replication. Instead, radiation treatment pushed cells into S phase, which H-1PV is able to take advantage of for its cytotoxicity [202].

Combination of H-1PV with the histone deacetylase (HDAC) inhibitor valproic acid (VPA) showed a synergistic effect *in vitro* against cervical and pancreatic carcinomas by exacerbating ROS-mediated DNA damage caused by the virus, increasing apoptosis in the cells. This was found to be mediated through an improvement in acetylation of the NS1 protein, leading to higher transactivation of the late p38 promoter and an increased viral load. Co-treatment of H-1PV with VPA was able to completely eradicate established cervical and pancreatic carcinomas at sub-effective doses of virus in a rat xenograft model [192].

Finally, the combination of H-1PV with the BH3 mimetic drugs ABT-199 and ABT-737 *in vitro* showed an improvement in virus-mediated apoptosis in a range of cancer cell lines including glioma, PDAC, lung, and colon adenocarcinomas [275]. The same combination in prostate cancer led to an improvement of cell killing in cells with normal Bcl2 expression through increased apoptosis and lysosomal membrane permeabilisation. Additionally, H-1PV and ABT-737 co-treatment increased ICD and subsequent DC maturation, and improved NK-based cell killing of infected cells [236].

5.7 Ledipasvir

While a deeper understanding of the viral life cycle and infection determinants is important to improving therapeutic regimens and biomarkers, this is a time-consuming process, and results may not always be quick to translate to the clinics. Likewise, second-generation parvoviruses would require regulatory scrutiny and approval that has already been granted for the wild-type H-1PV. Therefore, to speed the process from bench to bedside as much as possible, this work focusses on novel combination therapies of H-1PV combined with already clinically approved drugs.

To this end, our laboratory conducted a high-throughput screening of H-1PV in combination with clinically approved drugs in the United States and Europe, in collaboration with Laurent Brino and Anne Maglott-Roth (IGBMC, Strasbourg). This drug library includes 1443 compounds belonging to a wide range of functional classes, such as anticancer, anti-inflammatory, anti-diabetic, analgesic, anti-viral, and neuropsychiatric drugs [276]. Drugs were selected to maximise their chemical and pharmaceutical diversity within the library. As these compounds are already in use in the clinic, their bioavailability and activities are well characterised, which should accelerate the clinical translation of a combinatorial treatment with H-1PV. The results of this screening are described in more detail in Section 7.1 below; the top candidate emerged as the antiviral drug Ledipasvir (LDV). This work thus centres around validating this Ledipasvir/H-1PV combination and elucidating its mechanism of action in cancer cells.

Ledipasvir is an inhibitor of the hepatitis C virus (HCV), also known as GS-5885 [277]. It was developed using an HCV replicon system; autonomously replicating viral RNA comprising of the essential enzymes for HCV replication, without encoding the full virus [278]. Ledipasvir was rationally designed and iteratively tested to target the viral NS5A protein, as a complementary strategy to NS3 and NS5B inhibitors [277]. It binds the NS5A protein of HCV directly, with a suggestion that it preferentially binds and inhibits oligomeric forms of NS5A due to its structural symmetry and stoichiometry in *in vitro* binding assays [279] (Figure 24C). It is marketed by Gilead Sciences under the brand name Harvoni as a combination with the NS5B inhibitor Sofosbuvir, which has been approved by the United States Food and Drug Administration (FDA) for treatment of chronic HCV infection since 2014 [280; 281], and approved by the European Medicines Agency (EMA) for the same since 2014 [282].

The NS5A protein is a membrane-anchored phosphoprotein encoded by HCV which is involved in viral RNA replication and virion assembly, and binds RNA directly [283]. It is the only virally-encoded protein capable of forming the double membrane vesicles (DMVs) characteristic of HCV replication from the ER membranes. However, the efficiency of DMV formation increases dramatically

when NS5A is expressed together with the protease and helicase enzyme NS3 and the RNA-dependent RNA polymerase NS5B, termed the "replicase" [283]. Although the exact mechanism for this DMV formation is yet to be described, the N-terminal alpha helix which functions as a membrane anchor in NS5A may play a role, as insertion of this into membranes is sufficient to alter membrane shape *in vitro* [284]. NS5A forms homodimers and oligomers and recruits several cellular proteins to DMVs to aid HCV replication [283; 285]. Analysis of mutations in NS5A conferring resistance to Ledipasvir showed similarities to Daclatasvir, another NS5A inhibitor. This suggests that Ledipasvir is able to prevent the formation of the viral replication organelle by changing the conformation of NS5A near its membrane anchor through physical interaction [283; 286].

5.8 The PI3K/Akt/mTOR signalling pathway

Several of the mechanistic screens conducted in this study implicate the phosphoinositide 3 kinase (PI3K), protein kinase B (Akt), and mammalian target of rapamycin (mTOR) signalling pathway in the improved cell killing ability of the H-1PV-Ledipasvir combination. Therefore, it is important to understand the functions and regulation of PI3K/Akt/mTOR signalling. This is a proliferative signalling pathway, which controls the growth and division of cells in response to environmental stimuli, and centres around mTOR kinase (Figure 22). Hyperactive signalling of this pathway can lead to uncontrolled cell growth, and as such it is very often dysregulated in cancer [287].

PI3K signalling can be triggered by growth factor signalling, either through receptor tyrosine kinases or G protein-coupled receptors [288]. PI3K activity leads to Akt activation through phosphoinositide-dependent protein kinase 1 (PDK1). Akt requires two phosphorylation events to become fully active; one at the Thr308 position by PDK1, and one at the Ser473 by mTORC2 [288]. Active Akt can then activate mTOR signalling [287; 288]. mTOR associates with different co-factors to form two complexes, mTOR complex 1 and 2 (mTORC1 and mTORC2), with distinct functions. mTORC1 signalling is driven by environmental factors like oxygen, stress, and nutrient availability, whereas mTORC2 activation is less well understood, but seems to be dependent on PI3K activity [287; 289; 290].

Downstream targets of mTORC1 include the p70 S6 ribosomal kinase (p70S6K), which leads to proliferative and growth signalling through ribosomal protein S6 (RPS6). Phosphorylation and inhibition of eukaryotic initiation factor 4E (eIF-4E)-binding protein 1 (4E-BP1) allows cap-dependent translation through eIF-4E [291]. mTORC1 can also block autophagy and lysosome biogenesis through the phosphorylation of autophagy-initiating proteins like unc-51-like autophagy-activating kinase 1 (ULK1) and ATG13 [287]. One of the major

substrates of mTORC2 is Ser473 on Akt, driving a feedback loop whereby mTORC2 activation can drive mTORC1 activity through Akt [292]. mTORC2 also activates serum- and glucocorticoid-induced protein kinase (SGK), driving cell survival. Interestingly, it also phosphorylated protein kinase C (PKC) family members to control cytoskeleton rearrangement and cell motility [287; 290].

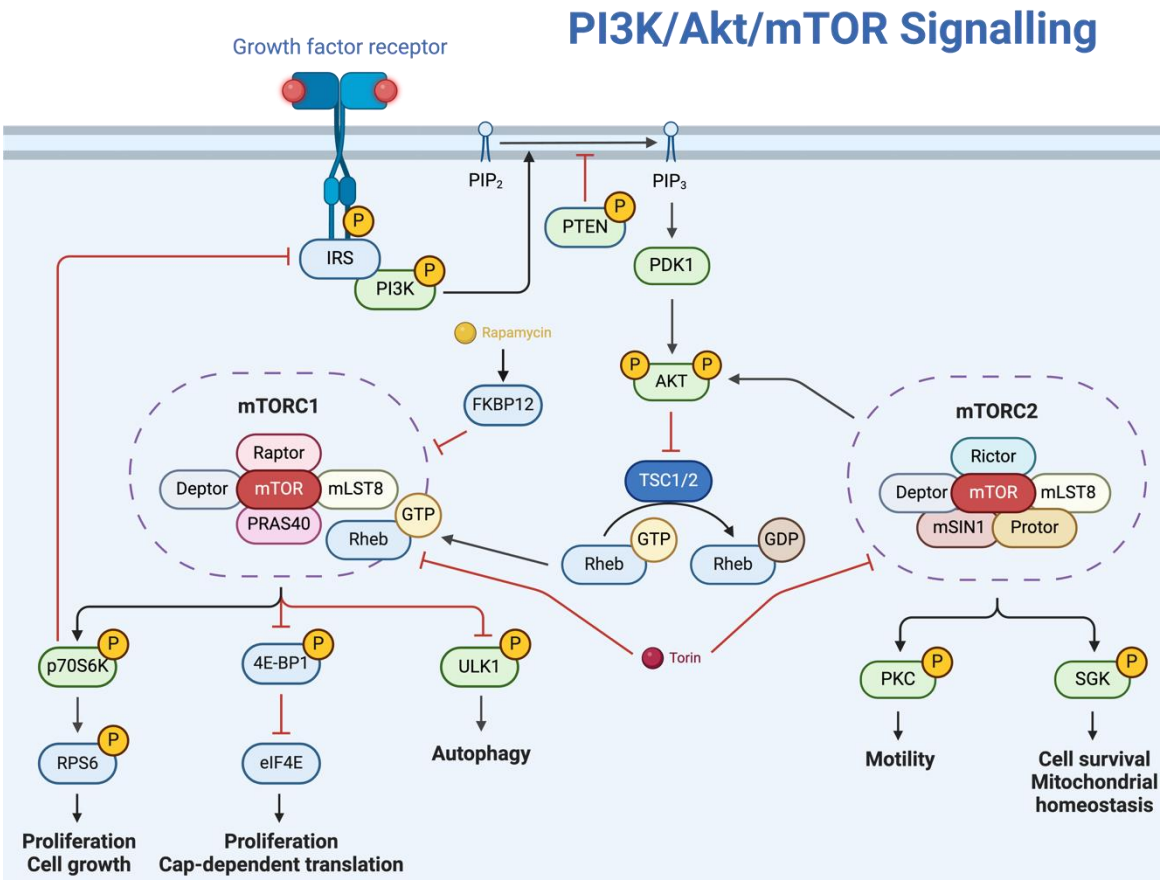

Figure 22. The PI3K/Akt/mTOR signalling pathway. Growth factor receptor signalling is transmitted through the insulin receptor substrate (IRS) to phosphoinositide 3 kinase (PI3K), activating it. PI3K then converts phosphatidylinositol (3,4)-bisphosphate (PIP_2) to phosphatidylinositol (3,4,5)-trisphosphate (PIP_3) within the plasma membrane, a process which is opposed by the tumour suppressor phosphatase and tensin homolog (PTEN). PIP_3 recruits protein kinase B (Akt) to the plasma membrane, allowing phosphorylation by phosphoinositide-dependent protein kinase 1 (PDK1) on the Thr308 residue in the activation loop of Akt. A second phosphorylation of Akt at Ser473 by mammalian target of rapamycin complex 2 (mTORC2) leads to its full activation. Active Akt goes on to phosphorylate and inhibit tuberous sclerosis complexes 1 and 2 (TSC1/2). TSC2 is a GTPase activating protein (GAP) for Ras-related GTPase Rheb (Rheb), so without this GAP activity Rheb-GTP accumulates, forming an essential component of the mammalian target of rapamycin complex 1 (mTORC1). Now in its active form, mTORC1 phosphorylates and activates p70 S6 ribosomal kinase (p70S6K), which can phosphorylate ribosomal protein S6 (RPS6) and lead to proliferative and growth signalling. P70S6K can also directly phosphorylate IRS, blocking PI3K activation and inhibiting hyperactivation of the whole pathway. Active mTORC1 also phosphorylates eukaryotic initiation factor 4E-binding protein 1 (4E-BP1), inhibiting its ability to bind and block eukaryotic initiation factor 4E (eIF-4E). eIF-4E is crucial for cap-dependent translation and proliferative signalling. By phosphorylating unc-51-like autophagy-activating kinase 1 (ULK1), mTORC1 can also downregulate autophagy. Activation of mTORC2 is less well understood but may be regulated through its subcellular localisation.

mTORC2 can phosphorylate Akt as well as the protein kinase C (PKC) family, regulating cytoskeletal organisation and cell motility, and serum- and glucocorticoid-induced protein kinase (SGK), modulating cell survival and controlling mitochondrial homeostasis. The activities of mTORC1 can be blocked by Rapamycin (yellow), which binds the FK506-binding protein 12 (FKBP12) and allows it to allosterically inhibit mTORC1. Torin (red) is a mTOR inhibitor which binds to the kinase site of mTOR, allowing it to block both mTORC1 and mTORC2 activity. Figure made using BioRender, based on Liu and Sabatini [287]; Manning and Toker [288]; Fu and Hall [290].

6 Aim of this project

The aim of this research project was to validate the novel combination of H-1PV with Ledipasvir and evaluate its potential for anticancer use. In addition, I aimed to characterise the mechanism of action of this novel combination. Notably, Ledipasvir exhibits picomolar activity against HCV replicon systems and is safe for human consumption with no known cellular targets in humans [277]. According to previous results from our group, up to micromolar concentrations of Ledipasvir are required to exert a synergistic anticancer effect with H-1PV infection. Therefore, the concentrations of Ledipasvir used in this study together with a lack of known cellular targets imply an off-target effect of the drug potentiating viral oncolysis. I aimed to find and characterise this novel effect of Ledipasvir.

The model systems that I chose for this characterisation were the glioma cell line U373-MG, and the PDAC cell line AsPC-1. This was for multiple reasons: firstly, H-1PV oncolytic activity has already been studied in these cell lines [192; 203; 230; 254; 293; 294]. Secondly, these cell lines represent the two cancer modalities for which H-1PV has undergone clinical testing [258; 263]. Finally, these cell lines display distinct sensitivity to H-1PV treatment alone, as U373-MG cells are relatively sensitive, but AsPC-1 cells are relatively resistant to viral oncolysis. Thus, any mechanism by which Ledipasvir can augment H-1PV oncolysis in both these cell lines is likely to be general, and not driven by specific properties of one cell line.

Specifically, in this project I aimed to:

i. Validate the synergistic anticancer effects of H-1PV and Ledipasvir in PDAC and glioma cell lines *in vitro*
ii. Assess the effects of Ledipasvir treatment on viral replication and cytotoxicity
iii. Investigate potential interactions of the Ledipasvir-H-1PV combination with cellular signalling, in particular kinases
iv. Extend these findings to translational models of PDAC

7 Results

7.1 Identification of Ledipasvir as a potentiator of H-1PV-mediated oncolysis

To identify novel drugs that could boost H-1PV oncolysis, our group in collaboration with Laurent Brino and Anne Maglott-Roth conducted a high-throughput screen of 1443 FDA-approved drugs from a SelleckChem library selected for a wide chemical and pharmaceutical diversity (described in Section 5.7 above). Drugs were tested alone or in combination with H-1PV infection in two glioma cell lines U373-MG and SNB-19 (Figure 23A). Cell viability was then measured by PrestoBlue viability assay. The results were first filtered for compounds which were toxic alone (viability <80% of mock) or which caused aberrant growth of the cells (viability >130% of mock). Compounds were considered as top hits if they were able to potentiate viral cell killing by at least 20% at low concentration, and at least 40% at high concentration (Figure 23B). These top hits were then validated in a second round of screening, again with a PrestoBlue viability readout, where five concentrations of each compound were tested, alone and in combination with H-1PV (Figure 23C). ABT-737 was used as a positive control in both rounds of screening, as our group has previously identified this compound as a booster of H-1PV oncolytic activity [236; 275]. Unsurprisingly then, another two BH3 mimetic compounds, ABT-236 and ABT-199, were also identified as top hits in this screen, confirming the validity of the results. The next top candidate was the antiviral drug Ledipasvir (Figure 24C).

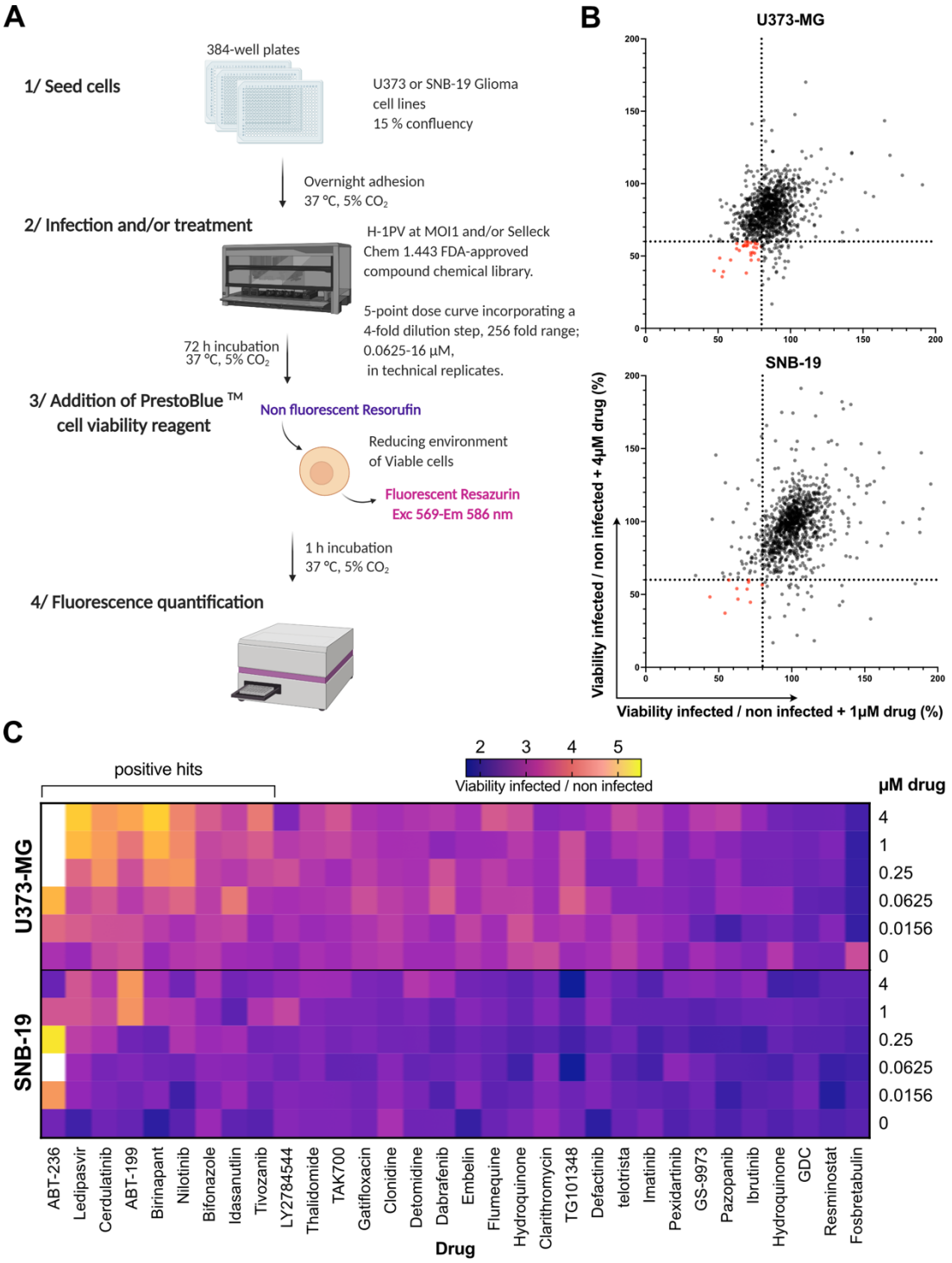

Figure 23 Screening to identify novel drug combinations potentiating H-1PV oncolysis. A Schematic of the screening design. U373-MG or SNB-19 glioma cells were treated with H-1PV at MOI 1 as well as a SelleckChem FDA-approved compound library, and viability was measured 72h post infection. **B** Primary screening results. Compounds were filtered for those with viability between 80% and 130% of mock to remove toxicity and abberant growth. Each dot on the graphs represents one compound, and the dotted lines respresent the upper thresholds for positive hits. **C** Validation screening results. U373-MG and SNB-19 glioma cells were treated as in A with compounds identified as top hits from the primary screen. Compounds were considered hits if the ratio of viability in infected to non-infected cells was greater than 120% of controls (0µM) in both cell lines.

Ledipasvir is an antiviral drug which targets the HCV protein NS5A (described in detail in Section 5.7 above). Given this novel finding that Ledipasvir may enhance oncolytic virotherapy, my colleagues Valérie Palissot and Tiina Marttila first validated the screening results using an independent assay. To this end, both glioma lines used in the original screening, U373-MG and SNB-19, were co-treated with H-1PV and various compounds for 96 hours, and cell lysis was measured by release of lactate dehydrogenase (LDH) into the culture medium. This is crucial to confirm active lysis of the cells, as a reduced viability measurement may simply be caused by a lack of growth of treated cells compared with their mock controls. Dimethyl sulfoxide (DMSO) and Hydroquinone were used as negative controls, while ABT-199 and ABT-263 were used as positive controls. LDH assays confirmed that Ledipasvir can potentiate H-1PV-mediated lysis of glioma cells at all concentrations tested (Figure 24A). Phenotypically, cells treated with the combination of Ledipasvir and H-1PV displayed increased cytopathic effects compared with treatment with H-1PV alone, while Ledipasvir treatment alone did not induce any noticeable changes (Figure 24B). In these assays, the concentrations of individual treatments were always kept equal to the concentrations used in combination.

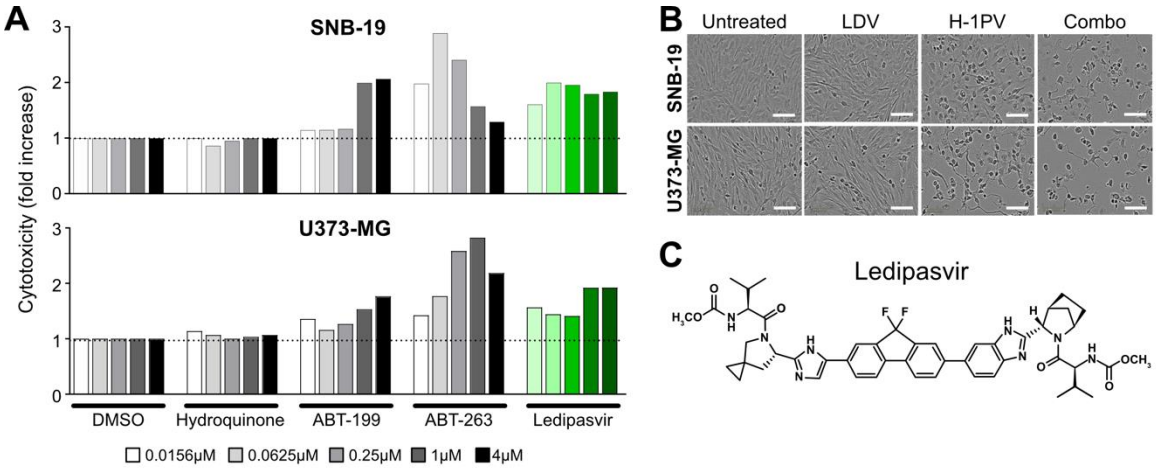

Figure 24. Validation of Ledipasvir as a top hit for potentiating H-1PV oncolysis. A Cytotoxicity was measured *in vitro* by measurement of lactate dehydrogenase (LDH) release 72h post infection with MOI 1 of H-1PV and the indicated drug. Values were normalised to the cytotoxicity of H-1PV with DMSO co-treatment. **B** Brightfield images of SNB-19 and U373-MG 96h post treatment with 4µM LDV, MOI 1 (SNB-19) or 100 (U373-MG) of H-1PV or the combination of both. Scale bar = 100µm. **C** Chemical structure of Ledipasvir. Data was produced by Valérie Palissot and Tiina Marttila.

To further validate these findings, the Ledipasvir-H-1PV combination was tested on a panel of cancer cell lines derived from different tumour entities (Figure 25). Again, active cell lysis was measured by lactate dehydrogenase release, and all cell lines tested showed a stronger cytolytic response to the combination treatment than H-1PV alone at the same dose, while Ledipasvir alone did not significantly affect cell lysis in almost all cell lines. Importantly, this result holds true across cells from diverse cancer entities, including glioma, pancreatic ductal adenocarcinoma (PDAC), prostate cancer, and lung and renal cell adenocarcinomas. This demonstrates that the mechanism of action of the combination treatment is general, and not limited to a certain type or types of cancer.

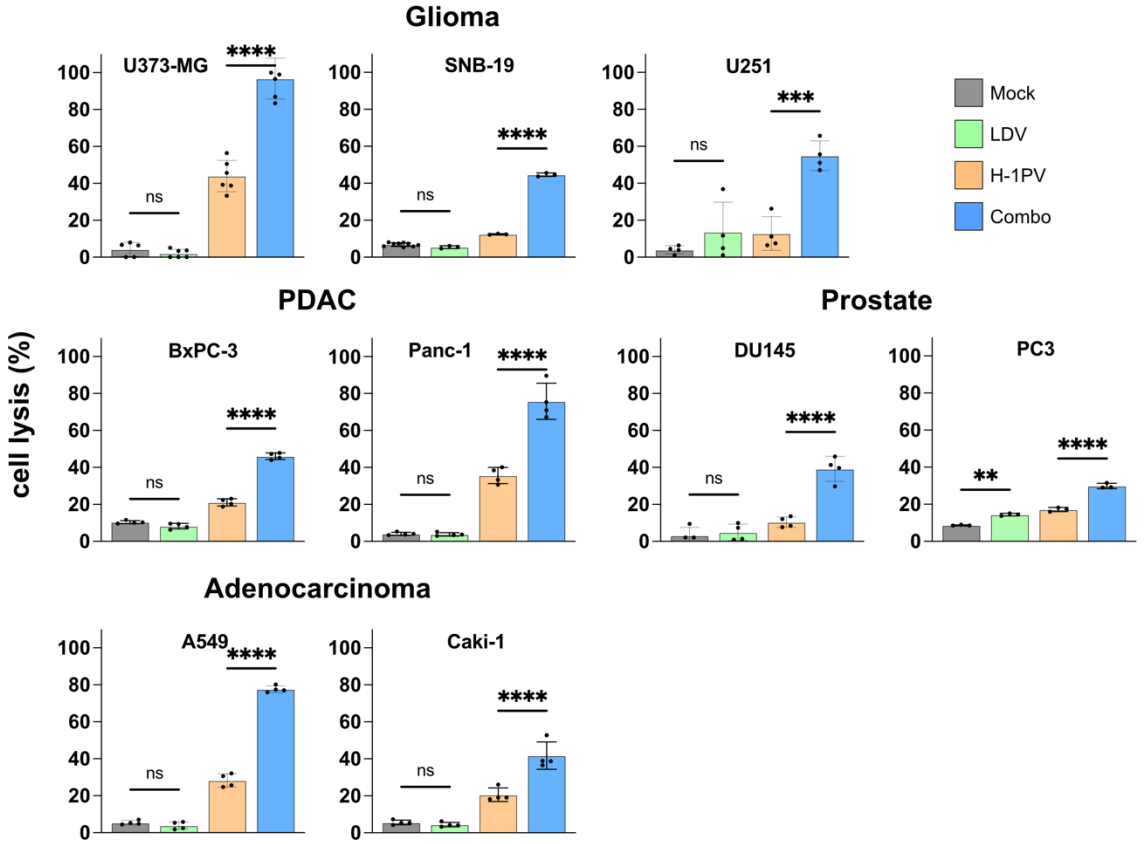

Figure 25. Ledipasvir can potentiate H-1PV-mediated oncolysis in a variety of cell lines from different cancer types. Cell lines were treated with Ledipasvir (LDV), H-1PV, or a combination (Combo) of both treatments and incubated for 96-120h. Cytotoxicity was quantified by measurement of lactate dehydrogenase (LDH) release and normalised to equivalent cells lysed directly before measurement. H-1PV was used at MOI 1 (SNB-19, U251, DU145), MOI 5 (BxPC-3, Panc-1), MOI 10 (PC3, A549), MOI 30 (Caki-1), and MOI 100 (U373-MG). Ledipasvir was used in concentrations of 1µM (U251, BxPC-3, Panc-1, DU145, A549, Caki-1) and 4µM (U373-MG, SNB-19, PC3). Data represent mean ± standard deviation. Significance was measured by one-way ANOVA, * = p≤0.05, ** = p≤0.01, *** = p≤0.001, **** = p≤0.0001. Data was produced by Valérie Palissot and Tiina Marttila.

In this study, I focussed my attention mainly on two cell lines: the glioma cell line U373-MG, and the PDAC cell line AsPC-1. This is for several reasons; firstly, the

oncolytic activity of H-1PV has previously been studied in these two cell lines [192; 203; 254; 293; 294], and they are representative of the two cancer modalities for which H-1PV has been tested in phase I/IIa clinical trials [258; 263]. Secondly, they present a markedly disparate sensitivity to H-1PV alone – while U373-MG cells are relatively sensitive to the virus, AsPC-1 cells are relatively resistant. Nevertheless, the oncolytic effect of H-1PV can be significantly augmented in both cancer cell lines by the addition of Ledipasvir, which alone was innocuous to these cells at all doses tested (Figure 26A-D). Both cell lines can even be sensitised over long time periods to completely sub-lethal doses of H-1PV by the addition of Ledipasvir, as assessed by crystal violet cell staining (Figure 26E and F). Taken together, these results provide evidence that H-1PV and Ledipasvir work in concert to kill cancer cells in a synergistic manner.

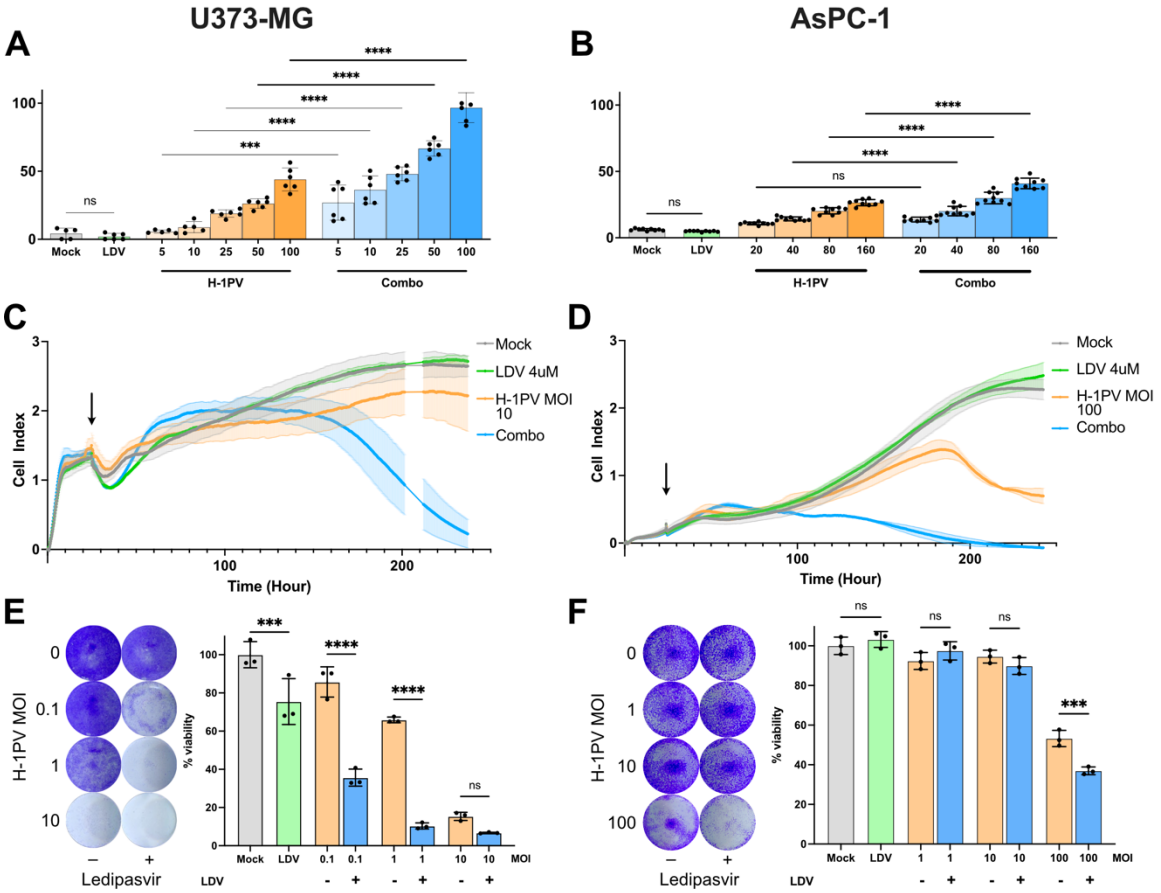

Figure 26. Ledipasvir improves H-1PV-mediated killing of U373-MG and AsPC-1 cell lines, including at sub-lethal doses of H-1PV. U373-MG glioma cells (left panels) and AsPC-1 pancreatic ductal adenocarcinoma cells (right panels) were infected with various MOIs of H-1PV with and without Ledipasvir. **A, B** Cell killing was measured by lactate dehydrogenase activity 96h (U373-MG) or 120h (AsPC-1) post infection. **C, D** Real-time cell growth was measured by the xCelligence system for 10 days and plotted as Cell Index. Arrows indicate the infection and treatment timepoint. **E, F** Cells were infected with H-1PV with or without Ledipasvir treatment and allowed to grow for 7 days, before crystal violet staining. Shown are representative examples of one staining (left) with quantification (right). Data show mean ± standard deviation representative of at least n=2. Significance was measured by one-way ANOVA, *** = p≤0.001, **** = p≤0.0001. xCelligence data and U373-MG assays in A were produced by Valérie Palissot and Tiina Marttila.

I next considered whether the increased cell death in infected and Ledipasvir-treated cells is due to apoptosis. For this, I used real-time microscopy with a caspase 3/7-reactive dye as established previously in our group [236]. I used the pan-caspase inhibitor zVAD-FMK to block apoptosis, as this has previously been shown to effectively block H-1PV- and NS1-mediated apoptosis in transformed cells [202; 236]. H-1PV treatment of both U373-MG and AsPC-1 cells caused an increase in caspase 3 and 7 cleavage, which increased even further upon addition of Ledipasvir (Figure 27A and B). This indicates that caspase-mediated apoptosis does contribute to the cell death caused by the Ledipasvir-H-1PV combination. However, while zVAD-FMK treatment was able to reduce this caspase cleavage, it was not blocked altogether, especially in Combo-treated cells. Furthermore, the addition of zVAD-FMK to either H-1PV or combination treatment with Ledipasvir was unable to affect cell lysis at any concentration tested (Figure 27C and D). Thus, it seems that reducing caspase 3/7 activity in H-1PV or Combo-treated U373-MG and AsPC-1 cells is insufficient to protect them from the oncolytic effects of these treatments. This indicates that there may be other cell death pathways triggered by these treatments able to compensate for the partial inhibition of caspase activity. I concluded that the H-1PV-Ledipasvir combination is associated with an increase in caspase-mediated apoptosis, although this may not be the sole cell death pathway caused by this treatment.

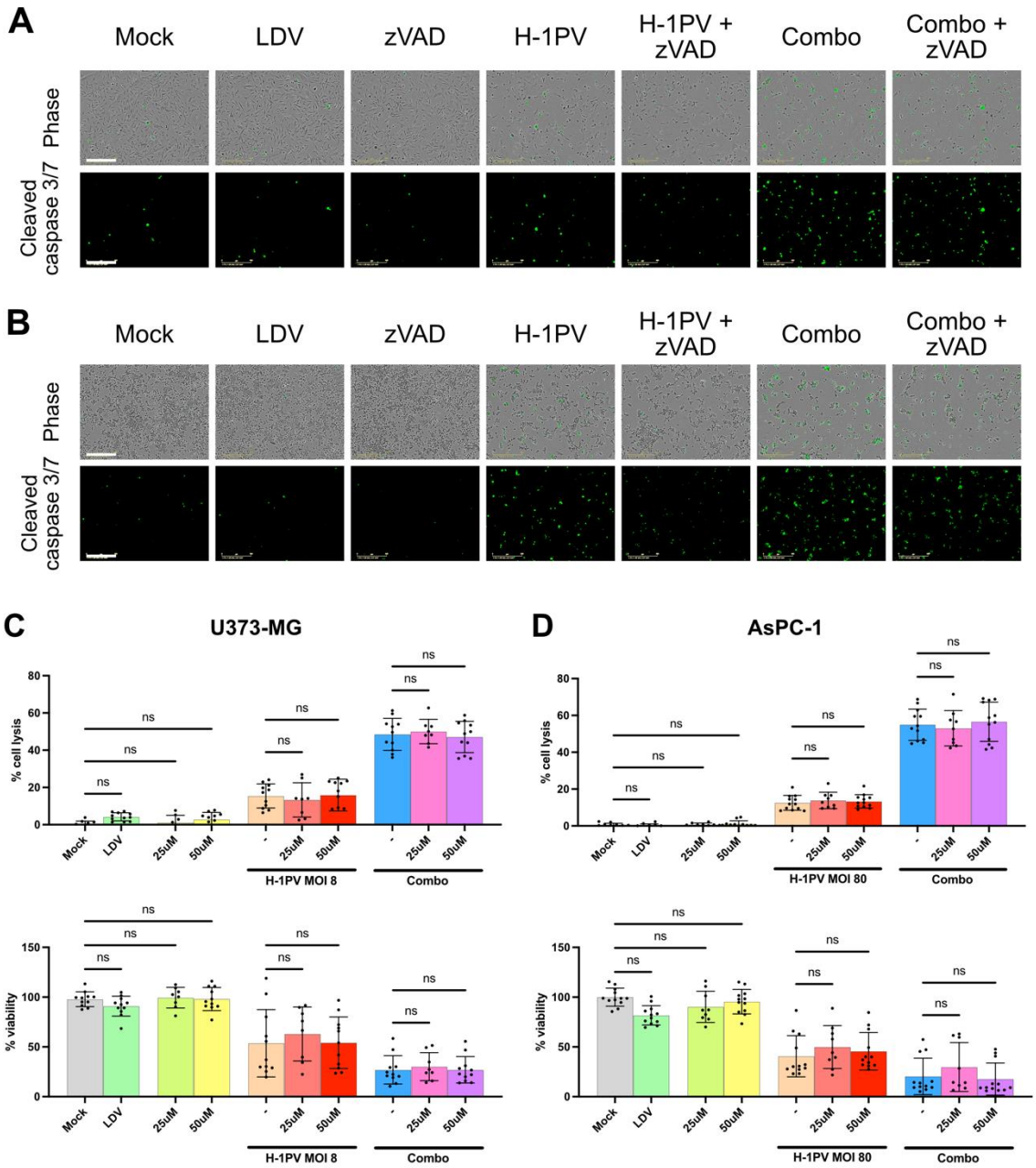

Figure 27. Ledipasvir-mediated oncolysis improvement is at least partially mediated through caspase cleavage. Cells were infected with H-1PV with or without 4μM Ledipasvir co-treatment, in addition to zVAD-FMK (caspase inhibitor) for 72h. Real-time imaging was conducted with a caspase-reactive dye, which emits green fluorescence upon cleavage by caspases 3 and 7. Representative images are shown for each treatment at the 48h timepoint. Co-treatment was tested in both **A** U373-MG cells (H-1PV MOI 8) and **B** AsPC-1 cells (H-1PV MOI 80). After treatment as above, cell lysis was measured by lactate dehydrogenase activity, and cell viability was measured by crystal violet staining in **C** U373-MG and **D** AsPC-1 cells. Scale = 400μm. Data represent mean ± standard deviation of four independent experiments, significance was measured by one-way ANOVA.

In summary, my colleagues identified the antiviral drug Ledipasvir as an FDA-approved candidate drug able to improve H-1PV-mediated oncolysis. They validated this complementarity in a panel of cancer cell lines, showing that the synergistic effect of the Ledipasvir-H-1PV combination is cancer type agnostic. I confirmed that Ledipasvir enhances H-1PV oncolysis and that cell lines particularly resistant to H-1PV can be sensitised to viral oncolysis in the presence of the drug. Finally, I did an initial study to investigate the mechanism of cell death by the Ledipasvir-H-1PV combination and found evidence that Ledipasvir enhances H-1PV-mediated caspase activation, leading to apoptosis. Thus, I set out to further investigate the molecular mechanisms underlying this synergistic anticancer effect.

7.2 Interaction of Ledipasvir with H-1PV

Ledipasvir can effectively potentiate the oncolytic activity of H-1PV in a wide range of cancer cell lines. This is a completely novel use of the drug, as it is an antiviral compound iteratively designed to target the HCV NS5A protein [277]. It is thus rather surprising that Ledipasvir would be capable of potentiating the anticancer activity of a virus unrelated to its target. Therefore, it is important to characterise the molecular mechanisms underlying the enhanced anticancer activity of H-1PV and Ledipasvir. A characterisation of the mechanism behind this synergistic effect may also help guide the identification of other molecules which can be used to potentiate H-1PV oncolysis.

7.2.1 Ledipasvir does not enhance viral replication

To address this, I first considered a potential interaction between Ledipasvir and H-1PV itself. An obvious possibility would be that Ledipasvir might increase viral replication, thus improving oncolysis. I thus performed quantitative polymerase chain reaction (qPCR) to quantify viral genomes after infecting U373-MG cells with and without Ledipasvir co-treatment (Figure 28). Cells were infected with low dose (MOI 0.5) of virus and cultured for up to 120 hours, with samples taken at 4 hours, 24 hours, and 120 hours post infection. Viral DNA was isolated from the samples using a spin-column based method (see Section 11.30 below) before qPCR to quantify the amount of viral DNA present. I assessed both cell pellets and culture supernatant to quantify all viruses present in the system. H-1PV and Combo-treated cells showed the same level of viral genomes in cell pellets 4h after infection and showed no significant differences in either pellets or supernatants 24h after infection. (Figure 28A, B). At the late (120h) timepoint, there was a significant shift in viral genomes from the cell pellet to the supernatant between H-1PV and Combo-treated cells. However, when summed, the total viral genome copies did not change between the treatments (Figure 28C). This result likely reflects the viability of the cells; at this timepoint, there are simply less viable cells left after

combination treatment than H-1PV alone, and therefore more of the virus has been released into the supernatant. Nevertheless, there was no significant difference in the total number of viral genomes produced by infection with H-1PV alone or in combination with Ledipasvir.

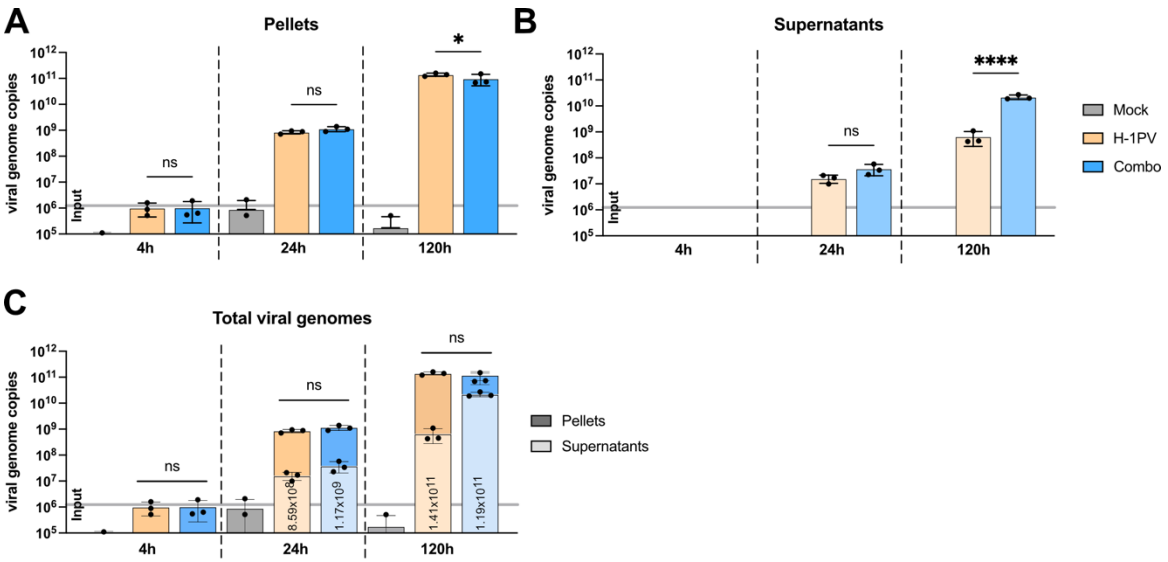

Figure 28. Co-treatment with Ledipasvir does not increase total viral genomes produced by H-1PV infection. U373-MG cells were infected with H-1PV at an MOI of 0.5 with or without Ledipasvir (4µM) co-treatment, and viral genomes were harvested and quantified by quantitative PCR at the indicated timepoints post infection from both **A** cell pellets and **B** cell supernatants. Viral genomes present in the medium mixes used for infection were also quantified (Input). **C** Viral copy numbers measured from both cell pellets and supernatants were added to quantify the total viral genomes present in the system at the indicated timepoints. Average total genome copies are shown written in selected data bars. Data shows mean ± standard deviation of one representative experiment from four independent replicates; significance was measured by one-way ANOVA, * = $p \leq 0.05$, **** = $p \leq 0.0001$.

To confirm this result, I assessed the expression of viral proteins in infected cells. At high multiplicities of infection (MOIs), there were only very small variations in the expression of viral NS1 and VP1/2 proteins with or without Ledipasvir addition in both U373-MG (Figure 29A-C) and AsPC-1 (Figure 29D-F) cells. However, at very low, sublethal MOIs, the expression of NS1 was slightly (albeit non-significantly) elevated in Combo-treated cells, and this discrepancy became increasingly pronounced with time (Figure 29G, H). Meanwhile, the expression of VP1 and 2 did not change (Figure 29G, I), in agreement with my previous observation that there was no increase in viral genomes upon addition of Ledipasvir. Thus, there is no evidence that Ledipasvir enhances H-1PV replication in either U373-MG or AsPC-1 cells.

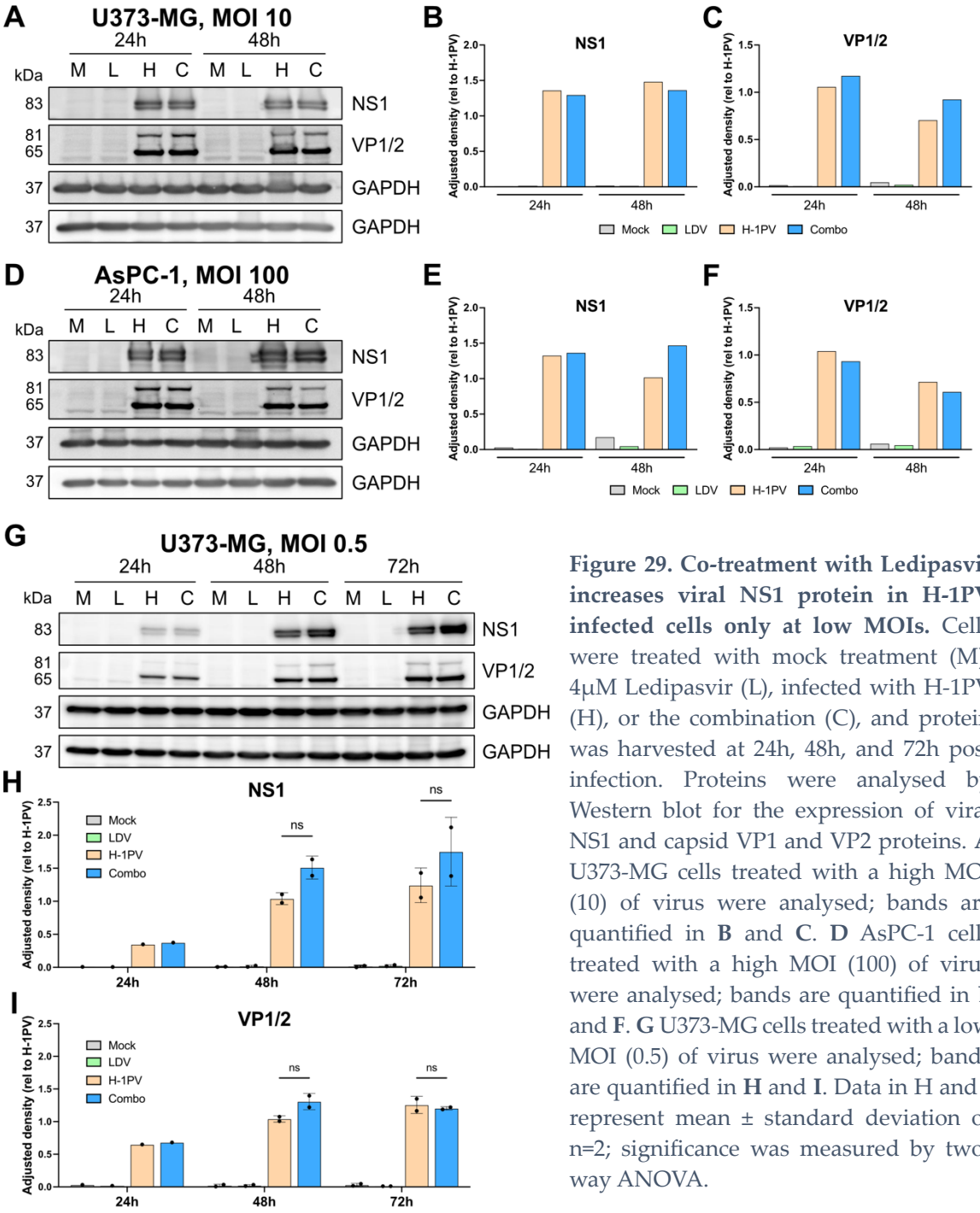

Figure 29. Co-treatment with Ledipasvir increases viral NS1 protein in H-1PV infected cells only at low MOIs. Cells were treated with mock treatment (M), 4µM Ledipasvir (L), infected with H-1PV (H), or the combination (C), and protein was harvested at 24h, 48h, and 72h post infection. Proteins were analysed by Western blot for the expression of viral NS1 and capsid VP1 and VP2 proteins. **A** U373-MG cells treated with a high MOI (10) of virus were analysed; bands are quantified in **B** and **C**. **D** AsPC-1 cells treated with a high MOI (100) of virus were analysed; bands are quantified in **E** and **F**. **G** U373-MG cells treated with a low MOI (0.5) of virus were analysed; bands are quantified in **H** and **I**. Data in H and I represent mean ± standard deviation of n=2; significance was measured by two-way ANOVA.

7.2.2 Ledipasvir enhances NS1-mediated cytotoxicity

I next delved deeper into the potential association between Ledipasvir and the viral NS1 protein, due to the observed increase in NS1 expression when cells were co-treated with Ledipasvir (Figure 29G, H). This is especially interesting, as it is known that NS1 is the main mediator of parvoviral oncotoxicity [195; 200; 202; 234]. As part of this prior work, Georgi Hristov and colleagues established HEK-293T and HeLa cell lines which express the H-1PV *NS1* gene unit under the control of a doxycycline-inducible CMV promoter [202] (Figure 30A). The expression of NS1 alone is enough to lyse these cells; moreover, I found that the addition of Ledipasvir upon induction of NS1 enhanced this cell death, both in HeLa-NS1 (Figure 30B, D, E) and in HEK-NS1 (Figure 30C) stable cell lines. Thus, the Ledipasvir-mediated potentiation of H-1PV oncolysis is at least in part due to an improvement in the cytotoxic effects of NS1 in cancer cells.

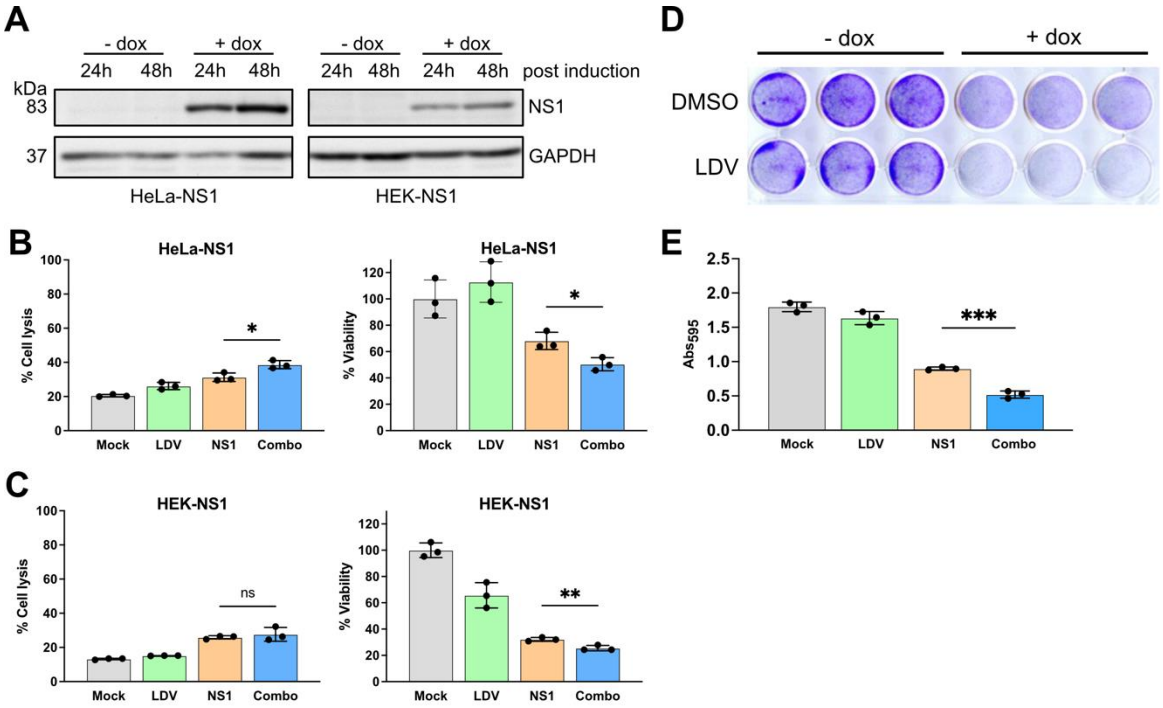

Figure 30. Ledipasvir can potentiate the cytotoxic effects of NS1 alone. A Expression of NS1 protein was induced in HeLa-NS1 and HEK-NS1 cells by 1µg/mL doxycycline (+dox) treatment, leading to efficient induction over 48h. **B** HeLa-NS1 cells were simultaneously induced and treated with 2µM Ledipasvir and cytotoxicity was quantified 72h post infection by lactate dehydrogenase assay (left), while cell viability was quantified by PrestoBlue viability assay (right). **C** HEK-NS1 cells were simultaneously induced and treated with 2µM Ledipasvir and cytotoxicity was quantified 72h post infection by lactate dehydrogenase assay (left), while cell viability was quantified by PrestoBlue viability assay (right). **D** HeLa-NS1 cells were simultaneously induced and treated with 4µM Ledipasvir, and stained with crystal violet 72h post infection. E shows a quantification of the staining. Significance in all graphs was measured by unpaired Student's t-test, * = p≤0.05, ** = p≤0.01, *** = p≤0.001. Data shown are mean ± standard deviation representative of three independent replicates.

Given that Ledipasvir enhanced parvoviral NS1 oncotoxicity, I next considered whether this might be due to a direct interaction between Ledipasvir and NS1. To address this, I used a cellular thermal shift assay (CETSA) [295; 296]. This assay relies on the principle that ligand-bound proteins are more thermostable than their unbound counterparts. Thus, if NS1 binds directly to Ledipasvir, this interaction should protect NS1 against denaturation at high temperatures. To test this, NS1 expression was induced in HEK-NS1 cells, which were lysed to release cellular proteins. This lysate was then incubated with Ledipasvir before dividing the mixture into equal aliquots. Each aliquot was heated to a different temperature, denaturing the NS1 protein. Denatured proteins were removed from solution by centrifugation, and the remaining soluble fraction was detected by Western blotting. If Ledipasvir-treated NS1 shows a stronger band by Western blotting than mock-treated NS1 after high temperature incubation, this would provide first evidence that Ledipasvir interacts directly with NS1 (Figure 31A). I chose to use ATP as a positive control substrate, as this is a known ligand of NS1 [190]. However, NS1 is known to hydrolyse ATP as part of this interaction, which accounts for the limited increase in thermostability of NS1 when incubated with ATP in my assay (Figure 31B and C, red curve). Nevertheless, Ledipasvir could not at any of the concentrations tested improve the thermostability of NS1 above control (Figure 31C, green curve), indicating that a direct interaction between NS1 and Ledipasvir is unlikely.

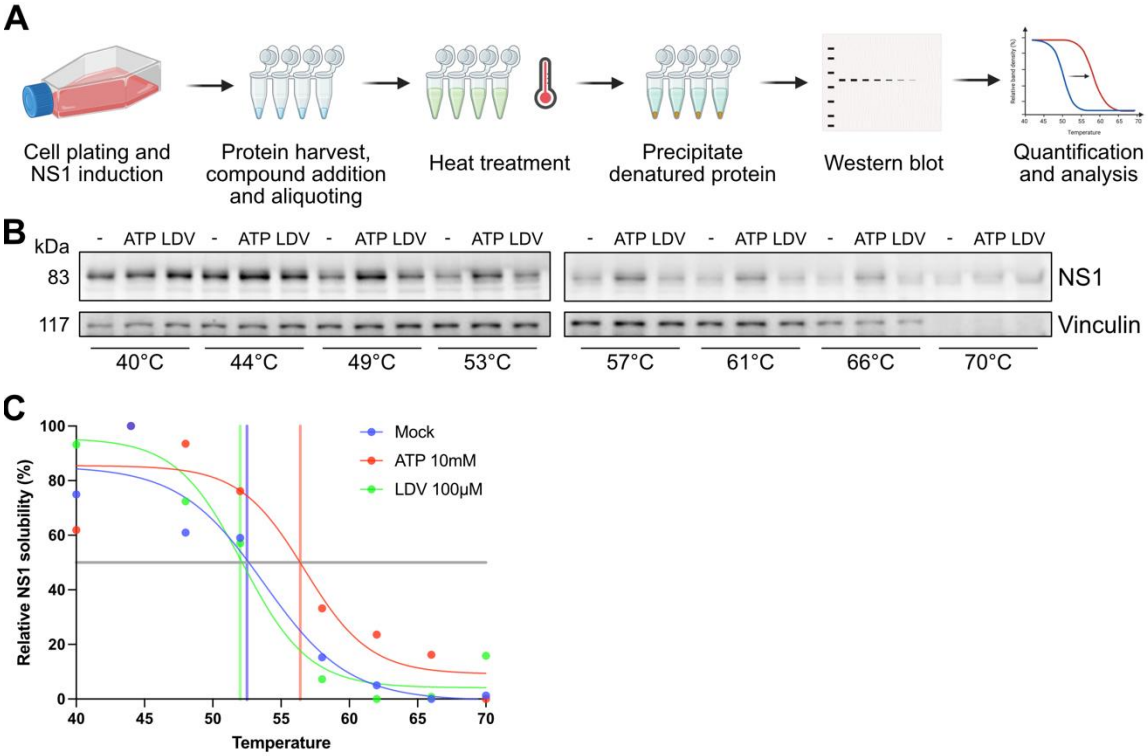

Figure 31. No evidence can be found of a direct interaction between Ledipasvir and NS1 by CETSA assay. A Schematic showing the principle of a Cellular Thermal Shift (CETSA) assay. In general, proteins are more thermostable when bound to a compound, so the thermostability of a protein can be used to infer its ability to bind a putative target. NS1 expression was first induced in HEK-NS1 cells, then protein was harvested from the cells and aliquoted equally. Compounds (ATP or Ledipasvir) were added to each aliquot, and each tube was subjected to heat treatment at a different temperature to denature the protein based on its thermostability. Denatured protein was removed by centrifugation, and remaining soluble protein was separated by SDS-PAGE and Western blotting, and the levels of NS1 remaining in solution at each temperature could then be quantified. Schematic modified from Jafari et al., Nat Protoc, 2014 [295] using BioRender. **B** Western blot showing HEK-NS1 lysates treated with vehicle (-), 10mM ATP, or 100µM Ledipasvir (LDV), showing specific stabilisation of NS1 at high temperatures. **C** Quantification of B, with a clear increase in thermostability of NS1 upon incubation with ATP, but not with Ledipasvir. Band intensities were quantified and normalised between 0-100%, then plotted against temperature. A Boltzmann sigmoidal curve was fit for each treatment. Data shown is representative of two independent experiments in both HEK-NS1 and HeLa cells.

7.3 Interaction of Ledipasvir with the cell

Thus far, I have shown that Ledipasvir is able to potentiate the oncolytic effects of the H-1PV virus in many cellular contexts, and that this potentiation is likely driven through an improvement in the cytotoxic capabilities of the viral NS1 protein. However, based on my results it is unlikely that there exists a direct interaction between Ledipasvir and NS1. Therefore, I now turned my attention towards any effects that Ledipasvir might have on cellular signalling to potentiate NS1 cytotoxicity. This section details three approaches used to investigate the impact of Ledipasvir and its combination with H-1PV on cellular signalling and processes. Firstly, a Cell Painting assay was used to infer the effect of Ledipasvir alone on cells, independently of H-1PV infection. Secondly, a kinosome screening was used to examine the interactions between Ledipasvir, H-1PV, and cellular signalling pathways. Finally, RNA sequencing was used to determine the impact of Ledipasvir and H-1PV, both alone and in combination, on gene expression.

7.3.1 Cell Painting provides evidence that Ledipasvir modulates PI3K signalling

To investigate which morphological changes, if any, Ledipasvir induces in cells independently of H-1PV infection, I considered a Cell Painting assay conducted and analysed by our collaborators Laurent Brino and Zahra Hanifehlou [297]. Here, U2OS osteosarcoma cells were treated with a library of 7120 different compounds, including Ledipasvir, with known modes of action at two different concentrations, 625nM and 1.25µM. After treatment, cells were stained with multiplexed fluorescent dyes to image eight different cellular organelles by fluorescent microscopy. High-throughput imaging and automated image analysis were then used to extract ~1500 morphological features and produce a morphological profile (or fingerprint) for each compound (Figure 32A). The fingerprint of Ledipasvir was then compared with the profiles of all other compounds in the library. It is presumed in this assay that compounds with a similar mode of action to each other will induce similar morphological changes in cells in response to treatment. Thus, compounds which induce a similar fingerprint to Ledipasvir may also perturb similar pathways and molecules. The top 12 compounds with the most similar fingerprints to Ledipasvir from this assay are shown in Figure 32B. Strikingly, five of these 12 compounds are known inhibitors of PI3K, while four others are inhibitors of PI3K-related pathways or upstream signalling receptors (Raf, MAPK, EGFR and VEGFR).

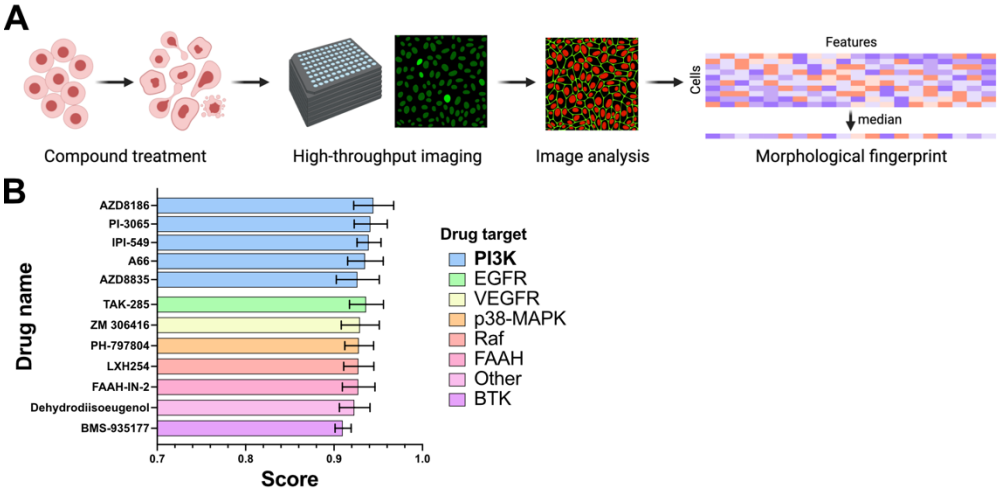

Figure 32. Cell Painting screen indicates the Ledipasvir may interact with the PI3K signalling axis. A Schematic showing the principle of Cell Painting. U2OS osteosarcoma cells were plated and treated with a library of compounds at two different concentrations (625nM and 2.5μM), after which distinct cellular organelles were visualised with multiplexed dyes in high-throughput immunofluorescent microscopy. Artificial intelligence-based image analysis defined morphological features to generate a "fingerprint" from each compound. Schematic adapted from Bray et al., Nat Protoc, 2016 [297] using BioRender. **B** Comparison of the Ledipasvir "fingerprint" to all other compounds in the dataset by K-nearest neighbour analysis led to a shortlist of 12 top compounds, grouped here by molecular target. Data is represented as mean score ± standard deviation. Cell Painting experiments and data analysis were executed by Laurent Brino and Zahra Hanifehlou, Ksilink, France.

7.3.2 PamGene kinase profiling suggests that Akt1 is activated by the Ledipasvir-H-1PV combination

Ledipasvir may also have an influence on cellular signalling in the context of an H-1PV infection. To this end, my colleagues Valérie Palissot and Tiina Marttila treated U373-MG cells with Ledipasvir, H-1PV, and the combination, and assessed the kinase activity in the cells by PamGene kinase activity profiling [298]. In this assay, cellular lysate is pumped over a chip with an array of covalently bound peptides, which serve as substrates for the kinases present in the lysate. The phosphorylation of these substrates on the chip can then be measured by fluorescence-conjugated antibody staining, leading to a phosphorylation pattern on the array which depends on the kinase activity in the cellular lysate (Figure 33A). Bioinformatic analysis can then be used to infer the most likely activity states of each kinase in the sample from the phosphorylation pattern. This assay was conducted for both phosphotyrosine kinases and serine-threonine kinases and analysed by PamGene. Interestingly, Ledipasvir alone at the concentration used does not majorly affect kinase activity in cells compared to DMSO-treated control cells, at any time (Figure 33B). Secondly, combination treatment of H-1PV and Ledipasvir seemingly flips the kinase activity profile in cells compared with H-1PV alone. In the case of phosphotyrosine kinases, this assay showed slight but significant decrease in global phosphotyrosine kinase activity upon H-1PV

treatment alone. However, in the Combo condition, there was a very significant increase in phosphotyrosine kinase activity, especially at the early timepoint (24h). In addition, H-1PV seems to have a highly time-dependent effect on serine-threonine kinases; early in infection (24h), their activity is strongly driven by the virus, but by late infection (72h), it is hindered. As before, in the Combo treatment there is a strong increase in serine-threonine kinase activity compared with mock-treated cells, regardless of timepoint.

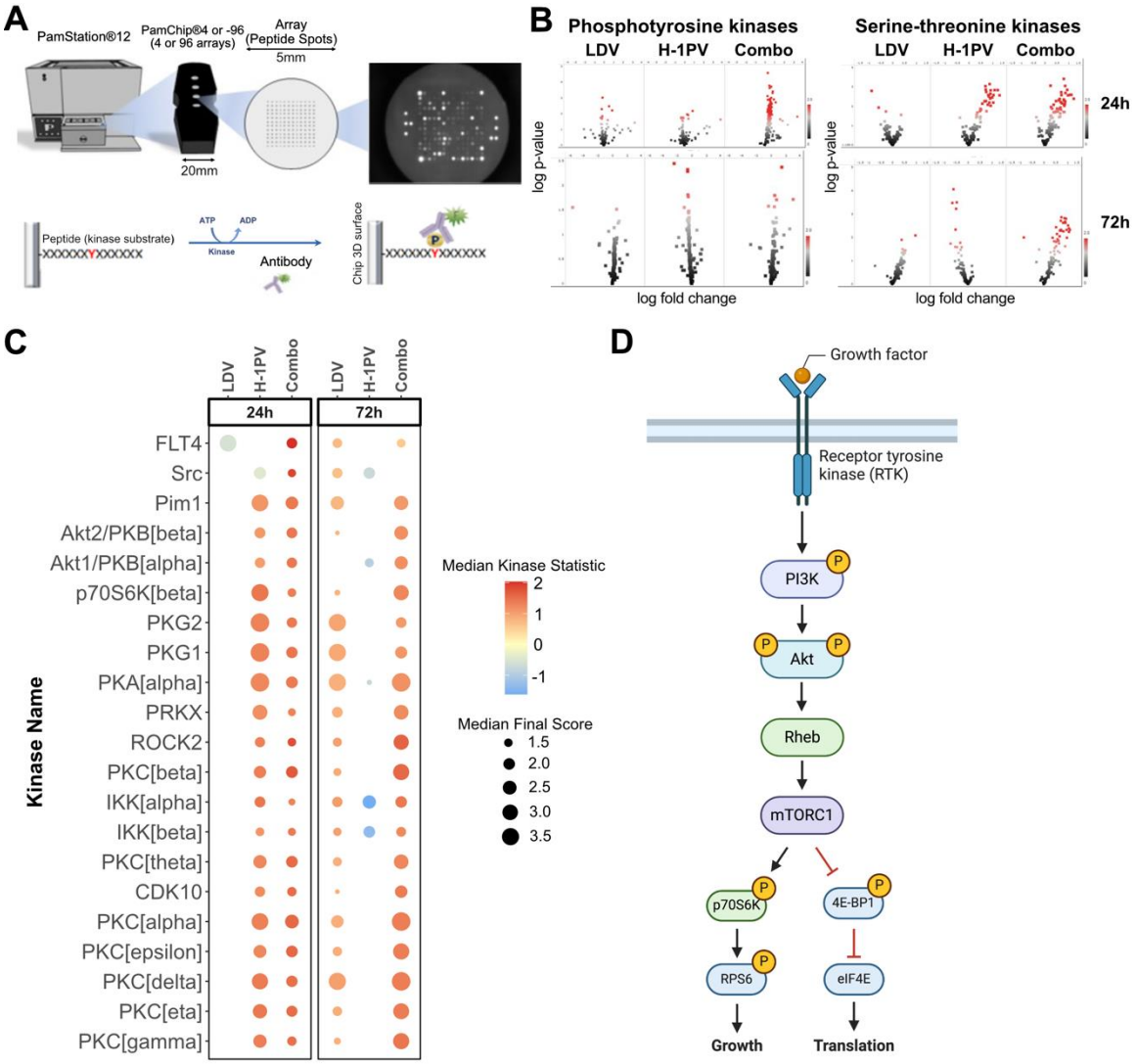

Figure 33. PamGene kinase screening indicates significant regulation of Akt signalling by the Ledipasvir-H-1PV combination. A Schematic of PamGene kinase screening (supplied, PamGene). Arrays of peptide spots are printed on PamChips, over which cellular lysate is washed in a PamStation. Active kinases in the lysate phosphorylate peptides in the spots, which can be detected by antibody-based fluorescence. The total kinase activity in the sample can thus be inferred, and bioinformatic Upstream Kinase Analysis (UKA) can be used to predict the activity of specific kinases based on the phosphorylation patterns on the PamChip. For this analysis, U373-MG cells were treated with 4μM Ledipasvir (LDV), H-1PV at MOI 10, or both treatments combined (Combo) for 72h and the kinase activity in cellular lysates was compared to control (0.08% DMSO) treatment. **B** Volcano plots showing total kinase activity in cells with the indicated treatments as measured by PamGene screening. Red spots are peptides that show significant difference compared to control

($p<0.05$). Two PamChips were used; one to measure phosphotyrosine kinase activity, and one for serine-threonine kinase activity. **C** Putative upstream kinases with differential activity identified in at least two of three treatments at both 24h and 72h post treatment. Kinases with the top significance scores (Median Final Score cutoff 1.2) are shown, with effect size and direction (Median Kinase Statistic) denoted by colour (blue is inhibition, red is activation compared to control treatment) and significant (Median Final Score) denoted by dot size. **D** Simplified schematic of the PI3K/Akt/mTORC1 signalling pathway. Activation of PI3K leads to Akt phosphorylation, which can activate mTORC1 through Rheb. mTORC1 phosphorylates both p70S6K and 4E-BP1, leading to cell growth and translation. For more details, see Section 5.8 above. Figure made using BioRender.

I next considered the predicted kinase activity from Upstream Kinase Analysis (UKA) by PamGene. Here, I combined the predicted activities of both phosphotyrosine and serine-threonine kinases from the UKA. I then filtered kinases for significance and effects in at least two of three conditions across both timepoints analysed (Figure 33C). Unexpectedly, this assay showed that Ledipasvir affects a greater number of distinct kinases than H-1PV after 72 hours of treatment (Figure 33C). This is despite the finding that there is lower differential regulation of global phosphorylation at the same timepoint (Figure 33B). In addition, at the late timepoint, H-1PV reduced the activity of all kinases that it influenced – a stark contrast with the strong activation seen at the early timepoint. Combining the two treatments once again flipped this phenotype, resulting in a stronger activation of kinases at the late timepoint than Ledipasvir alone.

UKA analysis additionally resulted in an enrichment of kinases known to affect replication and cytotoxicity of parvoviruses, especially the protein kinase C (PKC) family [195; 198; 299]. PKC family members were activated by H-1PV alone at the early timepoint, but by the late timepoint their activity was not significantly different to mock treatment. The combination of Ledipasvir and H-1PV, however, sustained the activation of PKC family members throughout both early and late infection, consistent with an increased oncotoxicity of the combination treatment compared with H-1PV alone. Additionally, Akt1 and p70S6K, both downstream kinases in the PI3K pathway (Figure 33D), show increased activity in Combo-treated cells compared with H-1PV alone at both timepoints. Ledipasvir alone was also able to activate Akt2 and p70S6K at 72h post treatment, consistent with Cell Painting analysis (Figure 32). This assay also revealed putative novel kinases that may play a role in H-1PV infection, or indeed the effect of the Combo treatment, most notably Src kinase. Src was the single kinase whose treatment was downregulated by H-1PV alone at both timepoints tested, in contrast to a strong activation of Src by the combination treatment at the early timepoint. Src is a proto-oncogene with pleotropic functions in cell proliferation, which can be activated by growth factor receptor signalling and functions together with Akt [300; 301].

7.3.3 Akt is hyperactivated by the Ledipasvir-H-1PV combination

Based on the integrated results from both the Cell Painting assay and the PamGene kinase profiling, I moved on to validate kinase activities in Combo-treated cells. I focussed on PI3K and Akt signalling as this pathway was strongly indicated by both screens, as well as Src kinase as a putative novel factor in H-1PV oncolysis. I was unable to verify the PamGene screening results that H-1PV inhibits the activity of Src kinase (data not shown). Western blotting for Akt phosphorylation indeed showed that there is a marked increase in the activating phosphorylation S473 on Akt in Combo-treated cells compared with H-1PV (Figure 34A). However, neither inhibition of PI3K (Figure 34B) nor Akt (Figure 34C) could block the effects of Ledipasvir addition to H-1PV oncolysis. Western blotting confirmed that both inhibitors at the doses used are functional in the context of H-1PV infection (Figure 34D). Therefore, I concluded that while Akt is hyperactivated by Ledipasvir-H-1PV combination treatment, this activation may not be the cause of increased oncolysis.

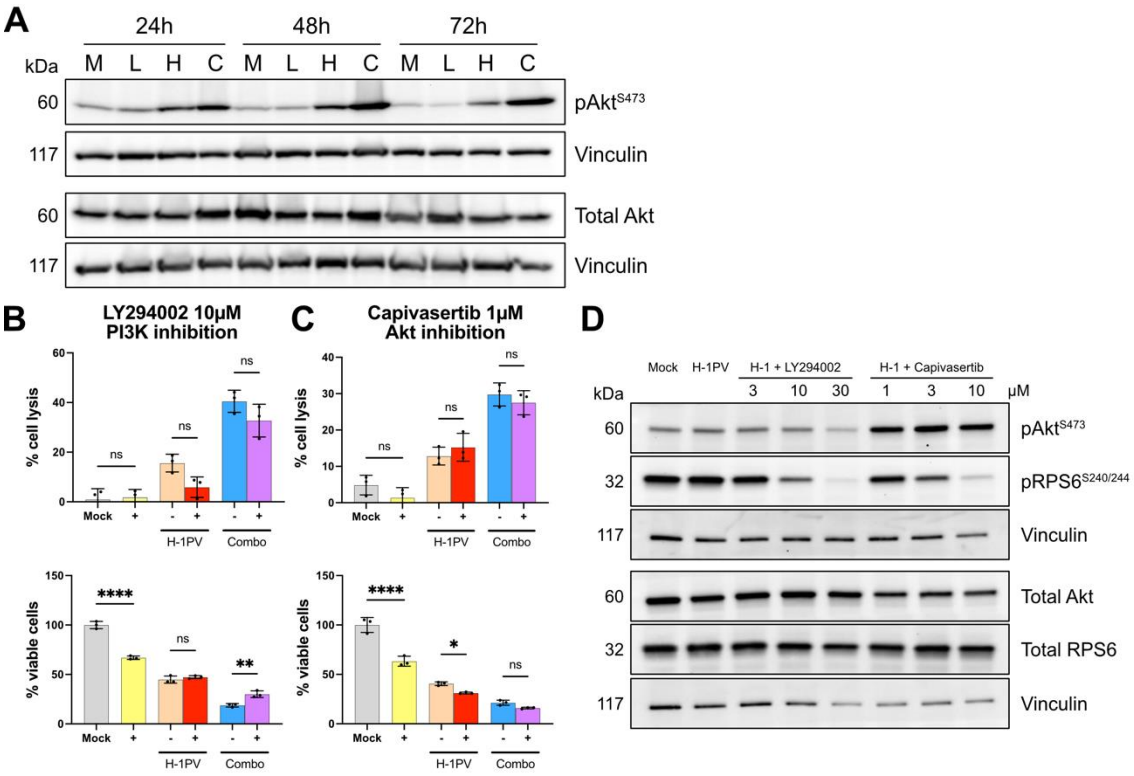

Figure 34. Ledipasvir and H-1PV combination treatment hyperactivates Akt. A Western blot of U373-MG cells treated with mock treatment (M), 4µM Ledipasvir (L), infected with H-1PV MOI 10 (H), or the combination (C) for 24h, 48h, and 72h, showing an increase in PI3K activity as measured by Akt phosphorylation at Ser-473. **B** U373-MG cells were infected with MOI 10 H-1PV with or without 4µM Ledipasvir co-treatment, in addition to 10µM LY294002 (PI3K inhibitor) for 72h. Cell lysis was measured by lactate dehydrogenase activity, and cell viability was measured by crystal violet staining. **C** U373-MG cells were infected with MOI 10 H-1PV with or without 4µM Ledipasvir co-treatment, in addition to 1µM Capivasertib (Akt inhibitor) for 72h. Cell lysis was measured by lactate dehydrogenase activity, and cell viability was measured by crystal violet staining. **D** Functionality of both inhibitors in the context of H-1PV infection was tested by Western blotting. U373-MG cells were infected with MOI 10 of H-1PV and co-treated with the indicated concentrations of inhibitors for 48h. Data for LY294002 is representative of two independent experiments in U373-MG and AsPC-1 cell lines, data for Capivasertib is from one experiment. Data represent mean ± standard deviation; significance was calculated by one-way ANOVA; * = p≤0.05, ** = p≤0.01, **** = p≤0.0001.

7.3.4 RNA sequencing implicates translation in the combinatorial mechanism

Concurrently with functional screening, my colleagues Valérie Palissot and Tiina Marttila also conducted RNA sequencing of U373-MG cells treated with Ledipasvir, H-1PV, and the combination of both, harvesting RNA from cells after 24, 72, and 96 hours. I then worked in collaboration with Yunhee Jeong to analyse the data from this experiment. From Uniform Manifold Approximation and Projection (UMAP) analysis it became clear that in the early timepoint (24h, Figure 35A, left panel), there are minimal disparities in gene expression between mock, Ledipasvir, H-1PV, and Combo-treated cells. However, samples diverge at the late timepoints (72h and 96h) and form two distinct clusters: one containing mock and Ledipasvir-treated cells, and the other containing H-1PV and Combo-treated cells (Figure 35A, middle panel). I therefore chose to perform Gene Set Enrichment Analysis (GSEA) on both late timepoints combined. Comparing each treatment to mock-treated cells, I saw that Ledipasvir has a minimal impact on cellular transcription at 72-96 hours, as there were no significantly enriched genesets (false discovery rate (FDR) < 5%) (Figure 35B). H-1PV treatment, on the other hand, showed significant enrichment of 20 genesets with differential regulation to mock treatment, the majority of which were upregulated upon infection (Figure 35C). Curiously, combination treatment reversed this phenotype, with a majority of 16 significantly enriched genesets being downregulated compared to the mock treatment (Figure 35D). Interestingly, I saw a significant enrichment of the PI3K-Akt-mTOR signalling pathway when comparing Combo to Mock treatment (Figure 35E). This pathway was not significantly enriched in Ledipasvir or H-1PV vs Mock comparisons, in line with the increased activation of Akt in Combo compared with H-1PV seen previously (Figure 34A).

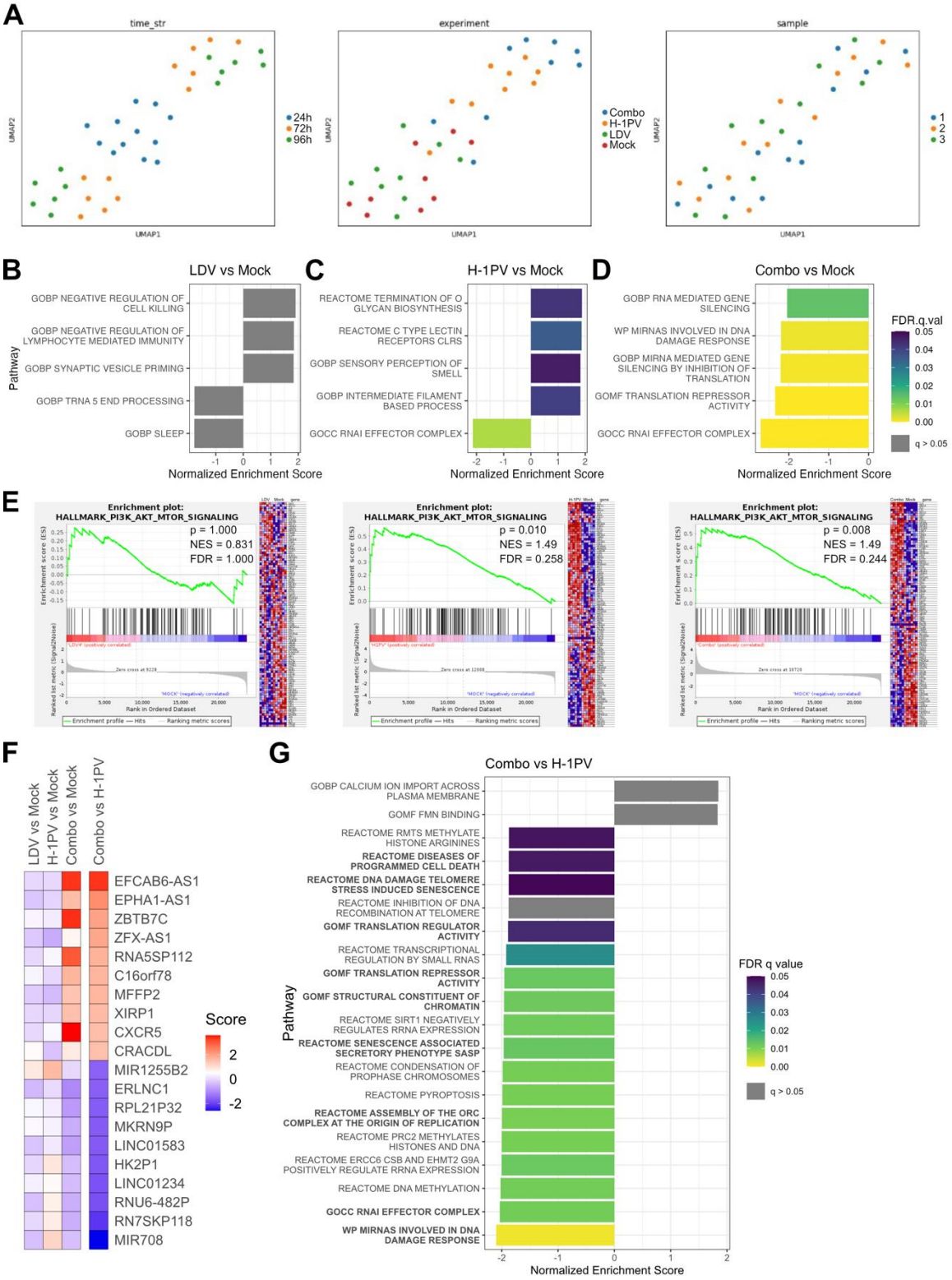

Figure 35. RNA sequencing indicates that cell death and translation are modulated in combination treatment. A UMAP plots of bulk RNA sequencing data showing divergence of cell expression over time (left panel) into Mock-Ledipasvir and H-1PV-Combo clusters (middle panel), and that there are no batch effects between sample replicates (right panel). Gene Set Enrichment Analysis (GSEA) was performed comparing **B** Ledipasvir, **C** H-1PV, and **D** Combo treatment to mock-treated cells at late timepoints (72h and 96h post infection). Pathways were considered enriched if they had a false discovery rate (FDR) below 5%. Plots show the 5 most significantly enriched genesets. **E** Activation of PI3K signalling was compared between the above-mentioned

conditions, with significance only reached in Combo-treated cells (FDR < 0.25). **F** Heatmap showing the top 10 up- and downregulated transcripts when comparing Combo treatment to H-1PV alone, compared with the relative expression of these transcripts in each comparison to Mock. **G** Barplot showing all significantly enriched (FDR < 0.05) pathways when comparing Combo treatment to H-1PV alone. Bioinformatic analysis was conducted in collaboration with Yunhee Jeong.

I also performed a comparison between Combo and H-1PV-treated cells in both late timepoints combined. This is a different approach than a comparison of each treatment to mock-treated cells, as has been performed here and in the screens described previously (Cell Painting and kinase profiling). The top 10 up- and downregulated genes in this comparison are shown in Figure 35F, together with their relative expressions in comparisons of each treatment to mock. Interestingly, there is an enrichment of antisense RNA species differentially regulated in Combo-treated cells compared to H-1PV. When performing GSEA analysis, 17 gene sets were significantly enriched (FDR < 5%) (Figure 35G). These genesets were all downregulated in the combination treatment compared to H-1PV alone. Most strikingly, and in agreement with the top differentially regulated genes, many genesets related to translation repression were significantly downregulated in the combination treatment, indicating that H-1PV and Ledipasvir co-treatment may affect translation. Several genesets related to chromosomal replication were also downregulated in combination-treated cells, which may point to an increase in cell cycle arrest induced by the virus-drug combination. Finally, senescence and apoptosis-associated genesets were also downregulated in Combo-treated cells compared with H-1PV alone, suggesting that cells treated with the combination of H-1PV and Ledipasvir are less capable of shielding themselves against H-1PV-mediated cell lysis by the induction of senescent or apoptotic signalling pathways (Figure 35F).

7.4 Inhibiting the Ledipasvir-H-1PV combination

I next integrated the three screens described – Cell Painting, kinase profiling, and RNA sequencing – as well as considered some other plausible possibilities based on my observations to perform a small-scale drug screening of potential candidates that could block the combination effect of Ledipasvir and H-1PV. I chose tauroursodeoxycholic acid (TUDCA, ER stress inhibitor), A23187 (calcium ionophore to induce ER stress), Vitamin C (deoxidase), Phenytoin (sodium channel blocker), and Torin (mTOR inhibitor). I tested the effects of each of these compounds when added to the Ledipasvir-H-1PV combination in U373-MG cells (Figure 36A). A23187 and Vitamin C were both toxic at the concentrations tested, and TUDCA was ineffective at blocking the combination effect. However, both Phenytoin (Figure 36B) and Torin (Figure 36C) were able to reduce the cell killing by Ledipasvir and H-1PV to comparable levels to H-1PV alone. In a second round of validation, Phenytoin could block the Ledipasvir-H-1PV combination in U373-MG cells (Figure 36D). However, in AsPC-1 cells, Phenytoin contributed

significantly to cell death when used in addition to H-1PV (Figure 36E). Furthermore, Phenytoin caused significant toxicity to both cell lines independent of Ledipasvir or H-1PV. Conversely, Torin was minimally effective at blocking H-1PV-mediated cell lysis in both U373-MG and AsPC-1 cells, while significantly reducing the effectiveness of the Ledipasvir-H-1PV combination treatment. It is important to note that Torin treatment did significantly reduce cell growth in both cell lines tested, leading to lower viability compared with mock treatment (Figure 36D and E, lower panel), however this does not reflect active lysis, except in the highest concentration treatment of U373-MG cells (Figure 36D, upper panel). Thus, the cell death caused by Ledipasvir and H-1PV combination treatment, but not H-1PV alone, can be blocked by Torin.

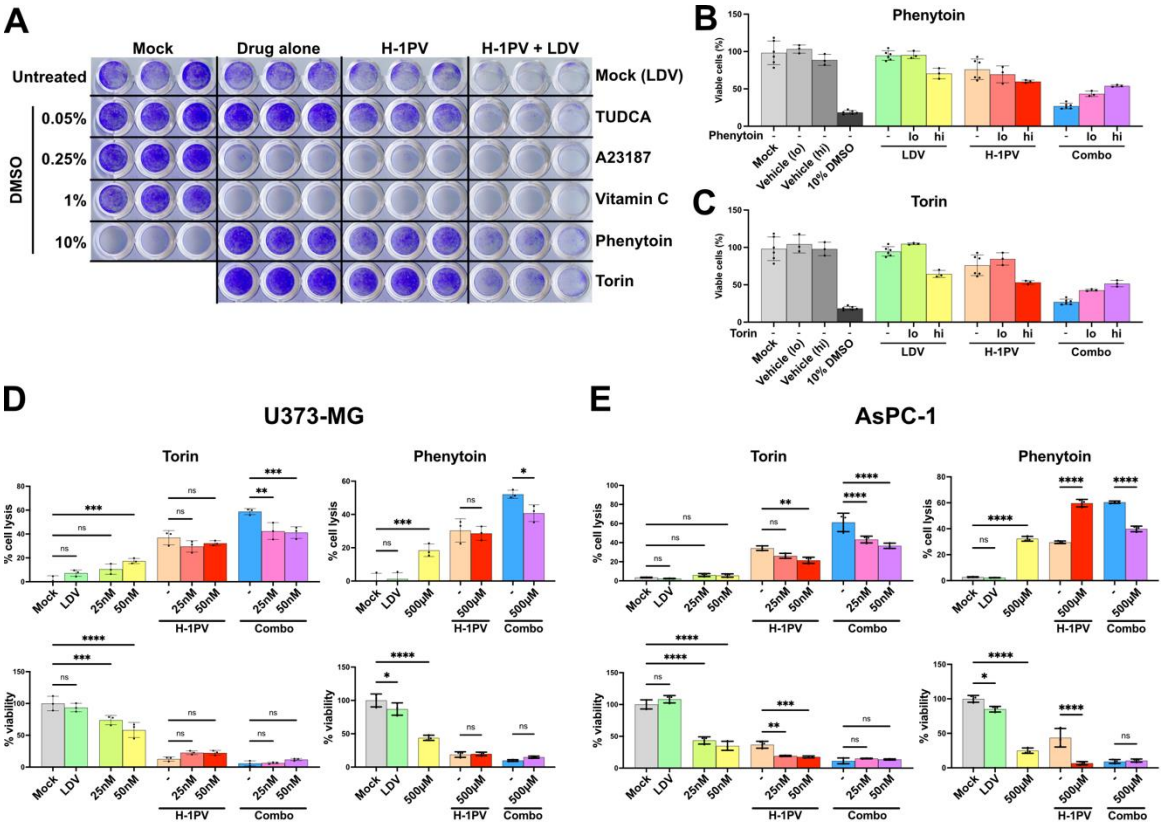

Figure 36. Small-scale drug screening identifies Torin as an inhibitor of improved oncolysis by Ledipasvir. A U373-MG cells were treated with each indicated drug at two different concentrations (Drug), H-1PV MOI 8 (H-1PV), or the combination of H-1PV MOI 10 with 4µM Ledipasvir (H-1PV + LDV) plus the indicated drug. Cells were stained with crystal violet after 72h. **B** Quantification of cell viability from A for the drug Phenytoin. Lo = 250µM, hi = 500µM. **C** Quantification of cell viability from A for the drug Torin. Lo = 25nM, hi = 50nM. A second validation screening to confirm the inhibitory effects of Torin and Phenytoin on combination treatment was then conducted. **D** U373-MG and **E** AsPC-1 cells were treated as in A, using H-1PV MOIs 10 (U373-MG) and 100 (AsPC-1), and cultured for 96h before measurement of cell lysis by lactate dehydrogenase assay and cell viability by crystal violet staining. Data represent mean ± standard deviation; significance was calculated by one-way ANOVA; * = p≤0.05, ** = p≤0.01, *** = p≤0.005, **** = p≤0.0001.

7.4.1 mTOR inhibitors can block the synergistic effects of Ledipasvir and H-1PV

Thus far, Torin is the only compound that I had tested which was able to block the combinatorial effect of Ledipasvir and H-1PV, while not affecting H-1PV lysis by itself. Therefore, I examined whether other inhibitors of mTOR would also be able to block the combination effect of Ledipasvir with H-1PV. I chose Rapamycin, as it uses a different mechanism than Torin to inhibit mTOR. Torin directly binds to mTOR in an ATP-competitive manner, blocking both mTOR complex 1 and 2 (mTORC1 and 2) functions [302], whereas Rapamycin binds to FKBP12, allowing the complex to inhibit mTORC1 only [289]. I saw in U373-MG cells that both inhibitors were able to significantly reduce cell lysis by the combination treatment while not affecting H-1PV alone, although Rapamycin was slightly less effective than Torin (Figure 37A and B). Real-time analysis of cells also showed that both Torin and Rapamycin could stunt cell killing by the combination treatment (Figure 37C and D). Note here that the confluence of each treatment was normalised to its respective control at each time point, to account for the effect of mTOR inhibition on the growth of the cells seen previously. To confirm that each inhibitor was indeed blocking mTOR at the concentrations used, I assessed phosphorylation of two major downstream targets of mTORC1, responsible broadly for cell size regulation (RPS6), and proliferation and translation (4E-BP1) [287] (Figure 37E). Here, it was clear that while both inhibitors efficiently abrogated RPS6 phosphorylation (Figure 37F), Torin was more effective at blocking 4E-BP1 phosphorylation than Rapamycin (Figure 37G).

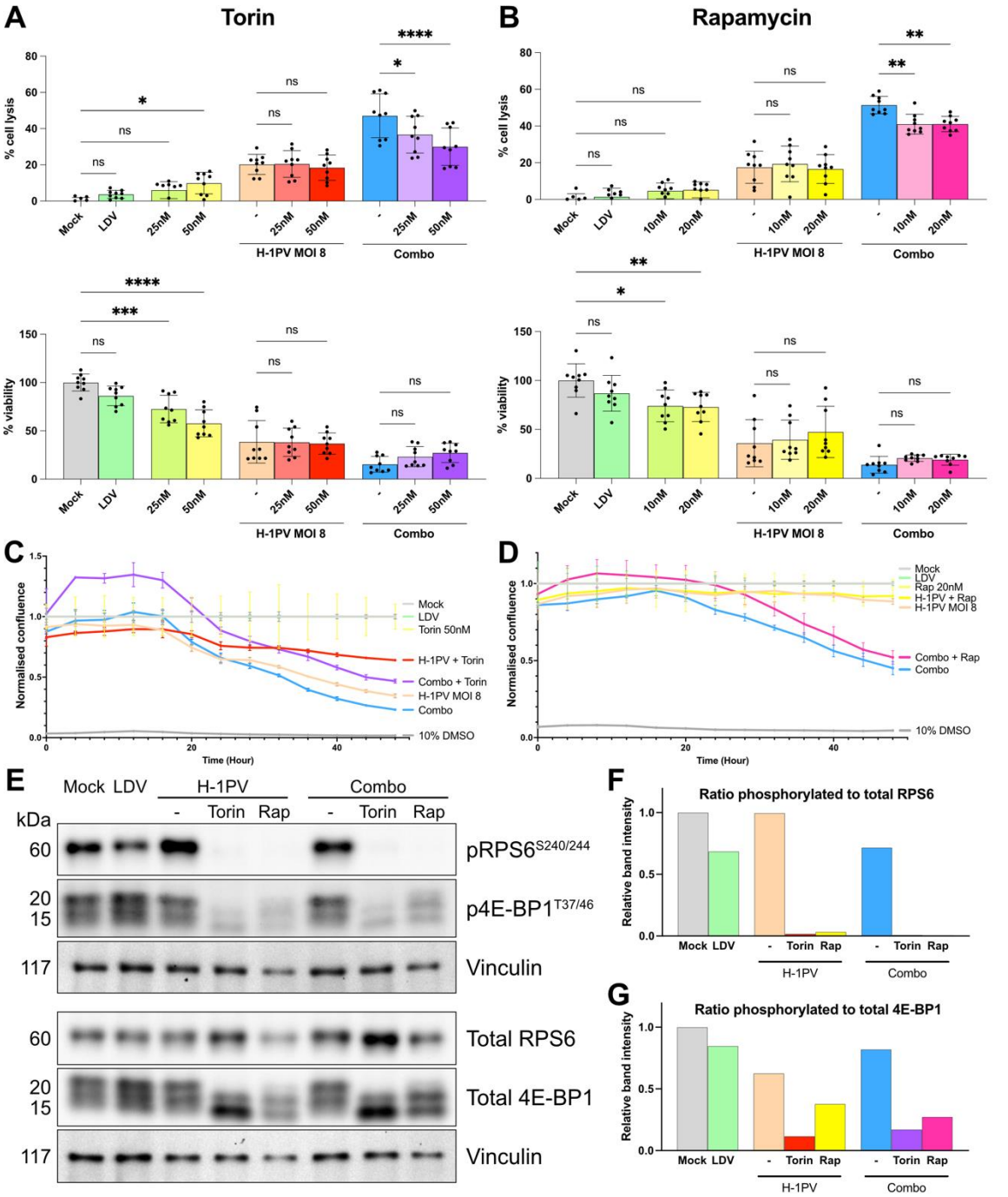

Figure 37. Ledipasvir-mediated improvement in oncolysis can be rescued by mTOR inhibition in U373-MG cells. U373-MG cells were infected with H-1PV MOI 8 with or without 4μM Ledipasvir co-treatment, in addition to **A** Torin or **B** Rapamycin treatment. Cell lysis was measured by lactate dehydrogenase activity, and cell viability was measured by crystal violet staining 72h after treatment. Real-time cell growth was also monitored by the Incucyte imaging system for 48h after infection of cells with H-1PV MOI 8 with or without 4μM Ledipasvir co-treatment, in addition to **C** Torin or **D** Rapamycin treatment. Cell confluence was normalised to the appropriate treatment controls, as mTOR inhibition hinders cell growth. **E** Cells were treated as above with the highest used concentrations of mTOR inhibitors for 48h before harvesting protein for Western blotting to test the functionality of both inhibitors in the context of H-1PV infection. **F** Quantification of the ratio between phosphorylated and total RPS6 in E, adjusted for vinculin signal. **G** Quantification of the ratio between phosphorylated and total 4E-BP1 in E, adjusted for vinculin signal. Cell killing and viability experiments show three independent experiments, Incucyte curves are representative of two independent experiments. Data represents mean ± standard deviation; significance was measured by one-way ANOVA, * = p≤0.05, ** = p≤0.01, *** = p≤0.001, **** = p≤0.0001.

The discrepancy in effect between Torin- and Rapamycin-mediated mTOR inhibition was even more striking in AsPC-1 cells (Figure 38). Here, only Torin was able to inhibit cell lysis by the combination treatment, whereas Rapamycin treatment was completely ineffective (Figure 38A and B). This effect was also mirrored in real-time analysis of cell growth under the same conditions (Figure 38C and D). Crucially, while both inhibitors were again able to abrogate most RPS6 phosphorylation (Figure 38F), Rapamycin was almost completely ineffective in these cells at blocking phosphorylation of 4E-BP1 (Figure 38G). These results indicate that activity of mTOR, particularly its downstream activation of cellular proliferation and translation through 4E-BP1, is necessary for the synergistic effect of Ledipasvir co-treatment with H-1PV.

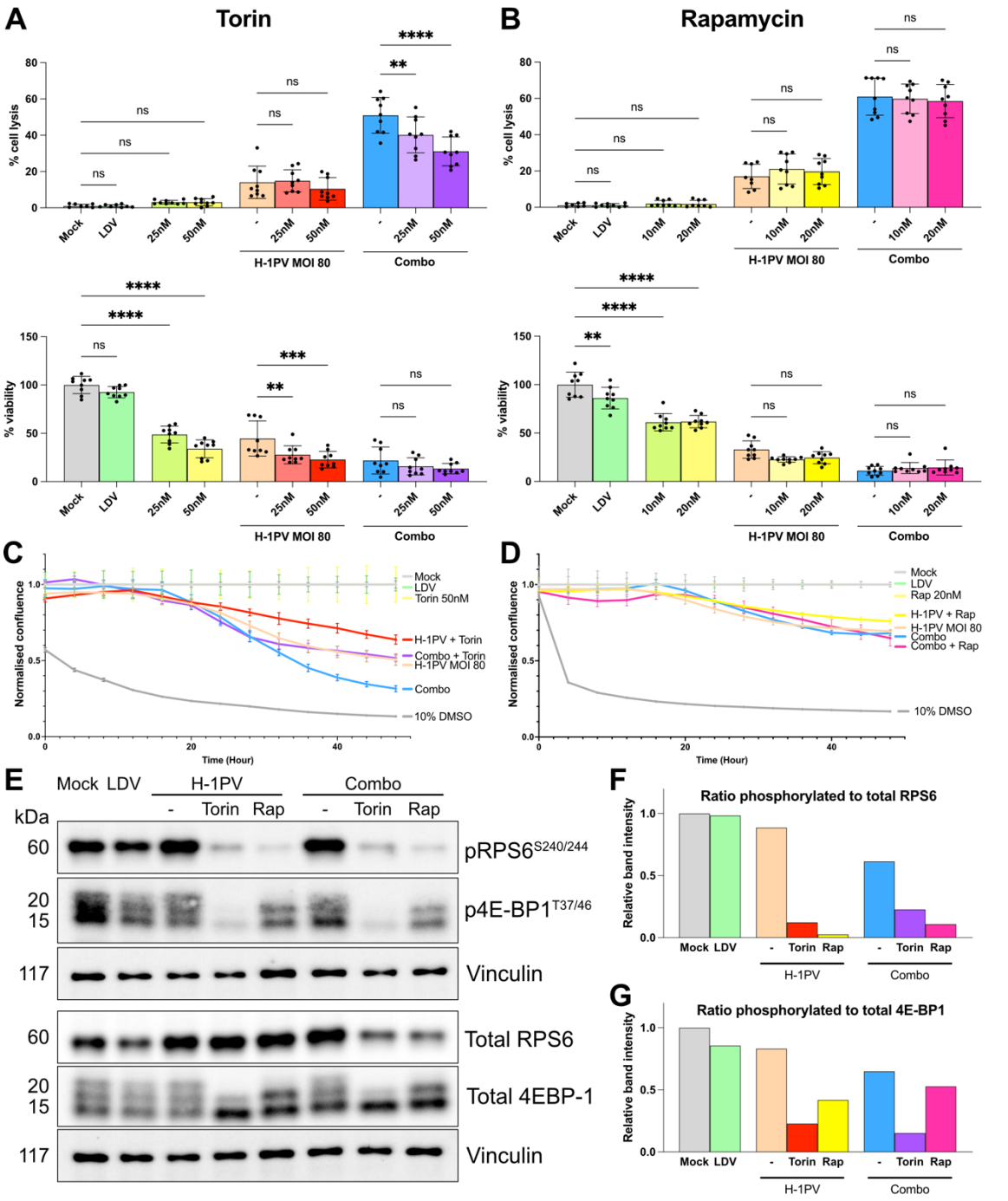

Figure 38. Ledipasvir-mediated improvement in oncolysis can be rescued by mTOR inhibition in AsPC-1 cells. AsPC-1 cells were infected with H-1PV MOI 80 with or without 4μM Ledipasvir co-treatment, in addition to **A** Torin or **B** Rapamycin treatment. Cell lysis was measured by lactate dehydrogenase activity, and cell viability was measured by crystal violet staining 72h after treatment. Real-time cell growth was also monitored by the Incucyte imaging system for 48h after infection of cells with H-1PV MOI 80 with or without 4μM Ledipasvir co-treatment, in addition to **C** Torin or **D** Rapamycin treatment. Cell confluence was normalised to the appropriate treatment controls, as mTOR inhibition hinders cell growth. **E** Cells were treated as above with the highest used concentrations of mTOR inhibitors for 48h before harvesting protein for Western blotting to test the functionality of both inhibitors in the context of H-1PV infection. **F** Quantification of the ratio between phosphorylated and total RPS6 in E, adjusted for vinculin signal. **G** Quantification of the ratio between phosphorylated and total 4E-BP1 in E, adjusted for vinculin signal. Cell killing and viability experiments show three independent experiments, Incucyte curves are representative of two independent experiments. Data represents mean ± standard deviation; significance was measured by one-way ANOVA, * = p≤0.05, ** = p≤0.01, *** = p≤0.001, **** = p≤0.0001.

7.5 Ledipasvir can enhance H-1PV oncotoxicity in a primary model of PDAC

Finally, I also wanted to assess the translational value of the discovery that Ledipasvir can potentiate H-1PV oncolysis. For this, I used five primary PDAC cell cultures derived through mouse xenotransplantation (PDX) by the group of Claudia Ball [303]. These five cultures showed widely divergent sensitivities to H-1PV, and have been classified by our collaborators Theresa Schäfer and Christine Engeland into two molecular subtypes, named quasi-mesenchymal, and classical-like, based on a comparison of gene expression in the cultures with previously published signatures [304]. I assessed both cell viability and active cell lysis after treatment with H-1PV alone or in combination with Ledipasvir. The quasi-mesenchymal cultures PC31, PC03, and PC20 were more sensitive to the combination treatment than H-1PV alone (Figure 39A-C). Surprisingly, the classical-like cultures PC09 and PC06 did not display any increased sensitivity to the combination treatment than H-1PV alone (Figure 39D and E) – the only two cultures in this entire study to display this phenotype. I therefore assessed whether this differential sensitivity to the combination treatment correlates with the basal activity of the PI3K/Akt/mTOR signalling pathway in the full dataset of 14 primary cultures characterised by Theresa Schäfer (Supplementary Figure 3). Indeed, analysis of microarray expression profiling of these cultures showed several genes with significant differential regulation between the two molecular subtypes. In particular, there was a reduction in the expression of genes associated with PI3K-Akt signalling (Figure 39F) and mTOR signalling (Figure 39G) in the classical-like cells compared with the quasi-mesenchymal cultures used in this study. Most notably, Akt1 itself was significantly downregulated in the two combination-resistant cell cultures compared with the sensitive ones. This analysis provides further evidence that the activity of the Akt/mTOR signalling axis is linked with the mechanism behind the enhanced cytotoxicity of the Ledipasvir-H-1PV combination.

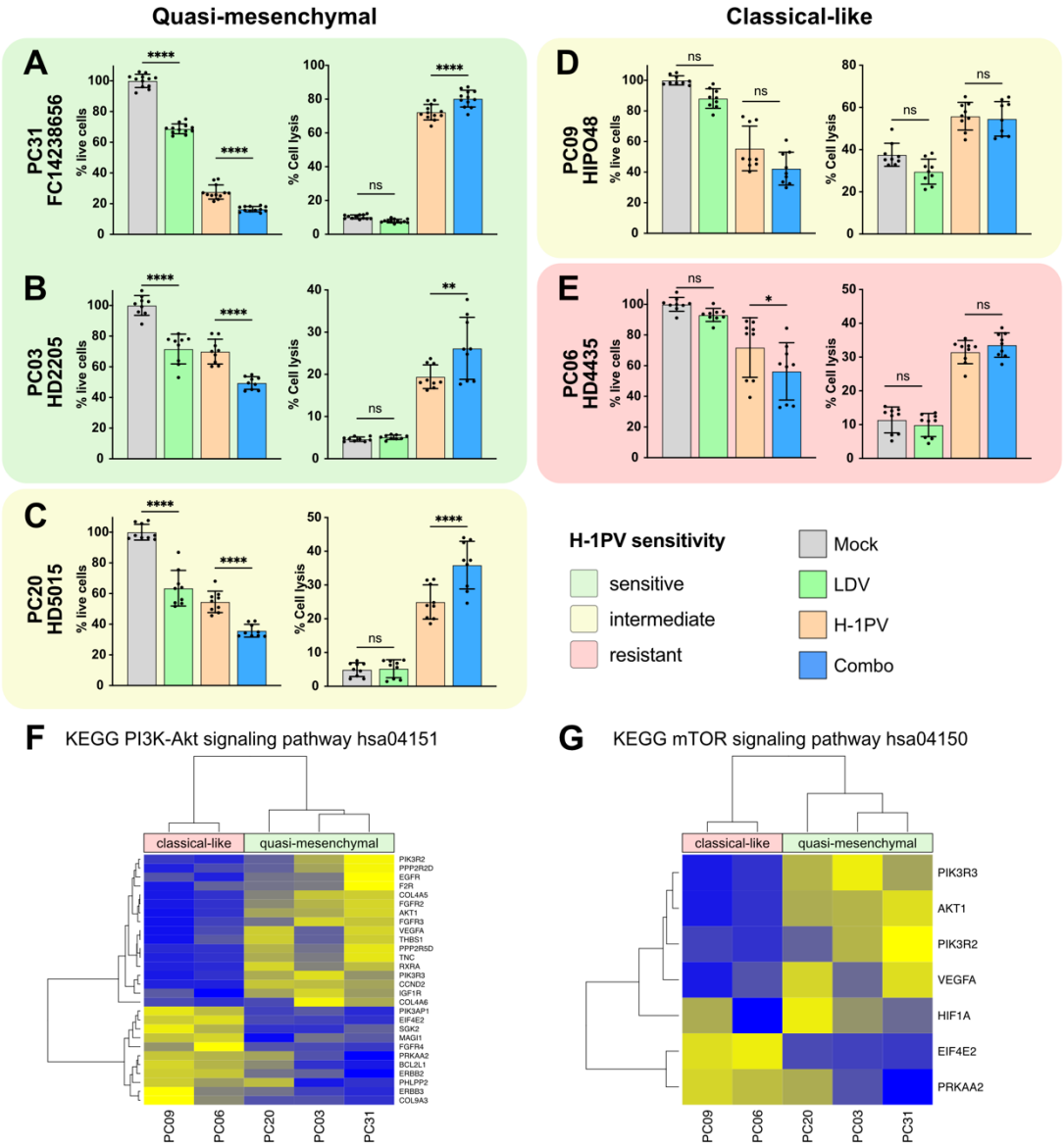

Figure 39. Ledipasvir is able to potentiate H-1PV-mediated oncolysis in primary PDAC cell cultures in 2D. Five primary pancreatic ductal adenocarcinoma cell cultures (established by Claudia Ball, NCT Dresden [303]) were tested for their sensitivity to both H-1PV and Ledipasvir (LDV). These cultures had previously been characterised for their sensitivity to H-1PV alone as well as their molecular subtype (quasi-mesenchymal or classical-like) by Theresa Schäfer. Cells were treated with **A** 10µM LDV and MOI 2.5 H-1PV, **B** 1µM LDV and MOI 4 H-1PV, **C** 2µM LDV and MOI 10 H-1PV, **D** 4µM LDV and MOI 50 H-1PV, **E** 10µM LDV and MOI 400 H-1PV and then cultured for 72-120h before measurement of cell viability by crystal violet staining and measurement of cell lysis by lactate dehydrogenase assay. **F** Heatmap of genes in the KEGG pathway hsa04151 significantly regulated ($p < 0.05$) between the classical-like and quasi-mesenchymal cultures, showing relative expression values for the five cultures used in this study. **G** Heatmap of genes in the KEGG pathway hsa04150 significantly regulated ($p < 0.05$) between the classical-like and quasi-mesenchymal cultures, showing relative expression values for the five cultures used in this study. Data represent mean ± standard deviation of at least n=3; significance was measured by one-way ANOVA, * = p≤0.05, ** = p≤0.01, *** = p≤0.001, **** = p≤0.0001. Microarray experiments were conducted by Theresa Schäfer.

7.6 Summary

H-1PV is emerging as a promising candidate for oncolytic virotherapy. Clinical trials in glioma and PDAC patients showed that treatment with this virus is safe in humans, with some indications of efficacy. However, thus far, monotherapeutic use of H-1PV has fallen short of achieving a cure. To this end, the goal of this study was to potentiate H-1PV-mediated oncolysis by novel combination with clinically approved drugs. Previous work in our group had identified the antiviral compound Ledipasvir as a potentiator of H-1PV-mediated oncolysis in a wide variety of cell lines from different cancer aetiologies (Figure 25). I was able to corroborate these findings in cell lines of glioma and PDAC origin and extend them to sub-lethal doses of H-1PV (Figure 26). I next investigated the mechanism by which Ledipasvir can potentiate H-1PV oncolysis. I found no indications that Ledipasvir improves viral replication in glioma cells (Figure 28, Figure 29). However, Ledipasvir could potentiate the cytotoxic effects of the viral effector protein NS1 in a virus free system (Figure 30), although I found no evidence of a direct interaction between Ledipasvir and NS1 (Figure 31). High-throughput image-based and functional screens of the interactions between Ledipasvir, H-1PV, and cellular kinases revealed a putative effect of Ledipasvir and the H-1PV-Ledipasvir combination on PI3K and Akt signalling (Figure 32, Figure 33). I could confirm that the combination treatment hyperactivates Akt in glioma cells (Figure 34) but neither inhibition of PI3K nor Akt could rescue the synergistic killing effect. RNA sequencing analysis further confirmed an activation of PI3K/Akt/mTOR signalling in combination-treated cells only, and comparison between H-1PV-infected cells with and without Ledipasvir co-treatment revealed links to translation inhibition and histone and DNA methylation (Figure 35). Additionally, treatment with the mTOR inhibitor Torin, but not Rapamycin, could effectively rescue cells from Ledipasvir-enhanced cell death upon H-1PV infection in both glioma and PDAC cell lines (Figure 37, Figure 38). This rescue effect appears to be driven by inhibition of 4E-BP1 phosphorylation, responsible for cellular translation. Finally, I translated these findings to primary patient-derived PDAC cultures, where cultures resistant to the combinatorial effects of Ledipasvir and H-1PV also showed a reduced basal expression of PI3K/Akt/mTOR pathway constituents (Figure 39). Therefore, I concluded that Ledipasvir together with H-1PV, in particular the NS1 protein, can interact with cellular signalling pathways, especially by activating mTOR signalling to improve H-1PV-mediated oncolysis in a diverse array of tumour type.

8 Discussion

8.1 High-throughput screening approaches to potentiate oncolytic viruses

The emerging field of oncolytic viruses is a promising avenue of research for cancer therapeutics. Four OVs to date have been approved for clinical use world-wide, with several others currently undergoing phase III clinical testing (Table 2). Oncolytic H-1PV has thus far been tested in early phase clinical trials for recurrent PDAC and glioma, and demonstrated a good safety profile and tolerability in both trials [258; 263]. However, as a monotherapy H-1PV was not sufficient to eradicate tumours. Thus, the work presented here employed a high-throughput screening approach to discover clinically approved drugs able to synergise with H-1PV and improve oncolysis. This is a promising approach which has been used previously to discover small molecule compounds able to improve OV therapy. The first example of such a screen from the group of John Bell focussed on compounds able to improve the replication and spread of an oncolytic VSV, culminating in the discovery of virus-sensitizer 1, a molecule able to potentiate VSV replication by disrupting the host antiviral response [305]. Similarly, work by the Chiocca and Lamfers groups identified four clinically approved compounds able to potentiate oncolytic AdV in glioblastoma stem-like cell cultures by increasing viral replication, cell apoptosis and necrosis [306]. The encouraging results from pre-clinical studies combining H-1PV with other small molecules such as HDAC inhibitors [192], pro-apoptotic BH3 mimetics [236; 275], and immunotherapies [272], as well as strong patient responses upon compassionate use in the clinics in combination with immunotherapy [261] suggest that multimodal treatment with H-1PV is a promising avenue of development for anti-cancer therapies.

8.2 Identification of Ledipasvir as a potentiator of H-1PV-mediated oncolysis

In this study, a high-throughput screen was used to identify drugs which can potentiate H-1PV-mediated oncolysis. Importantly, this library consisted of FDA- and EMA-approved drugs, which should accelerate the translation of any findings to the clinics. This is particularly relevant in light of the recent clinical trial showing that H-1PV is safe and well tolerated in metastatic PDAC, but not curative [263]. Thus, there is an urgent need for strategies to potentiate H-1PV oncolysis. The initial drug screen conducted in glioma cell lines found that the top candidate able to potentiate the oncolytic effects of H-1PV was the antiviral drug Ledipasvir (Figure 23). Ledipasvir was then tested in a wide variety of cancer cell lines to corroborate these findings and determine if it can potentiate H-1PV in a general fashion (Figure 25). The efficacy of the Ledipasvir-H-1PV combination in a wide range of cell lines from different cancer types shows that this combination works

in a cancer-agnostic fashion, which is particularly useful for an OV which is not restricted by cancer type. Ledipasvir is an antiviral drug directed at the NS5A protein of HCV [277], so its ability to improve the oncolytic capacities of H-1PV is unexpected. Thus, a major goal of this study was to elucidate the mechanisms by which Ledipasvir potentiates H-1PV oncolysis. This could lead to the identification of other molecules that could potentiate H-1PV by the same mechanism. H-1PV is known to translate well between cancers of different origin, such as PDAC and gliomas [258; 263]. Therefore, drugs able to potentiate H-1PV oncolysis in a cell type agnostic fashion should also be able to translate to different cancers together with H-1PV.

8.3 Ledipasvir enhances apoptosis without enhancing viral replication

The mechanism of cell death induced by the H-1PV-Ledipasvir combination is yet to be fully elucidated. Here, I show that there is an involvement of caspase 3- and 7-mediated apoptosis, as observed by a clear increase in caspase 3/7 activation in combination-treated cells (Figure 27), but there may also be other cell death pathways involved. Interestingly, treatment of cells with the pan-caspase inhibitor zVAD-FMK was not able to protect cells from H-1PV or combination-mediated apoptosis (Figure 27C, D). While the inhibitor could block most H-1PV-induced caspase activity in both glioma and PDAC cell lines tested, I observed a differential effect of caspase inhibition in the two cell lines after combination treatment. zVAD-FMK treatment more potently blocked the activation of caspases after Ledipasvir-H-1PV combination treatment in AsPC-1 PDAC cells than U373-MG glioma cells (Figure 27A, B). There are several possible explanations for these results. Firstly, it is possible that the induction of apoptosis by Ledipasvir and H-1PV together is so strong in these glioma cells that this caspase inhibitor is unable to abrogate it. Secondly, although the pan-caspase inhibitor attenuated much of the caspase 3 and 7 activity in PDAC cells, this did not reach 100% efficacy, and the remaining caspase activity may be sufficient to induce apoptosis in these cells. In this light, it could also be that apoptosis inhibition may drive the cells into other forms of cell death. It has been described that H-1PV alone can induce different cell death pathways, possibly depending on the cancer cell type [236; 256]. It follows that there may also be other cell death pathways in addition to apoptosis triggered by the Ledipasvir-H-1PV combination, such as necrosis or lysosomal cell death as described in H-1PV treatment alone [203; 245]. Importantly, these alternative pathways allow H-1PV to overcome cellular resistance to any one mode of cell death and may thus explain why inhibition of one cell death pathway does not affect the outcome of oncolysis [203]. The role of these pathways thus bears further investigating to discover the cellular pathways involved in Ledipasvir-H-1PV induced cell death.

An obvious cause of an increase in viral oncolysis as seen in the Ledipasvir-H-1PV combination would be an increase in replication of the virus. However, both by quantification of viral genomes (Figure 28) and viral proteins (Figure 29) I could find no evidence of an increase in viral replication upon Ledipasvir co-treatment in U373-MG or AsPC-1 cells. It is however possible that the viral particles produced by infection in the presence of Ledipasvir are more infectious than those produced by H-1PV alone. The parvoviral capsid goes through several stages of maturation before virion release [188; 238]. It is possible that co-treatment of cells with Ledipasvir modulates this maturation process, producing a higher rate of infectious particles. To address this, plaque assays could be performed using virus-containing supernatants from cells infected with and without Ledipasvir co-treatment. This would quantify truly infectious viral particles produced in the presence of the drug.

Aside from replicative capacity, the entry and egress of viral particles from cells with Ledipasvir co-treatment is yet to be considered. In qPCR experiments, all viral genomes measured in the input inoculum could be found within cell pellets four hours after infection, irrespective of Ledipasvir addition (Figure 28A). This is likely due to the low dose of virus used; only one virus per two cells (an MOI of 0.5). To measure whether or not Ledipasvir can influence the binding or entry of H-1PV to cells, an excess of viral particles, i.e. a higher MOI, could be used in similar binding-entry assays, as has been described before [213; 214]. However, the late timepoint 120 hours post infection showed a significant increase in viral genomes present in cell supernatants when co-treated with Ledipasvir, and a concomitant decrease in the viral genomes in cell pellets. This assay is not normalised to any cellular genes, so this effect may well simply be a natural consequence of higher cell lysis in the combination condition at this timepoint (Figure 26C). Nevertheless, it hints at a possible improvement in viral egress in the presence of Ledipasvir. This could be investigated by comparison of the intracellular locations of progeny virions with and without the drug over time, as well as more complete time-course studies of viral release from infected cells [206].

8.4 Ledipasvir enhances NS1-mediated cytotoxicity

Analysis of H-1PV protein production in the presence of Ledipasvir showed an increase, albeit not statistically significant, in expression of NS1 in the combination condition (Figure 29G, H). NS1 is the major cytotoxic effector protein of H-1PV, and its activity stimulates expression of its own p4 promoter [307], so this finding may indicate an increase in NS1 activity in the presence of Ledipasvir. Thus, I investigated whether Ledipasvir can potentiate NS1-mediated cytotoxicity. Indeed, in a virus free system where NS1 induction is controlled by doxycycline addition, I found that the addition of Ledipasvir could exacerbate the cytotoxic effects of NS1 expression (Figure 30). This suggests that the mechanism by which

Ledipasvir can improve H-1PV cytotoxicity is at least partially NS1 dependent. However, I found no evidence of a direct interaction between Ledipasvir and the NS1 protein when performing a CETSA using these cells (Figure 31). The CETSA can give a preliminary indication of direct interaction by measuring the thermostability of proteins, as this increases upon ligand binding [296]. Here, I saw no shift in thermostability of NS1 when incubated with Ledipasvir, in contrast to ATP, a known ligand of NS1 [190]. Therefore, it seems most likely that Ledipasvir can potentiate NS1-mediated cytotoxicity through interactions with cellular components.

8.5 Evidence for PI3K/Akt modulation by the Ledipasvir-H-1PV combination

To explore the cellular pathways which may be modulated upon Ledipasvir-H-1PV combination treatment, I analysed a series of unbiased experiments. The first of these is a Cell Painting experiment, in which osteosarcoma cells were treated with a library of drugs, including Ledipasvir, and their morphological changes were assessed by high-content imaging and AI-based analysis (Figure 32A). Importantly, this was done in the complete absence of H-1PV. These experiments showed that Ledipasvir treatment causes cells to adopt morphological phenotypes similar to that of PI3K inhibitors (Figure 32B). However, treatment of U373-MG and AsPC-1 cells with the PI3K inhibitor LY294002 somewhat inhibited the ability of H-1PV to kill these cells (Figure 34B), in contrast to Ledipasvir co-treatment. This indicates that in the presence of the virus, particularly viral NS1, Ledipasvir may be able to interact with cellular signalling in a different manner to monotherapy. The slight inhibition of H-1PV cytotoxicity in the presence of LY294002 may be due to a reduction in PDK1 activity, which is known to phosphorylate NS1 and increase its cytotoxic capacity (Figure 22) [299]. In fact, I saw an increase in the activating phosphorylation Ser473 on Akt by H-1PV infection, and to a greater extent combination with Ledipasvir, indicating an activation of Akt in infected cells (Figure 34A). This is in agreement with data from Lachmann and colleagues, who showed that MVM infection activates PDK1 [235]. PDK1 then phosphorylates Akt at Thr308, which is a prerequisite for its final activating phosphorylation at Ser473 as measured in this study [308]. Additionally, Bär and colleagues showed that H-1PV can cause an activation of PDK1 independently of PI3K through associations with PKCη and Radixin [299], which can activate Akt and prolong cell survival, allowing the virus to complete its replication before the death of its host [309].

The second unbiased analysis of the Ledipasvir-H-1PV combination was PamGene kinase profiling, in which the kinase activity in U373-MG glioma cells was measured after Ledipasvir, H-1PV, or combination treatment through a chip-based assay (Figure 33A). Aside from PI3K and Akt, this kinase profiling inferred

significant activation of the serine-threonine kinase PKC family by H-1PV at the early timepoint, and in particular by the combination with Ledipasvir (Figure 33C). This activation was restricted to the conventional PKCs (α, β, and γ), and the novel PKCs (δ, ϵ, η, and θ). PKC family kinases can both positively and negatively influence cell survival and death, depending on the isoform [310]. Interestingly, the first prerequisite for PKC family activation is phosphorylation by PDK1, again pointing towards an activation of PDK1 in combination-treated cells [311], in agreement with previous results in MVM [299]. In addition, mTORC2 is able to activate both conventional and novel PKCs (Figure 22) [290], so this concomitant activation of Akt and PKC family members may be due to an increase in mTORC2 activity in response to the H-1PV-Ledipasvir combination. This would benefit viral oncotoxicity, as activity of the novel PKCη is necessary to phosphorylate NS1 of MVM, and active PDK1/PKC signalling is important for the oncotropism of H-1PV [198; 299].

8.6 The Ledipasvir-H-1PV combination affects mTOR signalling

The final unbiased approach used here to understand the Ledipasvir-H-1PV mechanism of cell killing was RNA sequencing and GSEA in U373-MG cells. This again confirmed an activation of the PI3K/Akt/mTOR signalling pathway only in cells treated with both Ledipasvir and H-1PV, but neither treatment alone compared to untreated cells (Figure 35B-D). However, when comparing combination treatment with H-1PV alone, this pathway no longer showed significantly differential regulation (data not shown). One of the major downstream effects of mTOR signalling is an increase in translation, more specifically cap-dependent translation [287]. Indeed, pathways associated with translation repression are significantly downregulated in combination-treated cells compared with virus alone, which implies an increase in cellular translation. Therefore, I tested whether the inhibition of mTOR and thus cap-dependent translation may abrogate the combinatorial effect of Ledipasvir with H-1PV. I used both Rapamycin, which preferentially blocks the mTORC1-S6K signalling axis, or Torin, which blocks both the mTORC1-S6K and the mTORC1-4E-BP1 signalling axes [302]. The 4E-BPs are known to play a more prominent role in regulating translation than S6Ks [312; 313]. In support of this, inhibition of 4E-BP1 phosphorylation, and thus translation, by Torin and to a lesser extent Rapamycin treatment was able to weaken the Ledipasvir-H-1PV combination effect (Figure 37). Taken together, these results suggest that concomitant treatment of cells with Ledipasvir and H-1PV may increase cellular cap-dependent translation and that this may be a driver for improved oncolysis in these cells.

Interestingly, the most highly repressed gene in combination-treated cells compared with H-1PV was miR708 (Figure 35F). This is a microRNA with dual oncogenic and tumour-repressor properties depending on the tumour type.

MicroRNAs are noncoding RNAs which regulate post-transcriptional gene expression by association with the RNA-induced silencing complex (RISC) and interact with messenger RNA (mRNA), driving mRNA degradation. miR708 is most highly expressed in the brain and eyes, and its expression can be induced by ER stress or glucocorticoid signalling [314]. Importantly, miR708 has been shown to regulate PI3K/Akt signalling by increasing expression of PTEN, thus blocking Akt activation [315]. Thus, a downregulation of miR708 is consistent with an increase in the activating phosphorylation S473 on Akt seen in combination-treated cells (Figure 34A). Although miR708 is known to be downregulated in human glioblastoma [316; 317], its expression in the U373-MG cells used in this study is unknown. Therefore, downregulation of miR708 may contribute to the increased activation of Akt observed upon combination treatment, which could benefit viral oncotoxicity as discussed above. Indeed, miR708 may also be differentially regulated by Ledipasvir-H-1PV co-treatment in AsPC-1 PDAC cells, which remains to be investigated.

In this study, I show that inhibition of mTOR is able to weaken the combinatorial cytotoxic effect of H-1PV and Ledipasvir (Figure 37, Figure 38). It is crucial to note that while combination treatment (H-1PV + Ledipasvir) with either Torin or Rapamycin effectively blocked phosphorylation of RPS6, only Torin could reduce phosphorylation of 4E-BP1 in both U373-MG and AsPC-1 cells (Figure 37F and G, Figure 38F and G). Additionally, the oncolytic capabilities of H-1PV alone in these cells were unaffected by mTOR inhibition (Figure 37A and B, Figure 38A and B). Therefore, it seems that the mechanism by which Ledipasvir can potentiate H-1PV oncolysis may signal through 4E-BP1. 4E-BP1 phosphorylation primarily leads to an increase in cellular translation [287; 291], which aligns well with GSEA analysis showing a de-repression of translation in combination-treated cells (Figure 35G), corroborating this hypothesis. It is important to note that shutdown of cellular translation is a common antiviral response in human cells to limit viral replication and protein production [146]. Therefore, an increase in cellular translation in combination-treated cells may signal a reduced ability of these cells to trigger an antiviral response.

Importantly, inhibition of PI3K or Akt does not lead to the same protection against the combination treatment (H-1PV + Ledipasvir) as mTOR inhibition (Figure 34). This implies that there may be a PI3K/Akt-independent activation of mTOR in combination-treated cells. Indeed, Akt hyperactivation after combination treatment could well be a consequence of increased mTORC2 activity (Figure 22) [292]. This hyperactivation could nevertheless serve to improve the cytotoxic capabilities of NS1, and it would be interesting to examine the activity of Akt in cells treated with Torin as well as the H-1PV-Ledipasvir combination. Specific inhibition of mTORC2 without mTORC1 could also be explored, for example using RNA interference or an mTORC2-specific inhibitor such as JR-AB2-011 [318], to

identify whether Akt phosphorylation by mTORC2 plays a role in Ledipasvir-H-1PV mediated cell death. Given that regulation of 4E-BP1 appears to be a key nexus in this mechanism, it may also be informative to consider the phosphorylation levels of 4E-BP1 when cells are treated with the Ledipasvir-H-1PV combination together with PI3K or Akt inhibitors. Indeed, mTORC1 can be activated in a PI3K/Akt-independent way, such as through Ras/MAPK signalling [319], such that PI3K or Akt inhibition may not influence 4E-BP1 phosphorylation or activity.

It is noteworthy that Akt inhibition led to an increase in S473 phosphorylation on Akt, although downstream RPS6 phosphorylation was decreased (Figure 34D), which is in accordance with previous studies [320]. This is due to a feedback mechanism by which drug-inhibited Akt is hyperphosphorylated by mTORC2 at S473, a phenotype which mirrors kinase-dead Akt mutants, indicating that Akt is nonetheless inhibited by Capivasertib treatment [321]. However, at the dose of Capivasertib used in this study (1μM), it is possible that some Akt activity remains, as downstream RPS6 phosphorylation was not completely abrogated (Figure 34D). A higher dose of Capivasertib was not used due to adverse effects on cell growth (Figure 34C, lower panel). Thus, it would be prudent to explore other means of inhibiting Akt to conclusively show whether its activity is involved in the potentiation of H-1PV oncolysis by Ledipasvir.

Based on these combined results, I propose a tentative model of Ledipasvir-mediated H-1PV potentiation. This combination may be able to affect Akt activity, possibly through mTORC2 activation. Akt in turn may be able to directly increase the cytotoxicity of NS1 by a mechanism which is not yet fully understood. mTORC2 activation can also lead to PKC activation, which is known to phosphorylate NS1. Alternatively, Akt activity leads to activation of mTORC1, which drives cellular cap-dependent translation through phosphorylation and inhibition of 4E-BP1. This inhibition of 4E-BP1, and presumably the concomitant increase in translation, may also be able to increase NS1-mediated cytotoxicity by an as-yet unknown mechanism (Figure 40).

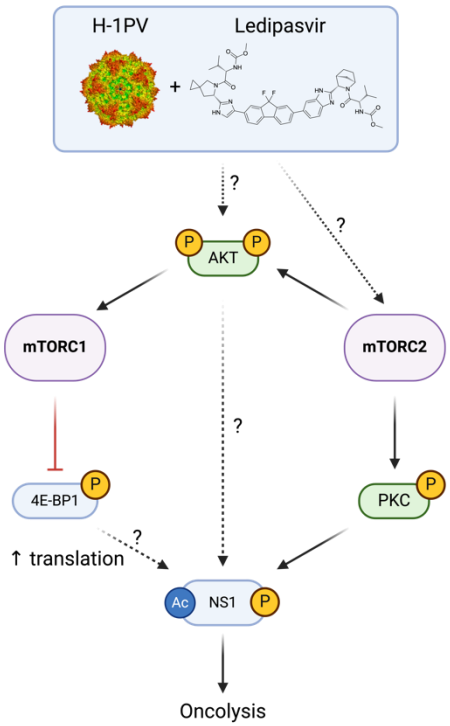

Figure 40. Tentative model for the potentiation of H-1PV by Ledipasvir. Together, H-1PV and Ledipasvir can modulate Akt/mammalian target of rapamycin (mTOR) signalling, possibly through direct activation of Akt, or through activation of mTOR complex 2 (mTORC2). mTORC2 activates Akt, whose activity may be beneficial to NS1 cytotoxicity by an as-yet uncharacterised mechanism. In addition, mTORC2 can drive activity of the protein kinase C (PKC) family, which may benefit NS1 oncotoxicity through phosphorylation of NS1. Alternatively, Akt activates mTOR complex 1 (mTORC1), which increases cellular cap-dependent translation through phosphorylation and inhibition of 4E-BP1. This derepression of cellular translation may also benefit NS1-mediated oncotoxicity by an unknown mechanism. Figure made using BioRender.

8.7 Possible interactions of Ledipasvir-H-1PV with other cellular pathways

Aside from the PI3K/Akt/mTOR signalling axis, RNA sequencing and GSEA analysis of U373-MG cells treated with the Ledipasvir-H-1PV combination identified several other pathways possibly involved in the combinatorial mechanism of oncolysis. Firstly, there was a downregulation of terms associated with DNA replication in cells treated with the Ledipasvir-H-1PV combination compared with H-1PV alone (Figure 35G). It is known that H-1PV induces cell cycle arrest through the NS1 protein, leading to cell lysis (reviewed in Nüesch, Lacroix et al. [309]). Putative stronger activity of NS1 through Ledipasvir could then also lead to a stronger cell cycle arrest in combination-treated cells than virus alone. The downregulation of DNA replication pathways in the combination-treated cells compared with H-1PV alone would be consistent with this hypothesis (Figure 35G).

Secondly, there was a decrease in cell death and senescence-associated pathways in combination-treated cells compared with virus treatment alone (Figure 35G). This decrease seems contradictory to the phenotype discussed above of increased caspase 3/7 activation after combination treatment, and the inference that combination-mediated cell death is therefore at least partially apoptotic (Figure 27). There are two potential explanations for this discrepancy. Firstly, RNA sequencing analysis was based on cells in the late stages of viral infection, at 72 and 96 hours post infection. Therefore, there is a possibility that those cells that were analysed by RNA sequencing were the few cells left able to survive H-1PV or the combination treatment. It would be instructive to analyse the gene expression of cells 48 hours after treatment, where cells have not yet died but may show higher virus-mediated effects than the early 24-hour timepoint (Figure 35A). Alternatively, this decrease in apoptotic and senescent signalling may indicate an inability of combination-treated cells to protect themselves against H-1PV-mediated lysis by triggering standard antiviral pathways leading to apoptosis or senescence [202; 322].

A further possibility is that Ledipasvir can potentiate H-1PV-mediated oncolysis through modulation of autophagy. Autophagy (*auto* = self, *phagy* = eating) is a homeostatic process to degrade and recycle cellular components, characterised by a double-membraned vesicle termed the autophagosome which engulfs cytoplasmic components. This autophagosome fuses with lysosomes to form an autolysosome, digesting the cellular components within, and providing components for protein synthesis and nutrients [323]. Autophagy can represent a double-edged sword in the cancer setting: on one hand, it can protect cells from ROS-induced damage by clearing misfolded proteins and hindering cellular transformation; on the other, autophagy can promote late-stage tumourigenesis by supplying nutrients and limiting DNA damage to promote cellular survival [324]. Importantly, Torin is a potent inducer of autophagy, whereas Rapamycin is only poorly able to induce autophagy, particularly in U373-MG cells [302; 325]. Torin inhibits autophagy through the inhibition of mTORC1-driven phosphorylation of autophagy-inducing proteins such as ULK1 (Figure 22). In the course of this project, I saw preliminary evidence that Ledipasvir treatment alone, as well as the Ledipasvir-H-1PV combination, is able to modulate autophagy (data not shown). Thus, Torin, but not Rapamycin, may be able to influence Ledipasvir and H-1PV-mediated modulation of autophagy by counteracting mTORC1-mediated autophagy suppression, ultimately activating autophagy.

Importantly, differential regulation of autophagy is a phenomenon that has already been recognised in the context of oncolytic virotherapy, for example in glioblastoma [326]. Here again, although the role of autophagy in OV therapy is well-recognised, it is two-fold and context dependent. Cells can trigger autophagy as an antiviral mechanism to degrade viral components, whereas hyperactivity of

autophagy by some OVs such as paramyxoviruses can aid their oncolytic capabilities [327; 328]. Parvoviruses are known to trigger ER stress through the SAT protein [210], and H-1PV more specifically is known to cause oxidative stress through NS1 [192; 202]. These two cellular stresses can both stimulate autophagy [326]. It therefore seems likely that H-1PV might be able to stimulate autophagy for its own replication and oncotoxicity, much like other OVs such as NDV and oncolytic Reovirus [148; 329; 330]. This is then in conflict with the idea that Torin, a potent inducer of autophagy, should be able to inhibit an autophagy-mediated increase in H-1PV oncotoxicity. Therefore, the possibility of Ledipasvir enhancing H-1PV oncotoxicity through autophagy regulation warrants cautious and critical examination.

8.8 Translational value of combination treatment

In this work, I also tested the capabilities of Ledipasvir to enhance H-1PV oncolysis in primary PDAC cultures [303]. These cultures represent the broad heterogeneity of PDAC tumours and recapitulate the histological features of the original patient tumours from which they were derived. This makes them an excellent resource to assess the translational value of the Ledipasvir-H-1PV combination *in vitro*. These cultures have previously been classified into two molecular phenotypes by Theresa Schäfer according to their transcriptional signatures. Interestingly, the two cultures falling into the classical-like phenotype showed a resistance to Ledipasvir-mediated H-1PV enhancement, in contrast to the three quasi-mesenchymal cultures (Figure 39A-E). Further examination of these two molecular phenotypes revealed that the classical-like cultures have markedly lower expression of PI3K/Akt/mTOR signalling components, including Akt1 (Figure 39F, G). This leads to the hypothesis that classical-like cultures may not rely on PI3K/Akt/mTOR signalling for their proliferation, rendering them insensitive to modulation of these pathways by Ledipasvir in the presence of H-1PV. The levels of PI3K/Akt/mTOR signalling in these two molecular phenotypes of PDAC cells therefore warrant further investigation and may even lead to identification of biomarkers predictive for response to Ledipasvir and H-1PV combination therapy.

8.9 Future directions

This work established that the oncolytic capabilities of H-1PV can be enhanced by concomitant treatment of cells with the antiviral compound Ledipasvir. The exact molecular mechanism of this enhancement remains elusive; however it appears to involve mTOR-mediated improvement in H-1PV oncotoxicity, and can be attributed at least in part to the activity of the viral NS1 protein. Ledipasvir is already approved for clinical use in the United States and Europe, which may accelerate clinical translation of these findings. Nevertheless, some aspects of Ledipasvir-H-1PV combination treatment must be considered before such translation can occur.

The exact mode(s) of cell death induced by the Ledipasvir-H-1PV combination remain to be fully elucidated. Here, I could show an involvement of caspase-mediated apoptosis in this improved cell killing (Figure 27); however, other modes of cell death caused by H-1PV have also been described. Apoptosis is not an unlikely mediator of combination-induced cell death, as I showed that Ledipasvir can synergise with NS1 alone to kill cells (Figure 30), and NS1-mediated cell death is known to be apoptotic due to the accumulation of ROS and DNA damage markers [202]. However, H-1PV has also been described to cause necrosis [245], lysosomal cell death [203], and ICD [158; 236]; all of which may be components of Ledipasvir-H-1PV-mediated cell death. Of particular interest would be whether Ledipasvir is able to augment the immunogenicity of cell death in combination-treated cells, for example by considering markers of ICD such as externalised HMGB1, ATP, and ecto-calreticulin. As a secondary effect, the stimulation of immune cells such as dendritic cells and T cells after cancer cell lysis using the Ledipasvir-H-1PV combination could be examined. An increase in ICD would be a highly desirable feature in combination treatment, as has been demonstrated for other OVs [123].

One crucial aspect to consider in combination treatment is safety. While H-1PV has been proven to be safe and well tolerated in patients [257; 263], its oncotropism when combined with Ledipasvir has not been examined here. Preliminary data suggests that neither H-1PV or Ledipasvir alone, nor the combination of the two pose significant toxicity to normal human foetal lung fibroblasts or umbilical vein endothelial cells in a 2D model (data not shown). Nevertheless, it is important to rigorously test the safety of the Ledipasvir-H-1PV combination to ensure that this is non-toxic to normal, untransformed cells.

Finally, all work done in this study was conducted using cell cultures *in vitro*. Aside from cell lines, primary cultures of PDAC tumours were also tested to increase the translational value of these findings. While these PDAC cultures do closely resemble the tumour histology of patients from which they were derived in xenograft models [303], they still represent a different setting to an entire organism with a tumour microenvironment and interactions with its surroundings. Thus, it is crucial to conduct rigorous pre-clinical testing of the H-1PV-Ledipasvir combination before translation into the clinics. This could be achieved using a tumour xenograft mouse model to look for a first-line combinatorial effect of H-1PV and Ledipasvir treatment. However, given the immune-stimulatory properties of H-1PV, in particular in the context of combination therapies [236; 247], it would also be interesting to test this combination in an immune-competent model. Given that H-1PV is unable to replicate in mouse cells [183], rat models such as RG2 rat glioma cells have previously been used in pre-clinical testing of H-1PV [254]. Such a model could be used to determine whether Ledipasvir is able to modulate the oncolytic activity, as well as the immune-stimulatory properties of H-1PV.

9 Supplementary figures

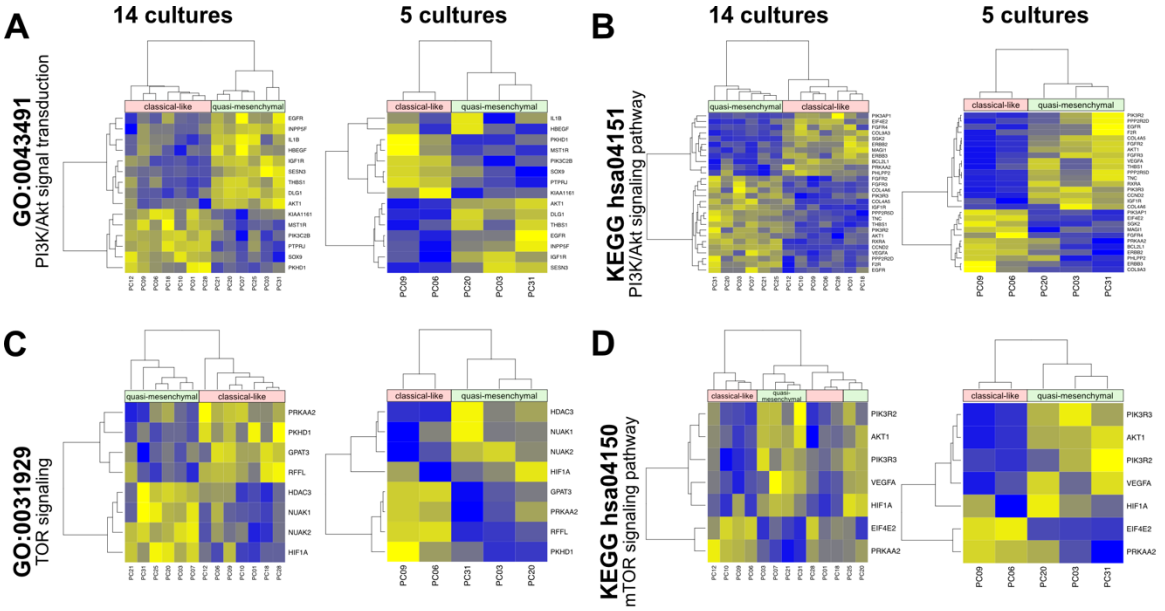

Supplementary Figure 3. Microarray analysis of PI3K/Akt and mTOR signalling pathways in primary PDAC cultures. Genes belonging to the indicated GO terms or KEGG pathways were extracted from global microarrays on 14 primary PDAC cultures (performed by Theresa Schäfer). Genes with significant ($p<0.05$) differences between the classical-like and the quasi-mesenchymal group were filtered and clustered into heatmaps using Pearson clustering. Expression values for the full dataset of 13 cultures are shown on the left, and for the 5 cultures used in this study on the right. Significance was measured using the Empirical Bayes method with Benjamini-Hochberg adjustment.

10 Materials

10.1 General materials

Table 3. List of general materials used in this study.

Material	Description	Company
Cell culture dishes	Ø 6 / 10 / 15 cm	greiner bio-one
Cell culture flasks	25/ 75 / 175 cm^2	greiner bio-one
Cell culture multidishes	6 / 12 /24/ 96 well	greiner bio-one / nunc
Cell scraper	28 cm length	greiner bio-one
Combitips	0.5 ml / 1 ml/ 5 ml	Eppendorf
Nalgene cryogenic vials	25 sterile tubes	Thermo Fisher Scientific/Nalgene
Falcon tubes	15 and 50ml	Falcon
Filtered tips	10, 20, 100, 200 and 1000µl	Nerbe
Filter unit	0.22 µm	GE Healthcare/Whatman
iBlot 2 Transfer Stacks, PVDF	Dry blotting system, 0.2µm pore polyvinylidene difluoride membrane	Life Technologies
PCR plate 96-well		Eppendorf
LUNA cell counting slides	disposable precision slides for Trypan blue and fluorescence cell counting	Logos Biosystems
Mini-PROTEAN Gels 4-20%	4–20% precast polyacrylamide gel, 8.6 × 6.7 cm (W × L), for use with Mini-PROTEAN Electrophoresis Cells. Separation of polypeptides ~2–400 kDa	Bio-Rad
Reagent reservoir	50ml deposits, sterile, polystyrene	Corning Incorporated
Transferpette multichannel	200ul	Brand
Multipette M4	multistep pipette with a range from 1µl to 10ml	Eppendorf
Nitrocellulose membrane	PROTAN®	Whatman (Maidstone, UK)

Material	Description	Company
Pasteur pipettes	9 inch, 5.5mm, Disposable, Bulk Pack, Non-Sterile, Unplugged	Corning Incorporated
PCR strips		Neolab
Plastic pipettes (sterile)	5, 10, 25 and 50ml	Corning/Costar
Safelock tubes	1.5 / 2.0 / 5.0 ml	Eppendorf
Sterile filter unit	Stericup E, 45mm thread, 0.22 µm, 500ml	MERCK Millipore
Syringes	3 / 5 / 10 / 50 ml	BD Biosciences
Whatman paper	3 mm	Whatman
µ-Plate 96 Well	µ-Plate 96 Well ibiTreat: #1.5 polymer coverslip, tissue culture treated, sterilised, black	ibidi
Scalpels	Disposable stainless steel blade with plastic handle	feather
Bacterial spreaders	individually wrapped, sterile	VWR
Cuvettes Gene Pulser	0.1cm gap (brown lid)	Bio-Rad

10.2 Equipment

Table 4. List of equipment used in this study.

Device	Company
Multiskan Ex	Thermo Labsystems
Fluoroskan Ascent FL	Thermo Labsystems
Amaxa II Nucleofector	Lonza
BD FACSAria II cell sorter	BD Biosciences
Cell culture hood Safe2020	Thermo Fisher Scientific
Centrifuge 5430R	Eppendorf
Centrifuge 5424R	Eppendorf
Centrifuge 5810	Eppendorf
Centrifuge rotor F10-6x-500y FiberLite	Thermo Fisher Scientific
Centrifuge Sorvall RC6+	Thermo Fisher Scientific
Electroporator MicroPulser	Bio-Rad

Device	Company
Gel basic power supply PowerPac™	Bio-Rad
Gel chambers PerfectBlue Wide Gel System ExM	Peqlab
iBlot 2	Invitrogen
Trans-Blot SD	Bio-Rad
ECL ChemoCam imager	Intas
Fusion SL gel documentation system	Vilber Lourmat
LUNA automated cell counter	Logos Biosystems
Microscope Eclipse Ti/X-Cite120Led	Nikon
Microscope phase contrast CK40	Olympus
Microscope phase contrast EVOS XL Core	Thermo Fisher Scientific
Microscope Stellaris 5 confocal	Leica
Live cell imager Incucyte SX5	Sartorius
Scanner Perfection V500	Epson
Microwave oven	Siemens
Mini-PROTEAN® Tetra Vertical Electrophoresis Cell	Bio-Rad
MS2 minishaker (vortex)	IKA
Nanodrop 2000C	Thermo Fisher Scientific
PCR thermocycler peqSTAR 2X/96X Universal Gradient	VWR Peqlab
PCR thermocycler S1000 Thermal Cycler	Bio-Rad
Realplex2 Mastercycler qPCR cycler	Eppendorf
CFX384 Real-Time PCR Detection System	Bio-Rad
UV transilluminator N90 LW366	Konrad Benda
Mr Frosty freezing container	Thermo Fisher Scientific

10.3 Software

Table 5. List of software used in this study.

Name	Description	Source/Company
Affinity Designer	Graphics design package	Pantone
Fiji (ImageJ)	Image processing package including plugins and macros	Schindelin, Arganda-Carreras et al. [331]
FlowJo 10	Flow cytometry analysis software	BD
SnapGene 4.0.1	Molecular biology tool for visualisation and cloning of DNA	Dotmatics
Endnote 21	Citation manager	Clarivate
Rstudio	Coding environment for statistical computing and graphics language R	Posit team (2023)
R	Coding language for statistical computing and graphics	R Core Team (2023)
dplyr	R package for data manipulation and analysis	Wickham, François et al. [332]
ggplot2	R package for graphical output	Wickham [333]
ggforce	R package to add functionality to ggplot2	Pedersen [334]
reshape	R package for reshaping data	Wickham [335]
scales	R package for scaling data in ggplot2	Wickham and Seidel [336]
affy	R package for analysis of Affymetrix microarray data	Gautier, Cope et al. [337]
limma	R package for statistical testing	Smyth [338]
amap	R package for clustering and heatmap generation	Lucas [339]
GraphPad Prism 10	Graphical analysis and statistics package	Dotmatics
BioRender	Online web tool for biological cartoon generation	BioRender
Incucyte 2020B	User interface software for recording and analysing Incucyte images	Sartorius
Gene Set Enrichment Analysis	Computational software for analysis of large sets of genomic data (used for RNA sequencing analysis)	Subramanian, Tamayo et al. [340]
Chipster	Analysis software for high-throughput data (used for microarray analysis)	Kallio, Tuimala et al. [341]

Name	Description	Source/Company
CFX Maestro	qPCR cycler software for calling CTs	Bio-Rad
Leica Application Suite - Advanced Fluorescence	Microscope software for SP5 confocal microscope	Leica
NIS-Elements	Microscope software for Eclipse Ti widefield microscope	Nikon
Phenogram Plot	Web-based plotting tool for genomic visualisation	Wolfe, Dudek et al. [342]
DeepL translator	AI-based translation software used to translate abstract	https://www.deepl.com/translator

10.4 Bacteria

Table 6. List of bacterial strains used in this study.

Name	Description	Reference/origin
MAX Efficiency® DH5a™ Competent Cells	Chemically competent *E. coli* used for routine subcloning	Life Technologies, 18258-012
NTC1050811-HF [dcm-]	Electrocompetent bacteria for nanovector cloning	Nature Technology Corporation, NTC-NP-CC11

10.5 DNA vectors

Table 7. List of DNA vectors used in this study.

Number	Vector series	Name	Description	Reference/Origin
		pMAX-GFP	pMAX backbone with CMV promoter driving expression of GFP	Lonza
p73	SMAR	pSMARt-hSK	pSMARt backbone with the CAG promoter driving expression of human Sox2-2A-Klf4, IFNβ SMAR	Roig-Merino [54]
p74	SMAR	pSMARt-hUL	pSMARt backbone with the CAG promoter driving expression of human L-Myc-2A-Lin28, IFNβ SMAR	Roig-Merino [54]
p75	SMAR	pSMARt-hO-shP53	pSMARt backbone with the CAG promoter driving expression of human Oct4, IFNβ SMAR and U6 driving shRNA for p53	Roig-Merino [54]
p76	SMAR	pSMARt-shP53	pSMARt backbone with the CAG promoter driving GFP-2A-Puro-IFNβ SMAR and U6 driving shRNA for p53	Roig-Merino [54]
p77	EBNA	pCXWB-EBNA1	Integration-free (episomal) expression of EBNA-1	Kind gift from Prof. Tristan McKay (MMU) [76]
p78	EBNA	pCXLE-hOct4-shP53	Integration-free (episomal) expression of human OCT3/4 and shRNA against p53	Kind gift from Prof. Tristan McKay (MMU) [21]
p79	EBNA	pCXLE-hSK	Integration-free (episomal) expression of human SOX2 and KLF4	Kind gift from Prof. Tristan McKay (MMU) [21]
p80	EBNA	pCXLE-hUL	Integration-free (episomal) expression of human L-MYC and LIN28	Kind gift from Prof. Tristan McKay (MMU) [21]

Number	Vector series	Name	Description	Reference/Origin
p101	EBNA	pCXLE-EBNA-GFP-2A-Puro	pCXLE backbone expressing EBNA and GFP-2A-Puro	Roig-Merino [54]
n1	nano SMAR	nCAG_hO_sp SMAR_shp53	CAG-driven Oct3/4 with spliced IFNβ SMAR and U6-driven shp53	Cloned in this study
n2	nano SMAR	nCAG_hSK_sp SMAR	CAG-driven Sox2-p2a-Klf4 with spliced IFNβ SMAR	Cloned in this study
n3	nano SMAR	nCAG_hML_sp SMAR	CAG-driven L-Myc-p2A-Lin28 with spliced IFNβ SMAR	Cloned in this study
n121	nano	nano-hOct4-shP53	pSMARt backbone with the CAG promoter driving expression of human Oct4 and U6 driving shRNA for p53	Cloned by Alicia Roig-Merino (DNA Vector Lab)
n122	nano	nano-hSK	pSMARt backbone with the CAG promoter driving expression of human Sox2-2A-Klf4	Cloned by Alicia Roig-Merino (DNA Vector Lab)
n123	nano	nano-hUL	pSMARt backbone with the CAG promoter driving expression of human L-Myc-2A-Lin28	Cloned by Alicia Roig-Merino (DNA Vector Lab)

10.6 Viruses

Table 8. List of viruses used in this study.

Name	Description	Reference/Origin
H-1PV	Wild-type H-1 parvovirus	Produced as part of this study by Tiina Marttila
H-1PV-rEGFP	Recombinant H-1PV expressing GFP in place of VP1/2 genes	El-Andaloussi, Leuchs et al. [343]

10.7 Buffers

Table 9. List of buffers used in this study.

Application	Buffers	Reagents	Amount	Company/ origin
General use	Phosphate-buffered saline (PBS), pH 7.4		500mL	Life Technologies, 10010-015
DNA Electro-phoresis	50x Electrophoresis Buffer (EP, 2L)	Tris (pH 7,8)	484.6g (2M)	home-made
		Sodium Acetate	41g (0.25M)	
		EDTA	37.2g (0.05M)	
		dH2O	1L (+1L)	
		pH to 7,8 with acetic acid	(approx 160ml)	
Western Blot	10x Tris-Glycine/SDS running buffer		1L	Bio-Rad, 1610732
	4x Laemmli Buffer		10mL	Bio-Rad, 1610747
	Cell Lysis Buffer (10x)		15mL	Cell Signaling Technology, 9803
	HALT Protease and Phosphatase Inhibitor Cocktail (100X)		100uL	Thermo Scientific, 78440
	Transfer buffer SD1 (1L)	Tris	36.3g (300mM)	home-made
		dH2O	800mL	
		Methanol	200mL (20%)	
		pH to 10.4 with NaOH		
	Transfer buffer SD2 (1L)	Tris	3.025g (25mM)	home-made
		dH2O	700mL	
		Methanol	200mL (20%)	
		pH to 10.4 with NaOH		
	Transfer buffer SD3 (1L)	Norleucine	5.24g (40mM)	home-made
		Tris	3.025g (25mM)	
		dH2O	1L	
		pH to 9.4 with NaOH		

Application	Buffers	Reagents	Amount	Company/ origin
Western Blot	10x Tris-buffered saline (TBS) (1L)	1M Tris Base (pH 7,6)	500 ml	home-made
		5M NaCl	300 ml	
		dH2O	200 ml	
	1x TBS(T)	1X TBS	100 ml	home-made
		dH2O	900 ml	
		(Tween 20)	1 ml	
	5% milk or BSA/TBST (w/v)	Milk powder/BSA	20g	home-made
		1x TBST	400mL	
Immuno-fluorescence	Fixation Solution	100% Methanol		home-made
	Permeabilisation solution	Triton-X100	0.1%	home-made
		PBS		
	Blocking solution	BSA	3%	home-made
		Tween20	0.1%	
		PBS		
	Storage solution	Vectashield Mounting Medium with DAPI		Vector Laboratories, H-1200-10
Flow Cytometry	FACS buffer (100mL)	PBS	98mL	home-made
		FBS	2mL (2%)	

10.8 Cell culture components

Table 10. List of cell culture components used in this study.

Reagent	Company	Cat. No.
Dimethyl Sulfoxide (DMSO)	Carl Roth	4720.1
Dulbecco's Phosphate-Buffered Saline (DPBS) (no calcium, no magnesium)	Gibco	14190094
Dulbecco's Modified Eagle's Medium (DMEM) - high glucose, with 4500 mg/L glucose, L-glutamine, and sodium bicarbonate, without sodium pyruvate	Sigma-Aldrich	D5796-6X500ML
Dulbecco's Modified Eagle's Medium - high glucose, with 4500 mg/L glucose and sodium bicarbonate, without L-glutamine, sodium pyruvate, and phenol red	Sigma-Aldrich	D1145-500mL
DMEM Advanced F12+	Life Technologies	12634-010
RPMI-1640 Medium, with L-glutamine and sodium bicarbonate, liquid, sterile-filtered, cell culture tested	Sigma-Aldrich	R8758-6X500ML
StemFit Basic04 Complete Type with bFGF	Ajinomoto	SFB-504-CT
Fetal Bovine Serum (FBS), lot 42Q0682K	Gibco	10270106
FBS, tetracycline free	Takara Bio	631106
B27 Supplement (50x) minus vitamin A	Gibco	12587-010
L-Glutamine	Gibco	25030-024
MEM Non-essential Amino Acid Solution (NEAA)	Gibco	11140-035
HEPES solution 1M	Sigma-Aldrich	H0887-100ML
Heparin sodium salt	R&D Systems	2812/100
Penicillin-Streptomycin (P/S)	Gibco	15140-122
Gelatin from porcine skin	Sigma-Aldrich	G1890-100G
Recombinant Laminin iMatrix-511 silk E8	Amsbio	AMS.892 021
Matrigel	Corning	354234
Glucose	Gibco	15023021
Fibroblast Growth Factor (FGF) basic	R&D Systems	233-FB-025
FGF-10	R&D Systems	345-FG-250
Nodal	R&D Systems	3218-ND-025

Reagent	Company	Cat. No.
Y-27632 dihydrochloride (rho-associated protein kinase (ROCK) inhibitor)	PeproTech	1293823
Trypsin-EDTA 0,25%	Sigma-Aldrich	T4049-100ML
Accutase	Sigma-Aldrich	A6964-100ML
StemPro Accutase Cell Dissociation Reagent	Thermo Fisher Scientific	A1110501
ReLeSR enzyme-free hiPSC passaging reagent	StemCell Technologies	05872
TrypLE Express Enzyme	Gibco	12605010
DMSO	Sigma-Aldrich	D2438
Trypan Blue solution 0.4%, liquid, sterile-filtered, suitable for cell culture	Logos biosystems	T13001

10.9 Cells

Table 11. List of cell cultures used in this study.

Name	Description	Reference/origin
HEK-293T	Human embryonic kidney cells expressing adenoviral E1A and E1B and the simian virus 40 (SV40) large T antigen	[344]
HEK-NS1	HEK-293T-Rex Flp-In cells (Invitrogen) expressing doxycycline-inducible H-1PV NS1 protein	[202]
HeLa-NS1	HeLa T-Rex cells (Invitrogen) expressing doxycycline-inducible H-1PV NS1 protein	[202]
U373-MG	Glioblastoma cell line	Iris Augustin, DKFZ
AsPC-1	Pancreatic adenocarcinoma call line	ATCC, CRL-1682
PC03	Patient-derived pancreatic adenocarcinoma culture	Kind gift from Claudia Ball [303]
PC06	Patient-derived pancreatic adenocarcinoma culture	Kind gift from Claudia Ball [303]
PC09	Patient-derived pancreatic adenocarcinoma culture	Kind gift from Claudia Ball [303]
PC20	Patient-derived pancreatic adenocarcinoma culture	Kind gift from Claudia Ball [303]

Name	Description	Reference/origin
PC31	Patient-derived pancreatic adenocarcinoma culture	Kind gift from Claudia Ball [303]
NHDF	Neonatal Human Dermal Fibroblasts, lot no. 2456041	Invitrogen, C-004-5C
SMAR1 iPSC	iPSCs derived from NHDF using SMAR vectors	Generated in this study
EBNA1 iPSC	iPSCs derived from NHDF using EBNA vectors	Generated in this study
EBNA2 iPSC	iPSCs derived from NHDF using EBNA vectors	Generated in this study
EBNA3 iPSC	iPSCs derived from NHDF using EBNA vectors	Generated in this study
SMAR5x.1 iPSC	iPSCs derived from NHDF using SMAR vectors	Generated in this study
SMAR5x.2 iPSC	iPSCs derived from NHDF using SMAR vectors	Generated in this study
SMAR5x.5 iPSC	iPSCs derived from NHDF using SMAR vectors	Generated in this study
SMAR5x.7 iPSC	iPSCs derived from NHDF using SMAR vectors	Generated in this study
SMAR5x.8 iPSC	iPSCs derived from NHDF using SMAR vectors	Generated in this study
SMAR5x.10 iPSC	iPSCs derived from NHDF using SMAR vectors	Generated in this study

10.10 Media composition

Table 12. Composition of cell culture media used in this study.

Cells	Media components	Amount
HEK-293T U373-MG	DMEM (With 4500 mg/L glucose, L-glutamine, and sodium bicarbonate, without sodium pyruvate)	
	FBS	10%
	Penicillin-Streptomycin	1%
	L-Glutamine	2mM

Cells	Media components	Amount
AsPC-1	RPMI-1640 Medium, with L-glutamine and sodium bicarbonate	
	FBS	10%
	Penicillin-Streptomycin	1%
	L-Glutamine	2mM
HEK-NS1	DMEM (with 4500 mg/L glucose, L-glutamine, and sodium bicarbonate, without sodium pyruvate)	
	FBS, tetracycline free	10%
	Penicillin-Streptomycin	1%
	Blasticidin	15ug/mL
	Hygromycin	50ugmL
	Doxycycline, for NS1 induction	1µg/mL
HeLa-NS1	DMEM (with 4500 mg/L glucose, L-glutamine, and sodium bicarbonate, without sodium pyruvate)	
	FBS, tetracycline free	10%
	Penicillin-Streptomycin	1%
	Blasticidin	6ug/mL
	Zeocin	200ug/mL
	Doxycycline, for NS1 induction	1µg/mL
PC31 PC03 PC20 PC09 PC06 (CSCN medium)	DMEM Advanced F12+	
	Glucose	0.6%
	L-Glutamine	2mM
	HEPES solution 1M	12ug/mL
	Heparin sodium salt	5mM
	B27 Supplement (50x) minus vitamin A	1x
	FGF basic (add fresh)	10ng/mL
	FGF-10 (add fresh)	20ng/mL
	Nodal (add fresh)	20ng/mL
NHDF	DMEM (With 4500 mg/L glucose, L-glutamine, and sodium bicarbonate, without sodium pyruvate)	
	FBS	10%
	Penicillin-Streptomycin	1%
	MEM Non-essential Amino Acid Solution (NEAA)	1%
	L-Glutamine	2mM
hiPSCs	StemFit Basic04 Complete Type with bFGF	
	Penicillin-Streptomycin	1%

10.11 Assay seeding densities

Table 13. List of assay seeding densities for cultured cells used in this study.

Cell culture	Cells per cm^2
AsPC-1	$1.25 \times 10^4 – 4.2 \times 10^4$, 1×10^4 for 7 day incubation
U373-MG	$1 \times 10^4 – 1.6 \times 10^4$, 5×10^3 for 7 day incubation
HeLa-NS1	$9.5 \times 10^3 – 2.3 \times 10^4$
HEK-NS1	4.69×10^4
PC03	1.25×10^4
PC06	2.50×10^4
PC09	2.50×10^4
PC20	3.13×10^4
PC31	3.13×10^4

10.12 Compounds

Table 14. List of compounds used in this study.

Name	Concentration(s) used	Company	Cat. No.
Ledipasvir	1-10µM	Selleck Chemicals	S7579
LY294002	10µM	Cayman Chemical Company	70920
Capivasertib	1µM	MedChem Express	HY-15431
Torin 1	50nM	Tocris Bioscience	4247
Rapamycin	20nM	Tocris Bioscience	1292
zVAD-FMK	up to 100µM	Selleck Chemicals	S7023
TUDCA	200µM	Selleck Chemicals	S3654
A23187	3µM	Sigma-Aldrich	C7522-1MG
Vitamin C	500µM	Sigma-Aldrich	255564-5G
Phenytoin	500µM	Sigma-Aldrich	D4505-25G

10.13 Kits

Table 15. List of kits used in this study.

Name	Company	Cat. No.
Molecular biology kits		
QIAprep Spin Miniprep Kit	QIAGEN	27106
QIAquick PCR purification kit	QIAGEN	28106
QIAGEN EndoFree Plasmid Maxi Kit	QIAGEN	12362
QIAquick Gel Extraction kit	QIAGEN	28704
Qubit dsDNA BR assay	Invitrogen	Q32850
Phire Tissue Direct PCR Master Mix	Thermo Fisher Scientific	F170S
Pierce™ BCA Protein Assay Kit	Thermo Fisher Scientific	23227
Alkaline Phosphatase Staining Kit II	Stemgent	00-0055
ReliaPrep RNA Miniprep from cells	Promega	Z6010
Wizard Genomic DNA purification kit	Promega	A1120
QIAamp MinElute Virus Spin kit	QIAGEN	57704
TaqMan Universal PCR Master Mix 2X	Applied Biosystems	4304437
Platinum Taq DNA polymerase	Thermo Fisher Scientific	10966083
Cell culture kits		
NHDF Nucleofection Kit	Lonza	VPD-1001
jetPEI	Polyplus	101-10N
STEMdiff Trilineage Differentiation kit	StemCell Technologies	05230
CytoTox 96 Non-Radioactive Cytotoxicity Assay	Promega	G1780
CellTiter-Glo 3D Cell Viability Assay	Promega	G9681
PrestoBlue Cell Viability Reagent	Thermo Fisher Scientific	A13261

10.14 Dyes

Table 16. List of dyes used in this study.

Name	Company	Catalogue Number
Incucyte Caspase 3/7 Green Dye	Sartorius	4440
Crystal Violet	Sigma Chemical Company	C-3886
DAPI	BD Pharmingen	564907
SYBR Green I	Sigma-Aldrich	S9430

10.15 Primary antibodies

Table 17. List of primary antibodies used in this study.

Target	Species	Clone	Use	Dilution	Company/ Source	Cat no.	kDa
4E-BP1	Rabbit	53H11	WB	1:2500	Cell Signaling Technology	9644	15-20
p4E-BP1$^{T37/46}$	Rabbit	236B4	WB	1:750	Cell Signaling Technology	2855	15-20
Akt	Rabbit		WB	1:1000	Cell Signaling Technology	9272	60
pAkt^{S473}	Rabbit		WB	1:1000	Cell Signaling Technology	9271	60
RPS6	Rabbit	5G10	WB	1:2500	Cell Signaling Technology	2217	32
pRPS6$^{S240/244}$	Rabbit	D68F8	WB	1:10,000	Cell Signaling Technology	5364	32
NS1	Rabbit	SP8	WB/ IF	1:50 (IF)/ 1:3000 (WB)	[185]		83
VP1/2	Rabbit		WB	1:4000	[345]		81/ 65
Oct3/4	Goat	n-19	WB	1:100	Santa Cruz Biotech	sc-8628	48
Klf4	Rabbit	H-180	WB	1:500	Santa Cruz Biotech	sc-20691	54-65
Sox2	Rabbit		WB	1:1000	Merck	AB5603	35
Lin28	Mouse	C-9	WB	1:200	Santa Cruz Biotech	sc-374460	28
α-tubulin	Mouse	DM1A	WB	1:5000	Thermo Fisher Scientific	62204	55
Vinculin	Mouse	H-10	WB	1:1000	Santa Cruz Biotech	sc-25336	117
GAPDH	Mouse	G-9	WB	1:1000	Santa Cruz Biotech	sc-365062	37
Tra-160	Mouse		IF	1:50	Santa Cruz Biotech	sc-21705	
Oct3/4	Rabbit		IF	1:300	Abcam	ab19857	
Nanog	Mouse		IF	1:50	Santa Cruz Biotech	sc-134218	
Nanog	Rabbit		IF	1:100	Abcam	ab21324	
Lin28	Mouse		IF	1:50	Santa Cruz Biotech	sc-374460	

Target	Species	Clone	Use	Dilution	Company/ Source	Cat no.	kDa
Sox17	Goat		IF	1:100	R&D Systems	AF1924	
NCAM (CD56)	Goat		IF	1:100	R&D Systems	AF2408	
β-tubulin	Mouse		IF	1:1000	Sigma-Aldrich	T8660	
SSEA-4	Mouse		IF	1:75	Abcam	ab16287	
Tra-1-81	Mouse		IF	1:150	Abcam	ab16289	

10.16 Secondary antibodies

Table 18. List of secondary antibodies used in this study.

Target	Species	Conjugation	Use	Dilution	Company	Cat. No.
Mouse IgG (H+L)	Goat	Alexa Fluor 546	IF	1:500	Invitrogen	A11003
Rabbit IgG (H+L)	Goat	Alexa Fluor 488	IF	1:500	Invitrogen	A11008
Goat IgG (H+L)	Donkey	Alexa Fluor 488	IF	1:500	Invitrogen	A11055
Mouse IgG (H+L)	Donkey	Alexa Fluor 488	IF	1:1000	Abcam	ab150105
Goat IgG (H+L)	Donkey	Alexa Fluor 647	IF	1:1000	Abcam	ab150131
Mouse	Goat	HRP	WB	1:5000	Jackson Immuno-Research	115-035-044
Rabbit	Donkey	HRP	WB	1:10,000	Life Technologies	A16023
Goat	Donkey	HRP	WB	1:10,000	Life Technologies	A15999

10.17 PCR primers

Table 19. List of PCR primers used in this study.

Name	Sequence (5' -> 3')	Target	Product size	Purpose
Ori_fwd	TTTCCATAGGCTCCGCCCCC	Bacterial origin of replication	589 bp	iPSC vector retention
Ori_rev	TTGAGATCCTTTTTTTCTGCGCGTAATCTGC			

Name	Sequence (5' -> 3')	Target	Product size	Purpose
nanoSMAR_Oct_fwd	CTCTGGGCTCTCCCATGCATTCAAACTGAGTCGACATGCATGCAGAAGTTG	IFNβ SMAR	2381 bp	Cloning nanoSMAR_hO-shp53
nanoSMAR_Oct_rev	CGGATCCTAGCGGCCGCACATGTAAGATACATTGATGAGTTTGGACAAACCACAAC			
nanoSMAR_SKML_fwd	AAAGGGCGAATTGCCTGCAGGGTCGACATGCATGCAGAAGTTG	IFNβ SMAR	2841 bp	Cloning nanoSMAR_hSK and hUL
nanoSMAR_SKML_rev	GTGGATCCGAGCTCGGTACCACTAGTCCTAATGATTTTTATCAAAATCATTAAGTTAAGGTAGATAC			

10.18 q(RT)-PCR primers

Table 20. List of q(RT)-PCR primers used in this study.

Name	Sequence (5' -> 3')	Target gene	Product size	Purpose	Source
H1-fwd	GCGCGGCAGAATTCAAACT	H-1PV NS1	141 bp	H-1PV genome quantification	[264]
H1-rev	CCACCTGGTTGAGCCATCAT				
H1-probe	6-FAM-ATGCAGCCAGACAGTTA-MGB	H-1PV NS1		H-1PV genome quantification	[264]
SOX17_fwd	GCTTTCATGGTGTGGGCTAA	Human SOX17	105 bp	trilineage differentiation of iPSCs, endoderm	[346]
SOX17_ rev	CGCCTTCCACGACTTGC				
FOXA2_fwd	TACAGGCGCAGCTACACGCACGCAAAG	Human FOXA2	216 bp	trilineage differentiation of iPSCs, endoderm	[346]
FOXA2_rev	GCGGGGCACCTTCAGGAAACAGTCGT				
KDR_fwd	CTGGCATGGTCTTCTGTGAAGCA	Human KDR	790 bp	trilineage differentiation of iPSCs, mesoderm	[347]
KDR_rev	AATACCAGTGGATGTGATGGCGG				
Brachyury_fwd	GGATGAAGGCTCCCGTCTC	Human TBXT	208 bp	trilineage differentiation of iPSCs, mesoderm	[346]
Brachyury_rev	GCTGTGATCTCCTCGTTCTGATA				

Name	Sequence (5' -> 3')	Target gene	Product size	Purpose	Source
Sox1_fwd	GGTCAAACGGCCCATGAACGC	Human SOX1	249 bp	trilineage differentiation of iPSCs, ectoderm	[346]
Sox1_rev	TCCTTCTTGAGCAGCGTCTTGGTCTT				
PAX6-fwd	TTTGCCCGAGAAAGACTAGC	Human PAX6	83 bp	trilineage differentiation of iPSCs, ectoderm	[348]
PAX6-rev	CATTTGGCCCTTCGATTAGA				
KLF4-fwd	TGATTGTAGTGCTTTCTGGCTGGGCTCC	Human KLF4	397 bp	iPSC phenotyping	[4]
KLF4-rev	ACGATCGTGGCCCCGGAAAAGGACC				
c-MYC-fwd	GCGTCCTGGGAAGGGAGTTCCGGAGC	Human MYC	325 bp	iPSC phenotyping	[4]
c-MYC-rev	TTGAGGGGCATCGTCGCGGGAGGCTG				
OCT3/4-S1165	GACAGGGGGAGGGGAGGAGCTAGG	Human POU5F1	144 bp	iPSC phenotyping	[4]
OCT3/4-AS1283	CTTCCCTCCAACCAGTTGCCCCAAAC				
SOX2-S1430	GGGAAATGGGAGGGGTGCAAAAGAGG	Human SOX2	151 bp	iPSC phenotyping	[4]
SOX2-AS1555	TTGCGTGAGTGTGGATGGGATTGGTG				
NANOG-S	CAGCCCTGATTCTTCCACCAGTCCC	Human NANOG	309 bp	iPSC phenotyping	[4]
NANOG-AS	CGGAAGATTCCCAGTCGGGTTCACC				
GDF3-S243	CTTATGCTACGTAAAGGAGCTGGG	Human GDF3	631 bp	iPSC phenotyping	[4]
GDF3-AS850	GTGCCAACCCAGGTCCCGGAAGTT				
REX1-RT-S	CAGATCCTAAACAGCTCGCAGAAT	Human ZFP42	305 bp	iPSC phenotyping	[4]
REX1-RT-AS	GCGTACGCAAATTAAAGTCCAGA				
FGF4-RT-S	CTACAACGCCTACGAGTCCTACA	Human FGF4	371 bp	iPSC phenotyping	[4]
FGF4-RT-AS	GTTGCACCAGAAAAGTCAGAGTTG				

Name	Sequence (5' -> 3')	Target gene	Product size	Purpose	Source
ESG1-S40	ATATCCCGCCGTGGGTGAAAGTTC	Human DPPA5	234 bp	iPSC phenotyping	[4]
ESG1-AS259	ACTCAGCCATGGACTGGAGCATCC				
TERT-S3234	CCTGCTCAAGCTGACTCGACACCGTG	Human TERT	446 bp	iPSC phenotyping	[4]
TERT-AS3713	GGAAAAGCTGGCCCTGGGGTGGAGC				
GAPDH_fwd	GCCAAAAGGGTCATCATCTC	Human GAPDH	117 bp	iPSC phenotyping	Self-made
GAPDH_rev	GGTGGTGCAGGAGGCATT				

11 Methods

11.1 Cloning

nanoSMAR vectors were cloned using In-Fusion cloning (Takara Bio). Briefly, this method involves *in vitro* homologous recombination of a 15bp region shared by both vector and insert(s). In this case, reprogramming vectors from the nano vector series were linearised by SbfI/KpnI double digestion (nanohSK and nanohUL) or NotI/NsiI double digest (nanohO-shp53) for use as vector backbones. The IFNβ S/MAR flanked by splicing sites was derived by polymerase chain reaction (PCR from the vector JP4.14 IL2RG flag sEF1-S/MAR IFN -NP, using primers to generate 15bp regions of homology with the vector backbones (see Table 19 for primer sequences). Digested vector backbones and PCR inserts were both separated by electrophoresis on a 1% agarose gel (1% agarose in EP buffer) and purified using a QIAquick Gel Extraction kit (QIAGEN). Digested backbones and PCR inserts were mixed at a mass ratio of 1:2 together with In-Fusion mix on ice and allowed to recombine at 50°C for 15 minutes, according to manufacturer's instructions. As the In-Fusion reaction is toxic to most bacteria, the resulting DNA was then precipitated by filling the volume up to 100µL with water and adding 10µL 3M sodium acetate (pH 5.2), then 250µL of 100% ethanol, and incubating at -20°C overnight. The next morning, precipitated DNA was pelleted by centrifugation at 16,000g for 30 minutes at 4°C, washed with ice-cold 70% ethanol and centrifuged again at 16,000g for 10 minutes at 4°C. After removal of as much ethanol as possible by pipetting, the DNA pellet was dried for 10-30 minutes at 40°C and resuspended in 3µL of nuclease-free water for electroporation into nanobacteria.

11.2 Electroporation of nanobacteria

Electrocompetent NTC1050811-HF bacteria (Nature Technologies) were thawed on ice before addition of 2.5µL ethanol purified In-Fusion reaction per 25µL aliquot of bacteria. The entire reaction was carefully transferred into a cold Gene Pulser cuvette (Bio-Rad, 165-2089) before electroporation with the Ec1 setting of a Micro Pulser device (Bio-Rad). 970µL of SOC medium was slowly added directly after electroporation and cells were then transferred to a 2mL Eppendorf tube for recovery at 30°C for 3 hours with gentle agitation. After this, cells were transferred to a 15mL Falcon tube to rest overnight at room temperature. The next day, cells were plated on LB-Agar plates containing sucrose as a selection medium and incubated overnight at 30°C before colony picking. Importantly, nanobacteria were never incubated above 30°C until a glycerol stock of bacteria with verified vector sequence was obtained.

11.3 Chemical transformation of bacteria

For handling of any vectors with a plasmid backbone, chemically competent DH5α bacteria (Life Technologies) were used. These were thawed on ice before addition of a small amount of target DNA (up to 50ng) was added and incubated on ice for 30 minutes. Bacteria were then subjected to heat shock at 42°C for 45 seconds, and immediately incubated on ice for 10 minutes. If the vector contained an ampicillin resistance cassette, the bacteria were then immediately plated onto LB-Agar plates containing ampicillin; if not, 1mL of warm LB broth without antibiotics was added to the cells, which were incubated for 30-60 min at 37°C with gentle shaking to allow them to recover. After recovery they were then plated on LB-Agar plates with the appropriate antibiotic.

11.4 Glycerol stocks

Frozen glycerol stocks of bacteria transformed with DNA were prepared for long-term storage of vectors. For this, equal volumes of overnight liquid cultures of transformed bacteria and a sterile 40% glycerol solution were mixed in a cryovial and immediately transferred to -80°C. To recover bacteria, a portion of the frozen glycerol stock was scraped out of the tube using a sterile Bac-loop and streaked onto a fresh LB-Agar plate containing the appropriate selection.

11.5 Vector purification

Vectors (nanovectors and plasmids) were purified from bacteria using the QIAGEN Spin Miniprep kit according to manufacturer's instructions for small-scale vector screening and cloning applications. For transfection into cells, vectors were purified using the QIAGEN EndoFree Plasmid Maxi kit, according to the manufacturer's instructions with the following modifications in the case of nanovectors: the volumes of P1, P2, P3 and ER buffers were doubled to ensure complete bacterial lysis and endotoxin removal. DNA concentrations for transfection were measured on a Qubit 4 (QIAGEN) using the dsDNA Broad Range assay.

11.6 Standard cell culture

All cells in this study were adherent cells and were cultured under 37°C and 5% CO_2. The media for each cell type is listed in Table 12**.** Unless otherwise required, cells were passaged on demand (2-3 times per week). Cells were washed once with PBS and then trypsinised using 0.25% Trypsin/EDTA for 5 minutes at 37°C. The culture vessel was tapped gently to release all cells, and they were resuspended in FBS-containing medium to inactivate the trypsin. Cells were then centrifuged at 250g for 5 minutes to remove the trypsin-containing medium and resuspended in an appropriate volume of fresh FBS-containing medium. Cells were then re-plated at the desired density in a new culture vessel. In general, cells were plated at similar densities for assays, regardless of the culture vessel (see Table 13).

Specialised cells such as primary NHDFs, patient-derived PDAC cultures, and iPSCs require specialised culturing conditions, described in detail below.

11.7 Cryopreservation and thawing of mammalian cells

Cells for cryopreservation were trypsinised as above, centrifuged, resuspended in appropriate medium with 10% FBS and 10% DMSO and transferred to cryovials. Cryovials were immediately transferred to an isopropanol-based freezing container (Mr Frosty) and stored at -80°C overnight to facilitate cooling at a rate of -1°C/minute. Cryovials were then transferred to liquid nitrogen for long-term storage.

To thaw cryopreserved cells, they were removed from liquid nitrogen and rapidly thawed in a 37°C water bath. Once only a small ice crystal remained, they were transferred to a sterile culture hood and disinfected with 80% ethanol. The cell suspension was transferred to a 50mL Falcon tube, and 10mL of pre-warmed culture medium (as appropriate for the cell type, see Table 12) was added dropwise while gently shaking the tube to ensure proper mixing. A small amount of culture medium was also used to wash out the cryovial, which was added to the cell suspension. Diluted cells were then centrifuged at 250g for 5 minutes and resuspended in fresh medium for plating at the desired density.

11.8 Cell culture plate coating

11.8.1 Gelatinisation of cell culture plates

Cell culture vessels for NHDF culture require a coating of gelatine on the vessel surface, prepared by covering the surface of a vessel with autoclaved 0.1% porcine gelatine in water and incubating for at least 20 minutes at 37°C and 5% CO_2. The gelatine mixture was then aspirated and ready to use.

11.8.2 Laminin coating of cell culture plates

iPSCs require laminin coating of cell culture vessels for attachment to the culture surface. For this, 4.8µL iMatrix Laminin-511 silk (Amsbio) per 1mL of PBS was mixed thoroughly and added to the desired culture vessel (2mL per 6-well plate, 1mL per 12-well plate, etc). This was incubated for 1 hour at 37°C and 5% CO_2, before aspiration and immediate addition of culture medium. Alternatively, laminin can be added directly to the culture medium, at half the concentration as for pre-coating – i.e. 2.4µL laminin per 1mL of culture medium. This must be mixed well, ideally before cells are added to avoid shear stress, and can be left in the culture medium overnight.

11.9 Primary cell culture

11.9.1 Neonatal human dermal fibroblasts (NHDFs)

NHDFs were cultured on gelatinised cell culture surfaces described in Section 11.8.1 above. Cells were thawed and cultured as described above (see Table 12 for medium), with the modification that all centrifugations were carried out at a maximum of 180g. For expansion, cells were seeded at the manufacturer's recommended density of 3500 cells/cm^2 of gelatinised culture vessel. Cells were assumed to be in passage 2 after thawing, so they were expanded and passaged once, before cryopreservation in passage 4 as described above for reprogramming.

11.9.2 Patient-derived PDAC cell cultures

Primary patient-derived PDAC cultures were cultured on standard cell culture surfaces, with CSCN medium changes every 3-4 days to replace cytokines (see Table 12 for details). To passage, cells were washed with PBS and released from the surface using Accutase incubation for at least 15 minutes at 37°C and 5% CO_2. The culture vessel was tapped to ensure complete release of cells, and they were washed from the surface using fresh CSCN medium (without cytokines). Cells were then centrifuged at 280g for 5 minutes, and resuspended in fresh CSCN medium before plating at the desired density (see Table 13). The cytokines FGF basic, FGF-10, and Nodal were always added fresh to CSCN medium in the appropriate concentrations when plating cells or exchanging the medium.
Primary PDAC cultures were cryopreserved in 55% RPMI 1640, 30% FBS, and 15% DMSO, following the procedure in Section 11.7 above. To thaw, freezing medium was first diluted using 50% unsupplemented CSCN medium and 50% FBS following the procedure above, before exchange for cytokine-supplemented CSCN medium for plating.

11.10 Stem cell culture

Human iPSCs were cultured on laminin-coated cell culture vessels (see Section 11.8.2 above), with Basic04 medium changes on a Mon-Wed-Fri schedule (see Table 12 for medium details). Since iPSCs do not survive as single cells, ROCK inhibitor was added to the medium at a concentration of 10µM at any time in which iPSC colonies were singularised, such as single-cell splitting or thawing cells [349]. However, prolonged ROCK inhibition also causes metabolic changes and possibly differentiation of iPSCs [350], so ROCKi-containing medium was always exchanged for fresh medium within 24 hours of plating.

11.10.1 Clump passaging of iPSCs

For routine passaging, iPSCs were split as clumps using ReLeSR (StemCell Technologies), or if a specific cell number was required, they were passaged using StemPro Accutase (Thermo Fisher Scientific). In general, iPSCs were cultured in a 6-well plate format.

For clump splitting, only 5mL plastic stripettes with a wide bore were used for pipetting to reduce shear stress on the cell clumps. Cells were washed once with PBS before addition of 1mL ReLeSR to the well for 30 seconds at room temperature. All ReLeSR was then removed from the well, and the dry plate was then incubated at 37°C and 5% CO_2 for 2 minutes. Cells were monitored under a microscope to ensure that holes had formed in each colony before careful addition of 1mL PBS to the side of the well. The plate was tapped firmly to dislodge all iPSC clumps, and an appropriate volume of cells was taken and added dropwise onto a pre-coated plate with fresh Basic04 medium (see Section 11.8.2 for coating method).

11.10.2 Single-cell passaging of iPSCs

For single-cell splitting, cells were washed once with PBS before addition of 200µL StemPro Accutase (Thermo Fisher Scientific) and incubation at 37°C and 5% CO_2 for 5-7 minutes. The plate was tapped firmly, and cells were resuspended in the Accutase solution to ensure complete detachment of cells. 500µL of Basic04 medium with 10µM ROCK inhibitor was added and the cell solution was transferred to an Eppendorf tube for counting using the LUNA cell counter (Logos Biosystems) if necessary. Then an appropriate volume of cells was added dropwise onto a pre-coated plate with fresh Basic04 medium supplemented with 10µM ROCK inhibitor (see Section 11.8.2 for coating method). The medium was changed 24 hours post plating to fresh Basic04 to remove ROCK inhibitor.

11.10.3 Cryopreservation and thawing of iPSCs

As cryopreservation is a stressful process, iPSCs were cryopreserved and thawed in medium containing 10µM ROCK inhibitor (Y-27632). In addition, only 5mL plastic stripettes with a wide bore were used for pipetting to reduce shear stress on the cells. Cells were passaged either as clumps or single cells as above and the desired volume of cell suspension for cryopreservation was aliquoted into an Eppendorf tube and centrifuged at 200g for 2 minutes. The supernatant was discarded, and 1mL of cold freezing medium (Basic04 + 10µM ROCKi + 10% DMSO) was added to the cell pellet without mixing. Cells were resuspended simply by transferring the pellet together with freezing media to a cryovial without pipetting up and down. This was immediately transferred to an isopropanol-based freezing container (Mr Frosty) and stored at -80°C overnight to facilitate cooling at a rate of -1°C/minute. Cryovials were then transferred to liquid nitrogen for long-term storage.

To thaw cryopreserved iPSCs, a fresh cell culture vessel was pre-coated with laminin and Basic04 medium supplemented with 10µM ROCK inhibitor was added to pre-warm at 37°C and 5% CO_2 (see Section 11.8.2 for coating method). Cryovials were removed from liquid nitrogen and rapidly thawed in a 37°C water bath. Once only a small ice crystal remained, they were transferred to a sterile

culture hood and disinfected with 80% ethanol. The cell suspension was transferred to a 50mL Falcon tube, and 7mL of Basic04 + ROCKi was added dropwise while gently shaking the tube to ensure proper mixing. A small amount of culture medium was also used to wash out the cryovial, which was added to the cell suspension. Diluted cells were then centrifuged at 100g for 5 minutes and resuspended slowly in fresh Basic04 + ROCKi and added dropwise to the prepared culture vessel. The medium was exchanged after a maximum of 24 hours to Basic04 without ROCK inhibitor.

11.11 Cell transfection

11.11.1 Nucleofection

Primary NHDFs were nucleofected using the Amaxa II Nucleofector device (Lonza) with the Human Dermal Fibroblast Nucleofector kit. One 6 well per transfection was prepared by gelatinising the culture surface (see Section 11.8.1 above) and prewarming 1.5mL of NHDF medium without antibiotics at 37°C and 5% CO_2. Per transfection, 90µL of Nucleofector solution was then mixed with 20µL supplement, and the appropriate mass of DNA was added. NHDFs growing on gelatinised culture flasks were harvested according to their culturing conditions (above) and counted using the LUNA cell counter (Logos Biosystems). $5x10^5$ cells per transfection were aliquoted into 1.5mL Eppendorf tubes and centrifuged for 7 minutes at 180g to remove all supernatant. Cells were then resuspended with the appropriate Nucleofector solution/DNA mix and transferred to a nucleofection cuvette. They were nucleofected with program P-022, and 500µL of pre-warmed NHDF medium without antibiotics was slowly added to the cells, before dropwise addition of the cell suspension using an eyedropper to the 6 well plate prepared earlier. The medium was exchanged one day post transfection to NHDF medium containing antibiotics, and the transfection efficiency was assessed by microscopy (see Section 2.2 above).

11.11.2 Chemical transfection

HEK-293T cells were transfected with jetPEI (Polyplus) according to the manufacturer's instructions. Cells were harvested by scraping 24 hours post transfection for Western blotting.

11.12 Virus production

H-1PV used in this study was produced by Tiina Marttila. Briefly, NB-324K cells were seeded in CellSTACK flasks and infected with an MOI of 0.01 plaque forming units (PFU) of H-1PV stock in a simultaneous seeding and infection step. Cells were incubated at 37°C and 5% CO_2 and observed for 4 days until cytopathic effect (CPE) was visible. CPE was defined as at least 30% dead or detached cells. Cells were harvested, and cell pellets were resuspended in Tris/EDTA lysis buffer (0.05M Tris-HCl, 0.5mM EDTA, pH 8.7). To release viral particles, pellets were subjected

to 3 freeze-thaw cycles. These crude cell extracts were then digested with 50U/mL Benzonase nuclease (Sigma) at 37°C for 30 minutes to remove all naked DNA. Viral particles were purified using iodixanol and Vis-Ringer density step gradients as previously described [351]. Viral titres were determined by plaque assay in NB-324K cells according to Daeffler, Horlein et al. [195] (see 11.13 below).

11.13 Titration of viral stocks

H-1PV used in this study was titrated by Tiina Marttila according to Daeffler, Horlein et al. [195]. Briefly, NB-324K cells were seeded and infected the next day with serial 10-fold dilutions of virus stocks for one hour at 37°C, 5% CO_2. After infection, the inoculum was removed and cells were covered with Minimal Essential Medium (MEM, Gibco) containing 0.65% Bacto agar (Becton Dickinson), 5 % FBS, 2 mM L-glutamine, 100 U/ml penicillin, and 100 mg/ml streptomycin. Cells were incubated at 37°C and 5% CO_2 for 4 days, and living cells were then stained for 18 hours with a neural red staining solution (0.2mg/mL neutral red, 0.85% Bacto agar in PBS). Plaques of dead cells were counted from duplicate experiments and titres calculated in terms of PFU per mL of virus stock.

11.14 Western blot

Whole cell lysates were obtained from cells in culture for Western blotting. Cells were either washed with PBS and trypsinised for 5 minutes at 37°C, then harvested in medium and centrifuged for 5 minutes at 350g, room temperature, or washed with PBS and harvested by scraping in PBS, then centrifuged for 5 minutes at 350g, room temperature. The supernatant was discarded and cells were lysed using Cell Lysis Buffer (Cell Signalling Technologies) with HALT protease and phosphatase inhibitor (Thermo Fisher) on ice for at least 20 minutes. Lysates were centrifuged for 30 minutes at 16000g, 4°C, and protein-containing supernatant was stored at -80°C. Protein concentration was measured using the Pierce BCA Protein Assay Kit (Thermo Fisher) according to the manufacturer's instructions. 20-30µg protein per well was mixed with 4x Laemmli (Bio-Rad) and denatured at 95°C for 5 minutes. Samples were separated on Mini-PROTEAN Gels 4-20% (Bio-Rad) in Tris-Glycine buffer (Bio-Rad) at 80-120V for 1-2h.

For Western blots analysing total protein, the protein was transferred from the SDS-PAGE gel to PVDF membrane using the iBlot2 dry blotting system (Invitrogen) according to the manufacturer's instructions, transferring with 20V for 7 minutes. Membranes were placed in deionised water immediately after transfer, then blocked in 5% milk in TBST (0.1% Tween-20) for 1 hour and incubated in primary antibody diluted in 5% milk in TBST at 4°C overnight. The next day, membranes were washed 3x 5 minutes with TBST before incubation in secondary antibody diluted in 5% milk in TBST for 1 hour. Membranes were washed a final 3x 5 minutes with TBST before developing using Western Lightning Plus ECL reagent (Perkin Elmer) in a ECL ChemoCam imager (Intas).

For Western blots analysing phosphoproteins, proteins were transferred from the SDS-PAGE gel to nitrocellulose membrane by semi-dry blotting using a Trans-Blot SD (Bio-Rad). An ionic gradient with three buffers (see Table 9) was set up by layering 6 filter papers soaked in buffer SD1, then 3 filter papers in buffer SD2 followed by the nitrocellulose membrane and SDS-PAGE gel both soaked in buffer SD2, and finally 9 filter papers soaked in buffer SD3. Proteins were transferred at 25V/300mA for 90 minutes. Membranes were then blocked in 5% BSA in TBST (0.1% Tween-20) for 1 hour and incubated in primary antibody diluted in 5% BSA in TBST at 4°C overnight. The next day, membranes were washed 3x 5 minutes with TBST before incubation in secondary antibody diluted in 5% BSA in TBST for 1 hour. Membranes were washed a final 3x 5 minutes with TBST before developing using Western Lightning Plus ECL reagent (Perkin Elmer) in a ECL ChemoCam imager (Intas). In general, two identical membranes were prepared simultaneously for analysis of both phospho- and total protein.

11.15 Reprogramming NHDFs

NHDFs were reprogrammed using a protocol established by Manuela Urban [75]. Cells were nucleofected with reprogramming vectors as described above (see Section 11.11.1 above), using 2µg of each EBNA vector, or 2/5/10µg of each S/MAR vector (see Section 2.4.1 above). After nucleofection, cells were plated on gelatinised 6 well plates in medium without antibiotics. Medium was exchanged for NHDF medium containing antibiotics (DMEM + 10% FBS + 1% NEAA, see Table 12) one day post nucleofection. Cells were confluent by day 2 post nucleofection, at which point they were trypsinised with 0.25% trypsin/EDTA at 37°C and 5% CO_2 and plated into one gelatinised T75 flask per transfection (one 6 well). Medium was refreshed every 2 to 3 days with fresh NHDF medium. On day 8, fresh culture vessels were coated with laminin (see Section 11.8.2 above). In general, 6-well plates were used for colony picking, and 12-well plates were used for AP staining (see Section 11.17 below). The cells were trypsinised as above, and $3x10^4$ cells were plated per well of 6-well plate and $1.09x10^4$ cells were plated per well of 12-well plate (cell density of $3.125x10^3$ cells/cm^2). The remaining cells were cryopreserved for further assays or continuation of the reprogramming process later. On day 9, the medium was replaced with iPSC medium (Basic04 + 1% P/S, see Table 12), and cells were fed every 2-3 days, on a Mon-Wed-Fri schedule. iPSC colonies appeared around day 20 and could be picked once a large enough colony size was reached (see 11.16 below). Importantly, only NHDFs younger than 5 passages were used for reprogramming to ensure efficiency of the reprogramming process. This protocol was partly developed in collaboration with Cornelia Wincek as part of a Master's internship.

11.16 iPSC colony picking

Once iPSC colonies had grown to a sufficient size (at least 100 cells), they were picked and transferred into fresh wells for further expansion. Per colony to be picked, one well of a 24-well plate was coated with laminin (see Section 11.8.2 above) and Basic04 medium supplemented with 10µm ROCK inhibitor (Y-27632) was pre-warmed in the coated plate at 37°C and 5% CO_2. An EVOS XL Core microscope (Thermo Fisher Scientific) was disinfected with ethanol, placed into a Safe2020 culture hood (Thermo Fisher Scientific), and exposed to UV irradiation for at least 30 minutes to ensure sterility. After this, the culture plate with the iPSC colony of interest was placed under the microscope, and a p200 pipette tip was used to carefully scratch an outline around the colony, separating it from the neighbouring fibroblasts. If the colony was not released from the culture surface by this, a cross-hatch pattern was scratched into the colony, to break it up into smaller clumps and release it from the culture surface. The p200 tip was then attached to a p200 pipette (Gilson), and the floating colony pieces were aspirated carefully, then transferred into the prepared well with pre-warmed medium. The medium was refreshed 24 hours post colony picking to fresh Basic04 to remove the ROCK inhibitor.

11.17 Alkaline phosphatase staining

Reprogrammed cells were stained for alkaline phosphatase (AP) expression as a marker for pluripotency using the Alkaline Phosphatase Staining Kit II (Stemgent) according to the manufacturer's instructions, with the modification that only 300µL of fixing and AP substrate solution was used per well of a 12 well plate. Plates were scanned using a Perfection V500 Photo scanner (Epson) and images of colonies were obtained on an EVOS XL Core Imaging System (Thermo Fisher Scientific).

11.18 Trilineage differentiation

Trilineage differentiation of iPSCs was performed using the STEMdiff Trilineage Differentiation kit (StemCell Technologies), according to the manufacturer's instructions. Briefly, cells were plated on Matrigel (Corning) coating and cultured using medium for endoderm (5 days), mesoderm (5 days), and ectoderm (7 days) differentiation with daily medium changes. After differentiation was complete, cells were either fixed for immunofluorescence, or RNA was harvested for qRT-PCR (described in Section 11.24 below).

11.19 Immunofluorescence

Cells fixed on culture slides (Sarsted) were treated with ice-cold methanol for 10 minutes and then washed once with PBS for 5 minutes. Cells fixed on glass-bottom plates (ibidi) were not methanol-treated, but both were then permeabilised in 0.1% Triton-X100 in PBS for 10 minutes at room temperature, followed by another 5-

minute PBS wash. Cells were blocked with 3% BSA/0.1% Tween-20 in PBS (filter sterilised) for 30 minutes, after which primary antibodies (see Table 17) diluted in blocking buffer were added for an overnight incubation at 4°C. Slides were then washed 3 times for 5 minutes each with PBS and incubated with a secondary antibody in blocking buffer (see Table 18) for 1 hour at room temperature. Following this, excess antibody was removed through a further 3 washes with PBS for 5 minutes each. Cells were mounted using Vectashield Mounting Medium with DAPI (Vector Laboratories).

11.20 Microscopy

Brightfield images of cells were taken on an EVOS XL Core Imaging System (Thermo Fisher Scientific). Fluorescent images of live cells were taken on an Eclipse Ti/X-Cite120Led microscope (Nikon). Images of immunofluorescence staining were acquired with a Stellaris 5 confocal microscope (Leica).

11.21 Incucyte imaging

For estimation of NHDF transfection efficiencies, cells were imaged once 24-48 hours post transfection using the Adherent Cell-By-Cell module of an Incucyte SX5 (Sartorius) with 10x objective capturing phase contrast and green fluorescence and analysed using the software Incucyte 2020B. Segmentation settings to define cells can be found in Table 21. Green cells were defined by a minimum Green Mean Intensity (GCU) set according to non-transfected cells.

For live cell imaging time courses, cells were seeded in 96-well plates in 100µL medium and left to settle overnight (see Table 13 for cell seeding densities). 50µL of medium was removed, and treatments were added in 50µL of fresh medium – drugs first, then virus. Plates were then imaged using the Adherent Cell-By-Cell module of an Incucyte SX5 (Sartorius) with 10x objective capturing phase contrast and fluorescence (as appropriate) and analysed using the software Incucyte 2020B. Segmentation settings to define cells can be found in Table 21. After imaging was complete, cells were used for further assays such as LDH and crystal violet staining (see Sections 11.27 and 11.28 below).

Table 21. Segmentation settings for each cell type analysed using Incucyte 2020B software.

		NHDF	AsPC-1	U373-MG
Cell Boundary	Segmentation adjustment	2	1.1	2
	Hole Fill (μm²)	1000	200	1600
	Adjust Size (pixels)		-2	-4
Object Seeding	Cell Detection Sensitivity	1.5	1	0.7
	Cell Contrast	1	1	2
	Cell Morphology	5	2	5
Cell-By-Cell Filters	Area	min: 300μm²		min: 400μm²
	Eccentricity			min: 0.5
	Green Mean Intensity			
	Green Integrated Intensity			
Fluorescent Background Subtraction	Top-Hat No Mask radius (μm)	40	50	50

11.22 Image processing

Microscopy images were processed using Fiji, a distribution of ImageJ [331]. Uneven illumination in images acquired with the EVOS XL Core microscope (Thermo Fisher Scientific) was corrected by pseudo-flat-field correction. A pseudo-flat-field image was generated by gaussian blur of the image (sigma = 50 pixels), and the original image was divided by the flat-field image with the Image Calculator plus plugin (k1 = mean flat-field intensity). For brightfield images, the white balance and brightness was adjusted manually. For fluorescent images, display ranges were normalised across all samples for each marker. Scale bars were added to images using the Analyze > Tools > Scale Bar function.

11.23 Flow cytometry

Transfection efficiency of NHDFs was estimated by flow cytometry. For this, $5x10^3$ transfected and untransfected NHDFs were harvested as described in Section 11.6 above and washed once with PBS. Cells were washed in PBS + 2% FBS (FACS buffer), then centrifuged and resuspended in FACS buffer with DAPI (1:500). Cells were filtered through a 35μm nylon mesh filter before analysis on a

FACSAria II cell sorter (BD Biosciences). Channels acquired and gating strategy is shown in Supplementary Figure 1.

11.24 Quantitative reverse-transcription polymerase chain reaction (qRT-PCR) for stemness markers

RNA was harvested from iPSCs before and after trilineage differentiation to characterise the gene expression of cells in each state using the ReliaPrep RNA Miniprep kit (Promega) according to the manufacturer's instructions. cDNA was synthesised from 2µg RNA per sample using the Superscript II RT (Invitrogen) using oligo(dT) primers (Invitrogen) according to the manufacturer's instructions. Gene expression was quantified using a SYBR green qPCR. Per reaction, 2µL of PCR buffer was mixed with 0.6µL 50mM $MgCl_2$, 0.4µL dNTPs, 0.4µL forward and reverse primers (10µM, see Table 20 for primer sequences), 0.6µL SYBR green (Sigma), 0.08µL Platinum Taq DNA polymerase (Thermo Fisher Scientific), and 9.52µL sterile water. This was mixed with 3µL of the synthesised cDNA in a 364-well plate and sealed with adhesive transparent cover. qPCR was performed in a CFX384 qPCR cycler (Bio-Rad); cycling conditions are listed in Table 22.

Table 22. Cycling conditions for qRT-PCRs to assay iPSC pluripotency and differentiation

Cycle step	Temperature	Time	Cycles
Initial denaturation	95°C	3 min	1
Denaturation	95°C	30 sec	40
Annealing	58°C	30 sec	
Extension	72°C	30 sec	
Final denaturation	95°C	1 min	1
Annealing	65°C	1 min	1
Melting curve	65°C – 95°C	0.5°C/sec	1

11.25 Copy number variant (CNV) analysis of iPSCs

For analysis of genomic integrity of iPSCs, cells were scraped off a high-density 6-well into PBS using a cell scraper and centrifuged at 2000g for 5 minutes. The cell pellet was stored at -20°C until ready for genomic DNA isolation using the Wizard Genomic DNA Purification kit (Promega) according to the manufacturer's instructions. Genotyping of iPSCs was performed by running 200ng of genomic DNA per clone on an Infinium Global Screening Array-24 v3.0 BeadChip (Illumina) at Erasmus MC, Rotterdam (Genomics Core Facility). Analysis of array data was performed using GenomeStudio software (Illumina) and R by Lieke Dons (Erasmus MC, Rotterdam). The genome of each cell line (including original fibroblasts) was aligned and compared to a reference human genome and copy number variants were called according to this reference. CNV calls were plotted with the Phenogram web tool (https://visualization.ritchielab.org/phenograms/plot) [342].

11.26 Polymerase chain reaction (PCR) for reprogramming vector retention

PCR to detect presence of reprogramming vectors was performed on snap-frozen cell pellets using the Phire Tissue Direct PCR kit (Thermo Fisher Scientific) according to the manufacturer's instructions, using kit-supplied internal control primers against *SOX21* and custom primers designed to detect the bacterial origin of replication (Ori) on plasmid vectors (see Table 19). Briefly, cell pellets were resuspended in Dilution Buffer with DNA Release Additive and incubated for 2-5min at room temperature, before boiling at 98°C for 2 minutes. Samples were diluted 1:50 in water, and 1µL of this was used as input for the PCR according to kit instructions. Primers were designed for a two-step PCR with annealing/extension at 72°C, and the PCR was run for 40 cycles (see Table 23 for cycling conditions). For positive controls, 10ng plasmid DNA was added directly to the PCR. PCR products were then separated on a 2% agarose gel and imaged using a Fusion SL gel documentation system (Vilber Lourmat).

Table 23. Cycling conditions for PCR to detect reprogramming vector retention in iPSCs.

Cycle step	Temperature	Time	Cycles
Initial denaturation	98°C	5 min	1
Denaturation	98°C	5 sec	40
Annealing/Extension	72°C	20 sec	
Final extension	72°C	1 min	1
	4°C	hold	

11.27 Lactate Dehydrogenase (LDH) assay

Active cell killing by H-1PV was assayed by measurement of free LDH enzyme in the supernatant, released by the lysis of cells. This was done using the CytoTox 96 Non-Radioactive Cytotoxicity Assay (Promega). For this measurement, it is crucial that the concentration of FBS in the culture medium is no more than 5%, to avoid high background signals. Cells were seeded and treated in 6 replicates of 100µL of 5% FBS-containing medium and cultured for the desired length of time (see Figure 41). At the end timepoint, three of six replicates were treated with 10µL of 10x lysis buffer (100% lysis controls), while 10µL PBS was added to the other three replicates. Meanwhile, one vial of Substrate Mix powder was dissolved in 12mL of Assay Buffer. After 30 minutes, the cells were monitored to ensure total lysis of the 100% lysis controls, and 50µL of supernatant from each well was transferred to a fresh 96-well plate. 50µL of prepared Substrate Mix was added to each well of supernatant and allowed to incubate in the dark at room temperature for at least 15 minutes, up to 30 minutes, until sufficient colour had developed. 50µL of Stop Solution was then added to halt the reaction, and absorbance was measured using a Multiskan Ex (Thermo Fisher Scientific) at 492nm.

Cell lysis was calculated by:

$$\%\ lysis = \frac{Abs_{492}\ sample - medium\ only}{Abs_{492}\ 100\%\ lysis - medium\ only} * 100$$

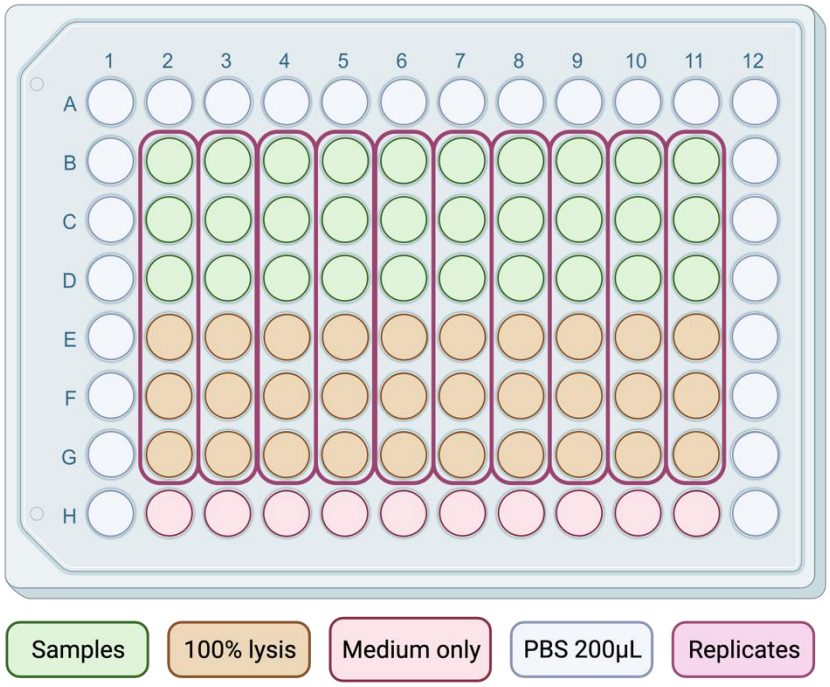

Figure 41. Schematic of cell plating for LDH assays.

11.28 Crystal violet cell staining

Cells were treated with crystal violet as an endpoint assay to assess how many cells remained after treatment. For 96-well plates, medium was removed (typically for measurement of LDH content, see Section 11.27 above), cells were washed once with PBS, then incubated in 0.2% crystal violet in water (w/v) with gentle agitation for at least 1 hour at room temperature (equal volumes for all wells). Cells were then washed with water until the water ran clear, then all liquid was removed, and the plate was dried overnight. For larger plate formats, cells were washed with PBS, then fixed using 0.5% glutaraldehyde in water for 1 hour at room temperature. Fixed cells were washed with distilled water, then all liquid was removed, and the plate was dried overnight. The next day, cells were incubated in 0.2% crystal violet in water (w/v) with gentle agitation for at least 1 hour at room temperature (equal volumes for all wells). Cells were washed with water until the water ran clear, then all liquid was removed, and the plate was dried overnight. Coloured staining was first imaged using a Perfection V500 Photo scanner (Epson), and then solubilised with 10% acetic acid in water with agitation for at least 30

minutes to quantify staining. Absorbance of solubilised crystal violet was measured using a Multiskan Ex (Thermo Labsystems) at 595nm.

Cell viability was calculated by:

$$\%\ viability = \frac{Abs_{595}\ sample - medium\ only}{Abs_{595}\ mock - medium\ only} * 100$$

11.29 PrestoBlue viability assay

PrestoBlue is a resazurin-based colourimetric and fluorescent indicator of cell viability by measuring mitochondrial dehydrogenase activity of intact cells. Cells were seeded and treated in 100µL of medium and cultured for the desired length of time. After removal of 50µL of culture medium for LDH assays (see Section 11.27 above), 10µL of PrestoBlue Cell Viability Reagent (Themo Fisher Scientific) was added to the remaining culture medium per well, including medium-only controls. The plate was incubated at 37°C for 1 hour before measurement of fluorescent resorufin using a Fluoroskan FL (Thermo Labsystems) with excitation at 544nm and emission at 590nm.

Cell viability was calculated by:

$$\%\ viability = \frac{Ex_{544}/Em_{590}\ sample - medium\ only}{Ex_{544}/Em_{590}\ mock - medium\ only} * 100$$

11.30 Quantitative polymerase chain reaction (qPCR) for viral genome

To measure the viral genome replication in H-1PV infected samples, $2x10^4$ U373-MG cells were seeded in 24-well plates and allowed to attach overnight at 37°C and 5% CO_2. Cells were infected with MOI 0.5 of H-1PV with or without 4µM Ledipasvir and incubated for a further 4 hours at 37°C and 5% CO_2. Leftover infection mix was snap-frozen and stored at -80°C for measurement of input virus. After 4 hours, cells were washed twice thoroughly with PBS before replacement of fresh medium, and cells were harvested at 4 hours, 24 hours and 120 hours post infection. At each timepoint, supernatant was removed from the wells, centrifuged at 300g for 5 minutes to remove all cellular material, and snap-frozen and stored at -80°C. Cells were harvested by trypsinisation as described in Section 11.6 above, and snap-frozen and stored at -80°C. When all samples (input, cells, and supernatants) were collected, they were subjected to 3 freeze-thaw cycles by alternating immersion in liquid nitrogen and 37°C with thorough mixing. Viral DNA was then extracted using the QIAamp MinElute Virus Spin kit (QIAGEN) according to the manufacturer's instructions.

Viral genomes were quantified using a parvovirus specific TaqMan probe with reference to a plasmid standard curve. Serial 10-fold dilutions of the plasmid pMVM+Δ800 were prepared (3.5–$3.5x10^7$ copies/µL). Per reaction, 10µL of TaqMan Universal PCR Master Mix 2X (Applied Biosystems) was mixed with 5.5µL dH_2O,

0.5µL of NS1-specific probe (10µM), and 0.5µL each of forward and reverse primers (10µM) (see Table 20 for primer and probe sequences). 17µL of this master mix was mixed with 3µL of each standard or sample in a 96-well PCR plate and sealed with adhesive transparent cover (Applied biosystems). The plate was centrifuged at 2360g for 5 minutes before cycling in a Realplex qPCR cycler (Eppendorf). Cycling conditions are listed in Table 24.

Table 24. Cycling conditions for NS1-specific qPCR for viral genome quantification.

Cycle step	Temperature	Time	Cycles
UNG incubation	50°C	2 min	1
Polymerase activation	95°C	10 min	1
Denaturation	95°C	15 sec	40
Annealing/Extension	60°C	1 min	

11.31 Cellular Thermal Shift Assay (CETSA)

The CEllular Thermal Shift Assay (CETSA) relies on the principle that ligand-bound proteins are more thermostable than their unbound counterparts. Thus, the potential of binding between a putative ligand-protein pair can be evaluated by assessing the temperature at which protein denaturation occurs when mixed with the ligand [296]. For this, NS1 expression was induced in HeLa-NS1 or HEK-NS1 cells by addition of 1µg/mL doxycycline to the culture medium, and cells were harvested by trypsinisation (see Section 11.6 above) 24 hours post induction. Cells were subjected to 3 freeze-thaw cycles by alternating incubation in liquid nitrogen and 37°C, and protein concentration of lysates was measured using the Pierce BCA Protein Assay Kit (Thermo Fisher) according to the manufacturer's instructions, and the concentration was adjusted to 2µg/µL. 400µL of this lysate was then treated with a final concentration of 10mM ATP, 100µM Ledipasvir, or equivalent volumes of DMSO on ice, and incubated for 15 minutes at room temperature to allow any ligand-protein interactions to occur without allowing too much hydrolysation of ATP by NS1. Each solution was divided into 8 50µL aliquots and heated for 3 minutes at a gradient of 40°C to 70°C in a peqSTAR PCR thermocycler (VWR Peqlab) to denature protein. Samples were then incubated at room temperature for 3 minutes before being placed on ice to halt any further protein denaturation. Samples were centrifuged at 20,000g for 30 minutes to precipitate all denatured protein, and the supernatants from each sample were assessed using Western blotting (see Section 11.14 above) using 16µg of protein per sample to detect all remaining soluble NS1. After data acquisition, relative band intensities for each treatment and temperature were calculated using Fiji [331] according to the method by Luke Miller [352]. Band intensity values were normalised between 0% – 100% (lowest intensity – highest intensity) for each treatment. This protocol

was developed in collaboration with Toros Taşgın as part of a Master's internship, based on the protocol by Jafari, Almqvist et al. [295].

11.32 Kinase activity profiling (PamGene)

Experimental procedures for kinase profiling were carried out by Valérie Palissot and Tiina Marttila. $8x10^5$ U373-MG cells were seeded in $75cm^2$ flasks and allowed to attach overnight at 37°C and 5% CO_2. Cells were infected 24 hours post seeding with MOI 10 of H-1PV with or without 4µM Ledipasvir and incubated at 37°C and 5% CO_2. Cells were harvested at each timepoint, and pellets were washed with ice-cold PBS, before lysis on ice using the Mammalian Protein Extraction Reagent (Thermo Fisher Scientific) including Protease Inhibitor Cocktail and Phosphatase Inhibitor Cocktail (Thermo Fisher Scientific) according to the manufacturer's recommendations. Lysates were centrifuged at 10,000g, 4°C for 10 minutes, and protein-containing supernatant was snap-frozen and stored at -80°C. Protein concentration was measured using the Pierce BCA Protein Assay Kit (Thermo Fisher) according to the manufacturer's instructions.
Kinase activity profiling was carried out using the PamChip® 12 serine/threonine (STK) and phosphotyrosine (PTK) peptide microarray system (PamGene International B.V.) according to the manufacturer's instructions. Array chips were blocked with 2% BSA and cell lysates were input at 1 µg/array for STK assays and 5 µg/array for PTK assays. Data quantification and visualisation was performed by PamGene using the BioNavigator software (PamGene International B.V). Peptides were filtered for those with signal above background in at least 80% of arrays in STK assays, and those with increasing signal over time for PTK assays, and statistical testing was used to define peptides with significant differential phosphorylation between conditions. Upstream kinase analysis was performed by PamGene using proprietary information about STK and PTK peptide chips.

11.33 RNA sequencing

Experimental procedures for RNA sequencing were carried out by Valérie Palissot and Tiina Marttila. $8x10^5$ U373-MG cells were seeded in $75cm^2$ flasks and allowed to attach overnight at 37°C and 5% CO_2. Cells were infected 24 hours post seeding with MOI 10 of H-1PV with or without 4µM Ledipasvir and incubated at 37°C and 5% CO_2. Cells were harvested at each timepoint, and pellets were washed in cold PBS, resuspended in TRIzol reagent, and stored at -80°C until RNA extraction. RNA was extracted in triplicate using the Direct-zol Miniprep extraction kit (Zymo Research) according to the manufacturer's protocol. RNA concentration was measured using the HSRNA kit on a Qubit 2.0 fluorometer (Invitrogen), and quality was measured with the Fragment Analyzer with the ssRNA kit (Agilent Technologies). All samples displayed RQN > 8.8. Sequencing libraries were prepared with 500ng of total RNA, and cytoplasmic and mitochondrial ribosomal RNA was depleted using the Ribo-Zero Human/Mouse/Rat Gold Kit (Illumina).

Library cDNA was generated using the TruSeq Stranded Total RNA Library Prep Gold kit (Illumina) was used following the manufacturer's recommendations and quantified using the dsDNA kit on a Qubit 2.0 fluorometer (Invitrogen). The size of each library was estimated using the Fragment Analyzer HS-NGS kit (Agilent Technologies). Libraries were pooled at 10nM and sequenced on a High and a Mid Output FlowCell (Illumina) in paired-end mode (75bp) on a Next Seq 550 sequencer (Illumina).
Gene Set Enrichment Analysis (GSEA) of RNA sequencing data was performed in collaboration with Yunhee Jeong. Genes with raw read counts below 10 were filtered out, and each sample was normalised by total counts. Afterwards, the counts were log1p- transformed. Combat correction was used to correct for batch effects over different samples [353]. GSEA software was used for analysis using default parameters [340]. Due to the low number of samples, gene sets were permuted rather than phenotypes. As a result, pathways were typically only considered significant with a false discovery rate (FDR) of below 5%.

11.34 Microarray expression profiling of PDAC cells

Microarray data for 14 primary PDAC cultures was kindly provided by Theresa Schäfer and Christine Engeland. This data was generated using an Affymetrix Human Clariom S assay (Affymetrix/Thermo Fisher Scientific), and analysed using Chipster [341]. Robust multichip average (RMA) from the *affy* package was used to subtract background, normalise, and summarise raw data [337]. All genes within the microarray data associated with the relevant KEGG pathway or GO term were extracted, and differential expression values for each gene were compared between classical and quasi-mesenchymal subgroups using an empirical Bayes test from the *limma* package with Benjamini-Hochberg adjustment and a p-value threshold of 0.05 [338]. Heatmaps were drawn using the *amap* package with Pearson correlation [339] either using the entire 14-culture dataset, or after extracting the five cultures used in this study.

References

[1] Malik, V., and Wang, J., 2022. 'Pursuing totipotency: authentic totipotent stem cells in culture', *Trends Genet*, 38: 632-36. https://doi.org/10.1016/j.tig.2022.03.012

[2] Waddington, C. H., 1957. *The Strategy of the Genes: A Discussion of Some Aspects of Theoretical Biology* (Allen & Unwin: London). https://doi.org/https://doi.org/10.4324/9781315765471

[3] Gurdon, J. B., 1962. 'Adult frogs derived from the nuclei of single somatic cells', *Developmental Biology*, 4: 256-73. https://doi.org/10.1016/0012-1606(62)90043-x

[4] Takahashi, K., Tanabe, K., Ohnuki, M., Narita, M., Ichisaka, T., Tomoda, K., and Yamanaka, S., 2007. 'Induction of pluripotent stem cells from adult human fibroblasts by defined factors', *Cell*, 131: 861-72. https://doi.org/10.1016/j.cell.2007.11.019

[5] Takahashi, K., and Yamanaka, S., 2006. 'Induction of pluripotent stem cells from mouse embryonic and adult fibroblast cultures by defined factors', *Cell*, 126: 663-76. https://doi.org/10.1016/j.cell.2006.07.024

[6] Warlich, E., Kuehle, J., Cantz, T., Brugman, M. H., Maetzig, T., Galla, M., Filipczyk, A. A., Halle, S., Klump, H., . . . Schambach, A., 2011. 'Lentiviral vector design and imaging approaches to visualize the early stages of cellular reprogramming', *Mol Ther*, 19: 782-9. https://doi.org/10.1038/mt.2010.314

[7] Carey, B. W., Markoulaki, S., Hanna, J., Saha, K., Gao, Q., Mitalipova, M., and Jaenisch, R., 2009. 'Reprogramming of murine and human somatic cells using a single polycistronic vector', *Proc Natl Acad Sci U S A*, 106: 157-62. https://doi.org/10.1073/pnas.0811426106

[8] Senís, E., Mosteiro, L., Wilkening, S., Wiedtke, E., Nowrouzi, A., Afzal, S., Fronza, R., Landerer, H., Abad, M., . . . Grimm, D., 2018. 'AAV vector-mediated in vivo reprogramming into pluripotency', *Nature Communications*, 9: 2651. https://doi.org/10.1038/s41467-018-05059-x

[9] Deyle, D. R., and Russell, D. W., 2009. 'Adeno-associated virus vector integration', *Curr Opin Mol Ther*, 11: 442-7. https://www.ncbi.nlm.nih.gov/pmc/articles/PMC2929125/pdf/nihms227900.pdf

[10] Hanlon, K. S., Kleinstiver, B. P., Garcia, S. P., Zaborowski, M. P., Volak, A., Spirig, S. E., Muller, A., Sousa, A. A., Tsai, S. Q., . . . György, B., 2019. 'High levels of AAV vector integration into CRISPR-induced DNA breaks', *Nature Communications*, 10: 4439. https://doi.org/10.1038/s41467-019-12449-2

[11] Lieu, P. T., Fontes, A., Vemuri, M. C., and MacArthur, C. C., 2013. 'Generation of Induced Pluripotent Stem Cells with CytoTune, a Non-Integrating Sendai Virus.' in Uma Lakshmipathy and Mohan C. Vemuri (eds.), *Pluripotent Stem Cells: Methods and Protocols* (Humana Press: Totowa, NJ). https://doi.org/10.1007/978-1-62703-348-0_5

[12] Warren, L., Manos, P. D., Ahfeldt, T., Loh, Y. H., Li, H., Lau, F., Ebina, W., Mandal, P. K., Smith, Z. D., . . . Rossi, D. J., 2010. 'Highly efficient reprogramming to pluripotency and directed differentiation of human cells with synthetic modified mRNA', *Cell Stem Cell*, 7: 618-30. https://doi.org/10.1016/j.stem.2010.08.012

[13] Yakubov, E., Rechavi, G., Rozenblatt, S., and Givol, D., 2010. 'Reprogramming of human fibroblasts to pluripotent stem cells using mRNA of four transcription factors', *Biochemical and Biophysical Research Communications*, 394: 189-93. https://doi.org/10.1016/j.bbrc.2010.02.150

[14] Cho, H.-J., Lee, C.-S., Kwon, Y.-W., Paek, J. S., Lee, S.-H., Hur, J., Lee, E. J., Roh, T.-Y., Chu, I.-S., . . . Kim, H.-S., 2010. 'Induction of pluripotent stem cells from adult somatic cells by protein-based reprogramming without genetic manipulation', *Blood*, 116: 386-95. https://doi.org/10.1182/blood-2010-02-269589

[15] Seo, B. J., Hong, Y. J., and Do, J. T., 2017. 'Cellular Reprogramming Using Protein and Cell-Penetrating Peptides', *Int J Mol Sci*, 18. https://doi.org/10.3390/ijms18030552

[16] Guan, J., Wang, G., Wang, J., Zhang, Z., Fu, Y., Cheng, L., Meng, G., Lyu, Y., Zhu, J., . . . Deng, H., 2022. 'Chemical reprogramming of human somatic cells to pluripotent stem cells', *Nature*. https://doi.org/10.1038/s41586-022-04593-5

[17] Kumar, D., Anand, T., Talluri, T. R., and Kues, W. A., 2020. 'Potential of transposon-mediated cellular reprogramming towards cell-based therapies', *World J Stem Cells*, 12: 527-44. https://doi.org/10.4252/wjsc.v12.i7.527

[18] Okita, K., Nakagawa, M., Hyenjong, H., Ichisaka, T., and Yamanaka, S., 2008. 'Generation of Mouse Induced Pluripotent Stem Cells Without Viral Vectors', *Science*, 322: 949-53. https://doi.org/10.1126/science.1164270

[19] Okita, K., Hong, H., Takahashi, K., and Yamanaka, S., 2010. 'Generation of mouse-induced pluripotent stem cells with plasmid vectors', *Nat Protoc*, 5: 418-28. https://doi.org/10.1038/nprot.2009.231

[20] Yu, J., Hu, K., Smuga-Otto, K., Tian, S., Stewart, R., Slukvin, II, and Thomson, J. A., 2009. 'Human induced pluripotent stem cells free of vector and transgene sequences', *Science*, 324: 797-801. https://doi.org/10.1126/science.1172482

[21] Okita, K., Matsumura, Y., Sato, Y., Okada, A., Morizane, A., Okamoto, S., Hong, H., Nakagawa, M., Tanabe, K., . . . Yamanaka, S., 2011. 'A more efficient method to generate integration-free human iPS cells', *Nat Methods*, 8: 409-12. https://doi.org/10.1038/nmeth.1591

[22] Yoshida, G. J., 2018. 'Emerging roles of Myc in stem cell biology and novel tumor therapies', *Journal of Experimental & Clinical Cancer Research*, 37: 173. https://doi.org/10.1186/s13046-018-0835-y

[23] Takahashi, J., 2020. 'iPS cell-based therapy for Parkinson's disease: A Kyoto trial', *Regen Ther*, 13: 18-22. https://doi.org/10.1016/j.reth.2020.06.002

[24] Takahashi, J., 2021. 'Clinical Trial for Parkinson's Disease Gets a Green Light in the US', *Cell Stem Cell*, 28: 182-83. https://doi.org/10.1016/j.stem.2021.01.013

[25] Liu, X., Robbins, S., Wang, X., Virk, S., Schuck, K., Deveza, L. A., Oo, W. M., Carmichael, K., Antony, B., . . . Hunter, D. J., 2021. 'Efficacy and cost-effectiveness of Stem Cell injections for symptomatic relief and strUctural improvement in people with Tibiofemoral knee OsteoaRthritis: protocol for a randomised placebo-controlled trial (the SCUlpTOR trial)', *BMJ Open*, 11: e056382. https://doi.org/10.1136/bmjopen-2021-056382

[26] Thornton, C. D., Fielding, S., Karbowniczek, K., Roig-Merino, A., Burrows, A. E., FitzPatrick, L. M., Sharaireh, A., Tite, J. P., Mole, S. E., . . . McKay, T. R., 2021. 'Safe and stable generation of induced pluripotent stem cells using doggybone DNA vectors', *Mol Ther Methods Clin Dev*, 23: 348-58. https://doi.org/10.1016/j.omtm.2021.09.018

[27] Davis, R. L., Weintraub, H., and Lassar, A. B., 1987. 'Expression of a single transfected cDNA converts fibroblasts to myoblasts', *Cell*, 51: 987-1000. https://doi.org/https://doi.org/10.1016/0092-8674(87)90585-X

[28] Wang, H., Yang, Y., Liu, J., and Qian, L., 2021. 'Direct cell reprogramming: approaches, mechanisms and progress', *Nature Reviews Molecular Cell Biology*, 22: 410-24. https://doi.org/10.1038/s41580-021-00335-z

[29] Mall, M., and Wernig, M., 2017. 'The novel tool of cell reprogramming for applications in molecular medicine', *J Mol Med (Berl)*, 95: 695-703. https://doi.org/10.1007/s00109-017-1550-4

[30] Mandai, M., Watanabe, A., Kurimoto, Y., Hirami, Y., Morinaga, C., Daimon, T., Fujihara, M., Akimaru, H., Sakai, N., . . . Takahashi, M., 2017. 'Autologous Induced Stem-Cell-Derived Retinal Cells for Macular Degeneration', *N Engl J Med*, 376: 1038-46. https://doi.org/10.1056/NEJMoa1608368

[31] Takagi, S., Mandai, M., Gocho, K., Hirami, Y., Yamamoto, M., Fujihara, M., Sugita, S., Kurimoto, Y., and Takahashi, M., 2019. 'Evaluation of Transplanted Autologous Induced Pluripotent Stem Cell-Derived Retinal

Pigment Epithelium in Exudative Age-Related Macular Degeneration', *Ophthalmol Retina*, 3: 850-59. https://doi.org/10.1016/j.oret.2019.04.021

[32] Kim, J. Y., Nam, Y., Rim, Y. A., and Ju, J. H., 2022. 'Review of the Current Trends in Clinical Trials Involving Induced Pluripotent Stem Cells', *Stem Cell Reviews and Reports*, 18: 142-54. https://doi.org/10.1007/s12015-021-10262-3

[33] Cynata Therapeutics, 2023. 'Recruitment Completed in Phase 3 SCUlpTOR Osteoarthritis Clinical Trial ', *ASX Announcement*, 13.12.2023. https://app.sharelinktechnologies.com/announcement/asx/e9300998deb38d9174c60a78dac400ef

[34] Xu, H., Wang, B., Ono, M., Kagita, A., Fujii, K., Sasakawa, N., Ueda, T., Gee, P., Nishikawa, M., . . . Hotta, A., 2019. 'Targeted Disruption of HLA Genes via CRISPR-Cas9 Generates iPSCs with Enhanced Immune Compatibility', *Cell Stem Cell*, 24: 566-78.e7. https://doi.org/10.1016/j.stem.2019.02.005

[35] Deuse, T., Hu, X., Gravina, A., Wang, D., Tediashvili, G., De, C., Thayer, W. O., Wahl, A., Garcia, J. V., . . . Schrepfer, S., 2019. 'Hypoimmunogenic derivatives of induced pluripotent stem cells evade immune rejection in fully immunocompetent allogeneic recipients', *Nature Biotechnology*, 37: 252-58. https://doi.org/10.1038/s41587-019-0016-3

[36] Hafeez, M. S., Awais, S. B., Razvi, M., Bangash, M. H., Hsiou, D. A., Malik, T. H., Haq, M. U., Awan, A. A. Y., and Rana, A. A., 2023. 'HLA mismatch is important for 20-year graft survival in kidney transplant patients', *Transplant Immunology*, 80: 101861. https://doi.org/https://doi.org/10.1016/j.trim.2023.101861

[37] Kekre, N., Mak, K. S., Stopsack, K. H., Binder, M., Ishii, K., Brånvall, E., and Cutler, C. S., 2016. 'Impact of HLA-Mismatch in Unrelated Donor Hematopoietic Stem Cell Transplantation: A Meta-Analysis', *American Journal of Hematology*, 91: 551-55. https://doi.org/https://doi.org/10.1002/ajh.24342

[38] Simkin, D., Papakis, V., Bustos, B. I., Ambrosi, C. M., Ryan, S. J., Baru, V., Williams, L. A., Dempsey, G. T., McManus, O. B., . . . Kiskinis, E., 2022. 'Homozygous might be hemizygous: CRISPR/Cas9 editing in iPSCs results in detrimental on-target defects that escape standard quality controls', *Stem Cell Reports*, 17: 993-1008. https://doi.org/https://doi.org/10.1016/j.stemcr.2022.02.008

[39] Taylor, Craig J., Peacock, S., Chaudhry, Afzal N., Bradley, J. A., and Bolton, Eleanor M., 2012. 'Generating an iPSC Bank for HLA-Matched Tissue Transplantation Based on Known Donor and Recipient HLA Types', *Cell Stem Cell*, 11: 147-52. https://doi.org/https://doi.org/10.1016/j.stem.2012.07.014

[40] Miura, K., Okada, Y., Aoi, T., Okada, A., Takahashi, K., Okita, K., Nakagawa, M., Koyanagi, M., Tanabe, K., . . . Yamanaka, S., 2009. 'Variation in the safety of induced pluripotent stem cell lines', *Nat Biotechnol*, 27: 743-5. https://doi.org/10.1038/nbt.1554

[41] Hossain, M. E., Cevallos, R. R., Zhang, R., and Hu, K., 2023. 'Attenuating iPSC reprogramming stress with dominant-negative BET peptides', *iScience*, 26: 105889. https://doi.org/10.1016/j.isci.2022.105889

[42] Banito, A., Rashid, S. T., Acosta, J. C., Li, S., Pereira, C. F., Geti, I., Pinho, S., Silva, J. C., Azuara, V., . . . Gil, J., 2009. 'Senescence impairs successful reprogramming to pluripotent stem cells', *Genes Dev*, 23: 2134-9. https://doi.org/10.1101/gad.1811609

[43] Hong, H., Takahashi, K., Ichisaka, T., Aoi, T., Kanagawa, O., Nakagawa, M., Okita, K., and Yamanaka, S., 2009. 'Suppression of induced pluripotent stem cell generation by the p53–p21 pathway', *Nature*, 460: 1132-35. https://doi.org/10.1038/nature08235

[44] Malik, N., and Rao, M. S., 2013. 'A review of the methods for human iPSC derivation', *Methods Mol Biol*, 997: 23-33. https://doi.org/10.1007/978-1-62703-348-0_3

[45] Cesana, D., Ranzani, M., Volpin, M., Bartholomae, C., Duros, C., Artus, A., Merella, S., Benedicenti, F., Sergi Sergi, L., . . . Montini, E., 2014. 'Uncovering and dissecting the genotoxicity of self-inactivating lentiviral vectors in vivo', *Mol Ther*, 22: 774-85. https://doi.org/10.1038/mt.2014.3

[46] Fusaki, N., Ban, H., Nishiyama, A., Saeki, K., and Hasegawa, M., 2009. 'Efficient induction of transgene-free human pluripotent stem cells using a vector based on Sendai virus, an RNA virus that does not integrate into the host genome', *Proceedings of the Japan Academy, Series B*, 85: 348-62. https://doi.org/10.2183/pjab.85.348

[47] Kunitomi, A., Hirohata, R., Arreola, V., Osawa, M., Kato, T. M., Nomura, M., Kawaguchi, J., Hara, H., Kusano, K., . . . Yamanaka, S., 2022. 'Improved Sendai viral system for reprogramming to naive pluripotency', *Cell Rep Methods*, 2: 100317. https://doi.org/10.1016/j.crmeth.2022.100317

[48] Humme, S., Reisbach, G., Feederle, R., Delecluse, H. J., Bousset, K., Hammerschmidt, W., and Schepers, A., 2003. 'The EBV nuclear antigen 1 (EBNA1) enhances B cell immortalization several thousandfold', *Proc Natl Acad Sci U S A*, 100: 10989-94. https://doi.org/10.1073/pnas.1832776100

[49] Frappier, L., 2012. 'Contributions of Epstein-Barr nuclear antigen 1 (EBNA1) to cell immortalization and survival', *Viruses*, 4: 1537-47. https://doi.org/10.3390/v4091537

[50] Kreppel, F., and Hagedorn, C., 2022. 'Episomes and Transposases—Utilities to Maintain Transgene Expression from Nonviral Vectors', *Genes*, 13. https://doi.org/10.3390/genes13101872

[51] De Belle, I., Cai, S., and Kohwi-Shigematsu, T., 1998. 'The Genomic Sequences Bound to Special AT-rich Sequence-binding Protein 1 (SATB1) In Vivo in Jurkat T Cells Are Tightly Associated with the Nuclear Matrix at the Bases of the Chromatin Loops', *The Journal of Cell Biology*, 141: 335-48. https://doi.org/10.1083/jcb.141.2.335

[52] Jenke, B. H., Fetzer, C. P., Stehle, I. M., Jonsson, F., Fackelmayer, F. O., Conradt, H., Bode, J., and Lipps, H. J., 2002. 'An episomally replicating vector binds to the nuclear matrix protein SAF-A in vivo', *EMBO Rep*, 3: 349-54. https://doi.org/10.1093/embo-reports/kvf070

[53] Hagedorn, C., Wong, S. P., Harbottle, R., and Lipps, H. J., 2011. 'Scaffold/matrix attached region-based nonviral episomal vectors', *Hum Gene Ther*, 22: 915-23. https://doi.org/10.1089/hum.2011.084

[54] Roig-Merino, A., 2018. 'Genetic Modification of Stem Cells Utilizing S/MAR DNA Vectors', Ruperto-Carola University of Heidelberg.

[55] Mirkovitch, J., Mirault, M.-E., and Laemmli, U. K., 1984. 'Organization of the higher-order chromatin loop: specific DNA attachment sites on nuclear scaffold', *Cell*, 39: 223-32. https://doi.org/10.1016/0092-8674(84)90208-3

[56] Cook, P. R., 1999. 'The Organization of Replication and Transcription', *Science*, 284: 1790-95. https://doi.org/doi:10.1126/science.284.5421.1790

[57] Bode, J., Kohwi, Y., Dickinson, L., Joh, T., Klehr, D., Mielke, C., and Kohwi-Shigematsu, T., 1992. 'Biological significance of unwinding capability of nuclear matrix-associating DNAs', *Science*, 255: 195-7. https://doi.org/10.1126/science.1553545

[58] Jenke, A. C. W., Scinteie, M. F., Stehle, I. M., and Lipps, H. J., 2004. 'Expression of a transgene encoded on a non-viral episomal vector is not subject to epigenetic silencing by cytosine methylation', *Molecular Biology Reports*, 31: 85-90. https://doi.org/10.1023/b:mole.0000031363.35839.46

[59] Forrester, W. C., Fernández, L. A., and Grosschedl, R., 1999. 'Nuclear matrix attachment regions antagonize methylation-dependent repression of long-range enhancer-promoter interactions', *Genes Dev*, 13: 3003-14. https://doi.org/10.1101/gad.13.22.3003

[60] Argyros, O., Wong, S. P., Niceta, M., Waddington, S. N., Howe, S. J., Coutelle, C., Miller, A. D., and Harbottle, R. P., 2008. 'Persistent episomal transgene expression in liver following delivery of a scaffold/matrix attachment region containing non-viral vector', *Gene Ther*, 15: 1593-605. https://doi.org/10.1038/gt.2008.113

[61] Stehle, I. M., Scinteie, M. F., Baiker, A., Jenke, A. C., and Lipps, H. J., 2003. 'Exploiting a minimal system to study the epigenetic control of DNA replication: the interplay between transcription and replication', *Chromosome Res*, 11: 413-21. https://doi.org/10.1023/a:1024962308071

[62] Piechaczek, C., Fetzer, C., Baiker, A., Bode, J., and Lipps, H. J., 1999. 'A vector based on the SV40 origin of replication and chromosomal S/MARs replicates episomally in CHO cells', *Nucleic Acids Research*, 27: 426-28. https://doi.org/10.1093/nar/27.2.426

[63] Baiker, A., Maercker, C., Piechaczek, C., Schmidt, S. B., Bode, J., Benham, C., and Lipps, H. J., 2000. 'Mitotic stability of an episomal vector containing a human scaffold/matrix-attached region is provided by association with nuclear matrix', *Nat Cell Biol*, 2: 182-4. https://doi.org/10.1038/35004061

[64] Schaarschmidt, D., Baltin, J., Stehle, I. M., Lipps, H. J., and Knippers, R., 2003. 'An episomal mammalian replicon: sequence-independent binding of the origin recognition complex', *The EMBO Journal*, 23: 191-201. https://doi.org/10.1038/sj.emboj.7600029

[65] Stehle, I. M., Postberg, J., Rupprecht, S., Cremer, T., Jackson, D. A., and Lipps, H. J., 2007. 'Establishment and mitotic stability of an extra-chromosomal mammalian replicon', *BMC Cell Biology*, 8: 33. https://doi.org/10.1186/1471-2121-8-33

[66] Hagedorn, C., Gogol-Doring, A., Schreiber, S., Epplen, J. T., and Lipps, H. J., 2017. 'Genome-wide profiling of S/MAR-based replicon contact sites', *Nucleic Acids Res*, 45: 7841-54. https://doi.org/10.1093/nar/gkx522

[67] Haase, R., Argyros, O., Wong, S. P., Harbottle, R. P., Lipps, H. J., Ogris, M., Magnusson, T., Vizoso Pinto, M. G., Haas, J., . . . Baiker, A., 2010. 'pEPito: a significantly improved non-viral episomal expression vector for mammalian cells', *BMC Biotechnol*, 10: 20. https://doi.org/10.1186/1472-6750-10-20

[68] Bozza, M., De Roia, A., Correia, M. P., Berger, A., Tuch, A., Schmidt, A., Zornig, I., Jager, D., Schmidt, P., . . . Harbottle, R. P., 2021. 'A nonviral, nonintegrating DNA nanovector platform for the safe, rapid, and persistent manufacture of recombinant T cells', *Sci Adv*, 7. https://doi.org/10.1126/sciadv.abf1333

[69] Luke, J., Carnes, A. E., Hodgson, C. P., and Williams, J. A., 2009. 'Improved antibiotic-free DNA vaccine vectors utilizing a novel RNA based plasmid selection system', *Vaccine*, 27: 6454-9. https://doi.org/10.1016/j.vaccine.2009.06.017

[70] Bozza, M., 2017. 'The development of a novel S/MAR DNA vector platform for the stable, persistent and safe Genetic Engineering of Dividing Cells', Ruperto Carola University Heidelberg.

[71] Chen, Z. Y., He, C. Y., Ehrhardt, A., and Kay, M. A., 2003. 'Minicircle DNA vectors devoid of bacterial DNA result in persistent and high-level transgene expression in vivo', *Mol Ther*, 8: 495-500. https://doi.org/10.1016/s1525-0016(03)00168-0

[72] Hodges, B. L., Taylor, K. M., Joseph, M. F., Bourgeois, S. A., and Scheule, R. K., 2004. 'Long-term transgene expression from plasmid DNA gene therapy vectors is negatively affected by CpG dinucleotides', *Mol Ther*, 10: 269-78. https://doi.org/10.1016/j.ymthe.2004.04.018

[73] Roig-Merino, A., Urban, M., Bozza, M., Peterson, J. D., Bullen, L., Buchler-Schaff, M., Stable, S., van der Hoeven, F., Muller-Decker, K., . . . Harbottle, R. P., 2022. 'An episomal DNA vector platform for the persistent genetic modification of pluripotent stem cells and their differentiated progeny', *Stem Cell Reports*, 17: 143-58. https://doi.org/10.1016/j.stemcr.2021.11.011

[74] Lufino, M. M. P., Manservigi, R., and Wade-Martins, R., 2007. 'An S/MAR-based infectious episomal genomic DNA expression vector provides long-term regulated functional complementation of LDLR deficiency', *Nucleic Acids Research*, 35: e98-e98. https://doi.org/10.1093/nar/gkm570

[75] Urban, M., 2021. 'Utilising S/MAR DNA vectors for the genetic modification of human induced pluripotent stem cells for cell and gene therapy', Ruperto Carola University Heidelberg.

[76] Okita, K., Yamakawa, T., Matsumura, Y., Sato, Y., Amano, N., Watanabe, A., Goshima, N., and Yamanaka, S., 2013. 'An efficient nonviral method to generate integration-free human-induced pluripotent stem cells from cord blood and peripheral blood cells', *Stem Cells*, 31: 458-66. https://doi.org/10.1002/stem.1293

[77] Wernig, M., Meissner, A., Foreman, R., Brambrink, T., Ku, M., Hochedlinger, K., Bernstein, B. E., and Jaenisch, R., 2007. 'In vitro reprogramming of fibroblasts into a pluripotent ES-cell-like state', *Nature*, 448: 318-24. https://doi.org/10.1038/nature05944

[78] Mittal, N., and Domian, I. J., 2014. 'Persistent Integration of Reprogramming Factors Impairs the In Vitro Cardiogenic Potential of Induced Pluripotent Stem Cells', *Circulation: Cardiovascular Genetics*, 7: 571-72. https://doi.org/10.1161/circgenetics.114.000825

[79] Herbst, F., Ball, C. R., Tuorto, F., Nowrouzi, A., Wang, W., Zavidij, O., Dieter, S. M., Fessler, S., van der Hoeven, F., . . . Glimm, H., 2012. 'Extensive methylation of promoter sequences silences lentiviral transgene expression during stem cell differentiation in vivo', *Mol Ther*, 20: 1014-21. https://doi.org/10.1038/mt.2012.46

[80] Esteban, M. A., Wang, T., Qin, B., Yang, J., Qin, D., Cai, J., Li, W., Weng, Z., Chen, J., . . . Pei, D., 2010. 'Vitamin C enhances the generation of mouse and human induced pluripotent stem cells', *Cell Stem Cell*, 6: 71-9. https://doi.org/10.1016/j.stem.2009.12.001

[81] Štefková, K., Procházková, J., and Pacherník, J., 2015. 'Alkaline Phosphatase in Stem Cells', *Stem Cells International*, 2015: 1-11. https://doi.org/10.1155/2015/628368

[82] Luke, J. M., Carnes, A. E., and Williams, J. A., 2014. 'Development of antibiotic-free selection system for safer DNA vaccination', *Methods Mol Biol*, 1143: 91-111. https://doi.org/10.1007/978-1-4939-0410-5_6

[83] Apostolou, E., and Stadtfeld, M., 2018. 'Cellular trajectories and molecular mechanisms of iPSC reprogramming', *Curr Opin Genet Dev*, 52: 77-85. https://doi.org/10.1016/j.gde.2018.06.002

[84] Milone, M. C., and O'Doherty, U., 2018. 'Clinical use of lentiviral vectors', *Leukemia*, 32: 1529-41. https://doi.org/10.1038/s41375-018-0106-0

[85] US Food and Drug Administration, 2023. 'FDA Investigating Serious Risk of T-cell Malignancy Following BCMA-Directed or CD19-Directed Autologous Chimeric Antigen Receptor (CAR) T cell Immunotherapies', Accessed 1.12.2023. https://www.fda.gov/vaccines-blood-biologics/safety-availability-biologics/fda-investigating-serious-risk-t-cell-malignancy-following-bcma-directed-or-cd19-directed-autologous.

[86] US Food and Drug Administration, 2024. 'FDA Roundup: January 23, 2024', Accessed 7.2.2024. https://www.fda.gov/news-events/press-announcements/fda-roundup-january-23-2024.

[87] Schlaeger, T. M., Daheron, L., Brickler, T. R., Entwisle, S., Chan, K., Cianci, A., Devine, A., Ettenger, A., Fitzgerald, K., . . . Daley, G. Q., 2015. 'A comparison of non-integrating reprogramming methods', *Nature Biotechnology*, 33: 58-63. https://doi.org/10.1038/nbt.3070

[88] Lim, S., Yocum, R. R., Silver, P. A., and Way, J. C., 2023. 'High spontaneous integration rates of end-modified linear DNAs upon mammalian cell transfection', *Scientific Reports*, 13. https://doi.org/10.1038/s41598-023-33862-0

[89] Canaan, A., Haviv, I., Urban, A. E., Schulz, V. P., Hartman, S., Zhang, Z., Palejev, D., Deisseroth, A. B., Lacy, J., . . . Weissman, S. M., 2009. 'EBNA1 regulates cellular gene expression by binding cellular promoters', *Proc Natl Acad Sci U S A*, 106: 22421-6. https://doi.org/10.1073/pnas.0911676106

[90] Westhoff Smith, D., Chakravorty, A., Hayes, M., Hammerschmidt, W., and Sugden, B., 2021. 'The Epstein-Barr Virus Oncogene EBNA1 Suppresses Natural Killer Cell Responses and Apoptosis Early after Infection of

Peripheral B Cells', *mBio*, 12: e0224321. https://doi.org/10.1128/mBio.02243-21

[91] Nakagawa, M., Koyanagi, M., Tanabe, K., Takahashi, K., Ichisaka, T., Aoi, T., Okita, K., Mochiduki, Y., Takizawa, N., . . . Yamanaka, S., 2008. 'Generation of induced pluripotent stem cells without Myc from mouse and human fibroblasts', *Nature Biotechnology*, 26: 101-06. https://doi.org/10.1038/nbt1374

[92] Li, W., Lu, L., Lu, J., Wang, X., Yang, C., Jin, J., Wu, L., Hong, X., Li, F., . . . Deng, L., 2020. 'cGAS-STING-mediated DNA sensing maintains CD8(+) T cell stemness and promotes antitumor T cell therapy', *Sci Transl Med*, 12. https://doi.org/10.1126/scitranslmed.aay9013

[93] Warren, L., and Lin, C., 2019. 'mRNA-Based Genetic Reprogramming', *Mol Ther*, 27: 729-34. https://doi.org/10.1016/j.ymthe.2018.12.009

[94] Lee, J., Sayed, N., Hunter, A., Au, K. F., Wong, W. H., Mocarski, E. S., Pera, R. R., Yakubov, E., and Cooke, J. P., 2012. 'Activation of innate immunity is required for efficient nuclear reprogramming', *Cell*, 151: 547-58. https://doi.org/10.1016/j.cell.2012.09.034

[95] Liu, C., Ameen, M., Himmati, S., Thomas, D., and Sayed, N., 2021. 'Generation of Human iPSCs by Protein Reprogramming and Stimulation of TLR3 Signaling', *Methods Mol Biol*, 2239: 153-62. https://doi.org/10.1007/978-1-0716-1084-8_10

[96] Tanabe, K., Nakamura, M., Narita, M., Takahashi, K., and Yamanaka, S., 2013. 'Maturation, not initiation, is the major roadblock during reprogramming toward pluripotency from human fibroblasts', *Proc Natl Acad Sci U S A*, 110: 12172-9. https://doi.org/10.1073/pnas.1310291110

[97] Samavarchi-Tehrani, P., Golipour, A., David, L., Sung, H.-k., Beyer, T. A., Datti, A., Woltjen, K., Nagy, A., and Wrana, J. L., 2010. 'Functional Genomics Reveals a BMP-Driven Mesenchymal-to-Epithelial Transition in the Initiation of Somatic Cell Reprogramming', *Cell Stem Cell*, 7: 64-77. https://doi.org/10.1016/j.stem.2010.04.015

[98] Gill, D., Parry, A., Santos, F., Okkenhaug, H., Todd, C. D., Hernando-Herraez, I., Stubbs, T. M., Milagre, I., and Reik, W., 2022. 'Multi-omic rejuvenation of human cells by maturation phase transient reprogramming', *Elife*, 11. https://doi.org/10.7554/eLife.71624

[99] Gonzalez, F., Barragan Monasterio, M., Tiscornia, G., Montserrat Pulido, N., Vassena, R., Batlle Morera, L., Rodriguez Piza, I., and Belmonte, J. C. I., 2009. 'Generation of mouse-induced pluripotent stem cells by transient expression of a single nonviral polycistronic vector', *Proceedings of the National Academy of Sciences*, 106: 8918-22. https://doi.org/10.1073/pnas.0901471106

[100] Cheng, L., Hansen, N. F., Zhao, L., Du, Y., Zou, C., Donovan, F. X., Chou, B. K., Zhou, G., Li, S., . . . Liu, P. P., 2012. 'Low incidence of DNA sequence variation in human induced pluripotent stem cells generated by nonintegrating plasmid expression', *Cell Stem Cell*, 10: 337-44. https://doi.org/10.1016/j.stem.2012.01.005

[101] Kang, X., Yu, Q., Huang, Y., Song, B., Chen, Y., Gao, X., He, W., Sun, X., and Fan, Y., 2015. 'Effects of Integrating and Non-Integrating Reprogramming Methods on Copy Number Variation and Genomic Stability of Human Induced Pluripotent Stem Cells', *PLOS ONE*, 10: e0131128. https://doi.org/10.1371/journal.pone.0131128

[102] Gruhne, B., Sompallae, R., and Masucci, M. G., 2009. 'Three Epstein–Barr virus latency proteins independently promote genomic instability by inducing DNA damage, inhibiting DNA repair and inactivating cell cycle checkpoints', *Oncogene*, 28: 3997-4008. https://doi.org/10.1038/onc.2009.258

[103] Turinetto, V., Orlando, L., and Giachino, C., 2017. 'Induced Pluripotent Stem Cells: Advances in the Quest for Genetic Stability during Reprogramming Process', *International Journal of Molecular Sciences*, 18: 1952. https://doi.org/10.3390/ijms18091952

[104] Haridhasapavalan, K. K., Raina, K., Dey, C., Adhikari, P., and Thummer, R. P., 2020. 'An Insight into Reprogramming Barriers to iPSC Generation', *Stem Cell Rev Rep*, 16: 56-81. https://doi.org/10.1007/s12015-019-09931-1

[105] Invitrogen, 2019. "Human Dermal Fibroblasts, neonatal (HDFn)." *Product Information Sheet*.

[106] Feng, B., Ng, J.-H., Heng, J.-C. D., and Ng, H.-H., 2009. 'Molecules that Promote or Enhance Reprogramming of Somatic Cells to Induced Pluripotent Stem Cells', *Cell Stem Cell*, 4: 301-12. https://doi.org/https://doi.org/10.1016/j.stem.2009.03.005

[107] Silva, J., Barrandon, O., Nichols, J., Kawaguchi, J., Theunissen, T. W., and Smith, A., 2008. 'Promotion of Reprogramming to Ground State Pluripotency by Signal Inhibition', *PLOS Biology*, 6: e253. https://doi.org/10.1371/journal.pbio.0060253

[108] Kim, J. B., Sebastiano, V., Wu, G., Arauzo-Bravo, M. J., Sasse, P., Gentile, L., Ko, K., Ruau, D., Ehrich, M., . . . Scholer, H. R., 2009. 'Oct4-induced pluripotency in adult neural stem cells', *Cell*, 136: 411-9. https://doi.org/10.1016/j.cell.2009.01.023

[109] Yu, J., Chau, K. F., Vodyanik, M. A., Jiang, J., and Jiang, Y., 2011. 'Efficient Feeder-Free Episomal Reprogramming with Small Molecules', *PLOS ONE*, 6. https://doi.org/10.1371/journal.pone.0017557

[110] Drozd, A. M., Walczak, M. P., Piaskowski, S., Stoczynska-Fidelus, E., Rieske, P., and Grzela, D. P., 2015. 'Generation of human iPSCs from cells of fibroblastic and epithelial origin by means of the oriP/EBNA-1 episomal reprogramming system', *Stem Cell Res Ther*, 6: 122. https://doi.org/10.1186/s13287-015-0112-3

[111] Rupprecht, S., Hagedorn, C., Seruggia, D., Magnusson, T., Wagner, E., Ogris, M., and Lipps, H. J., 2010. 'Controlled removal of a nonviral episomal vector from transfected cells', *Gene*, 466: 36-42. https://doi.org/10.1016/j.gene.2010.07.001

[112] Kelly, E., and Russell, S. J., 2007. 'History of oncolytic viruses: genesis to genetic engineering', *Mol Ther*, 15: 651-9. https://doi.org/10.1038/sj.mt.6300108

[113] Bierman, H. R., Crile, D. M., Dod, K. S., Kelly, K. H., Petrakis, N. I., White, L. P., and Shimkin, M. B., 1953. 'Remissions in leukemia of childhood following acute infectious disease. Staphylococcus and streptococcus, varicella, and feline panleukopenias', *Cancer*, 6: 591-605. https://doi.org/10.1002/1097-0142(195305)6:3<591::Aid-cncr2820060317>3.0.Co;2-m

[114] Bifulco, M., Di Zazzo, E., Napolitano, F., Malfitano, A. M., and Portella, G., 2023. 'History of how viruses can fight cancer: From the miraculous healings to the approval of oncolytic viruses', *Biochimie*, 206: 89-92. https://doi.org/10.1016/j.biochi.2022.10.008

[115] Hoster, H. A., Zanes, R. P., Jr., and Von Haam, E., 1949. 'Studies in Hodgkin's syndrome; the association of viral hepatitis and Hodgkin's disease; a preliminary report', *Cancer Res*, 9: 473-80. https://pubmed.ncbi.nlm.nih.gov/18134519/

[116] Southam, C. M., and Moore, A. E., 1952. 'Clinical studies of viruses as antineoplastic agents, with particular reference to egypt 101 virus', *Cancer*, 5: 1025-34. https://doi.org/10.1002/1097-0142(195209)5:5<1025::aid-cncr2820050518>3.0.co;2-q

[117] Levaditi, C., and Nicolau, S., 1922. 'Sur le culture du virus vaccinal dans les neoplasmes epithelieux', *CR Soc Biol*, 86: 928.

[118] Martuza, R. L., Malick, A., Markert, J. M., Ruffner, K. L., and Coen, D. M., 1991. 'Experimental therapy of human glioma by means of a genetically engineered virus mutant', *Science*, 252: 854-6. https://doi.org/10.1126/science.1851332

[119] Alberts, P., Tilgase, A., Rasa, A., Bandere, K., and Venskus, D., 2018. 'The advent of oncolytic virotherapy in oncology: The Rigvir(R) story', *Eur J Pharmacol*, 837: 117-26. https://doi.org/10.1016/j.ejphar.2018.08.042

[120] Garber, K., 2006. 'China Approves World's First Oncolytic Virus Therapy For Cancer Treatment', *JNCI: Journal of the National Cancer Institute*, 98: 298-300. https://doi.org/10.1093/jnci/djj111

[121] Harrington, K. J., Puzanov, I., Hecht, J. R., Hodi, F. S., Szabo, Z., Murugappan, S., and Kaufman, H. L., 2015. 'Clinical development of talimogene laherparepvec (T-VEC): a modified herpes simplex virus type-1-derived oncolytic immunotherapy', *Expert Rev Anticancer Ther*, 15: 1389-403. https://doi.org/10.1586/14737140.2015.1115725

[122] European Medicines Agency, 2022. 'Imlygic - talimogene laherparepvec', Accessed 02.02.2024. https://www.ema.europa.eu/en/medicines/human/EPAR/imlygic#ema-inpage-item-authorisation-details.

[123] Shalhout, S. Z., Miller, D. M., Emerick, K. S., and Kaufman, H. L., 2023. 'Therapy with oncolytic viruses: progress and challenges', *Nature Reviews Clinical Oncology*, 20: 160-77. https://doi.org/10.1038/s41571-022-00719-w

[124] Frampton, J. E., 2022. 'Teserpaturev/G47Δ: First Approval', *BioDrugs*, 36: 667-72. https://doi.org/10.1007/s40259-022-00553-7

[125] Todo, T., Ito, H., Ino, Y., Ohtsu, H., Ota, Y., Shibahara, J., and Tanaka, M., 2022. 'Intratumoral oncolytic herpes virus G47Δ for residual or recurrent glioblastoma: a phase 2 trial', *Nature Medicine*, 28: 1630-39. https://doi.org/10.1038/s41591-022-01897-x

[126] Hietanen, E., Koivu, M. K. A., and Susi, P., 2022. 'Cytolytic Properties and Genome Analysis of Rigvir(®) Oncolytic Virotherapy Virus and Other Echovirus 7 Isolates', *Viruses*, 14. https://doi.org/10.3390/v14030525

[127] Ma, R., Li, Z., Chiocca, E. A., Caligiuri, M. A., and Yu, J., 2023. 'The emerging field of oncolytic virus-based cancer immunotherapy', *Trends in Cancer*, 9: 122-39. https://doi.org/10.1016/j.trecan.2022.10.003

[128] Li, K., Zhao, Y., Hu, X., Jiao, J., Wang, W., and Yao, H., 2022. 'Advances in the clinical development of oncolytic viruses', *Am J Transl Res*, 14: 4192-206. https://www.ncbi.nlm.nih.gov/pmc/articles/PMC9274612/pdf/ajtr0014-4192.pdf

[129] Huang, Z., Guo, H., Lin, L., Li, S., Yang, Y., Han, Y., Huang, W., and Yang, J., 2023. 'Application of oncolytic virus in tumor therapy', *J Med Virol*, 95: e28729. https://doi.org/10.1002/jmv.28729

[130] U.S. Food & Drug Administration, 2022. 'FDA approves first adenoviral vector-based gene therapy for high-risk Bacillus Calmette-Guérin unresponsive non-muscle invasive bladder cancer', Accessed 31.01.2024. https://www.fda.gov/drugs/resources-information-approved-drugs/fda-

approves-first-adenoviral-vector-based-gene-therapy-high-risk-bacillus-calmette-guerin.

[131] Kaufman, H. L., Kohlhapp, F. J., and Zloza, A., 2015. 'Oncolytic viruses: a new class of immunotherapy drugs', *Nat Rev Drug Discov*, 14: 642-62. https://doi.org/10.1038/nrd4663

[132] Vaha-Koskela, M., and Hinkkanen, A., 2014. 'Tumor Restrictions to Oncolytic Virus', *Biomedicines*, 2: 163-94. https://doi.org/10.3390/biomedicines2020163

[133] McKee, T. D., Grandi, P., Mok, W., Alexandrakis, G., Insin, N., Zimmer, J. P., Bawendi, M. G., Boucher, Y., Breakefield, X. O., . . . Jain, R. K., 2006. 'Degradation of fibrillar collagen in a human melanoma xenograft improves the efficacy of an oncolytic herpes simplex virus vector', *Cancer Res*, 66: 2509-13. https://doi.org/10.1158/0008-5472.Can-05-2242

[134] Mok, W., Boucher, Y., and Jain, R. K., 2007. 'Matrix Metalloproteinases-1 and -8 Improve the Distribution and Efficacy of an Oncolytic Virus', *Cancer Research*, 67: 10664-68. https://doi.org/10.1158/0008-5472.Can-07-3107

[135] Schäfer, S., Weibel, S., Donat, U., Zhang, Q., Aguilar, R. J., Chen, N. G., and Szalay, A. A., 2012. 'Vaccinia virus-mediated intra-tumoral expression of matrix metalloproteinase 9 enhances oncolysis of PC-3 xenograft tumors', *BMC Cancer*, 12: 366. https://doi.org/10.1186/1471-2407-12-366

[136] Chen, Z., Han, F., Du, Y., Shi, H., and Zhou, W., 2023. 'Hypoxic microenvironment in cancer: molecular mechanisms and therapeutic interventions', *Signal Transduction and Targeted Therapy*, 8: 70. https://doi.org/10.1038/s41392-023-01332-8

[137] Shayan, S., Arashkia, A., and Azadmanesh, K., 2022. 'Modifying oncolytic virotherapy to overcome the barrier of the hypoxic tumor microenvironment. Where do we stand?', *Cancer Cell International*, 22: 370. https://doi.org/10.1186/s12935-022-02774-w

[138] Breitbach, C. J., De Silva, N. S., Falls, T. J., Aladl, U., Evgin, L., Paterson, J., Sun, Y. Y., Roy, D. G., Rintoul, J. L., . . . Bell, J. C., 2011. 'Targeting Tumor Vasculature With an Oncolytic Virus', *Molecular Therapy*, 19: 886-94. https://doi.org/10.1038/mt.2011.26

[139] Xiao, T., Fan, J. K., Huang, H. L., Gu, J. F., Li, L.-Y., and Liu, X. Y., 2010. 'VEGI-armed oncolytic adenovirus inhibits tumor neovascularization and directly induces mitochondria-mediated cancer cell apoptosis', *Cell Research*, 20: 367-78. https://doi.org/10.1038/cr.2009.126

[140] Choi, J.-W., Jung, S.-J., Kasala, D., Hwang, J. K., Hu, J., Bae, Y. H., and Yun, C.-O., 2015. 'pH-sensitive oncolytic adenovirus hybrid targeting acidic

tumor microenvironment and angiogenesis', *Journal of Controlled Release*, 205: 134-43. https://doi.org/10.1016/j.jconrel.2015.01.005

[141] Kaur, B., Antonio Chiocca, E., and P. Cripe, T., 2012. 'Oncolytic HSV-1 Virotherapy: Clinical Experience and Opportunities for Progress', *Curr Pharm Biotechnol*, 13: 1842-51. https://doi.org/10.2174/138920112800958814

[142] Bhattacharjee, S., and Yadava, P. K., 2018. 'Measles virus: Background and oncolytic virotherapy', *Biochemistry and Biophysics Reports*, 13: 58-62. https://doi.org/10.1016/j.bbrep.2017.12.004

[143] Hagedorn, C., and Kreppel, F., 2017. 'Capsid Engineering of Adenovirus Vectors: Overcoming Early Vector-Host Interactions for Therapy', *Hum Gene Ther*, 28: 820-32. https://doi.org/10.1089/hum.2017.139

[144] Geoffroy, K., and Bourgeois-Daigneault, M. C., 2020. 'The pros and cons of interferons for oncolytic virotherapy', *Cytokine Growth Factor Rev*. https://doi.org/10.1016/j.cytogfr.2020.07.002

[145] Gong, J., and Mita, M. M., 2014. 'Activated Ras Signaling Pathways and Reovirus Oncolysis: An Update on the Mechanism of Preferential Reovirus Replication in Cancer Cells', *Frontiers in Oncology*, 4. https://doi.org/10.3389/fonc.2014.00167

[146] Cesaro, T., and Michiels, T., 2021. 'Inhibition of PKR by Viruses', *Front Microbiol*, 12: 757238. https://doi.org/10.3389/fmicb.2021.757238

[147] Poppers, J., Mulvey, M., Khoo, D., and Mohr, I., 2000. 'Inhibition of PKR Activation by the Proline-Rich RNA Binding Domain of the Herpes Simplex Virus Type 1 Us11 Protein', *Journal of Virology*, 74: 11215-21. https://doi.org/10.1128/jvi.74.23.11215-11221.2000

[148] Schirrmacher, V., 2022. 'Molecular Mechanisms of Anti-Neoplastic and Immune Stimulatory Properties of Oncolytic Newcastle Disease Virus', *Biomedicines*, 10. https://doi.org/10.3390/biomedicines10030562

[149] Mansour, M., Palese, P., and Zamarin, D., 2011. 'Oncolytic specificity of Newcastle disease virus is mediated by selectivity for apoptosis-resistant cells', *J Virol*, 85: 6015-23. https://doi.org/10.1128/jvi.01537-10

[150] Adams, C. M., Clark-Garvey, S., Porcu, P., and Eischen, C. M., 2018. 'Targeting the Bcl-2 Family in B Cell Lymphoma', *Front Oncol*, 8: 636. https://doi.org/10.3389/fonc.2018.00636

[151] Kale, J., Osterlund, E. J., and Andrews, D. W., 2018. 'BCL-2 family proteins: changing partners in the dance towards death', *Cell Death Differ*, 25: 65-80. https://doi.org/10.1038/cdd.2017.186

[152] Angelova, A. L., Geletneky, K., Nüesch, J. P., and Rommelaere, J., 2015. 'Tumor Selectivity of Oncolytic Parvoviruses: From in vitro and Animal

Models to Cancer Patients', *Front Bioeng Biotechnol*, 3: 55. https://doi.org/10.3389/fbioe.2015.00055

[153] Gujar, S., Pol, J. G., Kim, Y., Lee, P. W., and Kroemer, G., 2018. 'Antitumor Benefits of Antiviral Immunity: An Underappreciated Aspect of Oncolytic Virotherapies', *Trends Immunol*, 39: 209-21. https://doi.org/10.1016/j.it.2017.11.006

[154] Elliott, M. R., Chekeni, F. B., Trampont, P. C., Lazarowski, E. R., Kadl, A., Walk, S. F., Park, D., Woodson, R. I., Ostankovich, M., . . . Ravichandran, K. S., 2009. 'Nucleotides released by apoptotic cells act as a find-me signal to promote phagocytic clearance', *Nature*, 461: 282-86. https://doi.org/10.1038/nature08296

[155] Fucikova, J., Kepp, O., Kasikova, L., Petroni, G., Yamazaki, T., Liu, P., Zhao, L., Spisek, R., Kroemer, G., . . . Galluzzi, L., 2020. 'Detection of immunogenic cell death and its relevance for cancer therapy', *Cell Death Dis*, 11: 1013. https://doi.org/10.1038/s41419-020-03221-2

[156] Koks, C. A., Garg, A. D., Ehrhardt, M., Riva, M., Vandenberk, L., Boon, L., Vleeschouwer, S. D., Agostinis, P., Graf, N., . . . Van Gool, S. W., 2015. 'Newcastle disease virotherapy induces long-term survival and tumor-specific immune memory in orthotopic glioma through the induction of immunogenic cell death', *International Journal of Cancer*, 136: E313-E25. https://doi.org/10.1002/ijc.29202

[157] Sieben, M., Schafer, P., Dinsart, C., Galle, P. R., and Moehler, M., 2013. 'Activation of the human immune system via toll-like receptors by the oncolytic parvovirus H-1', *Int J Cancer*, 132: 2548-56. https://doi.org/10.1002/ijc.27938

[158] Moehler, M. H., Zeidler, M., Wilsberg, V., Cornelis, J. J., Woelfel, T., Rommelaere, J., Galle, P. R., and Heike, M., 2005. 'Parvovirus H-1-induced tumor cell death enhances human immune response in vitro via increased phagocytosis, maturation, and cross-presentation by dendritic cells', *Hum Gene Ther*, 16: 996-1005. https://doi.org/10.1089/hum.2005.16.996

[159] Angelova, A., and Rommelaere, J., 2019. 'Immune System Stimulation by Oncolytic Rodent Protoparvoviruses', *Viruses*, 11. https://doi.org/10.3390/v11050415

[160] Liu, Z., Ravindranathan, R., Kalinski, P., Guo, Z. S., and Bartlett, D. L., 2017. 'Rational combination of oncolytic vaccinia virus and PD-L1 blockade works synergistically to enhance therapeutic efficacy', *Nature Communications*, 8: 14754. https://doi.org/10.1038/ncomms14754

[161] Conry, R. M., Westbrook, B., McKee, S., and Norwood, T. G., 2018. 'Talimogene laherparepvec: First in class oncolytic virotherapy', *Hum Vaccin Immunother*, 14: 839-46. https://doi.org/10.1080/21645515.2017.1412896

[162] Andtbacka, R. H., Agarwala, S. S., Ollila, D. W., Hallmeyer, S., Milhem, M., Amatruda, T., Nemunaitis, J. J., Harrington, K. J., Chen, L., . . . Kaufman, H. L., 2016. 'Cutaneous head and neck melanoma in OPTiM, a randomized phase 3 trial of talimogene laherparepvec versus granulocyte-macrophage colony-stimulating factor for the treatment of unresected stage IIIB/IIIC/IV melanoma', *Head Neck*, 38: 1752-58. https://doi.org/10.1002/hed.24522

[163] Soliman, H., Hogue, D., Han, H., Mooney, B., Costa, R., Lee, M. C., Niell, B., Williams, A., Chau, A., . . . Czerniecki, B., 2023. 'Oncolytic T-VEC virotherapy plus neoadjuvant chemotherapy in nonmetastatic triple-negative breast cancer: a phase 2 trial', *Nat Med*, 29: 450-57. https://doi.org/10.1038/s41591-023-02210-0

[164] Curiel, C. N., Stratton, D., Cui, H., Roe, D., Tiwari, H. A., and Sundararajan, S., 2022. 'A single arm phase 2 study of talimogene laherparepvec in patients with low-risk invasive cutaneous squamous cell cancer. interim analysis', *Journal of Clinical Oncology*, 40: e21583-e83. https://doi.org/10.1200/JCO.2022.40.16_suppl.e21583

[165] Chang, K. J., Senzer, N. N., Binmoeller, K., Goldsweig, H., and Coffin, R., 2012. 'Phase I dose-escalation study of talimogene laherparepvec (T-VEC) for advanced pancreatic cancer (ca)', *Journal of Clinical Oncology*, 30: e14546-e46. https://doi.org/10.1200/jco.2012.30.15_suppl.e14546

[166] Moreno, L., Teira, P., Croop, J. M., Gerber, N. U., André, N., Aerts, I., Gros Subias, L., De Wilde, B., Bautista, F., . . . Streby, K. A., 2023. 'A phase 1, first-in-child, multicenter study to evaluate the safety and efficacy of the oncolytic herpes virus talimogene laherparepvec in pediatric patients with advanced solid tumors', *Front Pediatr*, 11: 1183295. https://doi.org/10.3389/fped.2023.1183295

[167] Dummer, R., Gyorki, D. E., Hyngstrom, J., Berger, A. C., Conry, R., Demidov, L., Sharma, A., Treichel, S. A., Radcliffe, H., . . . Ross, M. I., 2021. 'Neoadjuvant talimogene laherparepvec plus surgery versus surgery alone for resectable stage IIIB-IVM1a melanoma: a randomized, open-label, phase 2 trial', *Nat Med*, 27: 1789-96. https://doi.org/10.1038/s41591-021-01510-7

[168] Gao, H., Zhang, X., Ding, Y., Qiu, R., Hong, Y., and Chen, W., 2019. 'Synergistic Suppression Effect on Tumor Growth of Colorectal Cancer by Combining Radiotherapy With a TRAIL-Armed Oncolytic Adenovirus', *Technol Cancer Res Treat*, 18: 1533033819853290. https://doi.org/10.1177/1533033819853290

[169] Kyula, J. N., Khan, A. A., Mansfield, D., Karapanagiotou, E. M., McLaughlin, M., Roulstone, V., Zaidi, S., Pencavel, T., Touchefeu, Y., . . . Harrington, K. J., 2014. 'Synergistic cytotoxicity of radiation and oncolytic Lister strain vaccinia in (V600D/E)BRAF mutant melanoma depends on JNK and TNF-alpha signaling', *Oncogene*, 33: 1700-12. https://doi.org/10.1038/onc.2013.112

[170] Pandha, H. S., Heinemann, L., Simpson, G. R., Melcher, A., Prestwich, R., Errington, F., Coffey, M., Harrington, K. J., and Morgan, R., 2009. 'Synergistic Effects of Oncolytic Reovirus and Cisplatin Chemotherapy in Murine Malignant Melanoma', *Clinical Cancer Research*, 15: 6158-66. https://doi.org/10.1158/1078-0432.ccr-09-0796

[171] Mahalingam, D., Fountzilas, C., Moseley, J., Noronha, N., Tran, H., Chakrabarty, R., Selvaggi, G., Coffey, M., Thompson, B., . . . Sarantopoulos, J., 2017. 'A phase II study of REOLYSIN(®) (pelareorep) in combination with carboplatin and paclitaxel for patients with advanced malignant melanoma', *Cancer Chemother Pharmacol*, 79: 697-703. https://doi.org/10.1007/s00280-017-3260-6

[172] Cohn, D. E., Sill, M. W., Walker, J. L., O'Malley, D., Nagel, C. I., Rutledge, T. L., Bradley, W., Richardson, D. L., Moxley, K. M., . . . Aghajanian, C., 2017. 'Randomized phase IIB evaluation of weekly paclitaxel versus weekly paclitaxel with oncolytic reovirus (Reolysin®) in recurrent ovarian, tubal, or peritoneal cancer: An NRG Oncology/Gynecologic Oncology Group study', *Gynecologic Oncology*, 146: 477-83. https://doi.org/10.1016/j.ygyno.2017.07.135

[173] Bommareddy, P. K., Aspromonte, S., Zloza, A., Rabkin, S. D., and Kaufman, H. L., 2018. 'MEK inhibition enhances oncolytic virus immunotherapy through increased tumor cell killing and T cell activation', *Sci Transl Med*, 10. https://doi.org/10.1126/scitranslmed.aau0417

[174] Ribas, A., Dummer, R., Puzanov, I., VanderWalde, A., Andtbacka, R. H. I., Michielin, O., Olszanski, A. J., Malvehy, J., Cebon, J., . . . Long, G. V., 2017. 'Oncolytic Virotherapy Promotes Intratumoral T Cell Infiltration and Improves Anti-PD-1 Immunotherapy', *Cell*, 170: 1109-19 e10. https://doi.org/10.1016/j.cell.2017.08.027

[175] Chesney, J. A., Ribas, A., Long, G. V., Kirkwood, J. M., Dummer, R., Puzanov, I., Hoeller, C., Gajewski, T. F., Gutzmer, R., . . . Gogas, H., 2023. 'Randomized, Double-Blind, Placebo-Controlled, Global Phase III Trial of Talimogene Laherparepvec Combined With Pembrolizumab for Advanced Melanoma', *Journal of Clinical Oncology*, 41: 528-40. https://doi.org/10.1200/jco.22.00343

[176] Chesney, J., Puzanov, I., Collichio, F., Singh, P., Milhem, M. M., Glaspy, J., Hamid, O., Ross, M., Friedlander, P., . . . Kaufman, H. L., 2018.

'Randomized, Open-Label Phase II Study Evaluating the Efficacy and Safety of Talimogene Laherparepvec in Combination With Ipilimumab Versus Ipilimumab Alone in Patients With Advanced, Unresectable Melanoma', *J Clin Oncol*, 36: 1658-67. https://doi.org/10.1200/JCO.2017.73.7379

[177] Toolan, H. W., Dalldore, G., Barclay, M., Chandra, S., and Moore, A. E., 1960. 'An Unidentified, Filtrable Agent Isolated from Transplanted Human Tumors', *Proc Natl Acad Sci U S A*, 46: 1256-8. https://doi.org/10.1073/pnas.46.9.1256

[178] Chandra, S., and Toolan, H. W., 1961. 'Electron Microscopy of the H-1 Virus. I. Morphology of the Virus and a Possible Virus-Host Relationship2', *JNCI: Journal of the National Cancer Institute*, 27: 1405-49. https://doi.org/10.1093/jnci/27.6.1405

[179] Toolan, H. W., and Ledinko, N., 1968. 'Inhibition by H-1 virus of the incidence of tumors produced by adenovirus 12 in hamsters', *Virology*, 35: 475-78. https://doi.org/10.1016/0042-6822(68)90226-2

[180] Dupressoir, T., Vanacker, J. M., Cornelis, J. J., Duponchel, N., and Rommelaere, J., 1989. 'Inhibition by parvovirus H-1 of the formation of tumors in nude mice and colonies in vitro by transformed human mammary epithelial cells', *Cancer Res*, 49: 3203-8. https://www.ncbi.nlm.nih.gov/pubmed/2541900

[181] Faisst, S., Guittard, D., Benner, A., Cesbron, J. Y., Schlehofer, J. R., Rommelaere, J., and Dupressoir, T., 1998. 'Dose-dependent regression of HeLa cell-derived tumours in SCID mice after parvovirus H-1 infection', *Int J Cancer*, 75: 584-9. https://doi.org/10.1002/(sici)1097-0215(19980209)75:4<584::aid-ijc15>3.0.co;2-9

[182] Van Pachterbeke, C., Tuynder, M., Cosyn, J. P., Lespagnard, L., Larsimont, D., and Rommelaere, J., 1993. 'Parvovirus H-1 inhibits growth of short-term tumor-derived but not normal mammary tissue cultures', *Int J Cancer*, 55: 672-7. https://doi.org/10.1002/ijc.2910550427

[183] Bretscher, C., and Marchini, A., 2019. 'H-1 Parvovirus as a Cancer-Killing Agent: Past, Present, and Future', *Viruses*, 11. https://doi.org/10.3390/v11060562

[184] Toolan, H. W., 1960. 'Experimental Production of Mongoloid Hamsters', *Science*, 131: 1446-48. https://doi.org/10.1126/science.131.3411.1446

[185] Faisst, S., Faisst, S. R., Dupressoir, T., Plaza, S., Pujol, A., Jauniaux, J. C., Rhode, S. L., and Rommelaere, J., 1995. 'Isolation of a fully infectious variant of parvovirus H-1 supplanting the standard strain in human cells', *Journal of Virology*, 69: 4538-43. https://doi.org/10.1128/JVI.69.7.4538-4543.1995

[186] Cotmore, S. F., and Tattersall, P., 2014. 'Parvoviruses: Small Does Not Mean Simple', *Annu Rev Virol*, 1: 517-37. https://doi.org/10.1146/annurev-virology-031413-085444

[187] Allaume, X., El-Andaloussi, N., Leuchs, B., Bonifati, S., Kulkarni, A., Marttila, T., Kaufmann, J. K., Nettelbeck, D. M., Kleinschmidt, J., . . . Marchini, A., 2012. 'Retargeting of rat parvovirus H-1PV to cancer cells through genetic engineering of the viral capsid', *J Virol*, 86: 3452-65. https://doi.org/10.1128/JVI.06208-11

[188] Halder, S., Nam, H. J., Govindasamy, L., Vogel, M., Dinsart, C., Salome, N., McKenna, R., and Agbandje-McKenna, M., 2013. 'Structural characterization of H-1 parvovirus: comparison of infectious virions to empty capsids', *J Virol*, 87: 5128-40. https://doi.org/10.1128/JVI.03416-12

[189] Nüesch, J. P. F., and Tattersall, P., 1993. 'Nuclear Targeting of the Parvoviral Replicator Molecule NS1: Evidence for Self-Association Prior to Nuclear Transport', *Virology*, 196: 637-51. https://doi.org/10.1006/viro.1993.1520

[190] Christensen, J., Cotmore, S. F., and Tattersall, P., 1995. 'Minute virus of mice transcriptional activator protein NS1 binds directly to the transactivation region of the viral P38 promoter in a strictly ATP-dependent manner', *J Virol*, 69: 5422-30. https://doi.org/10.1128/JVI.69.9.5422-5430.1995

[191] Cotmore, S. F., Christensen, J., Nüesch, J. P., and Tattersall, P., 1995. 'The NS1 polypeptide of the murine parvovirus minute virus of mice binds to DNA sequences containing the motif [ACCA]2-3', *Journal of Virology*, 69: 1652-60. https://doi.org/10.1128/jvi.69.3.1652-1660.1995

[192] Li, J., Bonifati, S., Hristov, G., Marttila, T., Valmary-Degano, S., Stanzel, S., Schnolzer, M., Mougin, C., Aprahamian, M., . . . Marchini, A., 2013. 'Synergistic combination of valproic acid and oncolytic parvovirus H-1PV as a potential therapy against cervical and pancreatic carcinomas', *EMBO Mol Med*, 5: 1537-55. https://doi.org/10.1002/emmm.201302796

[193] Christensen, J., and Tattersall, P., 2002. 'Parvovirus Initiator Protein NS1 and RPA Coordinate Replication Fork Progression in a Reconstituted DNA Replication System', *Journal of Virology*, 76: 6518-31. https://doi.org/10.1128/jvi.76.13.6518-6531.2002

[194] King, J. A., Dubielzig, R., Grimm, D., and Kleinschmidt, J. A., 2001. 'DNA helicase-mediated packaging of adeno-associated virus type 2 genomes into preformed capsids', *EMBO J*, 20: 3282-91. https://doi.org/10.1093/emboj/20.12.3282

[195] Daeffler, L., Horlein, R., Rommelaere, J., and Nüesch, J. P., 2003. 'Modulation of minute virus of mice cytotoxic activities through site-

directed mutagenesis within the NS coding region', *J Virol*, 77: 12466-78. https://doi.org/10.1128/jvi.77.23.12466-12478.2003

[196] Nüesch, J. P., Corbau, R., Tattersall, P., and Rommelaere, J., 1998. 'Biochemical activities of minute virus of mice nonstructural protein NS1 are modulated In vitro by the phosphorylation state of the polypeptide', *J Virol*, 72: 8002-12. https://doi.org/10.1128/jvi.72.10.8002-8012.1998

[197] Corbau, R., Salomé, N., Rommelaere, J., and Nüesch, J. P. F., 1999. 'Phosphorylation of the Viral Nonstructural Protein NS1 during MVMp Infection of A9 Cells', *Virology*, 259: 402-15. https://doi.org/10.1006/viro.1999.9786

[198] Lachmann, S., Rommeleare, J., and Nüesch, J. P., 2003. 'Novel PKCeta is required to activate replicative functions of the major nonstructural protein NS1 of minute virus of mice', *J Virol*, 77: 8048-60. https://doi.org/10.1128/jvi.77.14.8048-8060.2003

[199] Nüesch, J. P., Lachmann, S., Corbau, R., and Rommelaere, J., 2003. 'Regulation of minute virus of mice NS1 replicative functions by atypical PKClambda in vivo', *J Virol*, 77: 433-42. https://doi.org/10.1128/jvi.77.1.433-442.2003

[200] Nüesch, J. P., and Rommelaere, J., 2006. 'NS1 interaction with CKII alpha: novel protein complex mediating parvovirus-induced cytotoxicity', *J Virol*, 80: 4729-39. https://doi.org/10.1128/JVI.80.10.4729-4739.2006

[201] Nüesch, J. P., and Rommelaere, J., 2007. 'A viral adaptor protein modulating casein kinase II activity induces cytopathic effects in permissive cells', *Proc Natl Acad Sci U S A*, 104: 12482-7. https://doi.org/10.1073/pnas.0705533104

[202] Hristov, G., Kramer, M., Li, J., El-Andaloussi, N., Mora, R., Daeffler, L., Zentgraf, H., Rommelaere, J., and Marchini, A., 2010. 'Through its nonstructural protein NS1, parvovirus H-1 induces apoptosis via accumulation of reactive oxygen species', *J Virol*, 84: 5909-22. https://doi.org/10.1128/JVI.01797-09

[203] Di Piazza, M., Mader, C., Geletneky, K., Herrero, Y. C. M., Weber, E., Schlehofer, J., Deleu, L., and Rommelaere, J., 2007. 'Cytosolic activation of cathepsins mediates parvovirus H-1-induced killing of cisplatin and TRAIL-resistant glioma cells', *J Virol*, 81: 4186-98. https://doi.org/10.1128/JVI.02601-06

[204] Nüesch, J. P., and Rommelaere, J., 2014. 'Tumor suppressing properties of rodent parvovirus NS1 proteins and their derivatives', *Adv Exp Med Biol*, 818: 99-124. https://doi.org/10.1007/978-1-4471-6458-6_5

[205] Hashemi, H., Condurat, A. L., Stroh-Dege, A., Weiss, N., Geiss, C., Pilet, J., Cornet Bartolome, C., Rommelaere, J., Salome, N., . . . Dinsart, C., 2018.

'Mutations in the Non-Structural Protein-Coding Sequence of Protoparvovirus H-1PV Enhance the Fitness of the Virus and Show Key Benefits Regarding the Transduction Efficiency of Derived Vectors', *Viruses*, 10. https://doi.org/10.3390/v10040150

[206] Eichwald, V., Daeffler, L., Klein, M., Rommelaere, J., and Salomé, N., 2002. 'The NS2 proteins of parvovirus minute virus of mice are required for efficient nuclear egress of progeny virions in mouse cells', *J Virol*, 76: 10307-19. https://doi.org/10.1128/jvi.76.20.10307-10319.2002

[207] Mani, B., Baltzer, C., Valle, N., Almendral, J. M., Kempf, C., and Ros, C., 2006. 'Low pH-Dependent Endosomal Processing of the Incoming Parvovirus Minute Virus of Mice Virion Leads to Externalization of the VP1 N-Terminal Sequence (N-VP1), N-VP2 Cleavage, and Uncoating of the Full-Length Genome', *Journal of Virology*, 80: 1015-24. https://doi.org/10.1128/jvi.80.2.1015-1024.2006

[208] Zádori, Z., Szelei, J., Lacoste, M.-C., Li, Y., Gariépy, S., Raymond, P., Allaire, M., Nabi, I. R., and Tijssen, P., 2001. 'A Viral Phospholipase A2 Is Required for Parvovirus Infectivity', *Developmental Cell*, 1: 291-302. https://doi.org/10.1016/S1534-5807(01)00031-4

[209] Lombardo, E., Ramírez, J. C., Agbandje-McKenna, M., and Almendral, J. M., 2000. 'A beta-stranded motif drives capsid protein oligomers of the parvovirus minute virus of mice into the nucleus for viral assembly', *J Virol*, 74: 3804-14. https://doi.org/10.1128/jvi.74.8.3804-3814.2000

[210] Meszaros, I., Toth, R., Olasz, F., Tijssen, P., and Zadori, Z., 2017. 'The SAT Protein of Porcine Parvovirus Accelerates Viral Spreading through Induction of Irreversible Endoplasmic Reticulum Stress', *J Virol*, 91. https://doi.org/10.1128/JVI.00627-17

[211] Bretscher, C., 2018. 'The SAT Protein of the Minute Virus of Mice Induces the Lysis of the Cell through the Formation of Viroporin-like Structures. ', University of Heidelberg.

[212] Marchini, A., Bonifati, S., Scott, E. M., Angelova, A. L., and Rommelaere, J., 2015. 'Oncolytic parvoviruses: from basic virology to clinical applications', *Virol J*, 12: 6. https://doi.org/10.1186/s12985-014-0223-y

[213] Kulkarni, A., Ferreira, T., Bretscher, C., Grewenig, A., El-Andaloussi, N., Bonifati, S., Marttila, T., Palissot, V., Hossain, J. A., . . . Marchini, A., 2021. 'Oncolytic H-1 parvovirus binds to sialic acid on laminins for cell attachment and entry', *Nature Communications*, 12. https://doi.org/10.1038/s41467-021-24034-7

[214] Ferreira, T., Kulkarni, A., Bretscher, C., Nazarov, P., Hossain, J., Ystaas, L., Miletic, H., Röth, R., Niesler, B., . . . Marchini, A., 2022. 'Oncolytic H-1

Parvovirus Hijacks Galectin-1 to Enter Cancer Cells', *Viruses*, 14. https://doi.org/10.3390/v14051018

[215] Ferreira, T., Kulkarni, A., Bretscher, C., Richter, K., Ehrlich, M., and Marchini, A., 2020. 'Oncolytic H-1 Parvovirus Enters Cancer Cells through Clathrin-Mediated Endocytosis', *Viruses*, 12. https://doi.org/10.3390/v12101199

[216] Suikkanen, S., Antila, M., Jaatinen, A., Vihinen-Ranta, M., and Vuento, M., 2003. 'Release of canine parvovirus from endocytic vesicles', *Virology*, 316: 267-80. https://doi.org/10.1016/j.virol.2003.08.031

[217] Suikkanen, S., Aaltonen, T., Nevalainen, M., Välilehto, O., Lindholm, L., Vuento, M., and Vihinen-Ranta, M., 2003. 'Exploitation of Microtubule Cytoskeleton and Dynein during Parvoviral Traffic toward the Nucleus', *Journal of Virology*, 77: 10270-79. https://doi.org/10.1128/jvi.77.19.10270-10279.2003

[218] Porwal, M., Cohen, S., Snoussi, K., Popa-Wagner, R., Anderson, F., Dugot-Senant, N., Wodrich, H., Dinsart, C., Kleinschmidt, J. A., . . . Kann, M., 2013. 'Parvoviruses cause nuclear envelope breakdown by activating key enzymes of mitosis', *PLoS Pathog*, 9: e1003671. https://doi.org/10.1371/journal.ppat.1003671

[219] Cohen, S., Marr, A. K., Garcin, P., and Panté, N., 2011. 'Nuclear envelope disruption involving host caspases plays a role in the parvovirus replication cycle', *J Virol*, 85: 4863-74. https://doi.org/10.1128/jvi.01999-10

[220] Nicolson, S. C., and Samulski, R. J., 2014. 'Recombinant Adeno-Associated Virus Utilizes Host Cell Nuclear Import Machinery To Enter the Nucleus', *Journal of Virology*, 88: 4132-44. https://doi.org/10.1128/jvi.02660-13

[221] Sonntag, F., Bleker, S., Leuchs, B., Fischer, R., and Kleinschmidt, J. A., 2006. 'Adeno-associated virus type 2 capsids with externalized VP1/VP2 trafficking domains are generated prior to passage through the cytoplasm and are maintained until uncoating occurs in the nucleus', *J Virol*, 80: 11040-54. https://doi.org/10.1128/jvi.01056-06

[222] Ros, C., Baltzer, C., Mani, B., and Kempf, C., 2006. 'Parvovirus uncoating in vitro reveals a mechanism of DNA release without capsid disassembly and striking differences in encapsidated DNA stability', *Virology*, 345: 137-47. https://doi.org/10.1016/j.virol.2005.09.030

[223] Cotmore, S. F., Hafenstein, S., and Tattersall, P., 2010. 'Depletion of Virion-Associated Divalent Cations Induces Parvovirus Minute Virus of Mice To Eject Its Genome in a 3′-to-5′ Direction from an Otherwise Intact Viral Particle', *Journal of Virology*, 84: 1945-56. https://doi.org/10.1128/jvi.01563-09

[224] Cziepluch, C., Lampel, S., Grewenig, A., Grund, C., Lichter, P., and Rommelaere, J., 2000. 'H-1 parvovirus-associated replication bodies: a distinct virus-induced nuclear structure', *J Virol*, 74: 4807-15. https://doi.org/10.1128/jvi.74.10.4807-4815.2000

[225] Adeyemi, R. O., and Pintel, D. J., 2012. 'Replication of Minute Virus of Mice in Murine Cells Is Facilitated by Virally Induced Depletion of p21', *Journal of Virology*, 86: 8328-32. https://doi.org/10.1128/jvi.00820-12

[226] Bashir, T., Horlein, R., Rommelaere, J., and Willwand, K., 2000. 'Cyclin A activates the DNA polymerase delta -dependent elongation machinery in vitro: A parvovirus DNA replication model', *Proc Natl Acad Sci U S A*, 97: 5522-7. https://doi.org/10.1073/pnas.090485297

[227] Deleu, L., Pujol, A., Faisst, S., and Rommelaere, J., 1999. 'Activation of promoter P4 of the autonomous parvovirus minute virus of mice at early S phase is required for productive infection', *Journal of Virology*, 73: 3877-85. https://doi.org/10.1128/Jvi.73.5.3877-3885.1999

[228] Fuks, F., Deleu, L., Dinsart, C., Rommelaere, J., and Faisst, S., 1996. 'ras oncogene-dependent activation of the P4 promoter of minute virus of mice through a proximal P4 element interacting with the Ets family of transcription factors', *Journal of Virology*, 70: 1331-39. https://doi.org/10.1128/jvi.70.3.1331-1339.1996

[229] Perros, M., Deleu, L., Vanacker, J. M., Kherrouche, Z., Spruyt, N., Faisst, S., and Rommelaere, J., 1995. 'Upstream CREs participate in the basal activity of minute virus of mice promoter P4 and in its stimulation in ras-transformed cells', *Journal of Virology*, 69: 5506-15. https://doi.org/10.1128/jvi.69.9.5506-5515.1995

[230] Dempe, S., Stroh-Dege, A. Y., Schwarz, E., Rommelaere, J., and Dinsart, C., 2010. 'SMAD4: a predictive marker of PDAC cell permissiveness for oncolytic infection with parvovirus H-1PV', *International Journal of Cancer*, 126: 2914-27. https://doi.org/10.1002/ijc.24992

[231] Christensen, J., Cotmore, S. F., and Tattersall, P., 1997. 'A novel cellular site-specific DNA-binding protein cooperates with the viral NS1 polypeptide to initiate parvovirus DNA replication', *J Virol*, 71: 1405-16. https://doi.org/10.1128/jvi.71.2.1405-1416.1997

[232] Cotmore, S. F., and Tattersall, P., 1998. 'High-Mobility Group 1/2 Proteins Are Essential for Initiating Rolling-Circle-Type DNA Replication at a Parvovirus Hairpin Origin', *Journal of Virology*, 72: 8477-84. https://doi.org/10.1128/jvi.72.11.8477-8484.1998

[233] Cotmore, S. F., and Tattersall, P., 1992. 'In vivo resolution of circular plasmids containing concatemer junction fragments from minute virus of

mice DNA and their subsequent replication as linear molecules', *Journal of Virology*, 66: 420-31. https://doi.org/10.1128/jvi.66.1.420-431.1992

[234] Adeyemi, R. O., Landry, S., Davis, M. E., Weitzman, M. D., and Pintel, D. J., 2010. 'Parvovirus minute virus of mice induces a DNA damage response that facilitates viral replication', *PLoS Pathog*, 6: e1001141. https://doi.org/10.1371/journal.ppat.1001141

[235] Lachmann, S., Bär, S., Rommelaere, J., and Nüesch, J. P., 2008. 'Parvovirus interference with intracellular signalling: mechanism of PKCeta activation in MVM-infected A9 fibroblasts', *Cell Microbiol*, 10: 755-69. https://doi.org/10.1111/j.1462-5822.2007.01082.x

[236] Kavishwar, G., 2023. 'Boosting the Immune System: A Drug Combination Augments H-1 Parvovirus Mediated Oncolysis and Immunogenicity in Prostate Cancer', Ruperto Carola University Heidelberg.

[237] Riolobos, L., Valle, N., Hernando, E., Maroto, B., Kann, M., and Almendral, J. M., 2010. 'Viral oncolysis that targets Raf-1 signaling control of nuclear transport', *J Virol*, 84: 2090-9. https://doi.org/10.1128/JVI.01550-09

[238] Bär, S., Rommelaere, J., and Nüesch, J. P. F., 2013. 'Vesicular Transport of Progeny Parvovirus Particles through ER and Golgi Regulates Maturation and Cytolysis', *PLoS Pathogens*, 9: e1003605. https://doi.org/10.1371/journal.ppat.1003605

[239] Maroto, B., Valle, N., Saffrich, R., and Almendral, J. M., 2004. 'Nuclear Export of the Nonenveloped Parvovirus Virion Is Directed by an Unordered Protein Signal Exposed on the Capsid Surface', *Journal of Virology*, 78: 10685-94. https://doi.org/10.1128/jvi.78.19.10685-10694.2004

[240] Bär, S., Daeffler, L., Rommelaere, J., and Nüesch, J. P. F., 2008. 'Vesicular Egress of Non-Enveloped Lytic Parvoviruses Depends on Gelsolin Functioning', *PLoS Pathogens*, 4: e1000126. https://doi.org/10.1371/journal.ppat.1000126

[241] Nüesch, J. r. P. F., Bär, S. v., Lachmann, S., and Rommelaere, J., 2009. 'Ezrin-Radixin-Moesin Family Proteins Are Involved in Parvovirus Replication and Spreading', *Journal of Virology*, 83: 5854-63. https://doi.org/10.1128/jvi.00039-09

[242] Ohshima, T., Iwama, M., Ueno, Y., Sugiyama, F., Nakajima, T., Fukamizu, A., and Yagami, K., 1998. 'Induction of apoptosis in vitro and in vivo by H-1 parvovirus infection', *J Gen Virol*, 79 (Pt 12): 3067-71. https://doi.org/10.1099/0022-1317-79-12-3067

[243] Rayet, B. a., Lopez-Guerrero, J.-A., Rommelaere, J., and Dinsart, C., 1998. 'Induction of Programmed Cell Death by Parvovirus H-1 in U937 Cells: Connection with the Tumor Necrosis Factor Alpha Signalling Pathway',

Journal of Virology, 72: 8893-903. https://doi.org/10.1128/jvi.72.11.8893-8903.1998

[244] Moehler, M., Blechacz, B., Weiskopf, N., Zeidler, M., Stremmel, W., Rommelaere, J., Galle, P. R., and Cornelis, J. J., 2001. 'Effective infection, apoptotic cell killing and gene transfer of human hepatoma cells but not primary hepatocytes by parvovirus H1 and derived vectors', *Cancer Gene Ther*, 8: 158-67. https://doi.org/10.1038/sj.cgt.7700288

[245] Ran, Z., Rayet, B., Rommelaere, J., and Faisst, S., 1999. 'Parvovirus H-1-induced cell death: influence of intracellular NAD consumption on the regulation of necrosis and apoptosis', *Virus Res*, 65: 161-74. https://doi.org/10.1016/s0168-1702(99)00115-x

[246] Angelova, A. L., Grekova, S. P., Heller, A., Kuhlmann, O., Soyka, E., Giese, T., Aprahamian, M., Bour, G., Ruffer, S., . . . Giese, N. A., 2014. 'Complementary induction of immunogenic cell death by oncolytic parvovirus H-1PV and gemcitabine in pancreatic cancer', *J Virol*, 88: 5263-76. https://doi.org/10.1128/JVI.03688-13

[247] Moehler, M., Sieben, M., Roth, S., Springsguth, F., Leuchs, B., Zeidler, M., Dinsart, C., Rommelaere, J., and Galle, P. R., 2011. 'Activation of the human immune system by chemotherapeutic or targeted agents combined with the oncolytic parvovirus H-1', *BMC Cancer*, 11: 464. https://doi.org/10.1186/1471-2407-11-464

[248] Muharram, G., Le Rhun, E., Loison, I., Wizla, P., Richard, A., Martin, N., Roussel, A., Begue, A., Devos, P., . . . Stehelin, D., 2010. 'Parvovirus H-1 induces cytopathic effects in breast carcinoma-derived cultures', *Breast Cancer Res Treat*, 121: 23-33. https://doi.org/10.1007/s10549-009-0451-9

[249] Lacroix, J., Leuchs, B., Li, J., Hristov, G., Deubzer, H. E., Kulozik, A. E., Rommelaere, J., Schlehofer, J. R., and Witt, O., 2010. 'Parvovirus H1 selectively induces cytotoxic effects on human neuroblastoma cells', *Int J Cancer*, 127: 1230-9. https://doi.org/10.1002/ijc.25168

[250] Lacroix, J., Schlund, F., Leuchs, B., Adolph, K., Sturm, D., Bender, S., Hielscher, T., Pfister, S. M., Witt, O., . . . Witt, H., 2014. 'Oncolytic effects of parvovirus H-1 in medulloblastoma are associated with repression of master regulators of early neurogenesis', *Int J Cancer*, 134: 703-16. https://doi.org/10.1002/ijc.28386

[251] Herrero, Y. C. M., Cornelis, J. J., Herold-Mende, C., Rommelaere, J., Schlehofer, J. R., and Geletneky, K., 2004. 'Parvovirus H-1 infection of human glioma cells leads to complete viral replication and efficient cell killing', *Int J Cancer*, 109: 76-84. https://doi.org/10.1002/ijc.11626

[252] Josupeit, R., Bender, S., Kern, S., Leuchs, B., Hielscher, T., Herold-Mende, C., Schlehofer, J. R., Dinsart, C., Witt, O., . . . Lacroix, J., 2016. 'Pediatric and Adult High-Grade Glioma Stem Cell Culture Models Are Permissive to Lytic Infection with Parvovirus H-1', *Viruses*, 8. https://doi.org/10.3390/v8050138

[253] Kiprianova, I., Thomas, N., Ayache, A., Fischer, M., Leuchs, B., Klein, M., Rommelaere, J., and Schlehofer, J. R., 2011. 'Regression of glioma in rat models by intranasal application of parvovirus h-1', *Clin Cancer Res*, 17: 5333-42. https://doi.org/10.1158/1078-0432.CCR-10-3124

[254] Geletneky, K., Kiprianova, I., Ayache, A., Koch, R., Herrero, Y. C. M., Deleu, L., Sommer, C., Thomas, N., Rommelaere, J., . . . Schlehofer, J. R., 2010. 'Regression of advanced rat and human gliomas by local or systemic treatment with oncolytic parvovirus H-1 in rat models', *Neuro Oncol*, 12: 804-14. https://doi.org/10.1093/neuonc/noq023

[255] Geletneky, K., Leoni, A. L., Pohlmeyer-Esch, G., Loebhard, S., Leuchs, B., Hoefer, C., Jochims, K., Dahm, M., Huber, B., . . . Hajda, J., 2015. 'Bioavailability, biodistribution, and CNS toxicity of clinical-grade parvovirus H1 after intravenous and intracerebral injection in rats', *Comp Med*, 65: 36-45. https://www.ncbi.nlm.nih.gov/pubmed/25730755

[256] Hartley, A., Kavishwar, G., Salvato, I., and Marchini, A., 2020. 'A Roadmap for the Success of Oncolytic Parvovirus-Based Anticancer Therapies', *Annu Rev Virol*, 7: 537-57. https://doi.org/10.1146/annurev-virology-012220-023606

[257] Geletneky, K., Huesing, J., Rommelaere, J., Schlehofer, J. R., Leuchs, B., Dahm, M., Krebs, O., von Knebel Doeberitz, M., Huber, B., . . . Hajda, J., 2012. 'Phase I/IIa study of intratumoral/intracerebral or intravenous/intracerebral administration of Parvovirus H-1 (ParvOryx) in patients with progressive primary or recurrent glioblastoma multiforme: ParvOryx01 protocol', *BMC Cancer*, 12: 99. https://doi.org/10.1186/1471-2407-12-99

[258] Geletneky, K., Hajda, J., Angelova, A. L., Leuchs, B., Capper, D., Bartsch, A. J., Neumann, J. O., Schoning, T., Husing, J., . . . Rommelaere, J., 2017. 'Oncolytic H-1 Parvovirus Shows Safety and Signs of Immunogenic Activity in a First Phase I/IIa Glioblastoma Trial', *Mol Ther*, 25: 2620-34. https://doi.org/10.1016/j.ymthe.2017.08.016

[259] Chen, X., Liu, J., Li, Y., Zeng, Y., Wang, F., Cheng, Z., Duan, H., Pan, G., Yang, S., . . . Zhang, H., 2023. 'IDH1 mutation impairs antiviral response and potentiates oncolytic virotherapy in glioma', *Nat Commun*, 14: 6781. https://doi.org/10.1038/s41467-023-42545-3

[260] Philip, B., Yu, D. X., Silvis, M. R., Shin, C. H., Robinson, J. P., Robinson, G. L., Welker, A. E., Angel, S. N., Tripp, S. R., . . . Holmen, S. L., 2018. 'Mutant

IDH1 Promotes Glioma Formation In Vivo', *Cell Rep*, 23: 1553-64. https://doi.org/10.1016/j.celrep.2018.03.133

[261] Geletneky, K., Bartsch, A., Weiss, C., Bernhard, H., Marchini, A., and Rommelaere, J., 2018. 'ATIM-40. High rate of objective anti-tumor response in 9 patients with glioblastoma after viro-immunotherapy with oncolytic parvovirus H-1 in combination with Bevacicumab and PD-1 checkpoint blockade', *Neuro Oncol*, 20: vi10. https://doi.org/10.1093/neuonc/noy148.035

[262] Hajda, J., Lehmann, M., Krebs, O., Kieser, M., Geletneky, K., Jager, D., Dahm, M., Huber, B., Schoning, T., . . . Ungerechts, G., 2017. 'A non-controlled, single arm, open label, phase II study of intravenous and intratumoral administration of ParvOryx in patients with metastatic, inoperable pancreatic cancer: ParvOryx02 protocol', *BMC Cancer*, 17: 576. https://doi.org/10.1186/s12885-017-3604-y

[263] Hajda, J., Leuchs, B., Angelova, A. L., Frehtman, V., Rommelaere, J., Mertens, M., Pilz, M., Kieser, M., Krebs, O., . . . Ungerechts, G., 2021. 'Phase 2 trial of oncolytic H-1 parvovirus therapy shows safety and immune cell activity in patients with metastatic pancreatic ductal adenocarcinoma', *Clin Cancer Res*. https://doi.org/10.1158/1078-0432.CCR-21-1020

[264] El-Andaloussi, N., Endele, M., Leuchs, B., Bonifati, S., Kleinschmidt, J., Rommelaere, J., and Marchini, A., 2011. 'Novel adenovirus-based helper system to support production of recombinant parvovirus', *Cancer Gene Ther*, 18: 240-9. https://doi.org/10.1038/cgt.2010.73

[265] Raykov, Z., Grekova, S., Leuchs, B., Aprahamian, M., and Rommelaere, J., 2008. 'Arming parvoviruses with CpG motifs to improve their oncosuppressive capacity', *Int J Cancer*, 122: 2880-4. https://doi.org/10.1002/ijc.23472

[266] Grekova, S. P., Aprahamian, M., Giese, N. A., Bour, G., Giese, T., Grewenig, A., Leuchs, B., Hörlein, R., Heller, A., . . . Raykov, Z., 2014. 'Genomic CpG Enrichment of Oncolytic Parvoviruses as a Potent Anticancer Vaccination Strategy for the Treatment of Pancreatic Adenocarcinoma', *J Vaccines Vaccin*, 5: e1000227. https://doi.org/10.4172/2157-7560.1000227

[267] Marchini, A., Illarionova, A., Rommelaere, J., and Leuchs, B., 2012. 'Modified parvovirus useful for gene silencing', European Patent Office, EP2620503. https://data.epo.org/publication-server/document?iDocId=4338101&iFormat=0

[268] Marchini, A., Li, J., Rommelaere, J., Leuchs, B., Li-Weber, M., Nieto, K., Krammer, P., and De-Oliveira, A.-P., 2016. 'H-1 PV expressing RNAi effectors targeting CDK9', European Patent Office, EP 3 327 124 A1. https://data.epo.org/publication-server/document?iDocId=5615761&iFormat=0

[269] Grueso, E., Sanchez-Martinez, C., Calvo-Lopez, T., de Miguel, F. J., Blanco-Menendez, N., Fernandez-Estevez, M., Elizalde, M., Sanchez, J., Kourani, O., . . . Almendral, J. M., 2019. 'Antiangiogenic Vascular Endothelial Growth Factor-Blocking Peptides Displayed on the Capsid of an Infectious Oncolytic Parvovirus: Assembly and Immune Interactions', *J Virol*, 93. https://doi.org/10.1128/JVI.00798-19

[270] Paglino, J., and Tattersall, P., 2011. 'The parvoviral capsid controls an intracellular phase of infection essential for efficient killing of stepwise-transformed human fibroblasts', *Virology*, 416: 32-41. https://doi.org/10.1016/j.virol.2011.04.015

[271] El-Andaloussi, N., Bonifati, S., Kaufmann, J. K., Mailly, L., Daeffler, L., Deryckere, F., Nettelbeck, D. M., Rommelaere, J., and Marchini, A., 2012. 'Generation of an adenovirus-parvovirus chimera with enhanced oncolytic potential', *J Virol*, 86: 10418-31. https://doi.org/10.1128/JVI.00848-12

[272] Goepfert, K., Dinsart, C., Rommelaere, J., Foerster, F., and Moehler, M., 2019. 'Rational Combination of Parvovirus H1 With CTLA-4 and PD-1 Checkpoint Inhibitors Dampens the Tumor Induced Immune Silencing', *Front Oncol*, 9: 425. https://doi.org/10.3389/fonc.2019.00425

[273] Angelova, A. L., Aprahamian, M., Grekova, S. P., Hajri, A., Leuchs, B., Giese, N. A., Dinsart, C., Herrmann, A., Balboni, G., . . . Raykov, Z., 2009. 'Improvement of gemcitabine-based therapy of pancreatic carcinoma by means of oncolytic parvovirus H-1PV', *Clin Cancer Res*, 15: 511-9. https://doi.org/10.1158/1078-0432.CCR-08-1088

[274] Geletneky, K., Hartkopf, A. D., Krempien, R., Rommelaere, J., and Schlehofer, J. R., 2010. 'Improved killing of human high-grade glioma cells by combining ionizing radiation with oncolytic parvovirus H-1 infection', *J Biomed Biotechnol*, 2010: 350748. https://doi.org/10.1155/2010/350748

[275] Marchini, A., Li, J., Schroeder, L., Rommelaere, J., and Geletneky, K., 2015. 'Cancer therapy with a parvovirus combined with a Bcl-2 inhibitor', European Patent Office, EP 2 829 284 A1. https://data.epo.org/publication-server/document?iDocId=4757879&iFormat=0

[276] SelleckChem, 2013. 'FDA-approved Drug Library', Accessed 29.01.2024. https://www.selleckchem.com/screening/fda-approved-drug-library.html.

[277] Link, J. O., Taylor, J. G., Xu, L., Mitchell, M., Guo, H., Liu, H., Kato, D., Kirschberg, T., Sun, J., . . . Desai, M. C., 2013. 'Discovery of ledipasvir (GS-5885): a potent, once-daily oral NS5A inhibitor for the treatment of hepatitis C virus infection', *J Med Chem*, 57: 2033-46. https://doi.org/10.1021/jm401499g

[278] Khan, S., Soni, S., and Veerapu, N. S., 2020. 'HCV Replicon Systems: Workhorses of Drug Discovery and Resistance', *Front Cell Infect Microbiol*, 10: 325. https://doi.org/10.3389/fcimb.2020.00325

[279] Kwon, H. J., Xing, W., Chan, K., Niedziela-Majka, A., Brendza, K. M., Kirschberg, T., Kato, D., Link, J. O., Cheng, G., . . . Sakowicz, R., 2015. 'Direct binding of ledipasvir to HCV NS5A: mechanism of resistance to an HCV antiviral agent', *PLoS ONE*, 10: e0122844. https://doi.org/10.1371/journal.pone.0122844

[280] Balatow, P., Sandlin, A., and Cory, T. J., 2021. 'An evaluation of ledipasvir + sofosbuvir for the treatment of chronic hepatitis C infection', *Expert Opin Pharmacother*, 22: 1839-46. https://doi.org/10.1080/14656566.2021.1943359

[281] U.S. Food & Drug Administration, 2023. 'Drugs@FDA: Harvoni', Accessed 11.12.2023. https://www.accessdata.fda.gov/scripts/cder/daf/index.cfm?event=overview.process&ApplNo=205834.

[282] European Medicines Agency, 2023. 'Harvoni', Accessed 11.12.2023. https://www.ema.europa.eu/en/medicines/human/EPAR/harvoni.

[283] Tabata, K., Neufeldt, C. J., and Bartenschlager, R., 2020. 'Hepatitis C Virus Replication', *Cold Spring Harbor Perspectives in Medicine*, 10: a037093. https://doi.org/10.1101/cshperspect.a037093

[284] Palomares-Jerez, M. F., Guillen, J., and Villalain, J., 2010. 'Interaction of the N-terminal segment of HCV protein NS5A with model membranes', *Biochim Biophys Acta*, 1798: 1212-24. https://doi.org/10.1016/j.bbamem.2010.02.007

[285] Shanmugam, S., Nichols, A. K., Saravanabalaji, D., Welsch, C., and Yi, M., 2018. 'HCV NS5A dimer interface residues regulate HCV replication by controlling its self-interaction, hyperphosphorylation, subcellular localization and interaction with cyclophilin A', *PLoS Pathog*, 14: e1007177. https://doi.org/10.1371/journal.ppat.1007177

[286] Berger, C., Romero-Brey, I., Radujkovic, D., Terreux, R., Zayas, M., Paul, D., Harak, C., Hoppe, S., Gao, M., . . . Bartenschlager, R., 2014. 'Daclatasvir-like inhibitors of NS5A block early biogenesis of hepatitis C virus-induced membranous replication factories, independent of RNA replication', *Gastroenterology*, 147: 1094-105 e25. https://doi.org/10.1053/j.gastro.2014.07.019

[287] Liu, G. Y., and Sabatini, D. M., 2020. 'mTOR at the nexus of nutrition, growth, ageing and disease', *Nat Rev Mol Cell Biol*, 21: 183-203. https://doi.org/10.1038/s41580-019-0199-y

[288] Manning, B. D., and Toker, A., 2017. 'AKT/PKB Signaling: Navigating the Network', *Cell*, 169: 381-405. https://doi.org/10.1016/j.cell.2017.04.001

[289] Yang, H., Rudge, D. G., Koos, J. D., Vaidialingam, B., Yang, H. J., and Pavletich, N. P., 2013. 'mTOR kinase structure, mechanism and regulation', *Nature*, 497: 217-23. https://doi.org/10.1038/nature12122

[290] Fu, W., and Hall, M. N., 2020. 'Regulation of mTORC2 Signaling', *Genes*, 11: 1045. https://doi.org/10.3390/genes11091045

[291] Hara, K., Yonezawa, K., Kozlowski, M. T., Sugimoto, T., Andrabi, K., Weng, Q. P., Kasuga, M., Nishimoto, I., and Avruch, J., 1997. 'Regulation of eIF-4E BP1 phosphorylation by mTOR', *J Biol Chem*, 272: 26457-63. https://doi.org/10.1074/jbc.272.42.26457

[292] Sarbassov, D. D., Guertin, D. A., Ali, S. M., and Sabatini, D. M., 2005. 'Phosphorylation and Regulation of Akt/PKB by the Rictor-mTOR Complex', *Science*, 307: 1098-101. https://doi.org/10.1126/science.1106148

[293] Grekova, S. P., Aprahamian, M., Daeffler, L., Leuchs, B., Angelova, A., Giese, T., Galabov, A., Heller, A., Giese, N. A., . . . Raykov, Z., 2011. 'Interferon gamma improves the vaccination potential of oncolytic parvovirus H-1PV for the treatment of peritoneal carcinomatosis in pancreatic cancer', *Cancer Biol Ther*, 12: 888-95. https://doi.org/10.4161/cbt.12.10.17678

[294] Ferreira, T., 2021. 'Characterisation of Oncolytic H-1 Parvovirus Cell Entry Pathways', Ruperto Carola University Heidelberg.

[295] Jafari, R., Almqvist, H., Axelsson, H., Ignatushchenko, M., Lundback, T., Nordlund, P., and Martinez Molina, D., 2014. 'The cellular thermal shift assay for evaluating drug target interactions in cells', *Nat Protoc*, 9: 2100-22. https://doi.org/10.1038/nprot.2014.138

[296] Martinez Molina, D., Jafari, R., Ignatushchenko, M., Seki, T., Larsson, E. A., Dan, C., Sreekumar, L., Cao, Y., and Nordlund, P., 2013. 'Monitoring drug target engagement in cells and tissues using the cellular thermal shift assay', *Science*, 341: 84-7. https://doi.org/10.1126/science.1233606

[297] Bray, M. A., Singh, S., Han, H., Davis, C. T., Borgeson, B., Hartland, C., Kost-Alimova, M., Gustafsdottir, S. M., Gibson, C. C., . . . Carpenter, A. E., 2016. 'Cell Painting, a high-content image-based assay for morphological profiling using multiplexed fluorescent dyes', *Nat Protoc*, 11: 1757-74. https://doi.org/10.1038/nprot.2016.105

[298] Hilhorst, R., Houkes, L., Mommersteeg, M., Musch, J., van den Berg, A., and Ruijtenbeek, R., 2013. 'Peptide microarrays for profiling of serine/threonine kinase activity of recombinant kinases and lysates of cells and tissue samples', *Methods Mol Biol*, 977: 259-71. https://doi.org/10.1007/978-1-62703-284-1_21

[299] Bär, S., Rommelaere, J., and Nüesch, J. P., 2015. 'PKCeta/Rdx-driven phosphorylation of PDK1: a novel mechanism promoting cancer cell

survival and permissiveness for parvovirus-induced lysis', *PLoS Pathog*, 11: e1004703. https://doi.org/10.1371/journal.ppat.1004703

[300] Jiang, T., and Qiu, Y., 2003. 'Interaction between Src and a C-terminal proline-rich motif of Akt is required for Akt activation', *J Biol Chem*, 278: 15789-93. https://doi.org/10.1074/jbc.M212525200

[301] Parsons, S. J., and Parsons, J. T., 2004. 'Src family kinases, key regulators of signal transduction', *Oncogene*, 23: 7906-09. https://doi.org/10.1038/sj.onc.1208160

[302] Thoreen, C. C., Kang, S. A., Chang, J. W., Liu, Q., Zhang, J., Gao, Y., Reichling, L. J., Sim, T., Sabatini, D. M., . . . Gray, N. S., 2009. 'An ATP-competitive mammalian target of rapamycin inhibitor reveals rapamycin-resistant functions of mTORC1', *J Biol Chem*, 284: 8023-32. https://doi.org/10.1074/jbc.M900301200

[303] Ehrenberg, K. R., Gao, J., Oppel, F., Frank, S., Kang, N., Dieter, S. M., Herbst, F., Mohrmann, L., Dubash, T. D., . . . Ball, C. R., 2019. 'Systematic Generation of Patient-Derived Tumor Models in Pancreatic Cancer', *Cells*, 8. https://doi.org/10.3390/cells8020142

[304] Chan-Seng-Yue, M., Kim, J. C., Wilson, G. W., Ng, K., Figueroa, E. F., O'Kane, G. M., Connor, A. A., Denroche, R. E., Grant, R. C., . . . Notta, F., 2020. 'Transcription phenotypes of pancreatic cancer are driven by genomic events during tumor evolution', *Nat Genet*, 52: 231-40. https://doi.org/10.1038/s41588-019-0566-9

[305] Diallo, J.-S., Boeuf, F. L., Lai, F., Cox, J., Vaha-Koskela, M., Abdelbary, H., MacTavish, H., Waite, K., Falls, T., . . . Bell, J. C., 2010. 'A High-throughput Pharmacoviral Approach Identifies Novel Oncolytic Virus Sensitizers', *Molecular Therapy*, 18: 1123-29. https://doi.org/10.1038/mt.2010.67

[306] Berghauser Pont, L. M., Balvers, R. K., Kloezeman, J. J., Nowicki, M. O., van den Bossche, W., Kremer, A., Wakimoto, H., van den Hoogen, B. G., Leenstra, S., . . . Lamfers, M. L., 2015. 'In vitro screening of clinical drugs identifies sensitizers of oncolytic viral therapy in glioblastoma stem-like cells', *Gene Ther*, 22: 947-59. https://doi.org/10.1038/gt.2015.72

[307] Hanson, N. D., and Rhode, S. L., 1991. 'Parvovirus NS1 stimulates P4 expression by interaction with the terminal repeats and through DNA amplification', *Journal of Virology*, 65: 4325-33. https://doi.org/10.1128/jvi.65.8.4325-4333.1991

[308] Calleja, V., Alcor, D., Laguerre, M., Park, J., Vojnovic, B., Hemmings, B. A., Downward, J., Parker, P. J., and Larijani, B., 2007. 'Intramolecular and Intermolecular Interactions of Protein Kinase B Define Its Activation In Vivo', *PLoS Biology*, 5: e95. https://doi.org/10.1371/journal.pbio.0050095

[309] Nüesch, J. P., Lacroix, J., Marchini, A., and Rommelaere, J., 2012. 'Molecular pathways: rodent parvoviruses--mechanisms of oncolysis and prospects for clinical cancer treatment', *Clin Cancer Res*, 18: 3516-23. https://doi.org/10.1158/1078-0432.CCR-11-2325

[310] He, S., Li, Q., Huang, Q., and Cheng, J., 2022. 'Targeting Protein Kinase C for Cancer Therapy', *Cancers*, 14: 1104. https://doi.org/10.3390/cancers14051104

[311] Isakov, N., 2018. 'Protein kinase C (PKC) isoforms in cancer, tumor promotion and tumor suppression', *Semin Cancer Biol*, 48: 36-52. https://doi.org/10.1016/j.semcancer.2017.04.012

[312] Hsieh, A. C., Costa, M., Zollo, O., Davis, C., Feldman, M. E., Testa, J. R., Meyuhas, O., Shokat, K. M., and Ruggero, D., 2010. 'Genetic dissection of the oncogenic mTOR pathway reveals druggable addiction to translational control via 4EBP-eIF4E', *Cancer Cell*, 17: 249-61. https://doi.org/10.1016/j.ccr.2010.01.021

[313] Thoreen, C. C., Chantranupong, L., Keys, H. R., Wang, T., Gray, N. S., and Sabatini, D. M., 2012. 'A unifying model for mTORC1-mediated regulation of mRNA translation', *Nature*, 485: 109-13. https://doi.org/10.1038/nature11083

[314] Carvalho de Oliveira, J., Mathias, C., Oliveira, V. C., Pezuk, J. A., and Brassesco, M. S., 2022. 'The Double Face of miR-708: A Pan-Cancer Player with Dissociative Identity Disorder', *Genes*, 13: 2375. https://doi.org/10.3390/genes13122375

[315] Dileepan, M., Jude, J. A., Rao, S. P., Walseth, T. F., Panettieri, R. A., Subramanian, S., and Kannan, M. S., 2014. 'MicroRNA-708 regulates CD38 expression through signaling pathways JNK MAP kinase and PTEN/AKT in human airway smooth muscle cells', *Respiratory Research*, 15: 107. https://doi.org/10.1186/s12931-014-0107-0

[316] Guo, P., Lan, J., Ge, J., Nie, Q., Mao, Q., and Qiu, Y., 2013. 'miR-708 acts as a tumor suppressor in human glioblastoma cells', *Oncol Rep*, 30: 870-76. https://doi.org/10.3892/or.2013.2526

[317] Chen, Y., Deng, X., Chen, W., Shi, P., Lian, M., Wang, H., Wang, K., Qian, D., Xiao, D., . . . Long, H., 2019. 'Silencing of microRNA-708 promotes cell growth and epithelial-to-mesenchymal transition by activating the SPHK2/AKT/β-catenin pathway in glioma', *Cell Death & Disease*, 10: 448. https://doi.org/10.1038/s41419-019-1671-5

[318] Murray, E. R., and Cameron, A. J. M., 2017. 'Towards specific inhibition of mTORC2', *Aging (Albany NY)*, 9: 2461-62. https://doi.org/10.18632/aging.101346

[319] Mendoza, M. C., Er, E. E., and Blenis, J., 2011. 'The Ras-ERK and PI3K-mTOR pathways: cross-talk and compensation', *Trends Biochem Sci*, 36: 320-8. https://doi.org/10.1016/j.tibs.2011.03.006

[320] Davies, B. R., Greenwood, H., Dudley, P., Crafter, C., Yu, D.-H., Zhang, J., Li, J., Gao, B., Ji, Q., . . . Pass, M., 2012. 'Preclinical Pharmacology of AZD5363, an Inhibitor of AKT: Pharmacodynamics, Antitumor Activity, and Correlation of Monotherapy Activity with Genetic Background', *Molecular Cancer Therapeutics*, 11: 873-87. https://doi.org/10.1158/1535-7163.Mct-11-0824-t

[321] Okuzumi, T., Fiedler, D., Zhang, C., Gray, D. C., Aizenstein, B., Hoffman, R., and Shokat, K. M., 2009. 'Inhibitor hijacking of Akt activation', *Nature Chemical Biology*, 5: 484-93. https://doi.org/10.1038/nchembio.183

[322] Seoane, R., Vidal, S., Bouzaher, Y. H., El Motiam, A., and Rivas, C., 2020. 'The Interaction of Viruses with the Cellular Senescence Response', *Biology (Basel)*, 9. https://doi.org/10.3390/biology9120455

[323] Parzych, K. R., and Klionsky, D. J., 2014. 'An Overview of Autophagy: Morphology, Mechanism, and Regulation', *Antioxidants & Redox Signaling*, 20: 460-73. https://doi.org/10.1089/ars.2013.5371

[324] Sun, Y., Wang, H., Qu, T., Luo, J., An, P., Ren, F., Luo, Y., and Li, Y., 2023. 'mTORC2: a multifaceted regulator of autophagy', *Cell Communication and Signaling*, 21: 4. https://doi.org/10.1186/s12964-022-00859-7

[325] Takeuchi, H., Kondo, Y., Fujiwara, K., Kanzawa, T., Aoki, H., Mills, G. B., and Kondo, S., 2005. 'Synergistic Augmentation of Rapamycin-Induced Autophagy in Malignant Glioma Cells by Phosphatidylinositol 3-Kinase/Protein Kinase B Inhibitors', *Cancer Research*, 65: 3336-46. https://doi.org/10.1158/0008-5472.Can-04-3640

[326] Kamynina, M., Tskhovrebova, S., Fares, J., Timashev, P., Laevskaya, A., and Ulasov, I., 2021. 'Oncolytic Virus-Induced Autophagy in Glioblastoma', *Cancers*, 13: 3482. https://doi.org/10.3390/cancers13143482

[327] Wu, Y. Y., Sun, T. K., Chen, M. S., Munir, M., and Liu, H. J., 2023. 'Oncolytic viruses-modulated immunogenic cell death, apoptosis and autophagy linking to virotherapy and cancer immune response', *Front Cell Infect Microbiol*, 13: 1142172. https://doi.org/10.3389/fcimb.2023.1142172

[328] Chiramel, A. I., Brady, N. R., and Bartenschlager, R., 2013. 'Divergent roles of autophagy in virus infection', *Cells*, 2: 83-104. https://doi.org/10.3390/cells2010083

[329] Cheng, J.-H., Sun, Y.-J., Zhang, F.-Q., Zhang, X.-R., Qiu, X.-S., Yu, L.-P., Wu, Y.-T., and Ding, C., 2016. 'Newcastle disease virus NP and P proteins induce

autophagy via the endoplasmic reticulum stress-related unfolded protein response', *Scientific Reports*, 6: 24721. https://doi.org/10.1038/srep24721

[330] Jiffry, J., Thavornwatanayong, T., Rao, D., Fogel, E. J., Saytoo, D., Nahata, R., Guzik, H., Chaudhary, I., Augustine, T., . . . Maitra, R., 2021. 'Oncolytic Reovirus (pelareorep) Induces Autophagy in KRAS-mutated Colorectal Cancer', *Clinical Cancer Research*, 27: 865-76. https://doi.org/10.1158/1078-0432.Ccr-20-2385

[331] Schindelin, J., Arganda-Carreras, I., Frise, E., Kaynig, V., Longair, M., Pietzsch, T., Preibisch, S., Rueden, C., Saalfeld, S., . . . Cardona, A., 2012. 'Fiji: an open-source platform for biological-image analysis', *Nature Methods*, 9: 676-82. https://doi.org/10.1038/nmeth.2019

[332] Wickham, H., François, R., Henry, L., Müller, K., and Vaughan, D., 2023. 'dplyr: A Grammar of Data Manipulation.', R package version 1.1.3, https://CRAN.R-project.org/package=dplyr

[333] Wickham, H., 2016. *ggplot2: Elegant Graphics for Data Analysis* (Springer International Publishing). https://books.google.de/books?id=RTMFswEACAAJ

[334] Pedersen, T., 2022. 'ggforce: Accelerating 'ggplot2'', R package version 0.4.1, https://CRAN.R-project.org/package=ggforce

[335] Wickham, H., 2007. 'Reshaping Data with the reshape Package', *Journal of Statistical Software*, 21: 1 - 20. https://doi.org/10.18637/jss.v021.i12

[336] Wickham, H., and Seidel, D., 2022. 'scales: Scale Functions for Visualization', R package version 1.2.1, https://CRAN.R-project.org/package=scales

[337] Gautier, L., Cope, L., Bolstad, B. M., and Irizarry, R. A., 2004. 'affy--analysis of Affymetrix GeneChip data at the probe level', *Bioinformatics*, 20: 307-15. https://doi.org/10.1093/bioinformatics/btg405

[338] Smyth, G. K., 2004. 'Linear models and empirical bayes methods for assessing differential expression in microarray experiments', *Stat Appl Genet Mol Biol*, 3: Article3. https://doi.org/10.2202/1544-6115.1027

[339] Lucas, A., 2022. 'amap: Another Multidimensional Analysis Package', R package version 0.8-19, https://CRAN.R-project.org/package=amap

[340] Subramanian, A., Tamayo, P., Mootha, V. K., Mukherjee, S., Ebert, B. L., Gillette, M. A., Paulovich, A., Pomeroy, S. L., Golub, T. R., . . . Mesirov, J. P., 2005. 'Gene set enrichment analysis: A knowledge-based approach for interpreting genome-wide expression profiles', *Proceedings of the National Academy of Sciences*, 102: 15545-50. https://doi.org/10.1073/pnas.0506580102

[341] Kallio, M. A., Tuimala, J. T., Hupponen, T., Klemelä, P., Gentile, M., Scheinin, I., Koski, M., Käki, J., and Korpelainen, E. I., 2011. 'Chipster: user-

friendly analysis software for microarray and other high-throughput data', *BMC Genomics*, 12: 507. https://doi.org/10.1186/1471-2164-12-507

[342] Wolfe, D., Dudek, S., Ritchie, M. D., and Pendergrass, S. A., 2013. 'Visualizing genomic information across chromosomes with PhenoGram', *BioData Min*, 6: 18. https://doi.org/10.1186/1756-0381-6-18

[343] El-Andaloussi, N., Leuchs, B., Bonifati, S., Rommelaere, J., and Marchini, A., 2012. 'Efficient recombinant parvovirus production with the help of adenovirus-derived systems', *Journal of Visualized Experiments*: e3518. https://doi.org/10.3791/3518

[344] DuBridge, R. B., Tang, P., Hsia, H. C., Leong, P.-M., Miller, J. H., and Calos, M. P., 1987. 'Analysis of Mutation in Human Cells by Using an Epstein-Barr Virus Shuttle System', *Molecular and Cellular Biology*, 7: 379-87. https://doi.org/10.1128/mcb.7.1.379-387.1987

[345] Kestler, J., Neeb, B., Struyf, S., Van Damme, J., Cotmore, S. F., D'Abramo, A., Tattersall, P., Rommelaere, J., Dinsart, C., . . . Cornelis, J. J., 1999. 'cis requirements for the efficient production of recombinant DNA vectors based on autonomous parvoviruses', *Hum Gene Ther*, 10: 1619-32. https://doi.org/10.1089/10430349950017626

[346] Yuan, X., Braunstein, E. M., Ye, Z., Liu, C. F., Chen, G., Zou, J., Cheng, L., and Brodsky, R. A., 2013. 'Generation of glycosylphosphatidylinositol anchor protein-deficient blood cells from human induced pluripotent stem cells', *Stem Cells Transl Med*, 2: 819-29. https://doi.org/10.5966/sctm.2013-0069

[347] Möhle, R., Green, D., Moore, M. A., Nachman, R. L., and Rafii, S., 1997. 'Constitutive production and thrombin-induced release of vascular endothelial growth factor by human megakaryocytes and platelets', *Proc Natl Acad Sci U S A*, 94: 663-8. https://doi.org/10.1073/pnas.94.2.663

[348] Douvaras, P., Wang, J., Zimmer, M., Hanchuk, S., O'Bara, M. A., Sadiq, S., Sim, F. J., Goldman, J., and Fossati, V., 2014. 'Efficient generation of myelinating oligodendrocytes from primary progressive multiple sclerosis patients by induced pluripotent stem cells', *Stem Cell Reports*, 3: 250-9. https://doi.org/10.1016/j.stemcr.2014.06.012

[349] Watanabe, K., Ueno, M., Kamiya, D., Nishiyama, A., Matsumura, M., Wataya, T., Takahashi, J. B., Nishikawa, S., Nishikawa, S., . . . Sasai, Y., 2007. 'A ROCK inhibitor permits survival of dissociated human embryonic stem cells', *Nat Biotechnol*, 25: 681-6. https://doi.org/10.1038/nbt1310

[350] Vernardis, S. I., Terzoudis, K., Panoskaltsis, N., and Mantalaris, A., 2017. 'Human embryonic and induced pluripotent stem cells maintain phenotype but alter their metabolism after exposure to ROCK inhibitor', *Scientific Reports*, 7: 42138. https://doi.org/10.1038/srep42138

[351] Zolotukhin, S., Byrne, B. J., Mason, E., Zolotukhin, I., Potter, M., Chesnut, K., Summerford, C., Samulski, R. J., and Muzyczka, N., 1999. 'Recombinant adeno-associated virus purification using novel methods improves infectious titer and yield', *Gene Ther*, 6: 973-85. https://doi.org/10.1038/sj.gt.3300938

[352] Stael, S., Miller, L. P., Fernández-Fernández, Á. D., and Van Breusegem, F., 2022. 'Detection of Damage-Activated Metacaspase ActivityActivitiesby Western Blot in Plants.' in Marina Klemenčič, Simon Stael and Pitter F. Huesgen (eds.), *Plant Proteases and Plant Cell Death: Methods and Protocols* (Springer US: New York, NY). https://doi.org/10.1007/978-1-0716-2079-3_11

[353] Zhang, Y., Parmigiani, G., and Johnson, W. E., 2020. 'ComBat-seq: batch effect adjustment for RNA-seq count data', *NAR Genomics and Bioinformatics*, 2. https://doi.org/10.1093/nargab/lqaa078